

**POLYANILINE BASED MATERIALS FOR
ELECTROCHEMICAL SENSING AND SUPERCAPACITOR
APPLICATIONS**

*Thesis Submitted to the University of Calicut for the
Award of*

DOCTOR OF PHILOSOPHY IN CHEMISTRY

By

SIDHEEKHA M P

Under the Supervision of

Dr. YAHYA A.I.



DEPARTMENT OF CHEMISTRY

UNIVERSITY OF CALICUT

KERALA-673 635

JUNE 2023

Dedicated to the loving memory of my 'Umma',

*whose words continue to be the unwavering source of strength
in my life...*

CERTIFICATE

This is to certify that the thesis entitled “**Polyaniline Based Materials for Electrochemical Sensing and Supercapacitor Applications**” submitted by **Sidheekha M P** to the University of Calicut for the award of the degree of Doctor of Philosophy in Chemistry, is an authentic record of research work carried out at the Department of Chemistry, of the University of Calicut under my guidance and supervision. The contents of the thesis have been checked for plagiarism using the software ‘*DrillBit*’ and the similarity index falls under permissible limit, and I further certify that the thesis or part has not previously formed the basis for the award of any degree/diploma/associate ship of any other University or Institute. I also certify that the adjudicators have not suggested any major changes or corrections in the scientific content, results and interpretations the thesis. However, the minor suggestions recommended by the examiners are incorporated in the revised thesis.

Calicut University

Dr. Yahya A.I.

Associate Professor
Department of Chemistry
University of Cali

DECLARATION

I, **Sidheekha M P**, hereby declare that thesis entitled “POLYANILINE BASED MATERIALS FOR ELECTROCHEMICAL SENSING AND SUPERCAPACITOR APPLICATIONS” submitted to the University of Calicut by me, is a bonafide record of my research work done under the supervision and guidance of **Dr. Yahya A. I.**, Associate Professor, Department of Chemistry, University of Calicut, for the award of the degree of Doctor of Philosophy in Chemistry under the Faculty of Sciences, University of Calicut, Kerala. The contents of this thesis have not been presented previously for the award of any Degree/Diploma in any other University or Institution.

University of Calicut

Sidheekha M P

ACKNOWLEDGEMENTS

First and foremost, I thank Almighty “ALLAH” the most merciful and the beneficent for showering limitless blessings, being kind to me and also enabling this challenging task reach to its completion.

This thesis could not have been completed without the generous support that I have received from so many people over these years, and I owe my gratitude to all of them.

*It is definitely a pleasing privilege for me to express my heartfelt gratitude to my supervisor **Dr. Yahya A I**, Associate Professor, Department of Chemistry, University of Calicut, for his constant support and encouragement throughout this work. I was fortunate enough to have him as my mentor. I greatly appreciate his ability to stay kind, motivate and gave freedom though out my research period. I extend my most sincere regard and thanks to him for his comments, excellent advices and perceptive suggestions that eventually led to the final draft of this study.*

*I would also like to express my hearty thanks to **Dr. Rajeev S Menon**, the Head of the Department of Chemistry, and the former HODs of the department for providing me all the facilities to carry out my research work. I express my sincere gratitude to all the faculty members of this department for their suggestions and support. I extend my appreciation to the technician, lab assistants, and other non-teaching*

staff members in this department for their invaluable assistance and support.

I am extremely thankful to Dr. Mohamed Shahin Thayyil, Professor, Department of Chemistry, University of Calicut and his research group for providing me necessary arrangement and help for electrical characterization.

I would like to acknowledge the Central Sophisticated Instrument Facility (CSIF) of the University of Calicut and MNCF, IISc Bangalore, for their services in the characterization part. I am grateful to the University Grants Commission, Government of India, for the financial assistance, by providing me with JRF and SRF, that enabled me to complete this work.

I am deeply grateful for the unwavering help, support, care, and encouragement provided by my fellow research group members, Shabeeba A K, Lijin Rajan, Sivakrishna Prakash, Roopasri R, Razana P K, and Deepak Joshy and I thank each of them wholeheartedly. Additionally, I extend my gratitude to our former M. Phil scholars in the group, Anjali C, Geethu E R, and Athira A, for their valuable support. I express my heartfelt affection to Shabeeba with whom I shared personal and research-related matters with each other greatly contributed to making this place special for me. Furthermore, I am indebted to other research scholars, ex-research scholars who have contributed to fostering a positive working environment and offered their assistance and support.

I am grateful for the selfless efforts of my Uppa, who have given me the freedom to choose my path. I express my deep gratitude to My

stepmother, my sisters, and my little brother, for their love, support and prayers. I extend my gratitude to all other family members and in-laws for their support. I am indebted to my husband, Mr. Shameer, whose love, care, cooperation and sacrifices provided invaluable support in completing my research successfully. Words alone cannot fully convey the depth of my love and connection to my beloved daughter, Ifra Mol, who came to us during the research period. I take this moment to fondly remember my grandmother, who became a mother figure to me after the loss of my own mother, who passed away last year, her love and prayers were my genuine source of strength.

Apart from the ones mentioned here, I record my warm thanks to all those who have helped me directly or indirectly in making this thesis successful

Sidheekha M P

TABLE OF CONTENT

	Page No.
<i>Preface</i>	<i>i - iv</i>
<i>List of tables</i>	<i>v</i>
<i>List of figures</i>	<i>vii-xx</i>
<i>List of abbreviations</i>	<i>xxi-xxiii</i>
Chapter 1: Introduction	1-64
1.1 Conducting polymers	1
1.1.1. Examples of conducting polymers	3
1.1.2. The concept of doping	5
1.1.3. The charge transport mechanism of CPs	6
1.1.4. Factors affecting the electrical conductivity	9
1.1.5. Applications of conducting polymers	10
1.2. Polyaniline	12
1.2.1 A brief history	12
1.2.2 Molecular structure of PANI	13
1.2.3 Doping in polyaniline: A new concept	15
1.2.4. Synthesis of polyaniline	17
1.2.5. Polymerization mechanism of polyaniline	20
1.2.6. Applications of Polyaniline	23
1.2.7. Limitations of Polyaniline	26
1.2.8. Strategies adopted to overcome the limitations of polyaniline	27

1.3. Introduction to hydrogel	29
1.4. Conducting polymer/ hydrogel systems (CPHs)	31
1.4.1. Fabrication of CPHs	32
1.4.2. Characterization techniques to study the properties of CPHs	37
1.4.3. Applications of CPHs	39
1.5. Supercapacitors: A brief introduction	40
1.5.1. Electrical double layer capacitors (EDLCs)	40
1.5.2. Pseudocapacitors	41
1.5.3. Hybrid supercapacitors	42
1.5.4. Conducting polymers for supercapacitors	42
1.6. Electrochemistry of CPs: an overview	44
1.6.1. CPs are reactive redox materials	44
1.6.2. CPs as multistep molecular motors	47
1.6.3. Reaction driven biomimetic properties of CPs	49
1.7. The present investigation	50
1.8. The major research objectives	53
References	54

Chapter 2	Materials and methods	65-80
------------------	------------------------------	--------------

2.1. Materials used	65
2.2. Synthesis of PANI	65

2.3.	Fabrication of CP/hydrogel hybrid films	66
2.3.1.	Fabrication of Chitosan/PANI hybrid films	67
2.3.2.	Fabrication of PVA/PANI hybrid films	68
2.4.	Fabrication of supercapacitor device	69
2.5.	General characterization techniques	69
2.5.1.	Fourier transform infra-red spectroscopy (FTIR)	69
2.5.2.	Broadband dielectric spectroscopy (BDS)	70
2.5.3.	Thermogravimetric analysis (TGA)	71
2.5.4.	Universal testing machine (UTM) analysis-Mechanical studies	71
2.5.5.	Fourier transform scanning electron microscopy (FESEM)	72
2.5.6.	Energy-dispersive X-ray spectroscopy (EDX analysis)	72
2.6.	Electrochemical characterizations	73
2.6.1.	Preparation of working electrodes	73
2.6.2.	Cyclic voltammetry (CV)	74
2.6.3.	Galvanostatic charge discharge (GCD)	76
2.6.4.	Electrochemical impedance spectroscopy (EIS)	77
2.6.5.	Chronopotentiometry (for sensing studies)	78
2.6.6.	References	80

Characterization of Polyaniline with	
Chapter 3: special emphasis on electrochemical studies	81-105
<hr/>	
3.1. Introduction	81
3.2. Results and Discussion	82
3.2.1. General characterizations	82
3.2.2. Electrochemical characterization	85
3.2.2.1. Cyclic Voltammetry	85
3.2.2.2. Coulovoltammetry	88
3.2.2.3. Structural faradic processes in PANI electrode; characteristic potentials and related charges	90
3.2.2.4. Influence of the cathodic potential limit on voltametric and coulovoltammetric responses	95
3.2.2.5. Influence of the anodic potential limit on the voltammetric and coulovoltammetric responses	98
3.3. Conclusion	101
References	102
<hr/>	
Chapter 4: Reaction driven sensing characteristics of Polyaniline: A chronopotentiometric and voltammetric investigation	107-140
<hr/>	
4.1. Introduction	107
4.2. Results and Discussion	110

I.	Reaction driven sensing characteristics of PANI: A chronopotentiometric investigation	
4.2.1.	Theoretical description	110
4.2.2.	Sensing electrical working conditions: current sensor	114
4.2.3.	Sensing chemical working condition: concentration sensor	117
4.2.4.	Sensing thermal working condition: temperature sensor	119
II.	Reaction driven sensing characteristics of PANI: A voltammetric investigation	
4.2.5.	Sensing electrical working condition: scan rate sensor	122
4.2.6.	Sensing chemical working condition: concentration sensor	129
4.2.7.	Sensing thermal working condition: temperature sensor	134
4.3.	Conclusion	138
	References	139

Chapter 5	Reaction driven sensing characteristics and supercapacitor application of Chitosan/Polyaniline hybrid films	141-188
------------------	--	----------------

5.1.	Introduction	141
5.2.	Results and Discussion	143
I.	Characterization of Chitosan/PANI hybrid films	143
5.2.1.	FTIR spectra	143

5.2.2.	Electrical Conductivity	145
5.2.3.	Thermal characterization	146
5.2.4.	Mechanical characterization	147
5.2.5.	Morphological characterization	149
5.2.6.	Elemental analysis	151
5.2.7.	Electrochemical characterization	152
5.2.7.1.	Cyclic voltammetry	152
5.2.7.2.	Coulovoltammetry	155
II.	Reaction driven sensing characteristics of Cs/PANI hybrid films	156
5.2.8.	Sensing by chronopotentiometry	156
5.2.9.	Sensing by voltammetry	165
III.	Chitosan/PANI hybrid films as electrode materials for supercapacitors	175
5.2.10.	The areal specific capacitance of Cs/PANI hybrid film free-standing electrodes	175
5.2.11.	EIS analysis	179
5.2.12.	Cycling stability	180
5.2.13.	Charge storage kinetics of CPF4 electrode	181
5.3.	Conclusions	184
	References	185

Chapter 6 Polyvinyl alcohol/Polyaniline hybrid films as sensing macromolecular motors: electrochemical characterization and sensing supercapacitor application 189-256

6.1.	Introduction	189
6.2.	Results and Discussion	191
I.	Characterization of PVA/PANI hybrid films	191
6.2.1.	FTIR spectra	191
6.2.2.	Electrical conductivity	193
6.2.3.	Thermal characterization	194
6.2.4.	Mechanical characterization	195
6.2.5.	Morphological characterization	199
6.2.6.	Elemental analysis	201
6.2.7.	Electrochemical characterization	202
6.2.7.1.	Cyclic voltammetry	202
6.2.7.2.	Coulovoltammetry	204
II.	Reaction driven sensing characteristics of PVA/PANI hybrid films: A chronopotentiometric study	206
6.2.8.	Sensing working electrical working condition: current sensor	206
6.2.9.	Sensing the chemical working condition: concentration sensor	208

6.2.10.	Sensing the thermal working condition: temperature sensor	210
III.	Influence of working conditions on the cooperative actuation of multimolecular motors of PANI: A Voltammetric study	212
6.2.11.	Cooperative actuation in CP films	212
6.2.12.	Influence of chemical condition on the cooperative actuation of molecular motors of PANI present in PP4 hybrid film: concentration sensor	213
6.2.13.	Influence of thermal condition on the cooperative actuation of molecular motors of PANI present in PP4 hybrid film: temperature sensor	220
6.2.14.	Influence of electrical working condition on the cooperative actuation of molecular motors of PANI present in PP4 hybrid film: scan rate sensor	226
IV.	PVA/PANI films as supercapacitor electrode	233
6.2.15.	The specific areal capacitance of PVA/PANI hybrid film free-standing electrodes	235
6.2.16.	EIS analysis	236
6.2.17.	Cycling stability	237
6.2.18.	Charge storage kinetics of PP4 hybrid film	239

V. Sensing supercapacitor device using PVA/PANI hybrid films	241
6.2.19. Charge storage performance of the device	241
6.2.20. Sensing characteristics of the device	248
6.1. Conclusion	251
References	253
<hr/>	
Chapter 7 Summary and future outlook	257-263
<hr/>	
7.1. Summary	257
7.2. Future outlook	261
List of publications and presentations	265-269

Preface

Conducting polymers (CPs), notably polyaniline (PANI), have gained significant research attention due to their fascinating electrical and electrochemical characteristics leading to wide range of applications. Despite the substantial interest they have generated, the comprehensive understanding of their composition-dependent properties and applications are not much explored by the scientific world. Though PANI displays an impressive electroactivity, the fundamental electrochemical processes underlying its behavior are yet to be explored. Therefore, this thesis represents a progression from delving into the fundamental electrochemistry of PANI to the development of self-sensing motors utilizing PANI.

The thesis is divided into seven chapters.

Chapter 1 provides a detailed introduction to conducting polymers with special emphasis on polyaniline including a brief literature review. This section covers various aspects related to polyaniline and polyaniline/hydrogel systems, including synthesis methods and their applications. Additionally, a brief description of the electrochemistry of conducting polymers highlighting their reaction-driven biomimetic properties are also presented.

Chapter 2 provides a concise overview of materials employed, characterization techniques applied, and methodologies adopted for the current research. This section also offers a detailed explanation of the various electrochemical techniques, such as cyclic voltammetry,

chronopotentiometry, GCD and EIS studies employed in the presented work.

Chapters 3 to 6 represent the core of our investigative journey, each of these chapters has been designed to explore different aspects of our research in a detailed manner.

Chapter 3: ‘*Characterization of polyaniline with special emphasis on electrochemical studies.*’ This chapter comprises a discussion of the results of the characterization of synthesized polyaniline and offers a comprehensive exploration of PANI through in-depth electrochemical analysis. It provides a detailed examination of the structural faradaic processes in PANI and quantification of the charge consumed during each of these structural processes by utilizing coulombometry. The influences of cathodic and anodic potential limits on voltammetric and coulombometric responses are studied in this chapter. This chapter provides a profound understanding of PANI's electrochemical behavior and its reaction.

Chapter 4: ‘*Reaction driven sensing characteristics of polyaniline: A chronopotentiometric and voltammetric investigation.*’ This chapter is dedicated to the investigation of PANI's reaction-driven sensing characteristics under varying working conditions, such as electrical, thermal and chemical energetic working conditions. These characteristics are assessed using chronopotentiometry to measure consumed electrical energy and by cyclic voltammetry to monitor consumed charge during the reaction, both serving as key sensing parameters. Furthermore, the chapter includes an in-depth exploration of the theoretical foundation underpinning PANI's reaction-driven sensing capabilities.

Chapter 5: *‘Reaction driven sensing characteristics and supercapacitor application of Chitosan/Polyaniline hybrid films.’* The primary challenge associated with PANI lies in its limited processability, rendering it unsuitable for device applications. Thus, the main objective of this chapter is to develop a free-standing electrode material based on PANI, catering to the needs of both sensing and supercapacitor applications. In pursuit of this goal, Chitosan/PANI hybrid films are fabricated using a facile and cost-effective method. The chapter delves into the detailed characterization and an exploration of the reaction-driven sensing characteristics of Chitosan/PANI hybrid films as well as evaluates the efficacy of Chitosan/PANI hybrid films as a free-standing electrode material for supercapacitor applications.

Chapter 6: *‘Polyvinyl alcohol/Polyaniline hybrid films as sensing macromolecular motors: electrochemical characterization and sensing supercapacitor application.’* This chapter is dedicated to the fabrication of highly mechanically stable PVA/PANI free-standing hybrid films specifically fabricated for device applications. It delves into the detailed characterization and reaction-driven sensing capabilities of these PVA/PANI hybrid films. The chapter explores how various working conditions impact the cooperative actuation of multistep molecular motors of PANI present in these hybrid films. It is confirmed that the conformational and structural changes resulting from the cooperative actuation of constitutive chemical molecular machines within the PVA/PANI hybrid film are responsible for the film's self-sensing property. In addition, the chapter delves into the fabrication of a sensing supercapacitor device using PVA/PANI film, demonstrating the device's ability to sense working conditions without the necessity of additional connections or extra components. This fundamental study

offers a novel direction for the development of simple and compatible self-sensing motors.

Chapter 7 provides a comprehensive summary of the major findings and highlights of the present work. This chapter also outlines the future outlook of the present investigation, particularly focusing on the development of various biomimetic devices.

LIST OF TABLES

Table No.	Table caption	Page No.
1.1	Examples of conducting polymers	4
1.2	Applications of polyaniline and related properties	23
2.1	List of chemicals used and their purity	65
4.1	Structural faradic processes in PANI, characteristic potential ranges and associated electrical charges	94
5.1	Tensile strength, Young's Modulus and % elongation at break of Cs/PANI hybrid films	149
5.2	Anodic and cathodic peaks of Cs/PANI hybrid films at the scan rate 25 mV s^{-1}	153
5.3	Sensitivities of Cs/PANI hybrid films towards various working conditions, where consumed electrical energy and consumed charge during the reaction as sensing parameters	174
6.1	Tensile strength, Young's modulus and percentage elongation at break of PVA/PANI hybrid films in the dry and wet states	198
6.2	Anodic and cathodic peaks of PVA/PANI electrodes at the scan rate of 25 mV s^{-1}	203
6.3	Comparison of PVA/PANI hybrid film supercapacitor with other PANI-hydrogel-based supercapacitors reported in the literature	244
6.4	EIS fitting data of the device	247

LIST OF FIGURES

Figure No.	Figure captions	Page No.
1.1	Electrical conductivity range of conducting polymers	2
1.2	In trans-polyacetylene, (a) charge transportation as the soliton hops along the carbon chain, (b) and (c) the mechanism for transportation of a polaron and bipolaron respectively	8
1.3	Representation of energy band gaps of conducting polymer (a) undoped state and (b) with a polaron.	9
1.4	Representation of energy gap of (a) two polaron, (b) the coupling of two polarons forming bipolaron decreases the energy gap and (c) formation of bipolaron bands at high doping level.	9
1.5	Applications of conducting polymers	11
1.6	Principal unit of polyaniline: (a) reduced form and (b) oxidized form	14
1.7	Different forms of polyaniline	15
1.8	Resonance forms of aniline radical	21
1.9	Polymerization mechanism of aniline described by Wallace et al (steps 2 and 3).	22
1.10	Schematic showing the formation of PANI/Hydrogel via in-situ chemical polymerization of aniline within the hydrogel	33

	matrix; (a) chemical polymerization, (b) electrochemical polymerization and (c) interfacial polymerization	
1.11	Schematic representation of polymerization of aniline in the hydrogel solution/dispersion	34
1.12	Schematic representation of polyaniline/hydrogel from mixed precursors	35
1.13	Schematic illustrations CP gels formed by crosslinking with dopant molecules; (a) ATMP doped polyaniline gel, (b) phytic acid doped polyaniline gel, and (c) CuPcTs doped PPy hydrogel	37
1.14	The characterization techniques of CPHs	38
1.15	Schematic representation of (a) Exchange of anions and (b) exchange of cations during electrochemical reactions.	46
1.16	Formation/destruction of π bonds by oxidation/reduction of (a) polypyrrole and (b) polyaniline. (c) Schematic representation of reversible conformational movements reversible oxidation/reduction of CPs: an electrochemical molecular machine	48
1.17	Biomimetic properties of CPs driven by the electrochemical reaction, the mimicked biological functions and the related organs	49
2.1	Schematic representation of synthesis of PANI	66
2.2	Schematic representation of fabrication of CPH films	67

2.3	Schematic representation of supercapacitor device fabrication	69
2.4	Zahner Zennium Pro electrochemical workstation used for electrochemical studies	74
2.5	Cyclic voltammetry: (a) Symmetrical triangular potential wave applied to the working electrode, (b) corresponding current measured and (c) Cyclic voltammogram	75
2.6	(a) Square current waves applied to the working electrode and (b) resulting chronopotentiometric responses	79
3.1	FTIR spectra of PANI	82
3.2	TG curve of PANI	83
3.3	Frequency dependent conductivity of PANI	84
3.4	FESEM image of PANI	85
3.5	CV curve of PANI at scan rate of 25 mV s^{-1}	87
3.6	(a) CV of PANI at different scan rates and (b) linear variation of anodic and cathodic peak currents with the square root of scan rate	86
3.7	Schematic representation of the redox process in PANI	88
3.8	Coulovoltammogram of PANI at scan rate of 25 mV s^{-1}	89
3.9	Coulovoltammogram of PANI at a scan rate of 25 mV s^{-1}	71

3.10	Chronocoulogram attained from the QV (-0.25 V to 0.7 V at 25 25 mV s ⁻¹) showing the continuity of the faradic reduction compaction (Q _{rc}) during the anodic potential sweep.	93
3.11	(a) CVs obtained for PANI in 1 M HCl at 25mVs ⁻¹ from different cathodic potential limits. (b) QVs obtained by integration of the CVs from (a).	95
3.12	(a) Charge involved in the oxidation and reduction of PANI and (b) irreversible reduction charge for different cathodic potential limits (only magnitudes of the charges are considered for plotting)	98
3.13	(a) CVs obtained for PANI in 1M HCl at 25mVs ⁻¹ from different anodic potential limits. (b) Corresponding QVs. (c) Open loop QV shows the charge involved in the new irreversible oxidation process represented as Q _{irox}	99
3.14	(a) Charge involved in the oxidation and reduction of PANI and (b) irreversible reduction charge for different anodic potential limits (only magnitudes of the charges are considered for plotting)	101
4.1	Chronopotentiograms obtained when different anodic (a) and cathodic currents (b) from 1 M HCl by passing a constant oxidation/reduction charge of ± 60 mC, in absolute values	115
4.2	Linear dependence of consumed electrical energy with applied currents	116
4.3	anodic (a) and cathodic (b) chronopotentiograms obtained from different concentrations of the	117

	electrolyte by the flow of ± 1 mA current for 60 s (charge ± 60 mC) at room temperature	
4.4	Linear dependence of consumed electrical energy with the concentration of electrolyte	118
4.5	anodic (a) and cathodic (b) chronopotentiograms obtained at different temperatures by the flow of ± 1 mA current for 60 s (charge ± 60 mC) in 1 M HCl solution	119
4.6	Linear dependence of consumed electrical energy with reaction temperature	120
4.7	(a) CV at different scan rates and (b) QV obtained by integration of the corresponding CV	126
4.8	Schematic representation of extension of the electrochemically induced structural (volume) changes by reversible reaction of PANI at low and high scan rates	127
4.9	The double-logarithmic linear dependence between the charge consumed by the reaction of PANI with scan rate (a) and (b) frequency	129
4.10	(a) CVs at different electrolyte concentrations and (b) QVs obtained by integration of the corresponding CVs	130
4.11	Schematic representation of extension of the electrochemically induced structural (volume) changes by reversible reaction of PANI at low and high electrolyte concentration	132
4.12	The double-logarithmic dependence of charge consumed by the reaction of PANI with electrolyte concentration.	133

4.13	(a) CV at different temperatures and (b) Coulovoltammogram obtained by integration of the corresponding CV	136
4.14	Schematic representation of extension of the electrochemically induced structural (volume) changes by reversible reaction of PANI at low and high temperatures.	136
4.15	The logarithmic dependence of charge consumed by the reaction of PANI with the inverse of temperature (in Kelvin)	137
5.1	Structure of chitin and chitosan	142
5.2	Interaction between chitosan and PANI	143
5.3	FTIR spectra of chitosan, PANI and Cs/PANI hybrid films	144
5.4	Frequency dependent electrical conductivity of Cs/PANI hybrid films	146
5.5	The TGA of Cs and Cs/PANI hybrid films	147
5.6	Stress-strain curve of Cs/PANI hybrid films	148
5.7	FESEM images of (a) chitosan, (b) CPF1, (c) CPF2, (d) CPF3 and (e) CPF4 films	150
5.8	EDX spectra of chitosan and Cs/PANI hybrid films	151
5.9	CV plot of Cs/PANI hybrid films obtained at a scan rate of 25 mV s^{-1}	152
5.10	(a-d) CVs at different scan rates and (e-h) plots showing linear relation between the square root of	154

	scan rate with respect to anodic and cathodic peak currents of the Cs/PANI hybrid films	
5.11	(a) QVs of Cs/PANI hybrid films obtained by integration of CVs (Figure 5.9) (b) redox charges of Cs/PANI hybrid films obtained from QVs	155
5.12	Anodic (a-d) and cathodic (e-h) chronopotentiograms were obtained when different currents were applied to Cs/PANI hybrid films by passing a constant electrical charge in 1 M HCl solution	157
5.13	The linear variation of consumed electrical energy with the working current of Cs/PANI hybrid films	158
5.14	Current sensitivity of Cs/PANI hybrid films	159
5.15	Anodic (a-d) and cathodic (e-h) chronopotentiograms obtained at different electrolyte concentrations for Cs/PANI films	160
5.16	Linear variation of consumed electrical energy with the electrolyte concentration for (a) oxidation and (b) reduction process of Cs/PANI hybrid films	161
5.17	Concentration sensitivity of CPF electrodes	162
5.18	Anodic (a-d) and (e-h) cathodic chronopotentiograms obtained at different working temperatures for Cs/PANI hybrid films by passing a constant electrical charge in 1 M HCl solution	163
5.19	Linear variation of consumed electrical energy for (a) oxidation and (b) reduction process of	164

Cs/PANI hybrid films with the working temperature

5.20	Temperature sensitivity of Cs/PANI hybrid films	165
5.21	(a-d) CVs and (e-f) corresponding QVs for Cs/PANI hybrid films at different scan rates	167
5.22	(a) The double-logarithmic linear dependence between the charge consumed by the redox reaction of Cs/PANI hybrid films with scan rate and (b) sensitivity of Cs/PANI hybrid films toward scan rate	168
5.23	(a-d) CVs at different electrolyte concentrations and (e-f) corresponding QVs for Cs/PANI hybrid films	169
5.24	(a) The double-logarithmic linear dependence of consumed charge with the concentration of electrolytes and (b) concentration sensitivity of the Cs/PANI hybrid films	170
5.25	(a-d) CVs at different temperatures and (e-f) corresponding QVs for CPF1, CPF2, CPF3 and CPF4	172
5.26	(a) The logarithmic linear dependence of consumed charge during the reaction of Cs/PANI hybrid films with the inverse of temperature and (b) temperature sensitivity of Cs/PANI hybrid films	173
5.27	(a) CVs at a scan rate of 5 mV s^{-1} and (b) GCD curves at a current density of 0.4 mA cm^{-2} of Cs/PANI hybrid films	175

5.28	(a) GCD curves of CPF4 at different current densities and (b) variation of specific capacitance with current density	176
5.29	Schematic representation of structural features of Cs/PANI hybrid film enabling high electrochemical activity	177
5.30	(a) CVs at different scan rates and (b) variation of specific capacitance of CPF4 electrode with scan rate	178
5.31	Nyquist plot of Cs/PANI hybrid film electrodes	179
5.32	Cycling stability of CPF4 for 1500 cycles	181
5.33	Figure 5.33 (a) The determination of 'b' values at different potential regimes, (b) the obtained 'b' values, (c) separation of the capacitive and diffusion currents at a scan rate of 5 mV s ⁻¹ and (d) contribution ratios from non-faradaic double layer process (capacitive) and diffusion limited oxidation/reduction of CPF4 at various sweep rates.	183
6.1	Structure of PVA	190
6.2	Interaction between PVA and PANI	191
6.3	FTIR spectra of chitosan, PANI and PVA/PANI films	192
6.4	Frequency dependent conductivity of PVA/PANI films	193
6.5	TGA of PVA and PVA/PANI films	195

6.6	Photographs of PVA/PANI hybrid films in the dry state (a and b) and the wet state (c and d)	196
6.7	Stress-strain curve of PVA/PANI films in the dry state	197
6.8	Stress-strain curve of PVA/PANI films in wet condition	199
6.9	FESEM images of (a) PVA, (b) PP1, (c) PP2, (d) PP3 and (e) PP4 hybrid films	200
6.10	EDX spectra of PVA and PVA/PANI hybrid films	201
6.11	CVs of PVA/PANI hybrid films recorded at a scan rate of 25 mV s^{-1} in 1 M HCl	202
6.12	(a) CVs of PP4 at different scan rates from 1 M HCl aqueous solution at room temperature and (b) variation of peak current as a function of the square root of scan rate	204
6.13	(a) QVs of PVA/PANI hybrid films obtained by integration of CVs at the scan of 25 mV s^{-1} (b) redox charges of PVA/PANI hybrid films obtained from corresponding QVs	205
6.14	Anodic (a) and cathodic (b) chronopotentiograms were obtained when different currents were applied to PP4 hybrid film by passing a constant electrical charge of 84 mC in 1 M HCl solution	206
6.15	The linear variation of consumed electrical energy with the working current for the PP4 hybrid film	208

6.16	Anodic (a) and cathodic (b) chronopotentiograms obtained at different electrolyte concentrations for PP4 hybrid film	208
6.17	Linear variation of consumed electrical energy with the electrolyte concentration for the anodic and cathodic process of PP4 hybrid film	209
6.18	Anodic (a) and cathodic (b) chronopotentiograms obtained at different working temperatures for PP4 hybrid film by passing a constant electrical charge of ± 84 mC in 1 M HCl solution	210
6.19	Linear variation of consumed electrical energy with the working temperature for PP4 hybrid film	211
6.20	Schematic representation of experimental procedure adopted for studying influence of concentration (the number represent the order of CV cycling)	214
6.21	(a) Stationary CV obtained at different electrolyte concentrations of HCl solutions (indicated on each figure) in the potential window of -0.2 V to 0.75 V, (b) Control CV obtained in between every consecutive concentration under the same experimental condition from 0.25 M HCl solution	215
6.22	(a) QVs at different electrolyte concentrations obtained from CVs presented in Figure 6.21a (b) Control QVs obtained from CVs presented in Figure 6.21b	216
6.23	Schematic representation of extension of the electrochemically induced volume variations resulting from structural changes by reversible	218

	oxidation/reduction of the PP4 electrode at different concentration	
6.24	Double logarithmic variation of the charge consumed by the reversible oxidation/reduction of PP4 hybrid film with the HCl concentration	219
6.25	(a) Stationary CVs obtained at different working temperatures (indicated on each figure) (b) Control CVs obtained at 25 °C measured in between every consecutive temperature during increasing and decreasing temperature cycle under the same potential range and scan rate from 1 M HCl solution.	221
6.26	(a) QVs at different working temperatures obtained from CVs presented in Figure 6.25a (b) Control QVs (at 25 °C) obtained from CVs presented in Figure 6.25b	222
6.27	Schematic representation of extension of the electrochemically induced volume variations resulting from structural changes by reversible oxidation/reduction of the PP4 hybrid film electrode at different temperatures	224
6.28	Logarithmic variation of the charge consumed by the reversible oxidation/reduction of PP4 hybrid film with the working temperature	226
6.29	(a) Stationary CVs of PP4 hybrid film obtained at different scan rates in the potential window of -0.2 V to 0.75 V, and (b) Control CVs obtained in between every consecutive scan rate, under the same experimental conditions	227

6.30	(a) QVs at different scan rate obtained from CVs presented in Figure 6.29a (b) Control QVs obtained from CVs presented in Figure 6.29b	229
6.31	Schematic representation of extension of the electrochemically induced volume variations resulting from structural changes by reversible oxidation/reduction of the PP4 hybrid film at different scan rates	230
6.32	Logarithmic variation of the charge consumed by the reversible oxidation/reduction of PP4 hybrid film with the working scan rate	232
6.33	(a) CVs at a scan rate of 5 mV s^{-1} and (b) GCD curves at a current density of 0.4 mA cm^{-2} of PVA/PANI hybrid film electrodes	233
6.34	(a) GCD curves of PP4 hybrid film at different current densities and (b) variation of specific capacitance with current density	234
6.35	(a) CVs obtained for PP4 films at different scan rates and (b) variation of specific capacitance of PP4 hybrid film electrode with the CV scan rate	235
6.36	Nyquist plot of PVA/PANI hybrid films	237
6.37	Cycling stability of PP4 hybrid film for 1500 cycles	238
6.38	(a) Determination of b values at different potential regimes, (b) the obtained b values, (c) separation of the capacitive and diffusion currents at a scan rate of 5 mV s^{-1} and (d) contribution ratios from non-faradaic double layer process (capacitive) and diffusion limited	240

	oxidation/reduction of PP4 hybrid films at various scan rates from 5 mV s ⁻¹ to 100 mVs ⁻¹	
6.39	(a) CVs at different scan rates and (b) variation of specific capacitance of device with the CV scan rate	241
6.40	(a) GCD curves of the supercapacitor device at different current densities and (b) variation of specific capacitance with current density	242
6.41	Cycling stability of the device for 1500 cycles	243
6.42	EIS Nyquist plot of the super capacitor device	246
6.43	Ragone plot of the device	247
6.44	Normalized (a) anodic and (b) cathodic chronopotentiograms of the device corresponding to different working currents at the constant charge of ±38 mC	248
6.45	Linear variation of consumed electrical energy as a function of working current	249
6.46	Normalized (a) anodic and (b) cathodic chronopotentiograms of the device corresponding to different working temperatures at a constant charge of ±38 mC	250
6.47	Linear variation of consumed electrical energy as a function of working temperature	251
7.1	Possible biomimetic devices based on PVA/PANI hybrid films	263

LIST OF ABBREVIATIONS

<i>AC</i>	<i>Alternating Current</i>
<i>APS</i>	<i>Ammonium persulphate</i>
<i>ATMP</i>	<i>Aminotrimethylene phosphonic acid</i>
<i>ATR</i>	<i>Attenuated Total Reflectance</i>
<i>BDS</i>	<i>Broadband Dielectric Spectroscopy</i>
<i>CB</i>	<i>Conduction Band</i>
<i>CNFs</i>	<i>Cellulose Nanofibers</i>
<i>CNT(s)</i>	<i>Carbon Nanotube(s)</i>
<i>CP(s)</i>	<i>Conducting Polymer(s)</i>
<i>CPF</i>	<i>Chitosan/PANI hybrid film</i>
<i>CPH(s)</i>	<i>Conducting Polymer Hydrogel(s)</i>
<i>Cs</i>	<i>Chitosan</i>
<i>CSA</i>	<i>Camphor sulphonic acid</i>
<i>CuPcTs</i>	<i>copper phthalocyanine-3,4',4'', 4'''-tetra sulphonic acid tetrasodium salt</i>
<i>CV(s)</i>	<i>Cyclic Voltammogram(s)</i>
<i>DBSA</i>	<i>Dodecylbenzene sulphonic acid</i>
<i>DC</i>	<i>Direct Current</i>
<i>DSC</i>	<i>Differential Scanning Calorimetry</i>
<i>EDCLs</i>	<i>Electrical Double Layer Capacitors</i>
<i>EDX</i>	<i>Energy Dispersive X-ray Spectroscopy</i>
<i>EIS</i>	<i>Electrochemical Impedance Spectroscopy</i>
<i>EMI</i>	<i>Electromagnetic Interference</i>
<i>ER</i>	<i>Electro-rheological</i>
<i>ES</i>	<i>Emeraldine Salt</i>
<i>ESCR</i>	<i>Electrochemically Stimulated Conformational Relaxation</i>

<i>ESR</i>	<i>Equivalent Series Resistance</i>
<i>FED</i>	<i>Field Emitting Diodes</i>
<i>FESEM</i>	<i>Fourier Transform Scanning Electron Microscopy</i>
<i>FTIR</i>	<i>Fourier Transform Infra-red spectroscopy</i>
<i>GCD</i>	<i>Galvanostatic Charge-Discharge</i>
<i>GCE</i>	<i>Glassy Carbon Electrode</i>
<i>HOMO</i>	<i>Highest Occupied Molecular Orbital</i>
<i>ICP(s)</i>	<i>Intrinsic Conducting Polymer(s)</i>
<i>ITO</i>	<i>Indium tin oxide</i>
<i>LE</i>	<i>Leucoemeraldine</i>
<i>LED(s)</i>	<i>Light Emitting Diode(s)</i>
<i>LUMO</i>	<i>Lowest Unoccupied Molecular Orbital</i>
<i>NMP</i>	<i>N-methyl-2-pyrrolidone</i>
<i>NMR</i>	<i>Nuclear Magnetic Resonance</i>
<i>NLO</i>	<i>Non-Linear Optics</i>
<i>OCV</i>	<i>Open Circuit Voltage</i>
<i>PAA</i>	<i>Polyacrylic acid</i>
<i>PANI</i>	<i>Polyaniline</i>
<i>PEDOT</i>	<i>Poly(3,4-ethylenedioxythiophene)</i>
<i>PHE</i>	<i>Polymer Hydrogel Electrolyte</i>
<i>PHEA</i>	<i>Poly (N-hydroxyethyl acrylamide)</i>
<i>PIn</i>	<i>Polyindole</i>
<i>PLA</i>	<i>Polylactic acid.</i>
<i>PN</i>	<i>Pernigraniline</i>
<i>PP</i>	<i>PVA/PANI hybrid film</i>
<i>PPV</i>	<i>Polyphenylene vinylenes</i>
<i>Ppy</i>	<i>Polypyrrole</i>

<i>PTh</i>	<i>Polythiophene</i>
<i>PTSA</i>	<i>p-Toluene sulfonic acid</i>
<i>PVA</i>	<i>Polyvinyl alcohol</i>
<i>QV</i>	<i>Coulvoltammogram</i>
<i>rGO</i>	<i>Reduced Graphene Oxide</i>
<i>sulfo-PANI</i>	<i>Sulphonated PANI</i>
<i>SWCNT</i>	<i>Single-Walled Carbon Nanotube</i>
<i>TGA</i>	<i>Thermogravimetric Analysis</i>
<i>UTM</i>	<i>Universal Testing Machine</i>
<i>VB</i>	<i>Valence Band</i>

Chapter 1

Introduction

Conducting polymers (CPs), so-called Nobel prize winning materials, have garnered significant attention in the field of advanced materials research due to their tunable electrical conductivity, fascinating electrochemical properties, ease of synthesis and their ability to form composites/hybrid materials. These materials have opened up exciting avenues of research and find wide range of applications in modern science and technology. This chapter provides a general introduction to the conducting polymers. The focus is also placed on conducting polymer-based hydrogel systems, particularly polyaniline hydrogel systems. The chapter further delves into the electrochemical and biomimetic aspects of conducting polymers, providing a comprehensive understanding of their electrochemical properties and potential applications.

1.1. Conducting polymers

Until the middle of the twentieth century, research on organic polymers primarily focused on their insulating and anti-rusting properties, which offered practical advantages for various applications of plastics. However, the field of conducting polymers (CPs) emerged with the discovery of polyacetylene in 1958. The pioneering work of Alan G. McDiarmid, Hideki Shirakawa, and Alan J. Heeger in the late 1970s demonstrated that polyacetylene, previously known as an insulator, could become highly conductive when doped with iodine[1]. Their groundbreaking research on CPs led to the Nobel Prize in Chemistry in the year 2000 for the "discovery and development of conducting polymers," marking the beginning of a new era in the field of materials research. This recognition was significant, as it heralded the "dawn of the new plastic age"[2] and garnered immense interest from both industrial and academic researchers. CPs possess several advantages such as tunable electrical conductivity, fascinating electrochemical properties, low specific weight, ease of synthesis, low cost, and resistance to corrosion, etc. opening up exciting possibilities in materials science and technology.

"Intrinsically conducting polymers (ICPs) derive their electrical conductivity from their electronic structures. ICPs have alternate or conjugated double bonds along the polymer backbone. This conjugated structure is a fundamental requirement for a polymer to exhibit electrical conductivity. In ICPs, the polymer backbone consists of a π -conjugated chain, where the unpaired electrons of carbon atoms overlap and undergo delocalization over the entire polymeric chain. This extended

π -electron conjugation is responsible for the chemical or electrochemical redox processes, allowing for precise control of the electrical and optical properties of the polymers by modulating the oxidation and reduction levels. The unique redox property allows immense possibilities for designing and engineering CPs with desired electrical conductivity and optical properties, making them versatile materials for various applications in electronics, optoelectronics, and the field of electrochemical science and technology.

The electronic conduction in CPs is primarily dependent on (i) the presence of charge carriers, (ii) the overlap of molecular orbitals to aid carrier mobility, (iii) the extent of π conjugation and (iv) charge hopping between polymer chains [3]. Typically, undoped CPs are insulating in nature, and their electrical conductivity can be enhanced through doping. ICPs possess the unique ability to finely tune their electrical conductivity over a wide range by adjusting synthetic conditions. Higher dopant concentrations result in highly conductive polymers, allowing their conductivity to be adjusted to the metallic range. Consequently, heavily doped CPs are often referred to as "synthetic metals." [4]. The typical conductivity ranges are shown in Figure. 1.1.

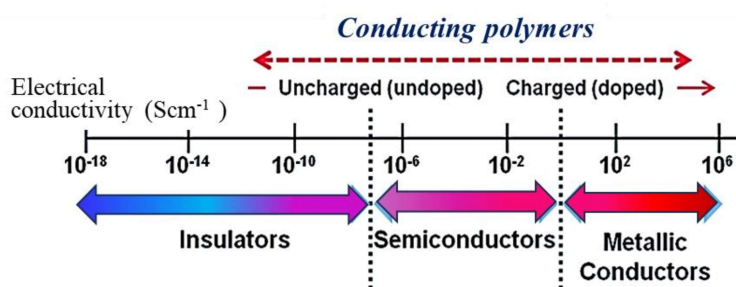


Figure 1.1 Electrical conductivity range of conducting polymers

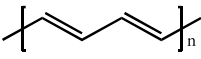
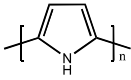
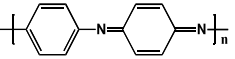
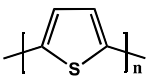
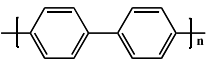
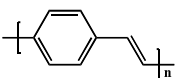
The physical and chemical properties of CPs are primarily determined during the synthesis stage. Various synthesis parameters, such as dopant type, dopant concentration, monomer concentration, synthesis time, synthesis temperature, and pH of the synthesis medium, can be adjusted to tailor the morphological, dielectric, microwave, electrical, and electrochemical properties of the CPs. Most of the ICPs are not processible due to very low solubility in common organic solvents. Therefore, extensive research has focused on improving the processability of CPs through various strategies such as the derivatization of polymer backbone with sulfonic acid groups or carboxyl groups into the main chain [5] and the use of surfactants [6]. Furthermore, CPs have poor mechanical properties when compared with conventional materials. Therefore, significant research has been carried out to improve mechanical strength through various strategies such as in-situ synthesis using conventional thermoplastics; preparation of composites/hybrid/blend with processable polymers [7]; incorporation of metallic nanoparticles [8, 9] or using polymeric/ hydrogel nanofibers and microfibers as templates [10-12].

1.1.1. Examples of conducting polymers

The simplest among the CPs is polyacetylene, with its highest reported electrical conductivity, it attracted much attention due to the simple molecular framework and was the subject of earlier conducting polymer research to understand the mechanism of conduction in CPs. Shirakawa et. al. reported conductivity up to 10^4 S cm⁻¹ for polyacetylene during chemical doping using iodine as an oxidizing agent. However, the infusibility, insolubility, and poor environmental

stability of polyacetylene were not suitable for its technological application. The technologically pertinent front runners belong to four families: Polyaniline (PANI), Polypyrroles (PPy), Polythiophenes (PTh), Polyindole (PIn) and Polyphenylene vinylenes (PPV). PPy and PTh consist of five-membered hetero-cyclic rings with nitrogen (PPy) and sulphur (PTh) respectively, as monomers, which are ideally linked at $\alpha - \alpha'$ positions (lowest energy bonding) providing free π -bond mobility. The list of some of the important CPs is given in Table 1.1.

Table 1.1 Examples of conducting polymers

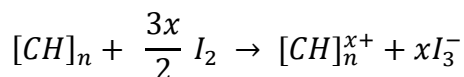
Polymer	Structure	Maximum conductivity (Scm^{-1})	Stability	Processability
Polyacetylene		1.5×10^5	React with air	The film is not soluble or fusible
Polypyrrole		2000	Reasonably stable	Insoluble and infusible
Polyaniline		10	Stable	Insoluble and infusible
Polythiophene		100	Stable	Soluble in neutral form
Polyphenylene		1000	Stable	Insoluble and infusible
Polyphenylene vinylene		1000	Stable in undoped form	Soluble precursor-route available

1.1.2. The concept of doping

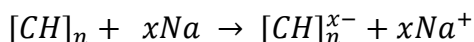
Doping is a process that transforms a π -conjugated polymer from an insulator to a semiconductor or conductor, and it differs significantly from doping in conventional inorganic semiconductors. A CPs is an insulator in its pure or undoped state, while becomes conductive after doping with a suitable oxidizing or reducing agent which increases the carrier concentration in the polymer [13, 14].

- The doping in CPs is attained through oxidation with electron acceptors (p-type doping) or reduction with electron donors (n-type), known as **redox doping**, instead of an atom replacement in inorganic semiconductors [15].

Example for p-type doping: oxidation of polyacetylene with halogen, form radical cation.



Example for n-type doping: Reduction of polyacetylene with alkali metal



- A **counter ion** is incorporated into the polymer chain during doping for charge balance. i.e., cation incorporation during p doping (electron withdrawal) and anion incorporation during n doping (electron addition). The counter ions are not present in inorganic semiconductors [13].
 - CPs can be converted back to insulators by neutralizing back to the uncharged state and the process is called **de-doping or un-doping**.
-

This kind of reversible doping is impossible in conventional inorganic semiconductors.

The de-doping of p-type (oxidatively doped) polymers can be attained through exposure to electron donors, conversely of n-type (reductively doped) polymers to electron acceptors.

- Chemical and electrochemical methods are commonly used for the doping process. Photo-doping, charge-injection doping, etc. are other methods of doping.
- Doping in polyaniline is based on acid-base chemistry- the protonation leads to an internal redox reaction which converts the semi-conducting emeraldine base into highly conducting emeraldine salt. The number of electrons associated with the polymer chain does not change in this type of doping [16].
- CPs can also be made conductive by the introduction of electrically conductive fillers into polymer matrices such as metal powders or metal oxides, carbon black graphite, graphene and carbon nanotubes.

1.1.3. The charge transport mechanism of Conducting polymers

The electrical conductivity of CPs is based on the transmission of quasi-particles such as solitons, polarons, and bipolarons (these are the charge carriers in CPs) acquired as a result of doping. Solitons carry the charge in degenerate CPs, while the polarons and bipolarons act as the charge carriers in non-degenerate CPs [17, 18].

The soliton is formed when one of the carbon atoms in the conjugated polymer chain does not share its electrons with either of its adjacent carbon atoms. In this state, one of the α -carbon atoms (adjacent

carbon atom) can change from its π bonded state with the β -carbon atom to form a π bond with the carbon atom in question, that is, a new π bond is formed and the radical moves to a third carbon atom (considering radical initially presented C atom as first C atom). Through this process, the soliton can be delocalized throughout the chain, and all the states formed by this process are in the degenerate state. Accordingly, this process can occur both naturally and spontaneously. The solitons are considered as most basic charge carriers of CPs and have a quantum spin value of $\pm\frac{1}{2}$ like a fermion, but they differ from the traditional charge carrier electrons because it is chargeless [19].

A polaron (radical ion) is another charge carrier in CPs with a quantum spin value of $\pm\frac{1}{2}$; unlike the soliton, the polarons have an electric charge of $\pm e$. When the intrinsic CP is doped with an electron acceptor, as is most common, some of the C atoms of the backbone chain get a positive formal charge, then, the polaron exists in the polymer chain as a coupling of this positive charge with the unpaired electron from a soliton. The polarons have a certain length - the distance between the coupled electron and hole (positive charge) and this length decreases as increasing of the dopant ion concentration. During charge transportation, the length of the polaron is allowed to vary, as the lone electron and hole move independently. The concentration of polarons also increases as more ions are added [19].

When the concentration of dopant increases above a certain limit, two polarons may couple to form another quasiparticle called bipolarons (dication or dianion). The bipolarons also have a certain length as polarons- the distance between two of the positively charged

atoms. Unlike solitons and polarons, bipolarons have quantum spin values of 0 or 1, like bosons, but have a charge of $\pm 2e$. The mechanism of transportation of a soliton, a polaron and a bipolaron along polymer chains is represented in Figure 1.2 [19].

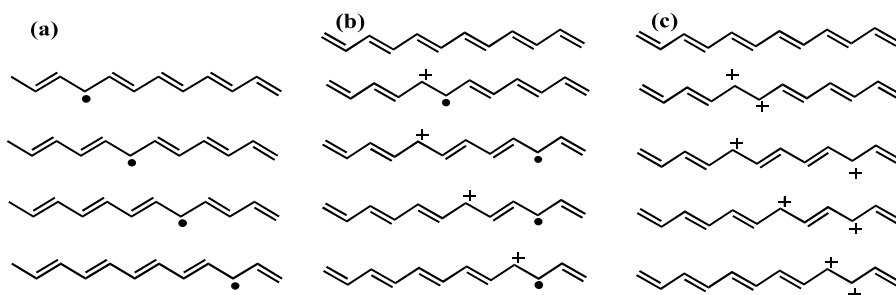


Figure 1.2 In *trans*-polyacetylene, (a) charge transportation as the soliton hops along the carbon chain, (b) and (c) the mechanism for transportation of a polaron and bipolaron respectively

The conductivity can be effectively described by band gap theory. The undoped CPs can be considered as semiconductors. That is the energy gap between the valence and the conduction band is relatively small. Certain conditions may be used to allow electrons from the highest occupied molecular orbital (HOMO) of the valance band to become excited up to the lowest unoccupied molecular orbital (LUMO) of the conduction band, with no assistance. In a polaron, the energy of HOMO increased and the energy of LUMO decreased by the value corresponding to the polaron's binding energy as depicted in Figure 1.3. That is, the energy gap decreases. In bipolaron, the energy gap further decreases by an amount corresponding to the coupling energy of two polarons as presented in Figure 1.4a and 14b. At higher doping levels, the bipolaron states overlap to form two wide bipolaron bands in the gap which is represented in Figure 1.4c [18, 19].

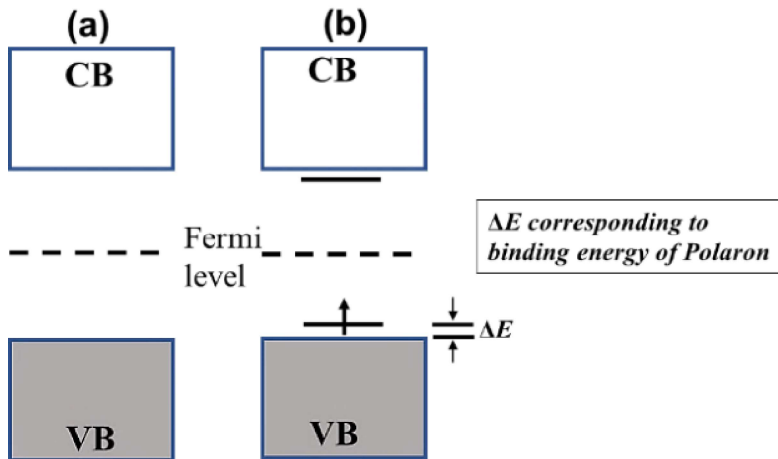


Figure 1.3 Representation of energy band gaps of conducting polymer
(a) undoped state and (b) with a polaron.

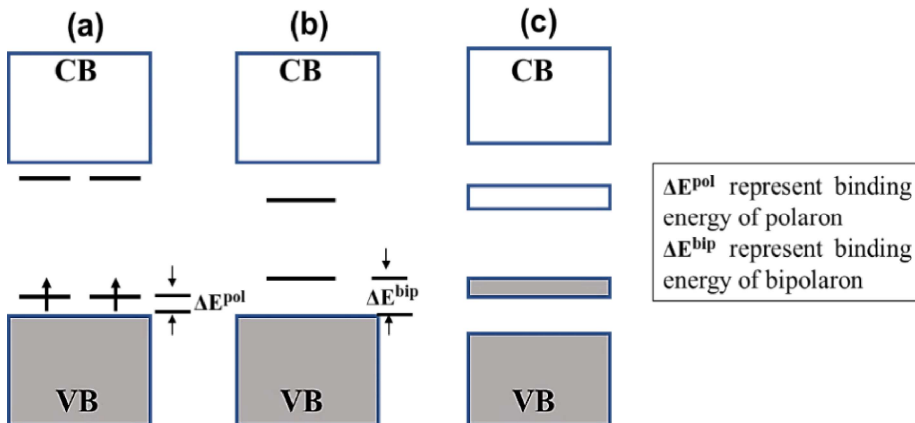


Figure 1.4 Representation of energy gap of (a) two polarons, (b) the coupling of two polarons forming bipolaron decreases the energy gap and (c) formation of bipolaron bands at high doping level.

1.1.4. Factors affecting the electrical conductivity

- *The chain structures*: the electrical conductivity of CPs increases with an increase in the length of the polymer chain, increasing

conjugation, and increasing the degree of crystallinity. The branched-chain has less crystallinity and hence has low electrical conductivity [20].

- *The nature of the dopant and degree of doping level:* In general, at room temperature, conductivity increases with an increase in the degree of doping till a saturation point is reached. The conductivity and solubility of CPs also depend on the molecular structure of the dopant [21, 22].
- *Temperature:* Like inorganic semiconductors, the electrical conductivity increases with an increase in temperature, sometimes, it becomes constant at a particular temperature [23, 24]
- *Frequency of applied current:* The conductivity of CPs increases with the frequency of applied current, as hopping is the transport mechanism in these materials [25].
- *Polymerization conditions:* The monomer concentration, concentration of dopant and oxidant, oxidant to monomer ratio, polymerization time, temperature, etc., have effects on the conductivity of synthesized polymer [26-28].

1.1.5. Applications of conducting polymers

The CPs have been used in a wide range of technological applications as depicted in Figure 1.5.

- Electronic devices: such as LEDs, solar cells, field emitting diodes (FED), Schottky diodes, etc.
 - EMI shielding and Microwave absorbing materials
-

- Rechargeable batteries and supercapacitors
- Sensors: CPs have been used in developing a variety of sensors in electronic, optoelectronic, or electromechanical devices and they can be used as biosensors.
- Electrochromic devices and Artificial muscles
- Used in various other fields such as corrosion protection materials, Electrostatic dissipation material, separation membranes, conducting textiles, desalination, electrocatalysis, tissue engineering, drug release systems, etc.

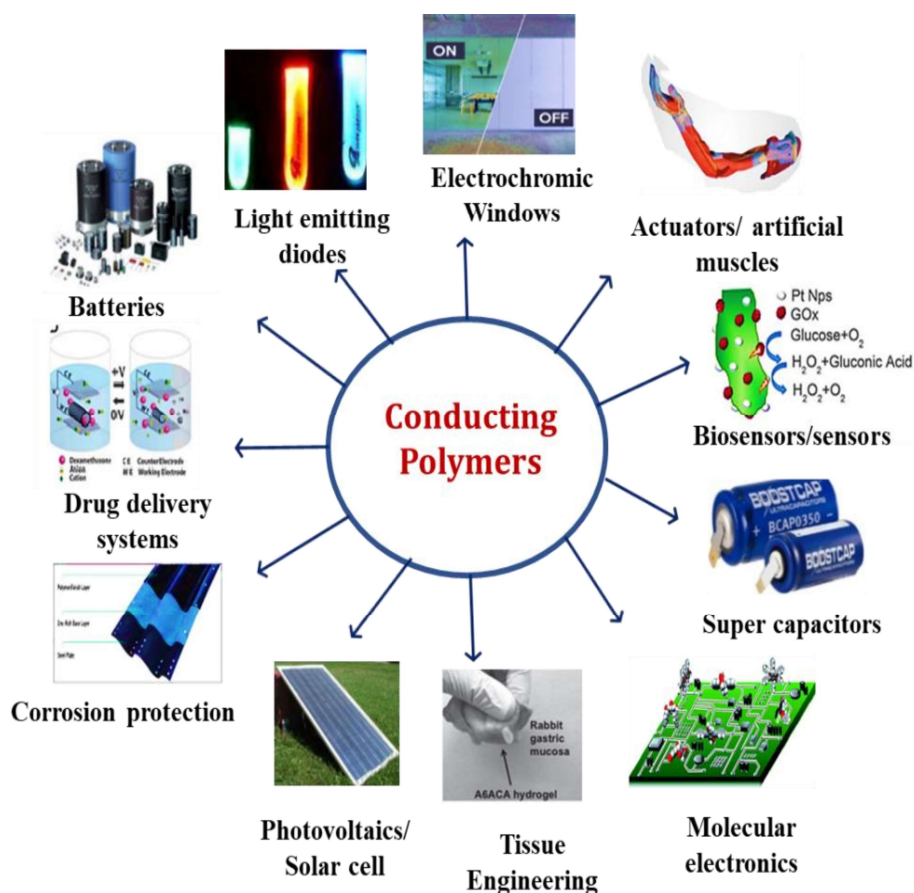


Figure 1.5 Applications of conducting polymers

1.2. Polyaniline

1.2.1. A brief history

Polyaniline (PANI), one of the oldest known synthetic organic polymers, has a rich history dating back to the 19th century. In 1835, the oxidation of aniline resulted in the formation of a dark-coloured product called "aniline black," which was used for dyeing textile fabrics. In 1862, Dr. Henry Letheby observed the formation of a blue substance during the electrolysis of aniline sulphate at a platinum electrode. This substance could be partially decolorized by reducing agents.[29]. In the early 20th century, scientists began investigating the structure of aniline black and its intermediate products. In 1907-1909, Willstatter and his colleagues proposed that aniline black was a derivative of an eight-nuclei chain compound resembling indamine. [30, 31]. However, the understanding of polyaniline's structure and constitution took further shape in 1910-1912 when Green and Woodhead described four different oxidation states of PANI: protoemeraldine, emeraldine, pernigraniline, and nigraniline [32, 33]. During this period, there was little investigation into the electrical and magnetic properties of PANI. It wasn't until 1911 that Mecoy and Moore first suggested the possibility of electrical conduction in organic polymers. In 1935, Yasui proposed a reaction scheme for the anodic oxidation of aniline at a carbon electrode. However, there were no significant advancements or reports on polyaniline until the middle of the 20th century.[34].

In 1985 MacDiarmid synthesized green powder of PANI by chemical oxidation of aniline monomer in an aqueous HCl solution using Ammonium persulphate (APS) as oxidant, which had a

conductivity as high as 10 S cm^{-1} [35, 36]. This was the first sample of a proton doped CP. Later, PANI attracted considerable attention not only from fundamental scientific interest but also from practical applications. PANI holds an important position in the field of conducting polymers due to its ease of synthesis, low cost of monomer, structural diversity, environmental stability, special proton doping mechanism and tuneable physical properties by controlling both oxidation and protonation states.

1.2.2. Molecular structure of polyaniline

PANI has a complex molecular structure due to different oxidation states and protonated states. PANI is typically a phenyl-based polymer having chemically flexible –NH groups flanked on either side by the phenylene ring of the polymer chain. Those –NH groups are responsible for protonation and deprotonation and various other physical and chemical properties of PANI.

The structure of PANI consists of an alternating arrangement of benzene rings and nitrogen atoms. The nitrogen atoms can exist in two different states: an imine (in sp^2 hybridized) state or an amine (sp^3 hybridized) state, depending on the oxidation state of the PANI. The relative composition of these nitrogen states is determined by the oxidation level of the polymer. The PANI consists of two forms, a fully oxidized form and a fully reduced form. In fully reduced form, the polymer chain is composed of benzenoid rings (Figure 1.6a) and the nitrogen atoms are in the amine state. The fully oxidized form consists of one benzenoid ring and one quinonoid ring with nitrogen in the imine

state (Figure 1.6b). In both cases, the N atom may or may not be protonated, depending on the pH of the solution. The unprotonated amine form is referred to as the base form. The general formula describing the PANI chain and the most prominent oxidation states are depicted in Figure 1.7. The fully reduced state is called leucoemeraldine, which consists only of benzenoid rings with hydrogen atoms attached to the nitrogen atoms in the base form. The fully oxidized state is called pernigraniline, where the quinonoid ring is formed, and there are no hydrogen atoms attached to the nitrogen atoms in the base form. The intermediate oxidation state, which includes both quinonoid and benzenoid rings, is known as the emeraldine state. It constitutes both quinonoid and benzenoid rings.

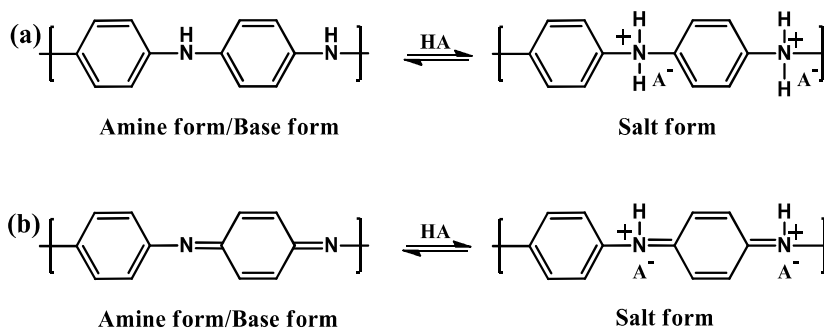


Figure 1.6 Principal unit of polyaniline: (a) reduced form and (b) oxidized form

The proportion of m and n determine the redox state of PANI (Figure 1.7), i.e., the ratio $m:n$ should be ideally 1:0 for leucoemeraldine, 0:1 pernigraniline, and 1:1 for emeraldine state. The redox state of PANI can be tuned by varying synthesis procedures, the extent of doping as well as varying the applied potential [37]. Both leucoemeraldine (light yellow) and pernigraniline (violet) are nonconducting forms, while the

doped emeraldine (emeraldine salt) is conducting a form of PANI. Therefore, it is generally practiced to keep a balance between the quinonoid and benzenoid rings in the emeraldine salt to accomplish the required electroactive performances. The Fourier transformation infrared spectra can be used for determining the proportion of Benzenoid: Quinonoid by taking the ratio of the intensities of corresponding peaks that appeared around 1460 cm^{-1} and 1560 cm^{-1} , respectively [38]. Besides, the doping process also has a very important role in tuning the electroactive behaviour.

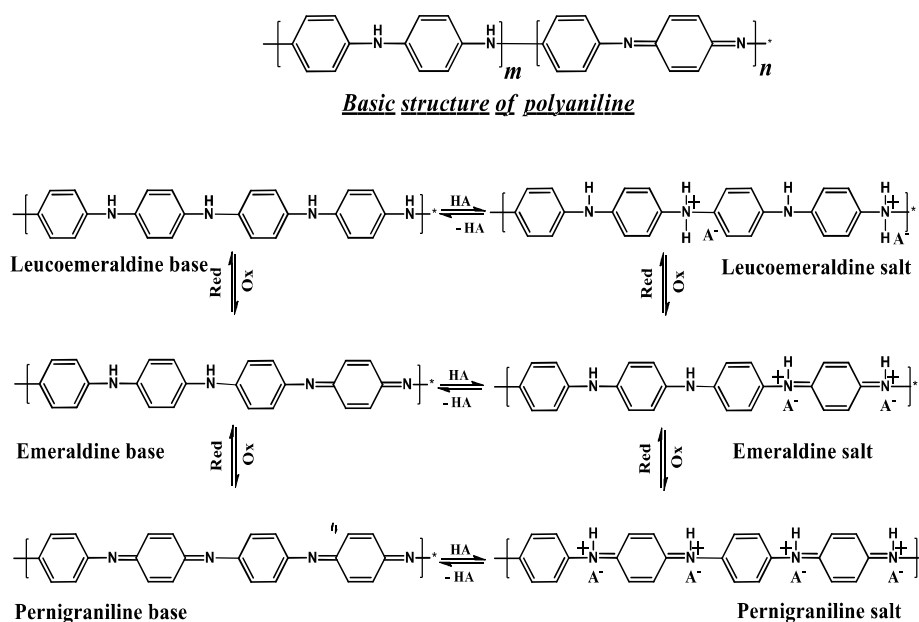


Figure 1.7 *Different forms of polyaniline*

1.2.3. Doping in polyaniline: A new concept

The redox doping of conducting polymer is briefly discussed in section 1.1.2. PANI shows a new type of doping rather than oxidation which occurs in the p-doping of all other CPs. PANI differs from other

CPs such as polyacetylene polypyrrole and polythiophene in that the electronic properties of PANI can be controlled by varying the number of electrons and the number of protons per repeat unit.

It has been found that the redox activity of PANI is pH-dependent in aqueous medium and established that the electro activity decreases considerably when $\text{pH} > 4$. Meanwhile, the electrochemical activity of PANI was also studied in an aprotic solvent, like propylene carbonate, in the presence of 1M lithium perchlorate as a supporting electrolyte. But this redox process vanished when a small amount of 2, 4, 6-trimethyl pyridine (a strong base) was added to the system. This dramatic effect of variation of pH on the conductivity (pH increased from 0 to 6 and the electrical conductivity decreased by six orders of magnitude) of PANI indicated that besides the dopants (counterions), the presence of protons invariably has a strong effect on the electrical conductivity. The studies indicate that the emeraldine base can be doped by protonic acids and the conductivity can be tuned up to the metallic regime by changing the pH of the medium without involving either oxidation or reduction of the polymer chain, thereby introducing a new concept of doping to the CPs. That is, **proton doping** means that the base form of PANI is doped with a protonic acid (HCl, HBr, H_2SO_4 , HClO_4 , H_3PO_4 , p-toluene sulfonic acid (PTSA), *d,l*-camphor sulfonic acid (CSA), dodecylbenzene sulfonic acid (DBSA), etc.) to produce a protonated PANI which is called as polyaniline salt form. Unlike redox doping, the number of electrons associated with the polymer chain does not undergo any change upon proton doping.

Initially, in 1985, it was believed that imine sites preferentially protonated during acid doping [16, 35, 39]. Later, the study show that some amine sites are also protonated before all the imine sites are protonated depending on the pH of the acid used and the oxidation state [40, 41]. The insulator-metal transition of PANI is a function of protonation and can be studied by various techniques like UV-Visible spectra, Electron Spin Resonance spectra, Fluorescence spectra as well as conductivity measurements.

In proton doping, the negatively charged ions (counter ions) from the acid solution exist in the close vicinity of the polymer main chain for electrical neutrality, which does not chemically interact or form any bond with the polymer. Depending on the type of counterion and its polarity, the electrical conductivity can be enhanced by reducing the bandgap. So, the molar ratio of aniline: oxidant as well as aniline: dopant has a strong effect on the molecular weight, microstructure, degree of crystallinity, solubility, and optical, electrical conductivity, as well as electrochemical properties of synthesized polyamine [42].

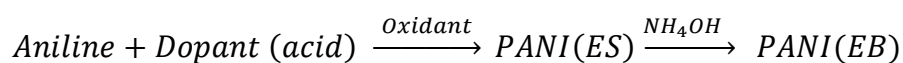
1.2.4. Synthesis of polyaniline

PANI is synthesized from the monomer aniline or its derivatives by two principal methods under acidic conditions: chemical synthesis and electrochemical synthesis. Chemical synthesis involves the direct polymerization of aniline using a chemical oxidant and electrochemical synthesis involves the anodic oxidation of aniline on an inert electrode.

(a) chemical synthesis

PANI in emeraldine salt form is generally synthesized by this method by dissolving aniline in an aqueous acid medium, like HCl, HBr,

H₂SO₄, and HClO₄, and polymerized by adding a solution of chemical oxidants like ammonium persulphate [26, 43-45]. Generally, the PANI is obtained as an insoluble residue during the oxidative polymerization of aniline, which has to be separated by filtration, washed with a copious amount of water and acetone to remove oligomers, and dried under a dynamic vacuum. The colour of the reaction medium changes to green during the reaction indicating the successful formation of PANI. The polymerization and doping occur concurrently in an acidic reaction medium. The obtained emeraldine salt can be converted into emeraldine base form by treating it with an alkali like NaOH or NH₃; the process called dedoping. The scheme of polymerization is represented as:



The chemical polymerization is conducted with the use of various oxidants, such as ammonium persulphate or potassium persulphate, ferric chloride [46], cupric chloride [47], cerium sulphate [47], potassium iodate [48], potassium dichromate [49], chloroaurate [50], benzoyl peroxide [51], sodium vanadate [52], hydrogen peroxide [53], etc.

The chemical synthesis is suitable for large-scale production at a reasonable cost. The reaction conditions affect the course of the reaction and the nature and properties of the final product. The major parameters are (1) the nature of the medium, (2) the concentration of the oxidant, (3) the duration of the reaction, (4) the temperature of the medium (5) the monomer-to-oxidant ratio and (6) the pH of the medium. Several different approaches for the chemical synthesis of PANI have

been documented in the literature, including interfacial polymerization, microemulsion polymerization, solid-state synthesis, and enzymatic synthesis.

(b) Electrochemical synthesis

Electrochemical synthesis does not require the use of any oxidant, rather the active species is generated on the electrode surface through electron transfer between the substrate molecule and the electrode by applying potential. The aniline molecule is transformed into a radical cation or anion and the reaction is diffusion-controlled, that is the radical generated reacts faster than diffuses away from the proximity of the electrode. It is a simple, fast and environmentally friendly method and useful for the fabrication of thin films having required uniformity and thickness. The electrochemical polymerization method also provides the possibility of exploring the kinetic parameters for the synthesis and doping/de-doping mechanism of PANI.

It can be performed either in two-electrode or three-electrode cells. The two-electrode cell consists of a working and counter electrode and the potential is applied between the working and the counter electrodes. Whereas, the three-electrode cell consists of working, counter, and reference electrodes. In this case, the potential is applied between the working and the reference electrodes, and the current is measured across the working and counter electrodes. Ag/AgCl and calomel electrodes are commonly used as reference electrodes. The commonly used working and counter electrode materials are graphite [54]; gold [55], platinum [56]; indium tin oxide (ITO) coated glass [57],

stainless steel [58], etc. In the electrochemical techniques, the initially formed PANI in the surface of the electrode will accelerate the further polymerization and this process is called auto acceleration or self-catalyzing [59]. Generally, the electrochemical synthesis is performed in three ways:

- (1) **potentiostatic method**: The potential between the working and reference electrodes is maintained constant (mostly, a potential in the range of 0.7-1.1 V versus reference electrode).
- (2) **Galvanostatic method**: potential varies to maintain current unchanged, (mostly, 1-10 mA during electrolysis).
- (3) **Potentiodynamic method** (cyclic voltammetry): by sweeping the potential of the working electrode within a specific range (mostly, ranging from -0.2 V to +1.0 V) with respect to the reference electrode at a certain scan rate (10, 20, 50 mV s⁻¹, etc.)

Dopant anions in the electrolyte influence the morphology, growth rate, as well as speed and extent of electrochemical deposition of PANI during its synthesis, It is commonly known as “anion effect” [60]. Several research groups reported the effect of anion on the growth rate of PANI in the order: H₂SO₄ >> HCl ~ HNO₃ >> HClO₄ [61-64].

1.2.5. Polymerization mechanism of polyaniline

Generally, chemical or electrochemical polymerization follows the radical polymerization mechanism. The mechanism of electrochemical polymerization of PANI was first described by Mohilner et al [65] and the most accepted mechanism was proposed by

Wei et al [66]. The main steps involved in the polymerization of aniline are as follows[67]:

Step 1: oxidation of monomer: Oxidation of aniline to a radical cation which is stabilized by resonance as shown in Figure 1.8. Among the resonance structures (c) is more reactive than the first due to an alternative induction effect and lack of a steric hindrance.

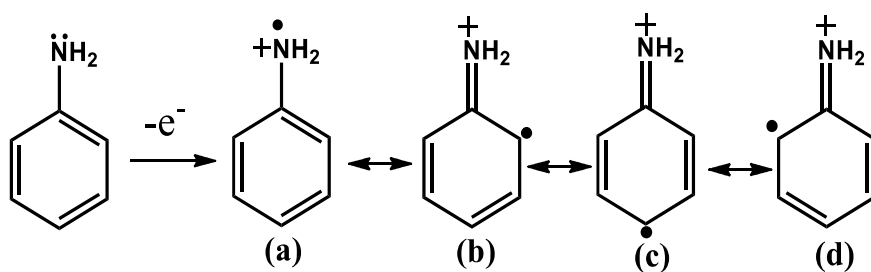


Figure 1.8 Resonance forms of aniline radical.

Step 2: Radical coupling and re-aromatization: The radical ions of aniline are coupled to form a dicationic dimer species. The coupling particularly takes place in a “head to tail” or “para-coupling” manner due to the low steric hindrance. Then the dimer undergoes re-aromatization to its neutral state, forming an intermediate p-amino diphenylamine (Figure 1.9).

Step 3: Chain propagation: via coupling of the dimer radical cation (at nitrogen atom) with an aniline radical cation (at para position) or coupling of two dimer radical cations in a head-to-tail manner.

Step 4: Oxidation and doping of polyaniline: The oxidation of the growing polymer to a radical cation and doping with acid (HX).

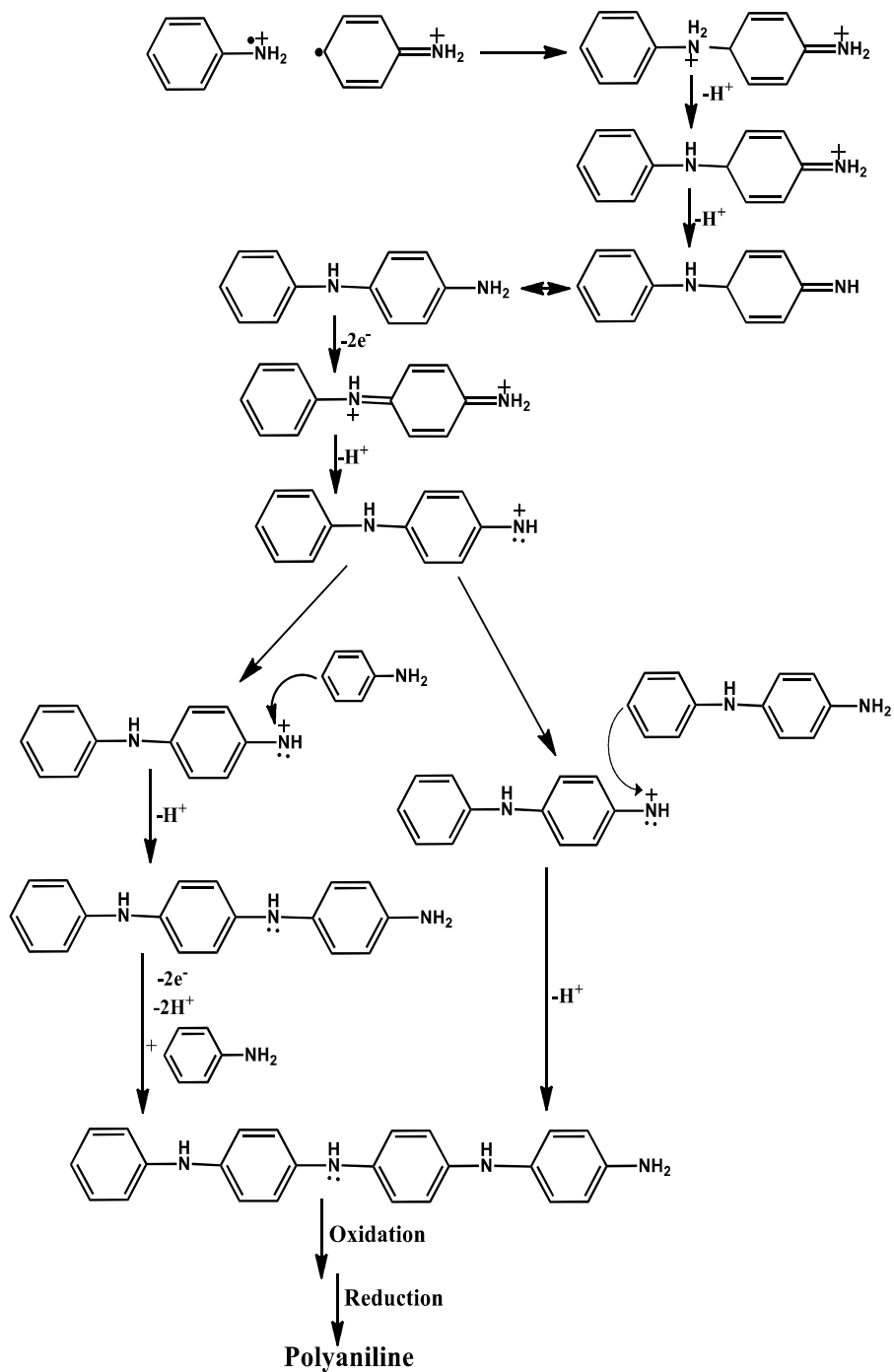


Figure 1.9 Polymerization mechanism of aniline described by Wallace et al [67] (steps 2 and 3).

1.2.6. Applications of Polyaniline

Table 1.2 *Applications of polyaniline and related properties [68].*

Special properties of polyaniline	Related applications
Electrically conductivity of PANI	Conductive adhesive, ink, paint, Antistatic textile Electrostatic discharge materials
Viscosity in solution increases under an electric field	Electro-rheological (ER) material
Electrical conductivity or color changes when exposed to acidic, basic and some neutral vapors or liquids	Gas sensor (CO ₂ , NH ₃ , NO ₂ , CO ₂ , CO, Cl ₂ , O ₃ , H ₂ O ₂ , Volatile organic compound, toxic gas sensor), Biosensor, Humidity sensor, pH sensor, Bacteria, vitamin C detector
Colour changes on change in the pH of the medium due to protonation–deprotonation	‘Acid-base’ indicator
Morphology changes due to protonation–deprotonation and oxidation-reduction processes	Membranes for gas separations Membranes for neutral solute separations pH switching actuator
Variation of oxidation states on charging and discharging, with concomitant diffusion of ions into and from the polymer	Ion-exchange material

Shows very high capacitance / very high dielectric constant	Capacitor, Super capacitor Energy storage devices
Ability to absorb and reflect electromagnetic radiation	Electromagnetic interference shielding
Response to an electromagnetic field in the optical regime	Medium for erasable optical information storage, Non-linear optics (NLO)
Can be converted from highly conducting to almost insulating	Digital memory device
Strain changes under pulsed current	Artificial muscle
Ability to accumulate and transform energy (including optical frequencies), and hence, to memorize (erase) information and unique electrochemical reaction	Electrode for rechargeable batteries, Super capacitors, Various sensors and actuators Anode for microbial fuel cell, Electrochromic displays and smart windows
Ability to change its electron donating or electron-accepting properties depending on the oxidation state	P-N heterojunctions Solar cell Diode
Emits colour under various excitations	Organic or polymer light-emitting diodes
Volume variation during the oxidation-reduction process	Actuators/artificial muscles

PANI has been used in various multidisciplinary fields due to its environmental stability, ease of synthesis, low cost, lightweight, high conductivity, thermal stability, optical properties, etc. Some applications of PANI due to its special properties are listed in Table 1.2. The existence of PANI in different oxidation states and the change of electrical conductivity upon exposure to acidic, basic and neutral vapours or liquids makes it a suitable candidate for electrochemical sensors [69]. PANI is also used for the construction of non-volatile memory devices that act as molecular switches between the two states [70]. Besides, the conducting nature of PANI can be widely used in the preparation of conductive inks, conductive paints, conductive adhesives, antistatic textiles, smart PANI fabrics etc.[71]. PANI exhibits diverse morphologies depending on the conditions under which it is synthesized. This characteristic has rendered it valuable in the fabrication of membranes for gas separation. The pH-dependent properties of PANI make it a viable material for pH-switching actuators. Moreover, the high dielectric constant, reversible oxidation/reduction process, ability to store/transform energy, high energy density and good portability make it a better material to use in rechargeable batteries and supercapacitors [72, 73]. In addition, the change of dielectric constant on interaction with radio waves and microwaves makes it a suitable candidate to shield electromagnetic interferences [74,75]. When subjected to different excitations, PANI emits light of various wavelengths which is suitable for the development of optical light-emitting devices and the fabrication of electrochromic displays [76]. The volume variation during the oxidation /reduction process is exploited for the fabrication of actuators and artificial muscles [77-79].

PANI is also employed as an anti-corrosive layer for metal protection where passivation takes place by the formation of an oxide layer on the metal surface. Apart from these applications, they find other applications such as biosensor [80], anti-static packaging and coatings [81], tissue engineering [82], catalysts [83], antioxidants [84], and in the metallization of printed circuit boards [85].

1.2.7. Limitations of polyaniline

Even though PANI has various interesting applications, they possess some inherent limitations.

- PANI is infusible and insoluble in common organic solvents which makes their processability difficult.
- PANI is brittle. Poor mechanical characteristics of PANI limit their practical application.
- The thermal stability of the emeraldine salt form of PANI is low compared to its base form. At high temperatures, the dopant ions are lost from the polymer chain inducing changes in structural and other characteristics [86]. So, at higher temperatures, there is a decrease in the mass of the material, a reduction in crystalline regions and hydrogen bonding that eventually reduces the stability of PANI.
- PANI shows electroactive only at acidic pH (up to $\text{pH} \leq 4$) and not electroactive at neutral or alkaline solutions [87] because at higher pH, the deprotonation of the nitrogen atoms in the PANI results in the loss of conductivity and thereby decreases its electroactivity.

This restricts its utility in biological applications which require a physiological working pH range.

- PANI shows relatively less rate capability and poor cycling stability when it is used in energy storage devices. Continuous inclusion/expulsion of the counter ions during the continuous charging/discharging process results in the swelling and shrinkage of the polymer leading to mechanical degradation [88]. It limits their technological applications.
- PANI is semi-crystalline in nature. The crystallinity depends upon the level of doping and the type of dopants. That is, the crystallinity increases with an increase in the doping level and the use of organic acid dopants increases the crystalline regions of PANI. The crystallinity of PANI has a direct dependence on its electrical conductivity, solubility and processability [89].

Thus, these limitations of PANI restrict their technological applications. Therefore, various research groups have been conducting systematic studies to overcome the various limitations of PANI to make them more effective for advanced and high-end technological applications. In the present study, we addressed this issue.

1.2.8. Strategies adopted to overcome the limitations of polyaniline

The literature shows that several strategies are adopted by the researchers to overcome the limitations of PANI, which are listed as follows:

- The difficulties associated with processability, and crystallinity are significantly overcome by using functionalized sulphonic

acids such as p-toluene sulphonic acid (PTSA) and dodecyl benzene sulphonic acid as dopants [90, 91], polyanions as templates [92], derivatization of the polymer backbone (functional groups enhances the interaction between the polymer dopant and the solvent, hence improving its solubility in organic solvents) [93] and use of colloidal PANI dispersions [94]. Among these, the bulky anion increases the inter-chain separation of the coiled polymer chains and sets in structural regularity thereby enhancing the crystallinity and in turn processability and conductivity of PANI.

- The loss of electroactivity at neutral pH which limits the application of PANI is overcome by adopting various strategies such as (i) synthesizing “self-doped polyaniline” [95] (ii) doping with negatively charged polyelectrolytes such as poly(vinyl sulphonate) [96] (iii) incorporating acid capped gold nanoparticles into the PANI polymer matrix forming PANI-Au nanocomposites, wherein the insertion of ionogenic groups into the polyaniline matrix change the microenvironment of the nitrogen atoms thereby shifting the local pH [97, 98].
- The limitation of low cyclic stability and rate capability of PANI is significantly overcome by combining it with suitable materials: carbon materials such as activated carbon, CNTs, graphene, etc. [99]. These materials provide high surface area and increase the conductivity of the combined material, thus increasing the pseudo-capacitance of the polymer. Besides, the presence of suitable

functional groups in carbon materials can enhance the interaction with PANI which enhances the stability.

- The mechanical properties and processibility of PANI are significantly improved by making composites/hybrid/blend with processable polymers like hydrogels [100-104]
- The use of surfactants can also improve the solubility and processibility of PANI [105].

Thus, among the different approaches adopted towards improving the properties of PANI, the synthesis and fabrication of composites/hybrid/blend with hydrogels are one of the most effective methods to improve the mechanical strength which is essential for device development. Therefore, the primary objective of the present investigation is to fabricate PANI/hydrogel systems for device applications. Furthermore, the attributes of hydrogels, such as their biocompatibility, responsive behaviour to stimuli, mechanical resilience, porous structure, and cost-effectiveness, confer upon them a range of significant advantages suitable for diverse applications.

1.3. Introduction to hydrogel

Hydrogels are soft hydrophilic, cross-linked three-dimensional (3D) polymeric materials that are insoluble and able to absorb water or other anatomical fluids up to a thousand times their initial weight [106]. Owing to their capability to imbibe higher water content, porosity and soft nature, they resemble more closely biological tissues than any other class of synthetic biomaterials. Natural hydrogels are gradually replaced by synthetic types due to their higher water absorption capacity, long

cycle life, and due to the availability of varieties of raw chemical resources for their synthesis. In recent years, hydrogels have received much attention in the research community as intelligent polymer materials, because they are able to alter their volume or other properties in response to external stimuli, such as pH, temperature and electric field, among others [107, 109].

The cross-linking between polymeric chains along with an increase in the ionic, covalent and hydrogen bonding interactions decreases their solubility in water [110] and thereby helps to retain a strong network structure even after squeezing most of its absorbed water. The cross-linking present in hydrogel also enhances the mechanical strength [111]. The swelling behaviour of hydrogels mainly depends on the degree of cross-linking, the chemical composition of the hydrogel polymer, and the interaction between the network and surrounding liquids [112]. The higher water retention of hydrogels is due to the presence of hydrophilic functional groups, like carboxylic acids, amides, and alcohols, in the polymer backbone and their resistance to dissolution is attributed to cross-links between the network chains [113].

Natural hydrogels are those gels that are derived from a natural source such as chitosan, gelatin and collagen, and synthetic hydrogels are those gels that are derived from synthetic polymers such as polyvinyl alcohol, polyamides and polyethylene glycol [114]. Over the last two decades, natural hydrogels have been slowly replaced by synthetic ones or hybridized with synthetic hydrogels, to achieve higher service life,

gel strength and water absorption capacity [115]. Two hydrogels are used in this thesis work: a natural hydrogel- chitosan and a synthetic hydrogel- polyvinyl alcohol.

1.4. Conducting polymer/ hydrogel systems

Conducting polymeric hydrogels is considered as a special type of soft material in the intelligent material category. Conducting polymer/hydrogels (CPHs) gels consist of organic conducting polymer (CPs) in the porous polymer network of hydrogel having the combined properties of hydrogel and conductive system. In 1994, Gilmore et al. reported the first CP/hydrogel system which is the hybrid composite of PPy and polyacrylamide, in which PPy is directly electropolymerized on a preformed hydrogel and these gels were shown to be electroactive and conductive. [116]. This study opened a new era in conducting polymer science.

CPHs show various advantages of both hydrogels and organic conducting polymers. The hydrogel component imparts swellability, a high degree of hydration, in vitro and in vivo biocompatibility and the high diffusivity of small molecules, while conducting polymer offers high electrical conductivity, ON–OFF electrical and optical switching and electrochemical redox properties. Besides, both are stimuli-responsive materials and viable candidates for sensory and actuation applications. CPHs can undergo physical/chemical changes in response to changes in environmental stimuli such as electric field, temperature, pH, ionic strength, salt type, solvent, external stress, light, or a combination of these. CPHs offer an excellent interface between (i) the

electronic transport (electrode) and the ionic-transport(electrolyte) phases, (ii) natural and synthetic biological systems and (iii) soft and hard materials. As a result, conducting polymer hydrogels are promising for a broad range of applications, ranging from energy storage devices, such as biofuel cells and supercapacitors, to molecular and bioelectronics and various sensors. They have been offered excellent processability and can be simply cast into thin films, wires and any other required shapes at its gelation stage and also can be easily ink-jet printed or screen printed into micropatterns.

1.4.1. Fabrication of CPHs

There are several successful methods reported for the fabrication of CP/hydrogel systems. The preparation procedure and synthetic conditions have a strong effect on the properties of the hydrogel system and this poses the main challenge in the production of a homogeneous hybrid system with reproducible properties by incorporating conducting polymer into the hydrogel system. The important methods of synthesis are discussed below.

(a) in situ polymerization of a CP monomer in a prefabricated hydrogel:

It is the simple and most common method of preparation of a conducting polymer hydrogel. Here, the fabricated dried hydrogel is allowed to swell in the monomer solution until attaining equilibrium, subsequently, this monomer absorbed hydrogel is immersed in the solution of oxidant resulting in the formation of conducting polymer penetrated hydrogel (Figure1.10a). The electrochemical polymerization

technique can be employed instead of chemical oxidation in which a hydrogel coated electrode is used as an anode (figure 1.10b) [117-119]. The interfacial polymerization method is also used for the synthesis of CPHs. In this method, the monomer and the oxidant are in two immiscible liquid phases. Here, the hydrogel is allowed to swell in an aqueous oxidant solution until attaining equilibrium, then this hydrogel is subjected to a monomer solution in an organic solvent and the polymerization will take place at the interface of two liquids which is directly diffused into a hydrogel matrix (Figure 1.10c) [120, 121].

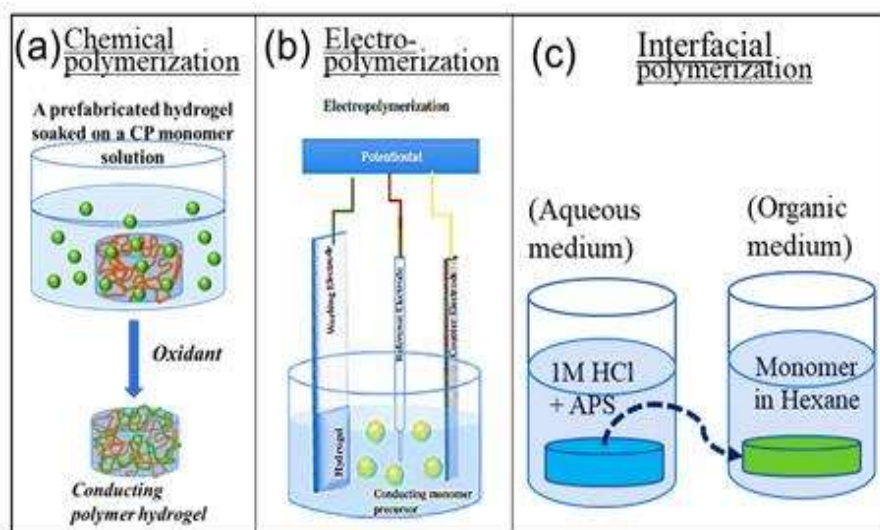


Figure 1.10 Schematic showing the formation of PANI/Hydrogel via in-situ chemical polymerization of aniline within the hydrogel matrix; (a) chemical polymerization, (b) electrochemical polymerization [117] and (c) interfacial polymerization

(b) Polymerization of conducting polymer in the matrix polymer solution/dispersion

It is a special type of one-pot synthesis of CPHs involving the chemical oxidative polymerization of conducting polymer in the solution of a suitable supporting hydrogel (Figure 1.11). It is well known that the polymerizations of aniline or pyrrole in the presence of water-soluble polymers such as polyvinyl alcohol, and polyethylene glycol, often in the presence of steric stabilizers, usually yield colloidal dispersions of the conducting polymer hydrogel composite. It can be precipitated in a suitable solvent like ethanol, methanol, acetone and ethanol/ether mixture, or can be cast into a required geometry like films or fibers [122, 123]. In these hydrogels, the formation of cross-linked network structures is mainly controlled by hydrogen bonding and chain entanglements instead of covalent or ionic bonds. Alternately, the freezing-thawing method is used along with in situ polymerization of aniline in the acidic aqueous solution of PVA to enhance the mechanical strength [124].

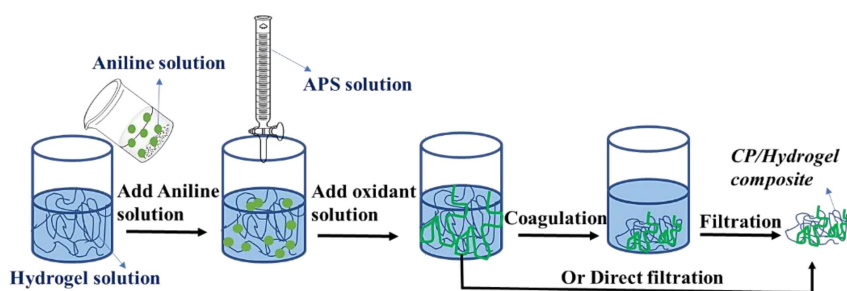


Figure 1.11 Schematic representation of polymerization of aniline in the hydrogel solution/dispersion

(c) The blending of conducting polymer with hydrogel:

The CPHs can be fabricated by blending the conducting polymer with hydrogel in a solution or in a melt state. The method consists of mixing the solution/dispersion of conducting polymer with the solution

of hydrogel with constant stirring to disperse conducting polymer uniformly throughout the matrix hydrogel polymer along with a crosslinker if needed [125]. Polyaniline/Chitosan blend could be easily prepared via mixing of the emeraldine base form of PANI in N-methyl-2-pyrrolidone (NMP) and 2 wt.% solutions of Chitosan in 2 % acetic acid with vigorous stirring and glutaraldehyde may use as the crosslinking agent. Since conducting polymers show poor solubility in common solvents, limits their versatility. In addition, in some cases, CP and hydrofoil are soluble in different solvents, polymers are known to be generally incompatible, and there is a possibility that solutions containing two different polymers may tend to separate into coexisting phases [126].

(d) Conducting polymer-hydrogels formed from mixed precursors:

This method is used for those hydrogels which can be easily prepared by polymerization of their monomer. Here, mixing the conducting polymer and hydrogel precursors are in the same vessel followed by chemical polymerization either simultaneously or in a two-step process to produce CPHs (Figure 1.12) [127].

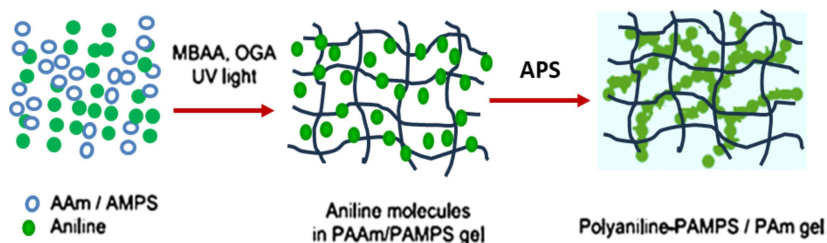


Figure 1.12 Schematic representation of polyaniline/hydrogel from Mixed Precursors

(e) Cross-Linking conducting polymer with Dopant Molecule

The above-described methods of fabrication of conductive polymer hydrogels usually result in a gel system that comprises of conductive component (conducting polymer) within the nonconductive components (hydrogel), thus, deteriorating the conductivity of the formed material as compared to pure conducting polymer. Apart from these methods, it is found that molecules with multiple acid functional groups, such as phytic acid, copper phthalocyanine-3,4',4'', 4'''-tetra sulphonic acid tetrasodium salt (CuPcTs), and amino trimethylene phosphonic acid (ATMP) can cross-link the polymer chains of conducting polymer, which can also act as a dopant and results in 3D networked structures to form CP gels with free of insulating components (Figure 1.13). CP gels show good electronic and electrochemical properties [128-132]. Generally, a two-component mixing strategy is employed for the synthesis of CP gels: a solution containing the oxidative initiator was mixed with a solution containing the monomer (aniline or pyrrole) and crosslinker dopant. The resulting solution gelled to form a hydrogel within a few minutes.

The mechanism is that each of these crosslinking molecules having multiple acid functional groups can react with more than one conductive polymer chain by protonating the nitrogen groups and through electrostatic interactions, thus acting as cross-linkers and dopant molecules. The formed heavily doped CP hydrogel frameworks provide well 3-D interconnected path for electron transport and a hierarchically porous structure for ion diffusion making them good electrical and ionic

conductors. The properties of the material can be tuned by changing the cross-linker, monomer to cross-linker ratio, oxidant, solvent, temperature, etc.

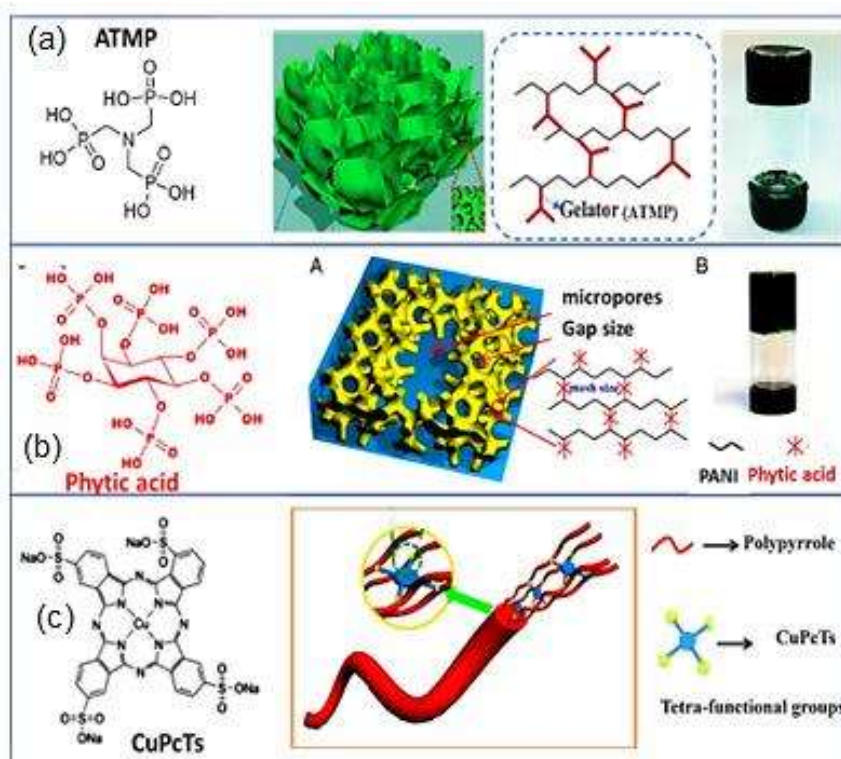


Figure 1.13 Schematic illustrations CP gels formed by crosslinking with dopant molecules; **(a)** ATMP doped polyaniline gel [128], **(b)** phytic acid doped polyaniline gel [129], and **(c)** CuPcTs doped PPy hydrogel [131]

1.4.2 Characterization techniques to study the properties of CPHs

CPHs have some prominent and distinct characteristics such as softness, plasticity, better mechanical strength than conducting polymers, high water absorption, porosity, high surface area specificity, electrical conductivity, and electrochemical activity. The structural

determination and characterization of the cross-linked network formation are essential for the fabrication of CPHs with desired properties. Physical, spectroscopic, thermal, morphological, mechanical electrical and electrochemical approaches are commonly used to gain insight into the complex structural intricacies and characteristics of hydrogels Figure 1.14. Electrical conductivity and electroactivity are an important characteristic of CPHs. The electrical conductivity measurement by broadband dielectric spectroscopic (BDS) measurement gives an idea about the dielectric characteristics as well as the charge transport characteristics of the material. The CPHs are electroactive due to the presence of conducting polymers. Various galvanostatic, potentiostatic as well as Potentiodynamic method including cyclic voltammetry (CV), galvanostatic charging-discharging (GCD), chronoamperometry, chronopotentiometry, electrochemical impedance measurement helps to evaluate the electrochemical behaviour and performance of CPHs.

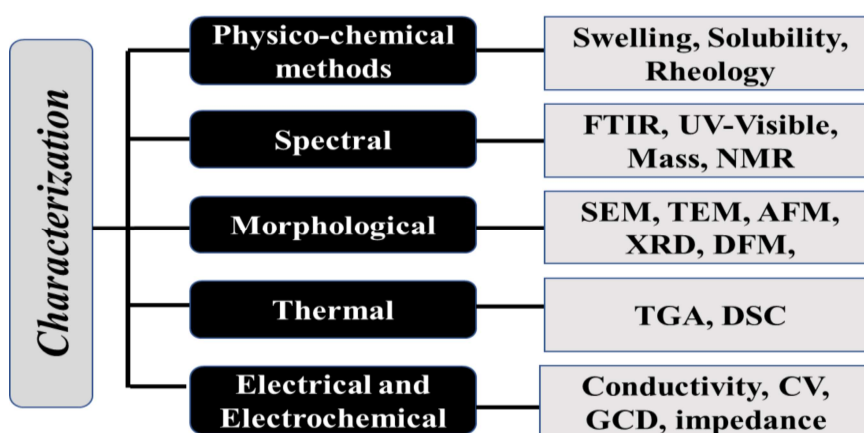


Figure 1.14 *The characterization techniques of CPHs*

1.4.3. Applications of CPHs

According to a web of science research, over the last 22 years, the biological applications of polyaniline-based hydrogels have been reported in 45 % of publications dealing with biomaterials science. The electrochemical properties of polyaniline-hydrogels were mentioned in about 33 % of the articles [133].

Biomedical applications: Conducting hydrogels have the ability to bind with bioactive molecules, nano templated to mimic extracellular matrix making them ideal for biomedical applications like controlled drug delivery, implantable biosensors, antimicrobial wound dressing, and a deep brain stimulator [134,135].

Actuator/artificial muscle application: the volume variation under external stimuli such as pH, electrical potential, etc., used for the development of actuators or artificial muscles [136,137].

Energy applications: CPHs are composite materials that combine the properties of both soft and hard materials, making them highly versatile for energy applications in various fields. One of the key advantages of CPHs is their excellent processability and biocompatibility. They can be easily cast into thin films or fibers, and their gelation state allows for shaping into desired forms. Additionally, CPHs can be printed using techniques such as inkjet or screen printing, enabling the creation of intricate micropatterns. The porous nature of CPHs promotes efficient charge transport, resulting in improved energy storage performance. CPHs have been successfully employed as flexible electrodes in supercapacitors, lithium-ion batteries, and solar cells [138].

1.5. Supercapacitors: A brief introduction

The increasing demand for lightweight and portable electronics is urging researchers to look for new energy storage devices with high energy density and power density. Flexible supercapacitors are considered an ideal power source for such devices, including wearable electronics. Extensive research has been focused on developing environmentally friendly energy storage devices with high power density and high energy density. Supercapacitors, also known as ultracapacitors or electrochemical capacitors, are a major class of energy storage devices that aim to bridge the gap between capacitors and batteries, offering intermediate energy and power densities [139, 140]. Supercapacitors can be classified into three types: electrical double layer capacitors, pseudocapacitors, and hybrid supercapacitors depending on their charge storage mechanisms.

1.5.1. Electrical double layer capacitors

Electrical double layer capacitors (EDLCs) store electric charge electrostatically through reversible adsorption of electrolyte ions onto electrode materials having high electrochemical stability and high surface area. The charge is accumulated on the surface of the electrode when a potential gradient is formed across the electrolytic medium as a result of an applied voltage. The developed potential gradient causes the positive and negative ions in the electrolyte to diffuse towards oppositely charged electrodes. At the same time, the solvent molecules also get polarized and attached to the electrode surface preventing the

oppositely charged ions from combining with the surface of the electrode. The charged electrode surface and a layer of adsorbed ions separated by solvent molecules together are known as the Helmholtz double layer [126]. The charge storage capacity of EDLCs increases with increasing the effective surface area of the electrode which is directly related to the porosity of the material used as electrode. Largeot and co-workers proposed that the capacitance of EDLC depends on both total porous volume and pore size distribution [141]. Generally, EDLCs have a very long lifetime and can undergo a very large number of charging-discharging cycles since there is no chemical reaction in electrodes. EDLCs have a sufficiently large power density due to their rapid charge-discharge ability but suffer from low energy density due to the limited accumulation of charges at the electrical double layer which is the major challenge experienced by EDLCs [141].

1.5.2. Pseudocapacitors

In pseudocapacitors, the charge storage mechanism is not only pure electrostatic as in the case of EDLCs but also involves a faradaic redox charge transfer process that occurs between electrode and electrolyte. It improves the capacitance as well as the energy density of supercapacitors. In pseudocapacitors, some specific ions of the electrolyte diffuse into the double layer and transfer their charge with the electrodes through highly reversible redox reactions, intercalation, and electrosorption processes. Pseudocapacitance from this charge transfer always occurs together with electrostatic double-layer capacitance. The magnitude of double layer contribution is remarkably

small in comparison with pseudocapacitance because the charge storage in pseudocapacitor occurs by redox reaction utilizing every part of the bulk of the electrode material in addition to the surface as in the case of EDLCs. Hence, pseudocapacitors can store a larger amount of charge thereby providing relatively larger specific energy than the EDLCs [142, 143].

1.5.3. Hybrid supercapacitors

A hybrid supercapacitor is a combination of both EDLC and pseudocapacitor. It consists of two asymmetric electrodes, one of the electrodes has high pseudocapacitance while the other has high electrostatics double-layer capacitance. The pseudocapacitive electrode offers high specific capacitance, large working voltage, and greater specific energy to the supercapacitor while the double-layer capacitive electrode provides good cyclic stability and high specific power. As a result, a hybrid supercapacitor attained improved electrochemical performance. Hybrid supercapacitors can also be developed by making /hybrid/blend/composites of pseudocapacitive materials with double-layer capacitive materials [144].

1.5.4. Conducting polymers for supercapacitors

CPs are pseudocapacitive materials whose Faradaic reversible oxidation/reduction reactions are responsible for charge storage property. They were first utilized in supercapacitors in the middle of the 1990s [145]. CPs are one of the prominent candidates among

pseudocapacitive materials due to their high charge density and low cost compared to the relatively more expensive metal oxides and hence can be used to develop devices with low equivalent series resistance (ESR), high power density, and high energy density. CPs are known to have relatively fast charge-discharge kinetics, easily tuneable morphology, and fast doping and dedoping processes [146]. The plastic properties of CPs allow easy manufacturing, particularly as thin films and can be used for the fabrication of flexible energy storage devices [147].

PANI has a very high theoretical specific capacitance value of approximately 2000 F g^{-1} [148] and can produce a high charge density of 140 mAh g^{-1} . When compared to metal oxide such as LiCoO_2 , it has lower charge density [149, 150] but has higher energy density when compared with carbon-based supercapacitors which often deliver less than 25 mAh g^{-1} [151]. Double-layer capacitors have high cycling stability, they can be cycled more than 0.5 million cycles [152] whereas CPs based pseudo-capacitors often begin to degrade even below a thousand cycles due to changes in their physical structure that are originated by the repeated insertion/expulsion of ions. The specific energy of CP electrodes can be improved by increasing the doping level. At the same time, in the cases where the larger degree of counter ion insertion and de-insertion with an accompanying volume change will cause the mechanical failure of the electrode under prolonged cycling [140]. The literature shows that, especially in actuators, the use of ionic liquid electrolytes improves the performance of CPs with greater life time [150, 154]. The major drawbacks of CP-based supercapacitors are poor mechanical characteristics and low cycle life. Therefore,

researchers are much more focused on improving these aspects by forming composites/hybrids between the CPs and other materials such as carbon based materials (including CNT and graphenes) [155-158], inorganic oxides and hydroxides [159-161], and other mechanically robust polymers [162-165].

1.6. Electrochemistry of CPs: an overview

1.6.1. CPs are reactive redox materials

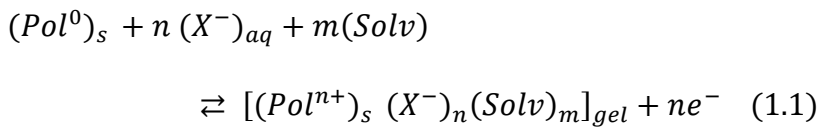
At the end of the 1970s, Professors MacDiarmid, Heeger, and Shirakawa made a significant discovery that CPs can undergo reversible oxidation and reduction processes, either through chemical or electrochemical means. This leads to the exchange of ions with the surrounding environment, known as doping and de-doping, resulting in a parallel variation of their electronic conductivity by several orders of magnitude, along with changes in the composition of CPs [1, 165]. The importance of these materials lies in their ability to be oxidized or reduced from their neutral state, allowing for the entry and exit of ions and solvents when an electric current is applied in the presence of suitable electrolytes. This reversible reaction induces changes in the benzenoid and quinoid structures of CPs, leading to conformational movements in the polymeric chains. Generally, CPs follow three basic electrochemical reactions:

(a) Oxidation (p-doping)

It is one of the predominant forms of doping in CPs. Many CPs have ionization potentials that allow them to be oxidized within the

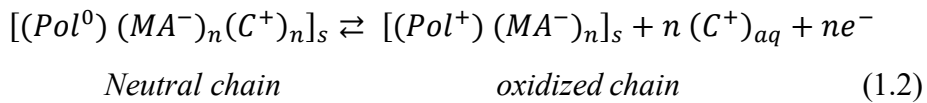
potential range of various electrolytes. When a CP chain is subjected to an anodic potential, it loses electrons, resulting in the generation of positive charges. These positive charges are balanced by the exchange of ions with the electrolyte, maintaining charge neutrality.[165, 166]. The transformation from a neutral polymer to an oxidized polymer usually occurs in two different ways:

Prevailing anion exchange: It is usually present in the case where the CPs have smaller counter ions. When oxidation occurs, positive charges are generated along the polymer chain, leading to conformational movements in the polymeric chains. These movements create free volume within the CPs. Additionally, anions from the electrolyte and solvent molecules penetrate the CPs to balance the positive charges and maintain osmotic balance, respectively. As a result, CPs undergo swelling during oxidation. Conversely, during neutralization or reduction processes, the CPs experience a decrease in volume. It is represented by the reaction (1.1):



where, *Pol* represents CP chains, X^- represents the anions exchanged for charge balance, *Solv* for solvent molecules and the different sub-indexes mean: *s*, solid and *aq*, aqueous solution. The material swells during oxidation by insertion of and shrinks during reduction with the expulsion of anions [167]. It is schematically represented in Figure 1.15a.

Prevailing cation exchange: If CPs are formed in the presence of larger macro anions, these anions become trapped within the polymer matrix regardless of the oxidation state of the CPs. In such cases, when the polymer is oxidized, cations are expelled to maintain charge neutrality, as shown in Equation 1.2. As a result, the material undergoes shrinkage during oxidation, while it swells during reduction. [167]. It is schematically represented in Figure 1.15b.



where MA^- stands for macroscopic anion trapped inside the CP during synthesis and C^+ represents the balancing cation present in CP.

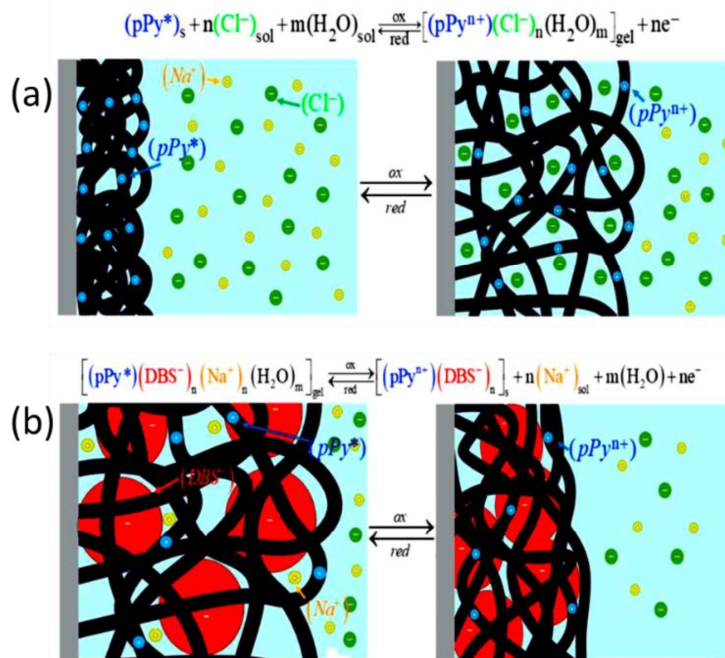
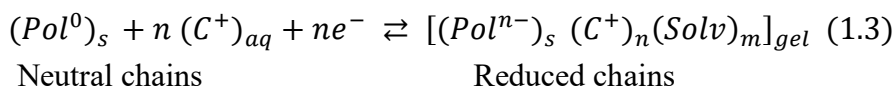


Figure 1.15 Schematic representation of (a) Exchange of anions and (b) exchange of cations during electrochemical reactions [166]

(b) Reduction (n-doping)

Certain CPs such as PEDOT, polythiophene, and polyfluorenes possess a high electronic affinity, which means they have the ability to undergo transitions from a neutral state to a reduced state [168-170]. This property enables them to effectively store negative charges by injecting electrons onto the polymer chains, particularly at high cathodic potentials. During the reduction process, these polymers experience a volumetric expansion or swelling as they uptake the additional electrons and undergo structural changes. Conversely, during the neutralization process, where the stored charges are neutralized or removed, the polymer chains undergo a contraction or shrinking. It is shown in reaction 1.3 [171].


1.6.2. CPs as multistep molecular motors

During a reversible electrochemical reaction in CPs, the insertion of ions and solvent molecules occurs only if there is enough free volume available to accommodate the balancing counterions and solvent. This means that the reaction must induce structural changes, particularly changes in volume, in the CPs. If the generated intra-chain free volume is insufficient and smaller than the volume of a counterion unit (intrachain distance is less than the solvated counterion's diameter), the reaction will be hindered due to structural constraints. In such cases, the ions and solvent molecules cannot be effectively inserted into the polymer structure [172].

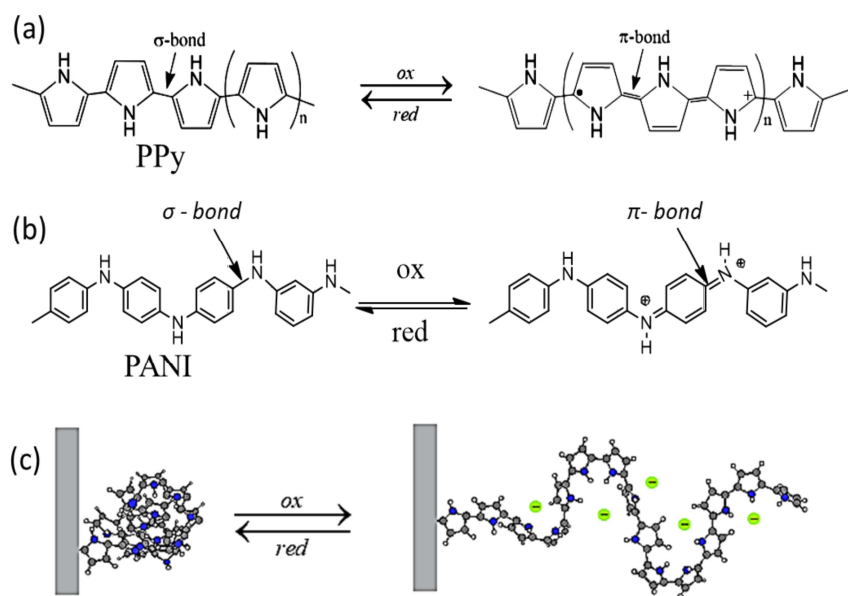


Figure 1.16 Formation/destruction of π bonds by oxidation/reduction of (a) polypyrrole and (b) polyaniline. (c) Schematic representation of reversible conformational movements reversible oxidation/reduction of CPs: an electrochemical molecular machine [173]

During the reverse oxidation/reduction process, there is a redistribution of sigma and pi bonds along the polymeric chain. Figure 1.16a and 1.16b show the change of a sigma bond to a pi bond during oxidation when bipolarons are formed. This bond redistribution induces conformational movements in the polymeric chain, where sigma bonds allow for free rotation while pi bonds hinder bond rotation. As a result, the polymer chains uncoil during oxidation (Figure 1.16c). These reaction-driven structural changes can be reversed by injecting an electron, i.e., reduction, into the polymer. Therefore, CPs are considered electrochemical molecular motors or machines. The redox reactions of CPs are highly complex. The extraction of 'n' electrons occurs through 'n' consecutive steps, with each step involving one electron transfer

following the first, second, and nth ionization potentials of the chain. Hence, CPs are regarded as multistep electrochemical molecular motors.[173].

1.6.3. Reaction driven biomimetic properties of CPs

In the wet state, CPs are reactive gels. Its composition, such as electric potential, polymer molecules, ions, and water, and properties mimic the intracellular matrix of living cells, making them ideal model materials for biological function [174]. During electrochemical reactions, CPs undergo reversible changes in properties such as volume, colour, and stored charge and these reversible properties of CPs have been harnessed for the development of various biomimetic devices [175, 176]. Figure 1.17 shows the properties of CPs that are changing during the redox reaction and the biomimetic devices that have been developed based on these property changes.

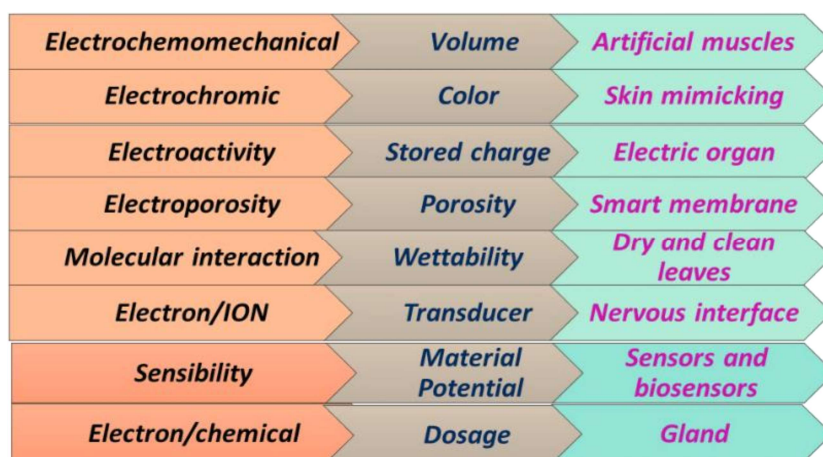


Figure 1.17 Biomimetic properties of CPs driven by the electrochemical reaction, the mimicked biological functions and the related organs

The cooperative actuation of molecular machines within CPs enables the generation or destruction of free volume required for the accommodation or expulsion of balancing counterions and solvents during electrochemical reactions. This transformation of electrical energy into mechanical energy replicates the cooperative actuation of conformational movements in myosin heads, which are responsible for muscular contraction and result in structural macroscopic changes [177, 178]. By harnessing the cooperative actuation of artificial multi-step molecular motors within CPs, it becomes possible to develop parallel macroscopic biomimetic electrochemical motors [167, 171].

1.7. The present investigation

In the past four decades, there has been a tremendous advancement in the field of CPs, especially in the field of polyaniline, owing to their unique optical, electrical and electrochemical characteristics. They found a variety of applications in different areas including microelectronic, medical, biomedical, environmental, robotics, etc. Most of the applications of CPs have been considering them as a dry material, i.e., based on their constant composition properties. When CPs are wet, the chemistry of CPs is different, the properties become composition dependent. The composition dependent properties and applications of CPs are not thoroughly explained by the scientific world. In this thesis, we are focusing on the composition dependent properties (reaction driven properties) of PANI.

Although a lot of research has been carried out on PANI, the basic electrochemistry of PANI has not been well explored yet. The

thesis started with electrochemical studies of the PANI by giving an insight into the structural chemical kinetics of the PANI. A detailed analysis of structural faradaic processes in PANI was carried out by voltammetry for the first time.

The Nernst equation is the fundamental equation of all equilibrium electrochemical reactions and is used for designing potentiometric and conventional electrochemical sensors. This Nernst equation is not applicable in the case of systems that are working outside the equilibrium conditions. CPs are working outside the equilibrium conditions. Therefore, the fundamental equilibrium electrochemical principles, such as the Le-Chatlier principle and Nernst equations are not applicable in the case of CPs. The new principle called the Otero principle, proposed by reformulating the Le-Chatlier principle, is only applicable to such condensed systems. This principle is the foundation of the reaction driven sensing characteristics of CPs.

One of the objectives of the present study is to establish that the reaction driven sensing (self-sensing) property is the general property of all CPs. In this thesis, studies are conducted to establish the reaction driven sensing capabilities of PANI by chronopotentiometry, where consumed electrical energy during the reaction as the sensing parameter and by voltammetry where consumed charge during the reaction as the sensing parameter. We argued that any electrochemical device, working based on the electrochemical reaction of PANI, can sense its working conditions because the reaction itself has sensing capabilities.

The major drawback of PANI is their poor processibility which limits their practical applications. Therefore, the work focused on the

development of mechanically stable PANI-based free-standing electrodes for device fabrication. Therefore, the work progressing with an aim to fabricate flexible and free-standing electrode material based on the PANI using hydrogels as templates. The two PANI/hydrogel hybrid films were fabricated through simple and inexpensive methods: (1) Chitosan/PANI hybrid films and (2) PVA/PANI hybrid films.

The present study aimed to verify the reaction driven sensing characteristics of Chitosan/PANI hybrid films. Besides, we aimed to analyze the performance of Chitosan/PANI hybrid films as supercapacitor electrodes. The investigations are carried out to prove that CP/hydrogel systems exhibit the capability to sense their working conditions such as electrical, chemical and thermal working conditions. The sensing and charge storage characteristics are originated from the same electrochemical reaction. By exploiting this aspect, we focused on developing a truly integrated sensing supercapacitor device: a supercapacitor that can sense their working conditions.

Since Chitosan/PANI hybrid films are only moderately mechanically stable, they are not suitable for device fabrication. Highly mechanically stable PVA/PANI hybrid films are then fabricated for the device application. Using PVA/PANI hybrid film, we aimed to analyze how the cooperative actuation of multimolecular motors of PANI changes with various working conditions and proved that the conformational and structural changes under faradaic control that arise due to the cooperative actuation of the constitutive chemical molecular machines are responsible for the self-sensing property of the hybrid film. Finally, we used this fundamental electrochemistry of PANI for the

development of a sensing motor: a sensing supercapacitor. We aimed to fabricate a symmetric supercapacitor using PVA/PANI hybrid films and verify the self-sensing capability of the device along with charge storage characteristics.

1.8. The major research objectives

- To characterize PANI with special emphasis on its reaction driven electrochemical sensing characteristics.
- To investigate the structural faradaic process in PANI by coulombometry and to analyze the influence of anodic and cathodic potential limits on voltammetric and coulombometric responses.
- To explore whether the PANI reaction has the capability to sense its working environmental conditions such as chemical, electrical and thermal conditions.
- To fabricate and characterize mechanically stable free-standing PANI/hydrogel hybrid films for their electrochemical sensing and energy store applications.
- To verify the reaction driven sensing characteristics in PANI/hydrogel hybrid films and to study their cooperative actuation characteristics.
- To study the charge storage characteristics of PANI/hydrogel films for supercapacitor applications
- To fabricate a sensing motor - a sensing supercapacitor based on PANI/hydrogel hybrid films.

References

1. H. Shirakawa, E.J. Louis, A.G. MacDiarmid, C.K. Chiang, A.J. Heeger, *Journal of the Chemical Society, Chemical Communications*, (1977) 578-580.
2. S. Ramakrishnan, *Resonance*, 2 (1997) 48-58.
3. G. Mitchell, F. Davis, M. Kiani, *British polymer journal*, 23 (1990) 157-164.
4. A.G. MacDiarmid, *Angewandte Chemie International Edition*, 40 (2001) 2581-2590.
5. Jaymand, Mehdi, *Progress in Polymer Science*, 38, (2013) 1287-1306
6. S. Xing, G. Zhao, *Journal of applied polymer science*, 104 (2007) 1987-1996.
7. Y.A. Ismail, A. K. Shabeeba, M. P. Sidheekha, L. Rajan, In: *Actuators: Fundamentals, Principles, Materials and Applications*, Wiley, 2022, pp211-252
8. T. Sen, S. Mishra, N.G. Shimpi, *RSC advances*, 6 (2016) 42196-42222.
9. Y. Wei, W. Luo, Z. Zhuang, B. Dai, J. Ding, T. Li, M. Ma, X. Yin, Y. Ma, *Advanced Composites and Hybrid Materials*, 4 (2021) 1082-1091.
10. Y.A. Ismail, J.G. Martínez, A.S. Al Harrasi, S.J. Kim, T.F. Otero, *Sensors and Actuators B: chemical*, 160 (2011) 1180-1190.
11. Y.A. Ismail, J.G. Martinez, T.F. Otero, *Journal of Electroanalytical Chemistry*, 719 (2014) 47-53.
12. J. Niu, J. Li, P. Liu, *Applied Materials Today*, 20 (2020) 100733.
13. J. Kanicki, T. Skotheim, Dekkker, New York, 543 (1986).
14. A.G. MacDiarmid, R. Mammone, R. Kaner, L. Porter, *Philosophical Transactions of the Royal Society of London. Series A, Mathematical and Physical Sciences*, 314 (1985) 3-15.
15. C.K. Chiang, C. Fincher Jr, Y.W. Park, A.J. Heeger, H. Shirakawa, E.J. Louis, S.C. Gau, A.G. MacDiarmid, *Physical review letters*, 39 (1977) 1098.
16. A. MacDiarmid, J. Chiang, A. Richter, Epstein, AJ, *Synthetic Metals*, 18 (1987) 285-290.

17. A. Heeger, *Philosophical Transactions of the Royal Society of London. Series A, Mathematical and Physical Sciences*, 314 (1985) 17-35.
18. J.L. Bredas, G.B. Street, *Accounts of Chemical Research*, 18 (1985) 309-315.
19. D.L. Gochnauer, T. Gilani, *Am. J. Undergrad. Res*, 14 (2018) 49-56.
20. K. Soga, M. Nakamaru, *Journal of the Chemical Society, Chemical Communications*, (1983) 1495-1496.
21. G. Tourillon, F. Garnier, *The Journal of Physical Chemistry*, 87 (1983) 2289-2292.
22. T.-H. Le, Y. Kim, H. Yoon, *Polymers*, 9 (2017) 150.
23. F. Zuo, M. Angelopoulos, A. MacDiarmid, A.J. Epstein, *Physical Review B*, 39 (1989) 3570.
24. -M.V. Kulkarni, A.K. Viswanath, R. Marimuthu, T. Seth, *Journal of Polymer Science Part A: Polymer Chemistry*, 42 (2004) 2043-2049.
25. R. Bianchi, G. Leal Ferreira, C. Lepienski, R. Faria, *The Journal of chemical physics*, 110 (1999) 4602-4607.
26. Y. Cao, A. Andreatta, A.J. Heeger, P. Smith, *Polymer*, 30 (1989) 2305-2311.
27. T. Hagiwara, M. Hirasaka, K. Sato, M. Yamaura, *Synthetic Metals*, 36 (1990) 241-252.
28. H.C. Kang, K. Geckeler, *Polymer*, 41 (2000) 6931-6934.
29. H. Letheby, *Journal of the Chemical Society*, 15 (1862) 161-163.
30. R. Willstätter, C.W. Moore, *Berichte der deutschen chemischen Gesellschaft*, 40 (1907) 2665-2689.
31. R. Willstätter, S. Dorogi, *Berichte der deutschen chemischen Gesellschaft*, 42 (1909) 4118-4135.
32. A.G. Green, A.E. Woodhead, *Journal of the Chemical Society, Transactions*, 97 (1910) 2388-2403.
33. A.G. Green, A.E. Woodhead, *Journal of the Chemical Society, Transactions*, 101 (1912) 1117-1123.
34. T. Yasui, *Bulletin of the Chemical Society of Japan*, 10 (1935) 305-311.

35. A.G. Macdiarmid, J.-C. Chiang, M. Halpern, W.-S. Huang, S.-L. Mu, L. Nanaxakkara, S.W. Wu, S.I. Yaniger, *Molecular Crystals and Liquid Crystals*, 121 (1985) 173-180.
 36. A.G. Macdiarmid, J.-C. Chiang, W. Huang, B.D. Humphrey, N. Somasiri, *Molecular Crystals and Liquid Crystals*, 125 (1985) 309-318.
 37. Z.A. Boeva, V.G. Sergeev, *Polymer Science Series C*, 56 (2014) 144-153.
 38. Y. Cao, S. Li, Z. Xue, D. Guo, *Synthetic metals*, 16 (1986) 305-315.
 39. A. MacDiarmid, J. Chiang, A. Richter, N. Somasiri, A. Epstein, *Polyaniline: synthesis and characterization of the emeraldine oxidation state by elemental analysis*, *Conducting polymers*, Springer, 1987, pp. 105-120.
 40. C. Menardo, M. Nechtschein, A. Rousseau, J. Travers, P. Hany, *Synthetic metals*, 25 (1988) 311-322.
 41. A.G. MacDiarmid, A.J. Epstein, *Faraday Discussions of the Chemical Society*, 88 (1989) 317-332.
 42. S. Bhandari, *Polyaniline: structure and properties relationship, Polyaniline Blends, Composites, and Nanocomposites*, Elsevier, 2018, pp. 23-60.
 43. A.G. MacDiarmid, L. Yang, W. Huang, B. Humphrey, *Synthetic metals*, 18 (1987) 393-398.
 44. S. Armes, J. Miller, *Synthetic metals*, 22 (1988) 385-393.
 45. T. Matsunaga, H. Daifuku, T. Nakajima, T. Kawagoe, *Polymers for Advanced Technologies*, 1 (1990) 33-39.
 46. S. David, Y. Nicolau, F. Melis, A. Revillon, *Synthetic Metals*, 69 (1995) 125-126.
 47. H. Ding, M. Wan, Y. Wei, *Advanced Materials*, 19 (2007) 465-469.
 48. S. Armes, M. Aldissi, *Polymer*, 32 (1991) 2043-2048.
 49. M. Ayad, M. Shenashin, *European polymer journal*, 40 (2004) 197-202.
 50. Y. Wang, Z. Liu, B. Han, Z. Sun, Y. Huang, G. Yang, *Langmuir*, 21 (2005) 833-836.
 51. S. Palaniappan, *Polymers for Advanced Technologies*, 15 (2004) 111-117.
-

52. Y. Lu, Y. Ren, L. Wang, X. Wang, C. Li, *Polymer*, 50 (2009) 2035-2039.
 53. Z. Sun, Y. Geng, J. Li, X. Wang, X. Jing, F. Wang, *Journal of applied polymer science*, 72 (1999) 1077-1084.
 54. Q. Zhou, X.M. Su, H. Zhang, Y.J. Weng, *Advanced Materials Research*, Trans Tech Publ, 2011, pp. 1124-1128.
 55. J.E. da Silva, S.I. de Torresi, M.L. Temperini, *Journal of the Brazilian Chemical Society*, 11 (2000) 91-94.
 56. P. Gaikwad, D. Shirale, V. Gade, P. Savale, H. Kharat, K. Kakde, S. Hussaini, N. Dhumane, M. Shirsat, *Bulletin of Materials Science*, 29 (2006) 169-172.
 57. E. Venancio, C. Costa, S. Machado, A. Motheo, *Electrochemistry communications*, 3 (2001) 229-233.
 58. T. Girija, M. Sangaranarayanan, *Synthetic Metals*, 156 (2006) 244-250.
 59. Y. Wei, Y. Sun, X. Tang, *The Journal of Physical Chemistry*, 93 (1989) 4878-4881.
 60. J. Lippe, R. Holze, *Journal of Electroanalytical Chemistry*, 339 (1992) 411-422.
 61. P. Nunziante, G. Pistoia, *Electrochimica acta*, 34 (1989) 223-228.
 62. L.J. Duić, Z. Mandić, F. Kovačiček, *Journal of Polymer Science Part A: Polymer Chemistry*, 32 (1994) 105-111.
 63. J. Desilvestro, W. Scheifele, *Journal of Materials Chemistry*, 3 (1993) 263-272.
 64. G. Zotti, S. Cattarin, N. Comisso, *Journal of electroanalytical chemistry and interfacial electrochemistry*, 239 (1988) 387-396.
 65. D.M. Mohilner, R.N. Adams, W.J. Argersinger, *Journal of the American Chemical Society*, 84 (1962) 3618-3622.
 66. Y. Wei, X. Tang, Y. Sun, W.W. Focke, *Journal of Polymer Science Part A: Polymer Chemistry*, 27 (1989) 2385-2396.
 67. G.G. Wallace, P.R. Teasdale, G.M. Spinks, L.A. Kane-Maguire, *Conductive electroactive polymers: intelligent materials systems*, CRC press, 2002.
 68. S. Bhadra, D. Khastgir, N.K. Singha, J.H. Lee, *Progress in polymer science*, 34 (2009) 783-810.
-

69. N. Shoaie, M. Daneshpour, M. Azimzadeh, S. Mahshid, S.M. Khoshfetrat, F. Jahanpeyma, A. Gholaminejad, K. Omidfar, M. Foruzandeh, *Microchimica Acta*, 186 (2019) 1-29.
70. R.J. Tseng, J. Huang, J. Ouyang, R.B. Kaner, Y. Yang, *Nano letters*, 5 (2005) 1077-1080.
71. E.K. Arora, V. Sharma, A. Ravi, A. Shahi, S. Jagtap, A. Adhikari, J.K. Dash, P. Kumar, R. Patel, *Energies*, 16 (2023) 6716
72. X. Chu, W. Yang, H. Li, *Materials Horizons*, 10 (2023) 670-697.
73. S. Goswami, S. Nandy, E. Fortunato, R. Martins, *Journal of Solid State Chemistry*, 317 (2023) 123679.
74. M. Zahid, R. Anum, S. Siddique, H.F. Shakir, Z. Rehan, *Journal of Thermoplastic Composite Materials*, 36 (2023) 1717-1761.
75. S. Akram, M. Ashraf, A. Javid, H.A. Abid, S. Ahmad, Y. Nawab, A. Rasheed, Z. Xue, A. Nosheen, *Synthetic Metals*, 294 (2023) 117305.
76. T.V. Nguyen, Q.V. Le, S. Peng, Z. Dai, S.H. Ahn, S.Y. Kim, *Advanced Materials Technologies*, 8 (2023) 2300474.
77. K. Kaneto, M. Kaneko, Y. Min, A.G. MacDiarmid, *Synthetic Metals*, 71 (1995) 2211-2212.
78. Y.A. Ismail, S.R. Shin, K.M. Shin, S.G. Yoon, K. Shon, S.I. Kim, S.J. Kim, *Sensors and Actuators B: Chemical*, 129 (2008) 834-840.
79. E. Smela, B.R. Mattes, *Synthetic metals*, 151 (2005) 43-48.
80. D. Yang, J. Wang, Y. Cao, X. Tong, T. Hua, R. Qin, Y. Shao, *ACS Applied Electronic Materials*, 5 (2023) 593-611.
81. S. Uppugalla, P. Srinivasan, *Journal of Applied Polymer Science*, 140 (2023) e54020.
82. J.A. Oyetade, R.L. Machunda, A. Hilonga, *RSC advances*, 13 (2023) 15467-15489.
83. J.R. Vaidya, Y.V. Durga Nageswar, *Physical Sciences Reviews*, 8 (2023) 4213-4231.
84. M. Mecwan, N. Falcone, A.H. Najafabadi, D. Khorsandi, *Antioxidant activity, Electrically Conducting Polymers and Their Composites for Tissue Engineering*, ACS Publications, 2023, pp. 71-80.

85. W. Huang, M. Angelopoulos, J. White, J. Park, *Molecular Crystals and Liquid Crystals*, 189 (1990) 227-235.
86. N. Chandrakanthi, M. Careem, *Polymer Bulletin*, 44 (2000) 101-108.
87. L. Duić, Z. Mandić, *Journal of Electroanalytical Chemistry*, 335 (1992) 207-221.
88. L. Lizarraga, E.M.a. Andrade, F.V. Molina, *Journal of Electroanalytical Chemistry*, 561 (2004) 127-135.
89. S. Bhadra, D. Khastgir, *Polymer Degradation and Stability*, 92 (2007) 1824-1832.
90. Y. Cao, P. Smith, A.J. Heeger, *Synthetic metals*, 48 (1992) 91-97.
91. G. Titelman, M. Zilberman, A. Siegmann, Y. Haba, M. Narkis, *Journal of applied polymer science*, 66 (1997) 2199-2208.
92. R. Nagarajan, *Enzymatic synthesis of polyaniline complexed with DNA and other polyelectrolyte templates*, University of Massachusetts Lowell, 2000.
93. A. Yahya, A. Ahmad, F. Mohammad, *Indian Journal of Chemistry - Section A*, 43A (2004) 1423-1427.
94. B. Vincent, J. Waterson, *Journal of the Chemical Society, Chemical Communications*, (1990) 683-684.
95. J. Yue, A.J. Epstein, *Journal of the American Chemical Society*, 112 (1990) 2800-2801.
96. P.N. Bartlett, P. Birkin, E. Wallace, *Journal of the Chemical Society, Faraday Transactions*, 93 (1997) 1951-1960.
97. S. Tian, A. Baba, J. Liu, Z. Wang, W. Knoll, M.K. Park, R. Advincula, *Advanced Functional Materials*, 13 (2003) 473-479.
98. H.D. Kyomuhimbo, U. Feleni, *Electroanalysis*, 35 (2023) e202100636.
99. A. Eftekhari, L. Li, Y. Yang, *Journal of Power Sources*, 347 (2017) 86-107.
100. U. Riaz, N. Singh, F. Rashnas Srambikal, S. Fatima, *Polymer Bulletin*, 80 (2023) 1085-1116.
101. J. Bhadra, A. Alkareem, N. Al-Thani, *Journal of Polymer Research*, 27 (2020) 1-20.

102. E.N. Zare, P. Makvandi, B. Ashtari, F. Rossi, A. Motahari, G. Perale, *Journal of Medicinal Chemistry*, 63 (2019) 1-22.
 103. J. Deng, X. Ding, W. Zhang, Y. Peng, J. Wang, X. Long, P. Li, A.S. Chan, *European Polymer Journal*, 38 (2002) 2497-2501.
 104. J. Anand, S. Palaniappan, D. Sathyanarayana, *Progress in Polymer Science*, 23 (1998) 993-1018.
 105. N. Kohut-Svelko, S. Reynaud, J. François, *Synthetic Metals*, 150 (2005) 107-114.
 106. W. Roorda, H. Bodde, A. De Boer, H. Junginger, *Pharmaceutisch Weekblad*, 8 (1986) 165-189.
 107. Y. Zhao, H. Su, L. Fang, T. Tan, *Polymer*, 46 (2005) 5368-5376.
 108. W.F. Lee, W.H. Chiang, *Journal of applied polymer science*, 91 (2004) 2135-2142.
 109. T. Zhu, Y. Ni, G.M. Biesold, Y. Cheng, M. Ge, H. Li, J. Huang, Z. Lin, Y. Lai, *Chemical Society Reviews*, 52 (2023) 473-509.
 110. N.A. Peppas, P. Bures, W. Leobandung, H. Ichikawa, *European Journal of Pharmaceutics and Biopharmaceutics*, 50 (2000) 27-46.
 111. J.A. Rowley, G. Madlambayan, D.J. Mooney, *Biomaterials*, 20 (1999) 45-53.
 112. S.W. Ali, S.A.R. Zaidi, *Journal of applied polymer science*, 98 (2005) 1927-1931.
 113. M.M. Zohourian, K. Kabiri, *Iranian Polymer Journal* 17(6), (2008), 451-477.
 114. M. Mahinroosta, Z.J. Farsangi, A. Allahverdi, Z. Shakoori, *Materials Today Chemistry*, 8 (2018) 42-55.
 115. C.M. Lopes, M.I. Felisberti, *Biomaterials*, 24 (2003) 1279-1284.
 116. K. Gilmore, A. Hodgson, B. Luan, C. Small, G. Wallace, *Polymer Gels and Networks*, 2 (1994) 135-143.
 117. D. Mawad, A. Lauto, G.G. Wallace, *Polymeric hydrogels as smart biomaterials*, (2016) 19-44.
 118. M. Molina, C. Rivarola, C. Barbero, *European Polymer Journal*, 47 (2011) 1977-1984.
-

119. Y. Xia, H. Zhu, *Soft Matter*, 7 (2011) 9388-9393.
120. H.-J. Lee, T.-J. Chung, H.-J. Kwon, H.-J. Kim, W.T.Y. Tze, *Cellulose*, 19 (2012) 1251-1258.
121. T. Dai, X. Qing, J. Wang, C. Shen, Y. Lu, *Composites Science and Technology*, 70 (2010) 498-503.
122. I.Y. Dmitriev, P.V. Vlasov, M.F. Lebedeva, et al, *Materials Chemistry and Physics*, 187 (2017) 88-95.
123. L. Li, J. Ge, B. Guo, P.X. Ma, *Polymer Chemistry*, 5 (2014) 2880-2890.
124. H. Huang, J. Yao, L. Li, F. Zhu, Z. Liu, X. Zeng, X. Yu, Z. Huang, *Journal of materials science*, 51 (2016) 8728-8736.
125. T. Thanpitcha, A. Sirivat, A.M. Jamieson, R. Rujiravanit, *Carbohydrate Polymers*, 64 (2006) 560-568.
126. J. Stejskal, *Chemical Papers*, 71 (2017) 269-291.
127. Q. Tang, J. Wu, H. Sun, J. Lin, S. Fan, D. Hu, *Carbohydrate Polymers*, 74 (2008) 215-219.
128. P. Dou, Z. Liu, Z. Cao, J. Zheng, C. Wang, X. Xu, *Journal of Materials Science*, 51 (2016) 4274-4282.
129. L. Pan, G. Yu, D. Zhai, H.R. Lee, W. Zhao, N. Liu, H. Wang, B.C.-K. Tee, Y. Shi, Y. Cui, *Proceedings of the National Academy of Sciences*, 109 (2012) 9287-9292.
130. K.-H. Sun, Z. Liu, C. Liu, T. Yu, T. Shang, C. Huang, M. Zhou, C. Liu, F. Ran, Y. Li, *Scientific reports*, 6 (2016) 1-11.
131. Y. Wang, Y. Shi, L. Pan, Y. Ding, Y. Zhao, Y. Li, Y. Shi, G. Yu, *Nano letters*, 15 (2015) 7736-7741.
132. K. Wang, X. Zhang, C. Li, H. Zhang, X. Sun, N. Xu, Y. Ma, *Journal of Materials Chemistry A*, 2 (2014) 19726-19732.
133. U. Riaz, N. Singh, F. Rashnas Srmbikal, S. Fatima, *Polymer Bulletin*, (2022) 1-32.
134. T. Zhu, Y. Ni, G.M. Biesold, Y. Cheng, M. Ge, H. Li, J. Huang, Z. Lin, Y. Lai, *Chemical Society Reviews*, 52 (2023) 473-509.
135. G. Kougkolos, M. Golzio, L. Laudebat, Z. Valdez-Nava, E. Flahaut, *Journal of Materials Chemistry B*, 11 (2023) 2036-2062.

136. Y.A. Ismail, A. Shabeeba, M.P. Sidheekha, L. Rajan, *Actuators: Fundamentals, Principles, Materials and Applications*, (2020) 211-252.
137. C. Qian, Y. Li, C. Chen, L. Han, Q. Han, L. Liu, Z. Lu, *Chemical Engineering Journal*, 454 (2023) 140263.
138. A.K. Nandi, D.P. Chatterjee, *Journal of Materials Chemistry A*, 11 (2023) 12593-12642.
139. Y. Han, L. Dai, *Macromolecular chemistry and physics*, 220 (2019) 1800355.
140. G.A. Snook, P. Kao, A.S. Best, *Journal of power sources*, 196 (2011) 1-12.
141. A. Schneuwly, R. Gallay, *Proceeding PCIM*, Citeseer, 2000.
142. C. Largeot, C. Portet, J. Chmiola, P.-L. Taberna, Y. Gogotsi, P. Simon, *Journal of the American Chemical Society*, 130 (2008) 2730-2731.
143. J. Libich, J. Máca, J. Vondrák, O. Čech, M. Sedlaříková, *Journal of Energy Storage*, 17 (2018) 224-227.
144. S. Najib, E. Erdem, *Nanoscale Advances*, 1 (2019) 2817-2827.
145. M. Mastragostino, F. Soavi, C. Arbizzani, W. van Schalkwijk, B. Scrosati, *Spring Nature*, (2002).
146. K.S. Ryu, Y.-G. Lee, Y.-S. Hong, Y.J. Park, X. Wu, K.M. Kim, M.G. Kang, N.-G. Park, S.H. Chang, *Electrochimica acta*, 50 (2004) 843-847.
147. M. Mastragostino, C. Arbizzani, F. Soavi, *Journal of power sources*, 97 (2001) 812-815.
148. H. Li, J. Wang, Q. Chu, Z. Wang, F. Zhang, S. Wang, *Journal of Power Sources*, 190 (2009) 578-586.
149. T. Nohma, H. Kurokawa, M. Uehara, M. Takahashi, K. Nishio, T. Saito, *Journal of power sources*, 54 (1995) 522-524.
150. Z. Peng, C. Wan, C. Jiang, *Journal of Power Sources*, 72 (1998) 215-220.
151. A. Du Pasquier, A. Laforgue, P. Simon, G.G. Amatucci, J.-F. Fauvarque, *Journal of the Electrochemical Society*, 149 (2002) A302.
152. A.G. Pandolfo, A.F. Hollenkamp, *Journal of power sources*, 157 (2006) 11-27.

153. W. Lu, A.G. Fadeev, B. Qi, E. Smela, B.R. Mattes, J. Ding, G.M. Spinks, J. Mazurkiewicz, D. Zhou, G.G. Wallace, *Science*, 297 (2002) 983-987.
 154. S. Sivakkumar, D.R. MacFarlane, M. Forsyth, D.-W. Kim, *Journal of the Electrochemical Society*, 154 (2007) A834.
 155. C. Peng, S. Zhang, D. Jewell, G.Z. Chen, *Progress in Natural science*, 18 (2008) 777-788.
 156. S. Bashir, K. Hasan, M. Hina, R.A. Soomro, M. Mujtaba, S. Ramesh, K. Ramesh, N. Duraisamy, R. Manikam, *Journal of Electroanalytical Chemistry*, 898 (2021) 115626.
 157. A. Laforgue, P. Simon, J. Fauvarque, M. Mastragostino, F. Soavi, J. Sarrau, P. Lailler, M. Conte, E. Rossi, S. Saguatti, *Journal of the Electrochemical Society*, 150 (2003) A645.
 158. H. Zhang, J. Wang, Y. Chen, Z. Wang, S. Wang, *Electrochimica Acta*, 105 (2013) 69-74.
 159. M. Mallouki, F. Tran-Van, C. Sarrazin, P. Simon, B. Daffos, A. De, C. Chevrot, J.-F. Fauvarque, *Journal of Solid State Electrochemistry*, 11 (2007) 398-406.
 160. L.-M. Huang, T.-C. Wen, A. Gopalan, *Electrochimica acta*, 51 (2006) 3469-3476.
 161. A. Ehsani, A.A. Heidari, H.M. Shiri, *The Chemical Record*, 19 (2019) 908-926.
 162. J. Stejskal, *Chemical Papers*, 71 (2017) 269-291.
 163. I. Shown, A. Ganguly, L.C. Chen, K.H. Chen, *Energy Science & Engineering*, 3 (2015) 2-26.
 164. Y.A. Ismail, J. Chang, S.R. Shin, R.S. Mane, S.-H. Han, S.J. Kim, *Journal of the Electrochemical Society*, 156 (2009) A313.
 165. W.-S. Huang, B.D. Humphrey, A.G. MacDiarmid, *Journal of the Chemical Society, Faraday Transactions 1: Physical Chemistry in Condensed Phases*, 82 (1986) 2385-2400.
 166. E. Tsai, T. Pajkossy, K. Rajeshwar, J. Reynolds, *The Journal of Physical Chemistry*, 92 (1988) 3560-3565.
 167. T.F. Otero, *The Chemical Record*, 18 (2018) 788-806.
-

168. H.J. Ahonen, J. Lukkari, J. Kankare, *Macromolecules*, 33 (2000) 6787-6793.
169. C. Arbizzani, M. Catellani, M. Mastragostino, C. Mingazzini, *Electrochimica Acta*, 40 (1995) 1871-1876.
170. M. Ranger, M. Leclerc, *Canadian Journal of Chemistry*, 76 (1998) 1571-1577.
171. J. Arias-Pardilla, T.F. Otero, J.G. Martínez, Y.A. Ismail, *Biomimetic sensing-actuators based on conducting polymers*, Intechopen, 2012.
172. T. F. Otero, in *Modern Aspects of Electrochemistry*, eds. R. E. White, J. O. Bockris and B. E. Conway, Springer US, New York, 1999, pp. 307–434.
173. T.F. Otero, *Electrochimica Acta*, 368 (2021) 137576.
174. T.F. Otero, J.G. Martinez, *Journal of Materials Chemistry B*, 1 (2013) 26-38.
175. T. Otero, J. Martinez, J. Arias-Pardilla, *Electrochimica Acta*, 84 (2012) 112-128.
176. T.F. Otero, *Polymer Reviews*, 53 (2013) 311-351.
177. T.F. Otero, *RSC advances*, 11 (2021) 21489-21506.
178. T.F. Otero, *International Journal of Smart and Nano Materials*, 8 (2017) 125-143.

Chapter 2

Materials and methods

The important chemicals, methodologies and the characterization techniques adopted for the investigations are presented in this chapter. The procedures for the synthesis of polyaniline, fabrication of conducting polymer hydrogel films (Chitosan/PANI and PVA/PANI) and fabrication of all solid-state symmetric supercapacitor device are discussed. The experimental aspects of characterizations and sensing and supercapacitive studies are also outlined here.

2.1. Materials used

A list of chemicals used for this research work is provided in Table 2.1. Except for aniline, all the chemicals used are of analytical grade and are used as received without any further purification. Aniline was distilled under vacuum before use and stored below 10 °C. The double distilled water was employed throughout the experiment.

Table 2.1 List of chemicals used and their purity

Consumable	Source
Aniline AR	Merck, India
Chitosan (high molecular weight)	Sigma Aldrich, USA
Polyvinyl alcohol (PVA), hot water soluble	Himedia, India
Glacial acetic acid	Merck, India
Acetone	Merck, India
Ammonium persulphate (APS)	Merck, India
Hydrochloric acid (HCl)	Merck, India
Methanol	Qualigens, India
Sodium hydroxide (NaOH)	Merck, India
Carbon conductive paste	MG chemicals, USA
Sulphuric acid (H ₂ SO ₄)	Merck, India

2.2. Synthesis of PANI

PANI was synthesized through chemical oxidative polymerization of aniline using ammonium persulphate as an oxidant. The process is illustrated schematically in Figure 2.1.

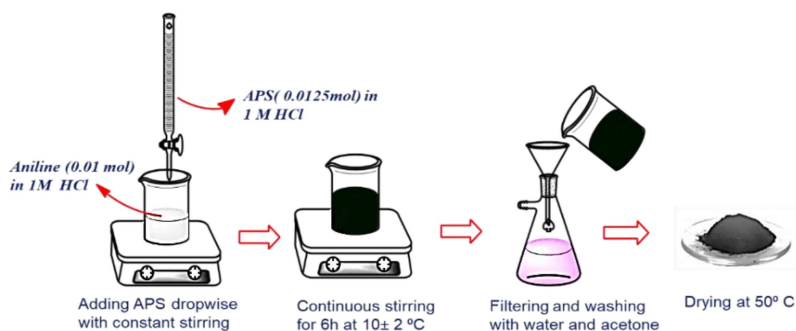


Figure 2.1 Schematic representation of the synthesis of PANI

Briefly, to the 100 mL of 0.01 M aniline solution prepared in 1 M HCl solution, 0.0125 M solution (100 mL) of APS prepared in 1 M HCl solution was added at a flow rate of 1 mL/min. The reaction was carried out at 10 ± 2 °C for 6 hours with constant stirring using a magnetic stirrer. The dark green coloured product was collected by filtration and the excess oxidant and oligomers were removed by continuous washing with double distilled water and then with acetone until a clear filtrate was obtained. The product was dried at 50 °C in a hot air oven for 24 hours. The final product was ground to fine powder and stored in a desiccator.

2.3. Fabrication of CP/hydrogel hybrid films

Conducting polymer/hydrogel hybrid films were fabricated through an in situ chemical polymerization of aniline using a prefabricated hydrogel film matrix in 1 M aqueous HCl solution using APS as an oxidant. Figure 2.2 shows a schematic representation of the fabrication process. It is a straightforward and cost-effective technique, making it suitable for large-scale fabrication of various CP/hydrogel hybrid films.

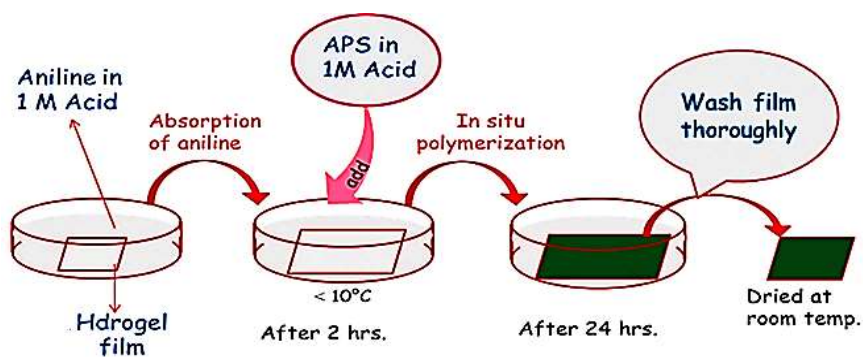


Figure 2.2 Schematic representation of fabrication of CPH films

2.3.1. Fabrication of Chitosan/PANI hybrid films

Fabrication of Chitosan film

Chitosan films were prepared by the solution casting method. 5 g of chitosan powder was dissolved in 500 mL of 2 % (w/v) acetic acid solution, by stirring at room temperature for 24 hours, to obtain a 1 % (w/v) solution of chitosan. The filtered clear solution was poured into a square glass plate dish (20 × 20 cm) and dried in the oven at 50 °C for 60 hours. The dry film was peeled off from the glass plate and soaked in 1 M NaOH solution for 12 hours to neutralize the film. Then the film was thoroughly washed with distilled water and methanol several times to remove excess NaOH and dried at room temperature. The thickness of the obtained chitosan films is 0.12 ± 0.02 mm.

Fabrication of Chitosan/Polyaniline hybrid films

The chitosan/polyaniline films (Cs/PANI) were fabricated through an in situ chemical polymerization of aniline using APS as an oxidant in 1 M aqueous HCl solution as depicted in Figure 2.2. In brief, the chitosan film was immersed in 100 mL of 0.01 M solution of aniline

prepared in 1 M HCl solution for 2 hours. Then, a 100 mL solution of 0.0125 M APS solution prepared in 1 M HCl was slowly added with gentle shaking. The reaction mixture was maintained at 10 ± 2 °C. After 24 hours, the first coated film was taken out and washed several times with a 1:1 methanol- water mixture to remove excess oxidant and oligomer, then dried at room temperature. The whole procedure was repeated to get high polyaniline content in the hybrid films. Here, up to four times of repeated coating was carried out and the films were named CPF1, CPF2, CPF3 and CPF4, respectively, for the first, second, third and fourth coated films.

2.3.2. Fabrication of Polyvinyl alcohol /PANI hybrid films

Fabrication PVA film

PVA films were prepared by the solution casting method. 5 g of PVA was dissolved in 250 mL double distilled water to obtain a 2 % (w/v) solution of PVA at a temperature of 80 °C. The filtered clear solution was poured into a square glass plate dish (20 × 20 cm) and dried in an air oven at 50 °C for 48 hours. Then the film was thoroughly washed with double distilled water and dried at room temperature. The thickness of the obtained PVA film is 0.1 ± 0.02 mm.

Fabrication of Polyvinyl alcohol/Polyaniline hybrid films

The Polyvinyl alcohol/Polyaniline (PVA/PANI) hybrid films were fabricated through the same procedure adopted for the fabrication of chitosan/PANI films using PVA film as the hydrogel matrix. Here, up to four times of repeated coating was carried out and the films were

named PP1, PP2, PP3 and PP4, respectively, for the first, second, third and fourth coated films.

2.4. Fabrication of supercapacitor device

An all-solid-state symmetric supercapacitor device was fabricated by sandwiching two PP4 hybrid films with filter paper containing PVA/H₂SO₄ as the separator and gel electrolyte. This configuration is illustrated in Figure 2.3. To prepare the electrolyte, 2 g of PVA was mixed with 20 mL of deionized water and 2 g of H₂SO₄ at 80 °C. The mixture was stirred continuously until it became transparent. A piece of filter paper was then immersed in the electrolyte, removed, and left to dry until excess water evaporated. The two PP4 hybrid films, each with an area of 10 mm x 20 mm, were stacked together, and the filter paper impregnated with PVA/H₂SO₄ was placed in between them as the middle layer. The entire assembly was pressed together to assemble the symmetric supercapacitor [1-3].

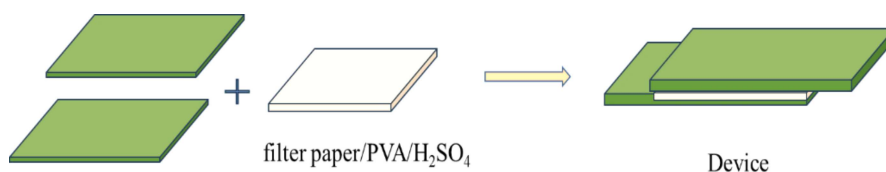


Figure 2.3 Schematic representation of supercapacitor device fabrication

2.5. General characterization techniques

2.5.1. Fourier transform infra-red spectroscopy (FTIR)

The structural analysis of PANI, chitosan, PVA, and the hybrid films, (Cs/PANI and PVA/PANI films) was carried out using FTIR analysis.

The FT-IR spectrum of PANI was recorded by pelletizing the sample with KBr and the spectra were recorded in the range of 4000 cm⁻¹ to 500 cm⁻¹ using JASCO FTIR-4600 FTIR spectrometer. For the films, the FTIR spectra were obtained through an attenuated total reflectance (ATR) mode using the JASCO FTIR-4700 instrument, recorded in the range of 4000 cm⁻¹ to 500 cm⁻¹. In ATR, an IR beam was directed onto an optically dense crystal with a high refractive index. The reflected beam interacts with the sample in contact with the crystal. The absorption bands are observed corresponding to the vibrational frequencies of various bonds of the polymer.

2.5.2. Broadband dielectric spectroscopy (BDS)

The electrical conductivities of all the samples were measured using a Broadband Dielectric Spectrometer (BDS) 'Novocontrol BDS concept 80'(Germany) at room temperature. The frequency range for the analysis was kept from 1 to 10⁷ Hz. PANI was pelletized using a stainless-steel die having a cross-sectional area of 13 mm. A pressure of 3 tons was applied using a hydraulic press (Spectra Lab India). For the films, circular samples with a diameter of 30 mm were taken for the analysis. During the measurement, an AC electric field was applied across the sample, which was sandwiched between two cylindrical gold-plated electrodes with an effective diameter of 30 mm. These electrodes were mounted within the BDS1200 sample cell. The DC electrical conductivity is obtained by fitting the frequency-dependent conductivity data with the universal power law, known as Jonscher's power law:

$$\sigma_{AC} = \sigma_{DC} + A\omega^S \quad (2.1)$$

where, ω is the angular frequency ($\omega=2\pi f$), and A and s are constant. The value of 's' usually lies between 0 and 1.

2.5.3. Thermogravimetric analysis (TGA)

Thermogravimetric Analysis (TGA) is a thermal analysis method used to measure changes in the physical and chemical properties of materials, particularly mass changes as the temperature increases at a constant heating rate. The thermal degradation behaviour of all the samples studied was investigated using a TGA analyzer (Model: Perkin Elmer) under a nitrogen atmosphere. The temperature range for the analysis was kept from 25 °C to 650 °C, and the heating rate was maintained at 10 °C/min. By plotting the percentage change of weight against temperature, thermograms were obtained. The thermograms provide insights into the thermal stability and decomposition patterns of the materials studied.

2.5.4. Universal testing machine (UTM) analysis- Mechanical studies

A Universal Testing Machine (UTM) is a versatile mechanical testing instrument used to evaluate the mechanical properties of materials. It applies controlled forces or displacements to the specimens to measure their response and behavior under different testing conditions. The UTM is widely used in research, to assess material strength, stiffness, and other mechanical properties. The mechanical characteristics of all the hybrid films were studied using a Universal Testing Machine (UTM). The films used for analysis had a length of

6 cm and a width of 1 cm. Three duplicate tests were performed for each film.

2.5.5. Fourier transform scanning electron microscopy (FESEM)

FESEM analysis is a powerful imaging technique used to investigate the surface morphology and topography of various types of materials at high magnification and resolution. In FESEM, a focused electron beam is scanned over the surface of the specimen, and the interaction between the beam and the sample produces various signals, corresponding to secondary electrons, backscattered electrons, and characteristic X-rays. These signals are detected and used to generate detailed images of the sample's surface. The surface morphologies of PANI, chitosan film, PVA film, and the fabricated hybrid films were analyzed using the ZEISS Gemini SEM 300 FESEM (Germany) instrument operated at 5 kV. To enhance conductivity and imaging quality, the samples were coated with a thin layer of gold-palladium using a Denton Desk II sputter coater. This preparation method allowed for detailed examination and visualization of the surface structures and features of the studied samples at high magnification and resolution.

2.5.6. Energy-dispersive X-ray spectroscopy (EDX analysis)

EDX analysis is one of the techniques used to determine the elemental composition of a sample. It is often performed in conjunction with SEM analysis. In EDX analysis, an electron beam used in SEM interacts with the sample, causing the emission of characteristic X-rays. These X-rays have energies that are specific to each element. These X-rays have been detected and analyzed, for the identification and

quantification of the elements in the sample. The EDX spectra of all the samples were recorded in the same instrument used for FESEM analysis after analyzing the morphology.

2.6. Electrochemical characterizations

Different electrochemical techniques were employed for the experiments presented in this thesis, including cyclic voltammetry, chronopotentiometry, electrochemical impedance analysis, and galvanostatic charge-discharge measurements for studying the electrochemical characteristics of the samples prepared. A Zenner Zennium Pro galvanostate/potentiostate electrochemical workstation (Germany) connected to a personal computer and supported by Thales XT software was used throughout the electrochemical experiments (Figure 2.4). In all the experiments, an Ag/AgCl (3 M KCl) electrode served as the reference electrode, while a platinum wire was used as the counter electrode. In the typical experimental setup, a current is applied between the working electrode and the counter electrode. Simultaneously, the potential of the working electrode is measured relative to the reference electrode. This configuration allowed the monitoring of the electrochemical behavior and reactions occurring at the working electrode.

2.6.1. Preparation of working electrodes

For studying the electrochemical characteristics of PANI powder, a glassy carbon electrode (GCE) modified with PANI was employed as the working electrode. Before use, the GCE was sequentially polished

with a wetted microcloth containing alumina powder to achieve a mirror-like finish. It was then thoroughly cleaned by sonication in ethanol and distilled water. 0.4 mg of PANI powder was coated onto the GCE using carbon paste.

In the case of hybrid films, films with an area of 20 mm² were attached to one end of a platinum wire using conductive carbon paste. These served as the working electrodes for the electrochemical studies.

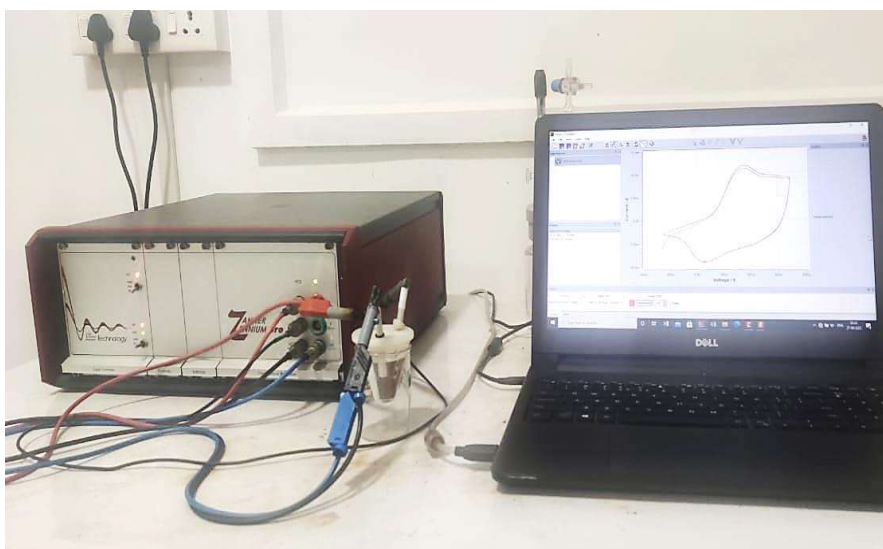


Figure 2.4 *Zahner Zennium Pro electrochemical workstation used for electrochemical studies*

2.6.2. Cyclic voltammetry (CV)

In cyclic voltammetry (CV), a potential sweep is applied between a cathodic potential limit and an anodic potential limit in such a way that the potential is varied at a constant scan rate during the sweep. Once a potential limit is reached, the potential sweep is reversed and carried out in the opposite direction towards the other potential limit,

maintaining the same scan rate. This results in a symmetrical triangular potential wave as shown in Figure 2.5a. This process is repeated as needed to gather the desired data and investigate the electrochemical behavior of the systems studied. During the potential sweep, the current flowing at any given time is recorded (Figure 2.5b), typically plotted as a function of the applied potential. Both the anodic and cathodic current values obtained during the potential sweeps are presented on the same potential axis, resulting in a closed loop when the system reaches a steady state, as illustrated in Figure 2.5c [4]. The coulouvoltammograms (QV) are obtained by integration of CV data.

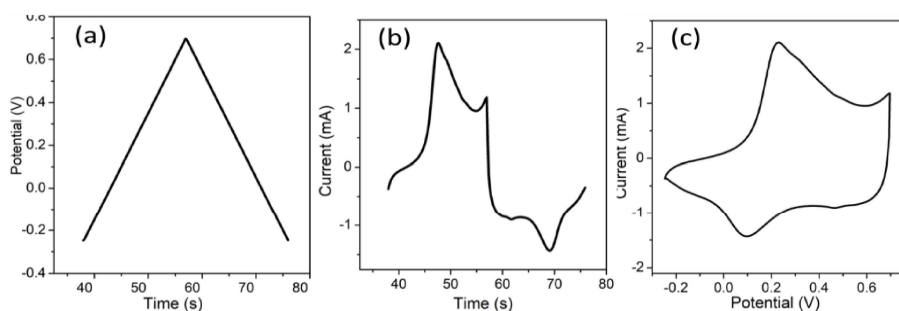


Figure 2.5 Cyclic voltammetry: **(a)** Symmetrical triangular potential wave applied to the working electrode, **(b)** corresponding current measured and **(c)** Cyclic voltammogram

The specific capacitances of the fabricated chitosan/PANI and PVA/PANI hybrid films were calculated using CV curves. The CVs are recorded using films having an area of 20 mm² as the working electrodes. The capacitance values were expressed as areal specific capacitance, which represents the capacitance per unit area of the electrode material. This normalization allows for a fair comparison of the energy storage capabilities of different films. The specific areal capacitance from CV can be determined using the Equation 2.2 [5, 6]:

$$C_s = \frac{\int_{V_1}^{V_2} IdV}{Av(V_2 - V_1)} \quad (2.2)$$

where the integral implies the total area under the CV curve recorded between the potentials of V_1 and V_2 . 'v' is the scan rate and 'A' is the total area of the electrode in contact with the electrolyte or the total area of the device.

2.6.3. Galvanostatic charge-discharge (GCD)

The galvanostatic charge-discharge (GCD) experiment is one of the electrochemical techniques used to assess the energy storage capabilities of energy storage devices such as batteries and supercapacitors. In a galvanostatic charge-discharge experiment, a constant current is applied to the device. During the charging process, the electrode or device stores electrical energy, while during discharging, the stored energy is released. The experiment involves monitoring the voltage across the electrode material or device with respect to time during the charging or discharging process. By measuring the charge and discharge currents and by monitoring the voltage changes, various characteristics of the energy storage materials or devices can be studied. These include the charge/discharge time, voltage profiles, energy efficiency, capacity, and power density. GCD experiments are essential for evaluating the performance and understanding the behavior of materials or devices. They help in optimizing device design, assessing the efficiency and stability of the system, and comparing different materials and configurations for energy

storage applications. The specific areal capacitance from GCD can be determined using the Equation 2.3 [7, 8]:

$$C_s = \frac{i\Delta t}{A\Delta V} \quad (2.3)$$

where 'i' represents the discharging current and Δt stands for the time-lapse for discharging in seconds through the potential interval of ΔV , ($V_2 - V_1$) in volts. The areal energy density (E) and power density (P) of the supercapacitor device are obtained from GCD data. It is calculated using Equation (2.4) and Equation (2.5), respectively [9, 10].

$$E = \frac{C_s * \Delta V^2}{2 * 3600} \quad (2.4)$$

$$P = \frac{3600E}{\Delta t} \quad (2.5)$$

2.6.4. Electrochemical impedance spectroscopy (EIS)

It is one of the important techniques used to characterize the electrochemical behavior of materials, interfaces, and electrochemical systems. It gives information about the electrical behaviour, charge transfer and kinetics of electrochemical reactions. In EIS analysis, a small amplitude sinusoidal signal is applied to the system for a range of frequencies. The resulting response, in terms of the complex impedance, is measured. The impedance is a frequency-dependent parameter that comprises both resistance (real part) and reactance (imaginary part). The impedance spectra are often fitted using equivalent circuit models, which consist of resistors, capacitors, and inductors. This modeling can

help in understanding the underlying electrochemical mechanisms and provides quantitative information about the system [11, 12].

For all the samples, the EIS spectra were recorded at an open-circuit voltage (OCV). The amplitude of the applied sinusoidal signal was 10 mV, and the measurements were performed over a frequency range of 1 Hz to 100 kHz. The EIS experiments were conducted at room temperature. The results are presented as a Nyquist plot (the real part of the impedance is plotted against the negative imaginary part of the impedance). The Zmann software was utilized to fit the experimental data obtained from the EIS measurements.

2.6.5. Chronopotentiometry (for sensing studies)

In a chronopotentiometric experiment, a constant current is applied in an electrochemical system, and the resulting potential variations over time are monitored. This technique is useful for the investigation of the behavior and kinetics of electrochemical reactions occurring at the electrode/electrolyte interface.

To study the sensing characteristics of PANI, Cs/PANI and PANI/PVA, a square wave of current is applied to the systems under study for a specific duration of time. During the flow of current, the potential change between the working electrode and the reference electrode is recorded. In this thesis, a constant square wave of current ' i ' is passed through the electrode for a fixed time period, ' t ', in order to consume a constant amount of charge, ' Q '. The time required to consume a fixed amount of charge was calculated using Equation 2.6 [13]. This

controlled application of current and measurement of potential was used for the investigation of the sensing behavior and response of the materials

$$i = Q/t, \text{ therefore } t = Q/i \quad (2.6)$$

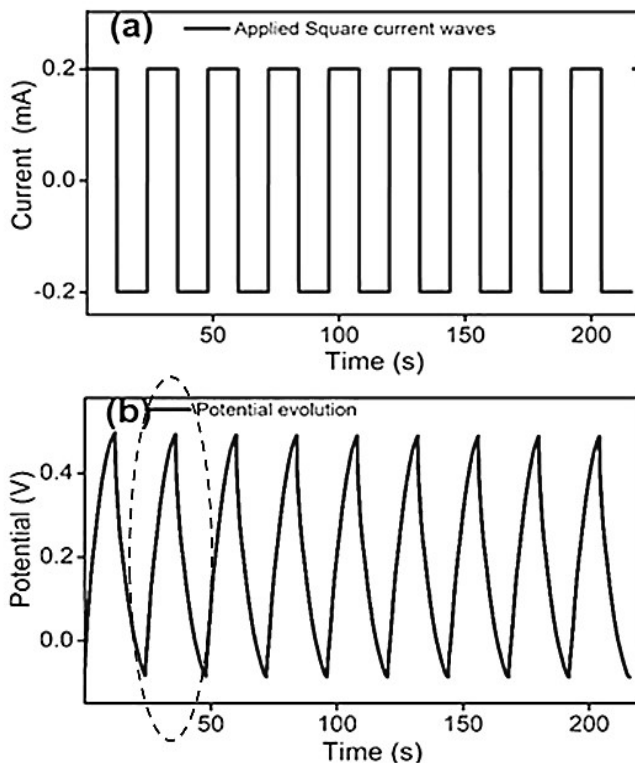


Figure 2.6. (a) Square current waves applied to the working electrode and (b) resulting chronopotentiometric responses

By applying a square current wave to the working electrode in both directions, the same amount of charge is consumed during both the oxidation and reduction processes. It ensures that the oxidation and reduction processes occur with the same initial and final conditions [14]. During the chronopotentiometric experiments, presented in this thesis,

the stationary chronopotentiograms are obtained from the second cycle onwards. A cycle refers to one consecutive oxidation and reduction process. In this case, the second cycle was used for analysis. The normalized chronopotentiograms are plotted for sensing studies.

References

1. E. Tsai, T. Pajkossy, K. Rajeshwar, J. Reynolds, *The Journal of Physical Chemistry*, 92 (1988) 3560-3565.
2. H. Zhang, J. Wang, Y. Chen, Z. Wang, S. Wang, *Electrochimica Acta*, 105 (2013) 69-74.
3. Z. Karami, M. Youssefi, K. Raieisi, M. Zhiani, *Journal of Materials Science*, 57 (2022) 16776-16794.
4. D.H. Evans, K.M. O'Connell, R.A. Petersen, M.J. Kelly, ACS Publications, 1983.
5. L. Cao, S. Huang, F. Lai, Z. Fang, J. Cui, X. Du, W. Li, Z. Lin, P. Zhang, Z. Huang, *Ionics*, 27 (2021) 3431-3441.
6. M.Z. Iqbal, M.M. Faisal, M. Sulman, S.R. Ali, A.M. Afzal, M.A. Kamran, T. Alharbi, *Journal of Energy Storage*, 29 (2020) 101324.
7. Z. Huang, Z. Ji, Y. Feng, P. Wang, Y. Huang, *Polymer International*, 70 (2021) 437-442.
8. W. Li, X. Li, X. Zhang, J. Wu, X. Tian, M.-J. Zeng, J. Qu, Z.-Z. Yu, *ACS Applied Energy Materials*, 3 (2020) 9408-9416.
9. R. Vinodh, Y. Sasikumar, H.-J. Kim, R. Atchudan, M. Yi, *Journal of Industrial and Engineering Chemistry*, 104 (2021) 155-171.
10. J. Huang, X. Song, C. He, Z. Zhang, L. Qu, D. Zhao, *Ionics*, 26 (2020) 2525-2536.
11. M. Ates, *Progress in Organic Coatings*, 71 (2011) 1-10.
12. K. Rossberg, L. Dunsch, *Electrochimica acta*, 44 (1999) 2061-2071.
13. J.G. Martínez Gil, Thesis, (2015).
14. Y.A. Ismail, J.G. Martínez, A.S. Al Harrasi, S.J. Kim, T.F. Otero, *Sensors and Actuators B: chemical*, 160 (2011) 1180-1190.

Chapter 3

Characterization of polyaniline with special emphasis on electrochemical studies

The oxidation/reduction reaction of PANI is revisited here and explored through voltammetric studies. This is the first-time study of detailed analysis of coulovoltammogram of PANI. The electrochemical reaction of PANI induces various molecular structural changes such as relaxation, swelling, shrinking, and compaction which are identified from coulovoltammetric responses. The charge and potentials associated with the reversible processes and irreversible processes are also quantified from coulovoltammograms. The influence of cathodic and anodic potential limits on voltametric and coulovoltammetric Responses are also presented in this chapter.

3.1. Introduction

During the last few decades, PANI has received much attention in both fundamental and practical studies due to its unique electrical and electrochemical properties. Owing to the excellent characteristics such as lightweight, tunable conductivity, low cost of monomer, ease of synthesis, structural diversity and controllable electrical properties of PANI, they are attractive for fabricating a new generation of lightweight, soft and flexible electronic devices [1]. PANI has been studied extensively due to its potential applications in supercapacitors and batteries [1-8], artificial muscles or actuators [9-11], sensors [12-15], electrochromic devices [16-18], electrocatalysts [19-21], solar cells [22, 23], fuel cells [24, 25], tissue engineering [26-28], electromagnetic interference shielding [29, 30], desalination [31], etc. In most of the electronic applications of PANI and the devices based on PANI, the composition is kept constant. Much less attention has been given to PANI to explore its composition dependent properties by the research communities and to design devices based on the electrochemical reaction of PANI. Besides, the structural electrochemistry of PANI has also not been explored yet.

Though, there have been a lot of studies carried out in the field of PANI, the electrochemistry of PANI is not much explored yet. Therefore, the present work is aimed at exploring the electrochemical reaction of PANI with special emphasis on the structural electrochemistry of PANI. The various structural process during the electrochemical reaction is identified and analyzed in terms of consumed charge.

3.2. Results and Discussion

The PANI in the green emeraldine form was synthesized by oxidative chemical polymerization as described in section 2.2 and characterized by FTIR, TGA, BDS, SEM, EDX, cyclic voltammetry and coulombometry. The results are discussed below.

3.2.1. General characterizations

(a) Structural characterization (FTIR spectra)

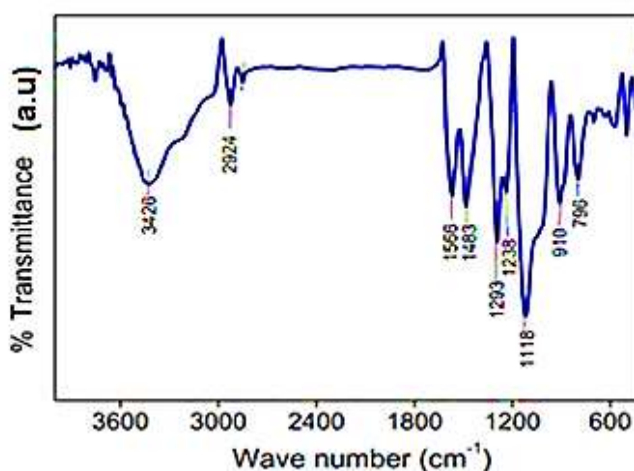


Figure 3.1 FTIR spectra of PANI

The FTIR spectrum of polyaniline recorded in the frequency range of 4000–400 cm^{-1} is shown in Figure 3.1. The broad band at 3426 cm^{-1} corresponds to the stretching vibration of N–H bonds. The peak at 2924 cm^{-1} is attributed to the stretching vibration of C–H in the aromatic ring. The two characteristic peaks of 1566 cm^{-1} and 1483 cm^{-1} correspond to the quinonoid and benzenoid ring C=C vibrations of PANI respectively. Since the intensities of these peaks are almost the same almost equal number of oxidized and reduced rings are present in

the synthesized PANI [32]. The peak at 1293 cm^{-1} is due to C-N stretching vibrations, while the band at 1238 cm^{-1} is ascribed to the C-N⁺ stretching vibration in the polaron structure [33]. The peak at 1118 cm^{-1} is due to the in-plane bending of C-H and the bands at 796 cm^{-1} are assigned to the out-of-plane bending vibration of C-H bonds [34].

(b) Thermal characterization

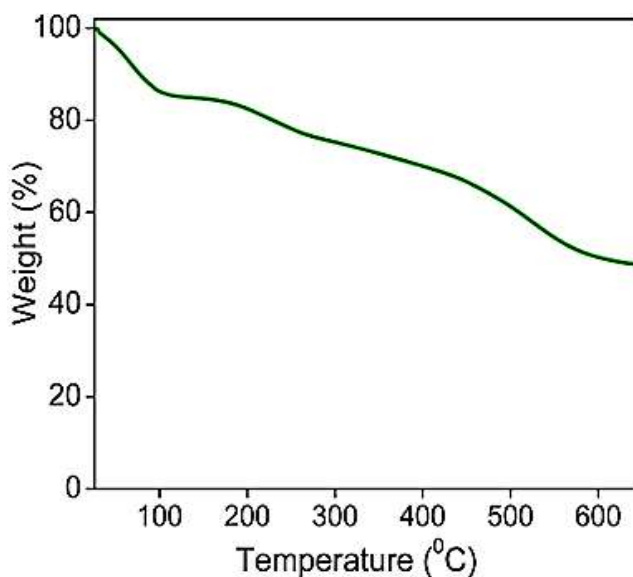


Figure 3.2 TG curve of PANI

The thermal stability of as prepared PANI is analyzed by thermogravimetry and the obtained thermogram is presented in Figure 3.2. The PANI presents three stages of mass loss. The first stage of mass loss up to 105 °C with a weight loss of 15 % corresponds to the loss of water molecules; the second stage, between 180 °C and 270 °C with a weight loss of 12 % is ascribed to the release of low molecular weight oligomers and dopant ions [35]; the third stage, from 450 °C to 580 °C with 18 % of weight loss, is attributed to the degradation of the

polymer chains of PANI through the rupture of the benzene rings and 47 % residue is left at 700 °C. The degradation temperature of PANI is 525 °C [36].

(c) Electrical characterization

The electrical conductivity of pelletized PANI was measured using a broad-band dielectric spectrometer, and the frequency-dependent conductivity is illustrated in Figure 3.3. The electrical conductivity values were obtained by fitting the curve with Jonscher's power law. The conductivity is $4.9 \times 10^{-2} \text{ S cm}^{-1}$, which indicates the semiconducting nature of PANI.

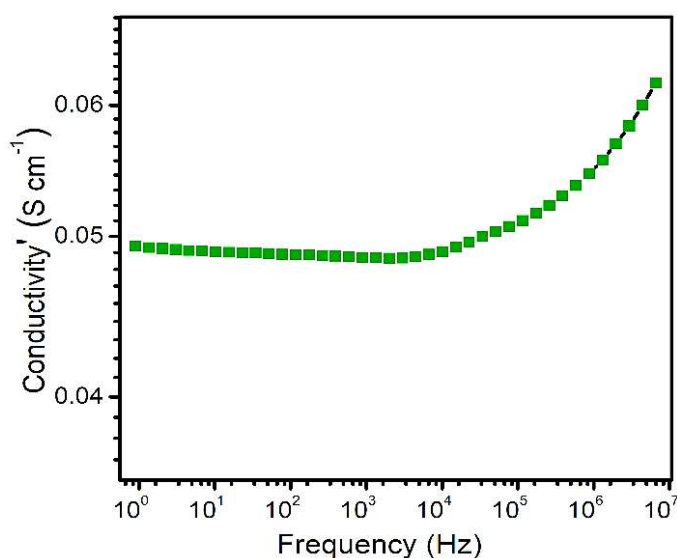


Figure 3.3 Frequency dependent conductivity of PANI

(d) Morphological characterization

The morphology of synthesized PANI was investigated by FESEM analysis. Figure 3.4 is the FESEM image and it revealed that

polyaniline grown with coral-like nanowire structures during the chemical polymerization of aniline. The figure demonstrates the presence of substantial porosity in PANI, which facilitates the diffusion of ions and solvent molecules for efficient electrochemical reactions.

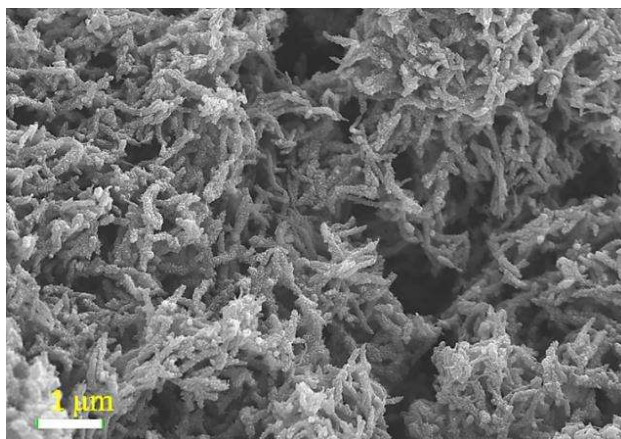


Figure 3.4 FESEM image of PANI

3.2.2. Electrochemical characterization

3.2.2.1. Cyclic Voltammetry

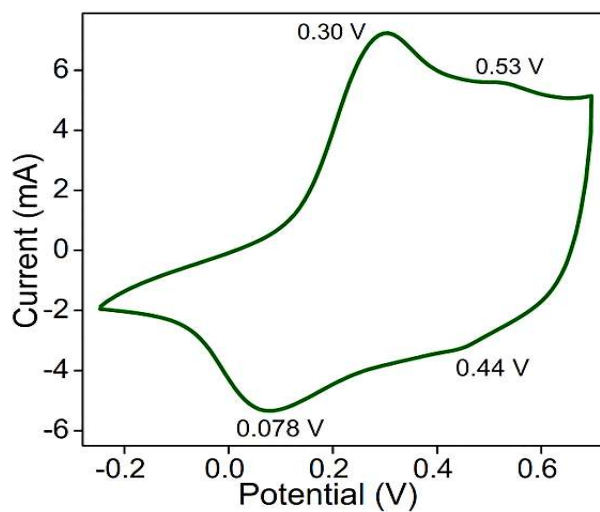


Figure 3.5 CV curve of PANI at a scan rate of 25 mV s^{-1}

The electrochemical activity of PANI was studied by cyclic voltammetry. The stationary cyclic voltammogram of PANI at a scan rate of 25 mV s^{-1} in 1M HCl between the potential limits of -0.25 V and $+0.7 \text{ V}$ after 30 consecutive cycles (for stabilizing the film) is shown in Figure 3.5. A pair of the anodic and cathodic peaks corresponding to PANI oxidation and reduction, respectively, are observed in CV. During oxidation, the characteristic peaks at 0.30 V and 0.53 V correspond to the transition from leucoemeraldine (LE) to emeraldine (ES) and emeraldine to pernigraniline (PN) form of PANI, respectively. During reduction, it comes back to the leucoemeraldine state through two transitions and the corresponding peaks are observed at 0.44 V and 0.078 V , respectively.

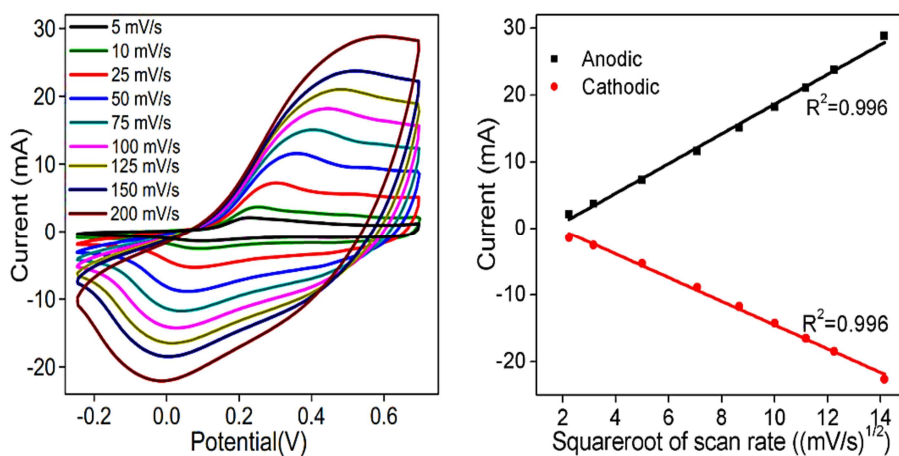
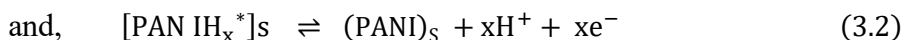
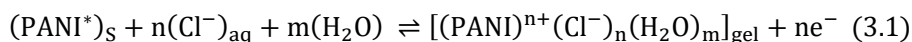


Figure 3.6 (a) CV of PANI at different scan rates and **(b)** linear variation of anodic and cathodic peak currents with the square root of scan rate

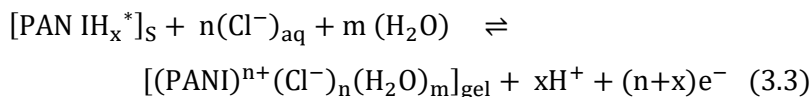
The CVs of PANI recorded at various scan rates are depicted in Figure 3.6a. As the scan rate increases, the oxidations are shifted to more positive values and reductions are shifted to more negative values, because the redox reaction becomes more resistive at a higher scan rate

due to the slow entry/ejection of counter ions through the electrode [37, 38]. Figure 3.6b exhibits good linear dependence of oxidation or reduction peak currents with the square root of scan rate up to 200 mV s⁻¹, which reveals that the redox process of the PANI electrode is diffusion controlled up to 200 mV s⁻¹ [38].

During the anodic oxidation, the PANI polymer chain becomes positively charged. The Cl⁻ ions and H₂O molecules from the electrolyte are diffused into the polymer chain for charge neutrality and osmotic balance, respectively, and followed by the expulsion of the proton. During the cathodic reduction, the reverse process happens; protons are reduced and incorporated into the polymer chain and the Cl⁻ ions and the H₂O molecules are expelled out. The reactions concerning the PANI oxidation/reduction can be written as:



The overall reaction can be written as:



Where PANI* or PANIH_x* represents the electroactive center. During the electrochemical reaction, the subindex means solid. The composition changes from [PANIH_x*] to dense polymer gel [(PANI)ⁿ⁺(Cl⁻)_n(H₂O)_m]. This process takes place through *n* consecutive steps of one electron per

step, which is the formation of one polaron on the chain per step. There is a continuous variation of composition by continuous insertion/extraction of electrons from the polymer chains under faradaic control which are responsible for the composition-dependent material properties. Polymer swells during oxidation and shrinks during reduction. The schematic representation of the oxidation/reduction process in PANI is depicted in Figure 3.7.

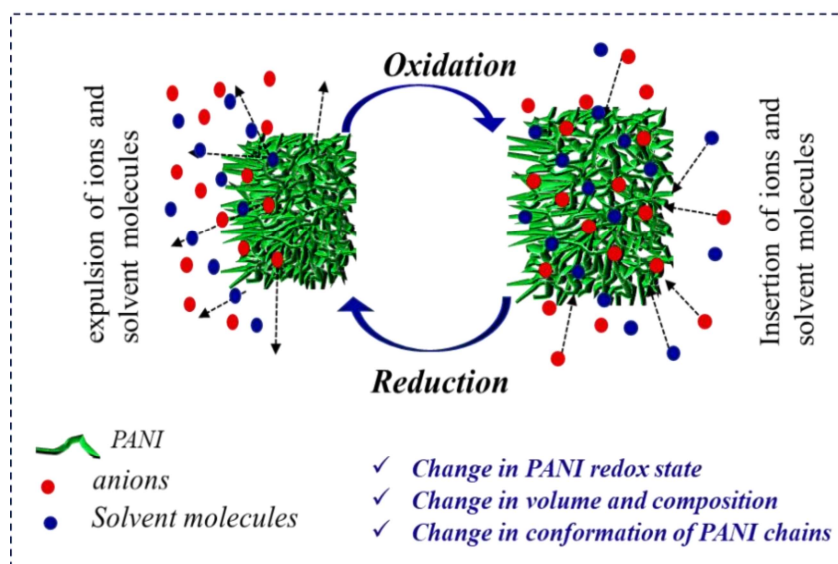


Figure 3.7 Schematic representation of the redox process in PANI

3.2.2.2. Coulovoltammetry

Coulovoltammogram (QV, plot of consumed charge vs. applied potential) is the representation of charge consumed during the oxidation/reduction reaction obtained by the integration of CVs. Figure 3.8 is the normalized QV of PANI obtained by the integration of CV recorded at a scan rate of 25 mV s^{-1} (Figure 3.6).

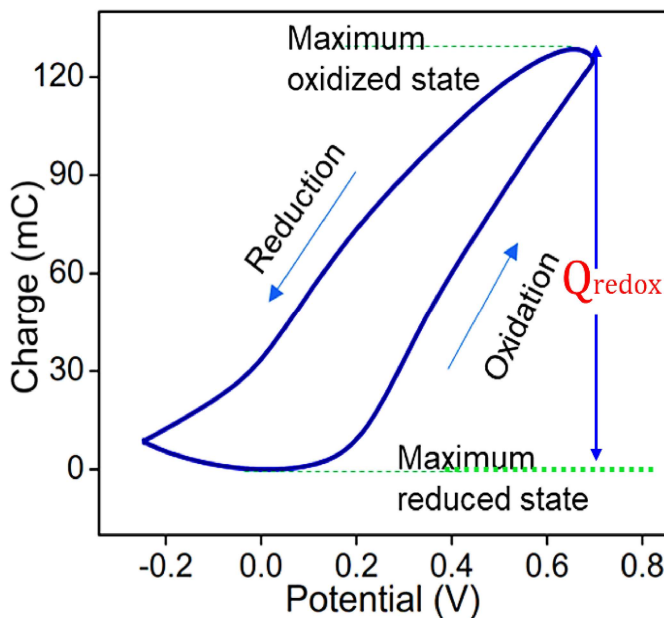


Figure 3.8 Coullovoltammogram of PANI at a scan rate of 25 mV s^{-1}

The minimum of QV response is taken as the zero-charge reference and the oxidation processes give positive charge increments while reduction processes give negative charge increments. A practically closed QV loop is obtained in the full studied potential range (-0.25 V to 0.7 V). This implies that the anodic charge is equal to the cathodic charge and only reversible oxidation/reduction reactions are involved in the studied potential range [39]. The charge difference between the minimum and maximum of the closed loop is the **redox charge** (Q_{redox}) involved in the reversible oxidation/reduction reaction (reaction 3.3). This closed loop has an abrupt slope (Q/E) variation. The charge (Q) depends on the number (n) of exchanged ions, according to Faraday's second law:

$$n = \frac{Q}{zF} \quad (3.4)$$

where z represents the charge of the exchanged ion and F is the Faraday constant. The reaction rate (r) is defined by the rate of change of the specific (per unit of polymer mass, w) concentration of ions in the polymer. For an empirical potential sweep rate, $v = dE/dt$, the PANI reaction rate is written as:

$$r = \frac{dn}{dt} = \frac{d\left(\frac{Q}{zF}\right)}{d\left(\frac{E}{v}\right)} = \frac{dQ \cdot v}{zF \cdot dE} = \frac{v}{zF} \cdot \frac{dQ}{dE} \quad (3.5)$$

Where dQ/dE is the slope at any point in Figure 3.8 and the slope change indicates a parallel change in the reaction rate (r) which is associated with structural changes.

3.2.2.3. Structural faradic processes in PANI; characteristic potentials and related charges

QV is a graphical tool for the separation of the different structural processes during the electrochemical reaction that is mathematically defined by the Electrochemically Stimulated Conformational Relaxation (ESCR) model [38, 40]. It enables the quantitative determination of the charge consumed by each of these constitutive structural faradic processes during reaction 3.3.

The closed QV loop of PANI has six types of basic structural slope variations during the electrochemical reactions of PANI: as shown in Figure 3.9. They are reduction-shrinking (comprises two stages), reduction-compactation, oxidation-relaxation and oxidation-swelling (comprises two stages).

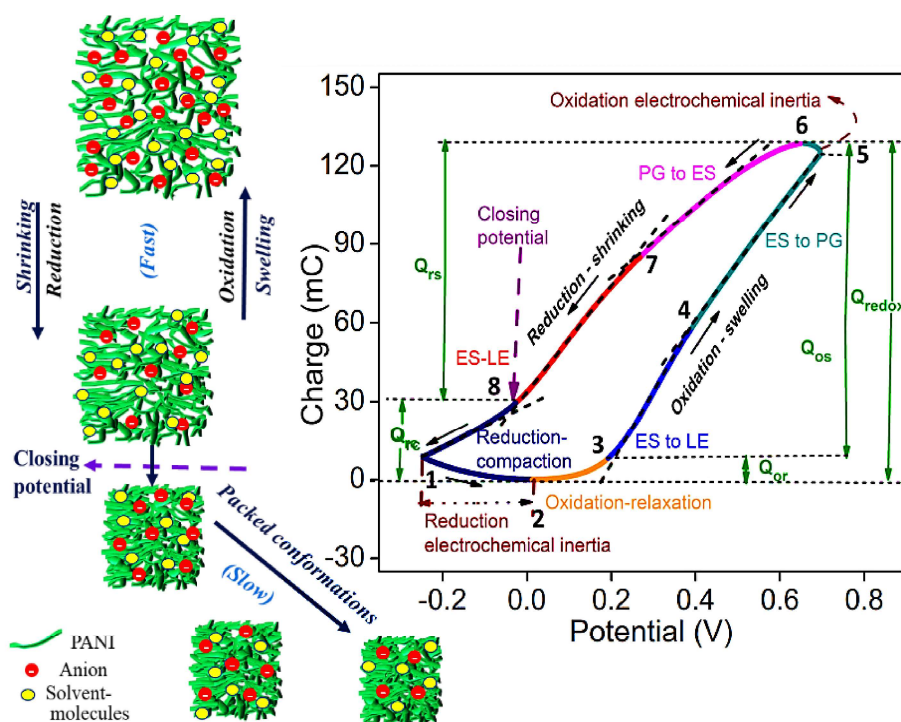


Figure 3.9 Coulo Voltammogram of PANI at a scan rate of 25mV s^{-1}

The maximum of QV corresponds to the highest oxidized state of PANI (point 6 in Figure 3.9). From this point, the **fast reduction process** (high Q/E slope in Figure 3.9) is initiated (backward reaction in 3.3) which includes two processes: insertion of proton to the polymeric chain (pernigraniline to emeraldine conversion, points 6 to 7 in Figure 3.9) and followed by the expulsion of anions (Cl^-) and solvent molecules (emeraldine to leucoemeraldine conversion, points 7 to 8 in Figure 3.9). The fast reduction causes the fast shrinking of polymer chains. This **reduction-shrinking** of the material goes on under kinetic control of diffusion of the counterions to the solution. After that (from point 8), polymer reduction continues with a slower reduction rate (lower slope) upon increasing the cathodic potential. As the reduction/shrinking goes

on, the average distance between neighboring polymeric chains becomes equal to the diameter of the hydrated counterion unit at a certain potential (at point 8), and the dense polymer closes the gel structure. This potential is referred to as ***closing potential, Ec***. At this stage, a large number of counter ions involved in the oxidation process are trapped between polymer chains [38]. Ionic trapping is one of the well-described processes in the electrochemistry of CPs [41-44]. On rising the cathodic potential beyond the closing potential, the reduction does not stop but continues with a lower reaction rate. Because the anions leaving from the material must push the polymer chains apart (conformational movements) to open their way toward the solution. That is, after closing potential, the reaction occurs under kinetic control of those slow conformational movements of the polymer chains [38]. Thus, the polymer compacts (shrinks further) to give more packed conformational energetic states and this structural process is termed as ***reduction-compaction***. This slow reduction (negative increment of the charge) or reduction compaction continued at the beginning of subsequent anodic potential sweep up to 0.0124 V i.e., up to the QV minimum (from point 1 to 2 in Figure 3.9). Because the reduction overpotential and conformational mobility is still high enough at the beginning of the anodic sweep, the polymer still is partially oxidized at -0.25 V and the reduction goes on. This is the ***oxidation electrochemical inertia***. The continuity of the reduction compaction process ahead of the cathodic potential sweep inside the anodic potential sweep is fully realized by presenting the coulombometric responses as chronocoulometric (Q vs t) responses. Figure 3.10 represents the Chronocoulogram attained from the QV (-0.25 V to 0.7 at 25 mV s⁻¹) and the red slope region represents the

reduction compaction process. The continuous decrease of the charge corroborates the faradic nature of the process.

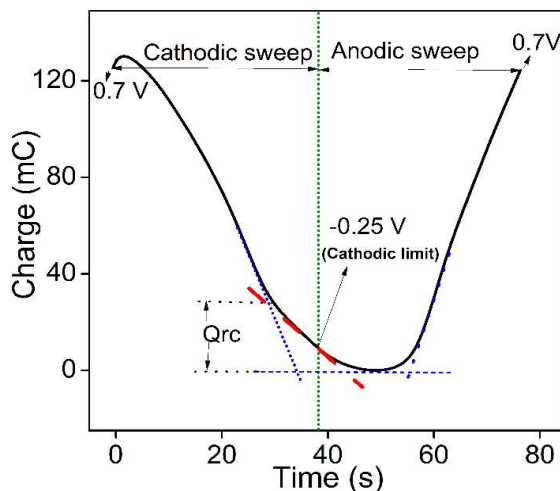


Figure 3.10 Chronocouloulogram attained from the QV (-0.25 V to 0.7 V at 25 mV s^{-1}) showing the continuity of the faradic reduction compaction (Q_{rc}) during the anodic potential sweep.

The oxidation of the PANI chains is initiated from the QV minimum. At the onset, the conformational relaxation of polymer chains initiates the opening of the compact structure, generating the required free volume for anions to enter from the solution. This structural process is the **oxidation-relaxation** (from 2 to 3) and the potential at a minimum of QV is the **relaxation potential (E_r)**. After this relaxation process **fast oxidation process** (high anodic Q/E slope in Figure 3.9) is initiated (reaction 3.3) which includes two processes: insertion of anions and water molecule from solution for charge and osmotic balance to the polymeric chain (leucoemeraldine to emeraldine conversion, 3 to 4 in Figure 3.9) which is followed by the expulsion of proton (emeraldine to pernigraniline conversion, 4 to 5 in Figure 3.9). The fast oxidation causes fast swelling of polymer chains. This **oxidation-swelling** of PANI goes

on under kinetic control through diffusion of the counterions from the solution. At 0.7 V, the anodic potential limit, (point 5 in figure 3.9) the maximum anodic over potential is attained but the polymer does not get enough time to complete the oxidation: its oxidation is completed at just the beginning of the cathodic potential sweep until the coulovoltammetric maximum. This is the *oxidation electrochemical inertia* (5 to 6). The characteristic potential ranges of each structural process associated with the electrochemical reaction of PANI are listed in Table 4.1.

Table 4.1 Structural faradic processes in PANI, characteristic potential ranges and associated electrical charges

Structural Process	Potential range (V)	Consumed charge (mC)
Fast reduction/ shrinking	0.657 to -0.052	$Q_{\text{frs}} = -98.95$
Reduction compaction	-0.052 to 0.0124	$Q_{\text{rc}} = -29.48$
Oxidation relaxation	0.0124 to 0.182	$Q_{\text{or}} = 6.83$
Fast oxidation/ swelling	0.182 V to 0.7 V	$Q_{\text{fos}} = 117.6$
Oxidation inertia	0.7 V to 0.657 V	$Q_{\text{oi}} = 4.092$
Total oxidation process	0.0124 to 0.657	$Q_{\text{ox}} = Q_{\text{or}} + Q_{\text{fos}} + Q_{\text{oi}} = 128.5$
Total reduction process	0.657 to -0.2 (potential minima) to 0.0124	$Q_{\text{red}} = Q_{\text{frs}} + Q_{\text{rc}} = -128.5$

3.2.2.4. Influence of the cathodic potential limit on voltammetric and coulometric responses

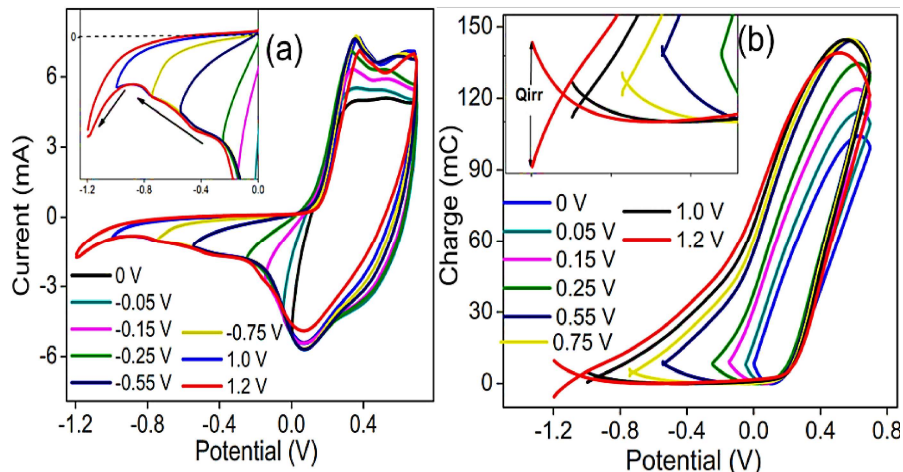


Figure 3.11 (a) CVs obtained for PANI in 1 M HCl at 25 mV s^{-1} from different cathodic potential limits. (b) QVs obtained by integration of the CVs from (a).

Figure 3.11a represents the steady state CVs corresponding to different cathodic potential limits to a constant anodic potential limit of 0.7 V. All the CVs obtained after two consecutive potential cycles applied to the PANI electrode recorded at 25 mV s^{-1} in 1 M HCl solution at room temperature. The memory of any previous structural changes is deleted during the first potential cycle and attains steady-state CV responses from the second cycle onwards. The figure can convey insight into the following facts:

- (i) On the cathodic side only small current flows as the reduction goes on beyond -0.2 V until the beginning of the subsequent anodic potential sweep. This fact arises an important question: In which cathodic potential limits does the PANI reduction end?

- (ii) As the cathodic potential limit increases, the oxidation peak current increases, which indicates that PANI undergoes deeper reduction upon increasing the cathodic potential limit. The question arises is that: what is the maximum potential range for reversible oxidation/reduction of this PANI electrode?
- (iii) During the potential sweep beyond -0.8 V, the reduction current increases, which indicates the presence of a new reduction process. The question is: what will be the nature of the new reduction process? Is it reversible or irreversible?

The coulombometry helps explain the above facts, which separate different reactions and structural processes in terms of involved charge during the reaction [45]. Figure 3.11b represents the coulombometric responses attained by the integration of the CVs depicted in Figure 3.11a and the following inferences are obtained from the figure.

- (i) The small current flows as the reduction goes on beyond -0.2 V due to the slow reduction compaction of PANI.
- (ii) The closed QV loops are obtained up to a cathodic potential limit of -0.25 V. Concluding that inside the potential range from -0.25 V to 0.7 V, this PANI electrode has only reversible redox processes (oxidation charge equals the reduction charge).
- (iii) Beyond -0.25 V, QVs show two parts: (1) A closed loop that quantifies the charge involved in the reversible redox processes and (2) an open part outside the loop related to irreversible reduction. The difference between the beginning and the end of the open part of QV gives the irreversible reduction charge (Q_{irr}).

Therefore, $Q(\text{reduction}) = Q_{\text{redox}} + Q_{\text{irr}}$

- (iv) Beyond -0.25 V the PANI reversible reaction overlaps with irreversible reduction attributed to the hydrogen evolution from the electrode
- (v) The reduction goes on beyond the voltammetric reduction maximum. The oxidation/reduction charge variation for the cathodic potential limit is shown in Figure 3.12a.
- From 0 to -0.3 V oxidation and reduction charges are overlapped (reversible reaction) and follow a linear variation with the cathodic potential limit.
 - Beyond -0.3 V the charge has two components: Q_{redox} and Q_{ir} .
 - From -0.3 V to -1 V, the redox charge shows a linear increase, but at a slower rate.
 - The redox charge decreases at -1.2 V. This decrease is due to incomplete oxidation of the reduced PANI at the anodic limit of 0.7 V, which is caused by the anodic shift of the oxidation peak to higher potentials. It is clear from Figure 3.11a, the second oxidation peak shifted beyond the potential limit. Consequently, only a fraction of the reduced state attained at high cathodic potential is re-oxidized during the subsequent anodic potential sweep.
- (vi) The irreversible charge consumed by this irreversible reduction also increases for increasing cathodic potential limits. Figure 3.12b depicts the exponential increase of irreversible reduction charge with respect to the cathodic potential limit.
-

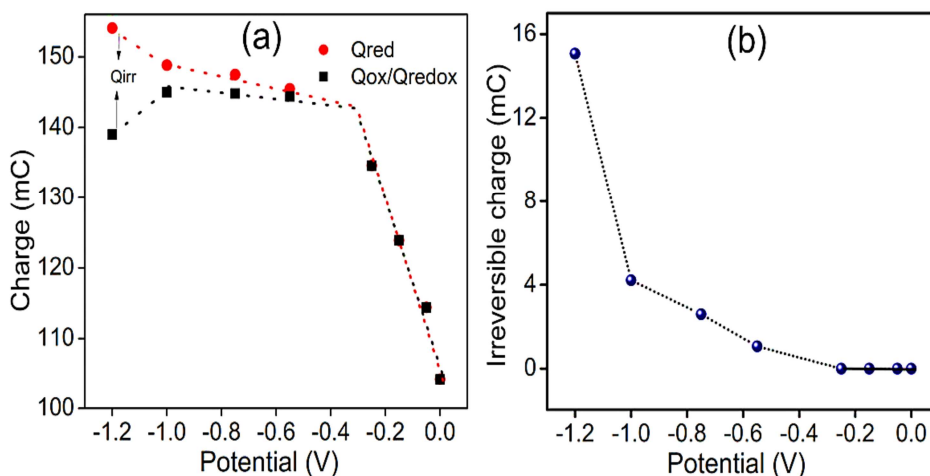


Figure 3.12 (a) Charge involved in the oxidation and reduction of PANI and **(b)** irreversible reduction charge for different cathodic potential limits (only magnitudes of the charges are considered for plotting)

3.2.2.5. Influence of the anodic potential limit on the voltammetric and coulometric responses

From the above discussion, it is clear that only the reversible processes during the electrochemical reaction of PANI can take place (gives closed charge loops) for a range of cathodic potential limits between 0 V and -0.3 V. So, an intermediate potential of -0.25 V was taken as the cathodic potential limit to investigate the influence of the anodic potential limit on the PANI electrode processes. Figure 3.13a represents the stationary CV responses obtained after two consecutive potential sweeps for different anodic potential limits. All the CVs are recorded at a scan rate of 25 mV s^{-1} in 1 M HCl at room temperature and pressure. Figure 3.13b represents the corresponding QV responses. The following inferences are made from this study.

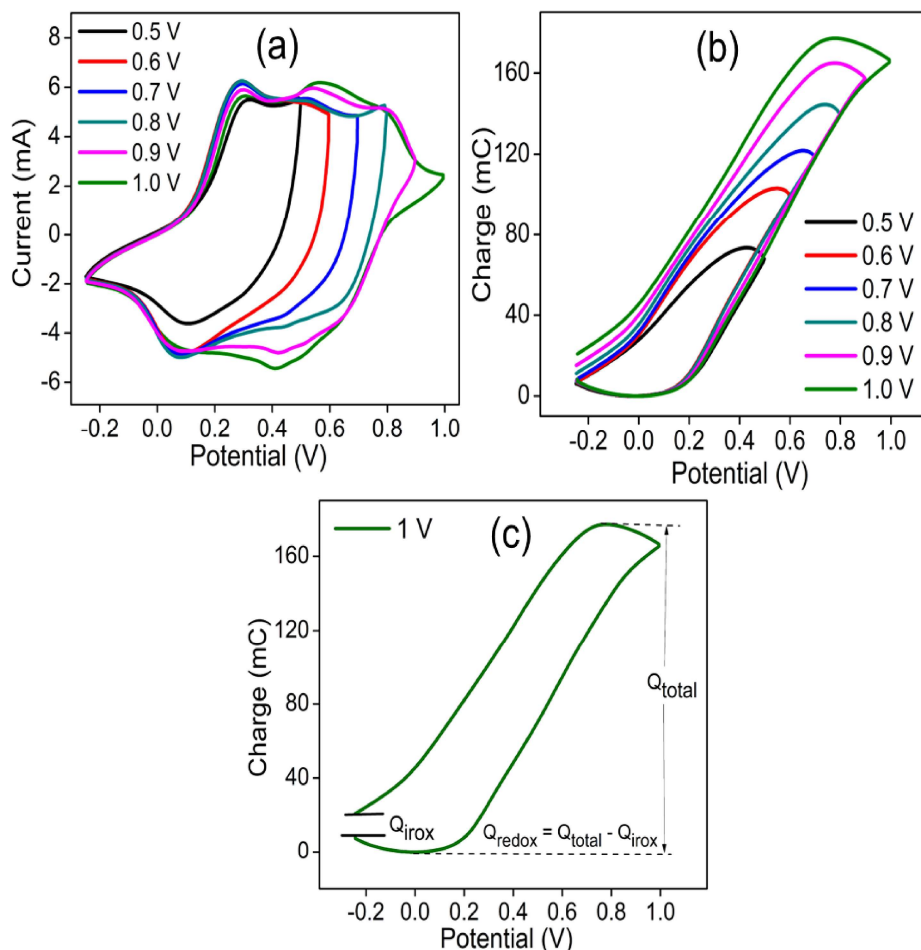


Figure 3.13 (a) CVs obtained for PANI in 1M HCl at 25 mV s⁻¹ from different anodic potential limits. (b) Corresponding QVs. (c) Open loop QV shows the charge involved in the new irreversible oxidation process represented as Q_{irox}

- (i) The anodic limits lower than 0.7 V give closed QV loops. That is only the reversible reaction occurs up to the anodic potential of 0.7V.
- (ii) Anodic potential limits higher than 0.7 V give open QV loops (Figure 3.13c): the oxidation charges are higher than the reduction charges which means that a new irreversible oxidation occurs.

-
- (iii) The charge consumed during this irreversible oxidation process (Q_{irox}) is equal to the difference between charges at the beginning and the end of the open loop (Figure 3.13c). So, the reversible charge (Q_{redox}) is obtained by:

$$Q_{\text{redox}} = Q_{\text{total}} - Q_{\text{irox}}$$

$$Q_{\text{total}} = QV_{\text{maximum}} - QV_{\text{minimum}}$$

- (vii) Beyond 0.7 V the PANI reversible reaction overlaps with irreversible oxidation which is attributed to the overoxidation, incomplete reduction or oxygen evolution from the electrode.
- (viii) The oxidation/reduction charge variation with respect to the anodic potential limit is shown in Figure 3.14a. From 0.5 V to 0.7 V oxidation and reduction charges are overlapped with each other, i.e., only reversible oxidation/reduction reactions are involved in these potential limits. It follows a linear variation with the anodic potential limits. Then the redox charge increases at a slower rate. Beyond 0.7 V the charge has two components: reversible and irreversible charge.
- (ix) The irreversible charge consumed by this irreversible oxidation also increases for increasing anodic potential limits as shown in Figure 3.14b.
- (x) In the studied potential ranges the coul voltammograms show the same structural processes as described above.

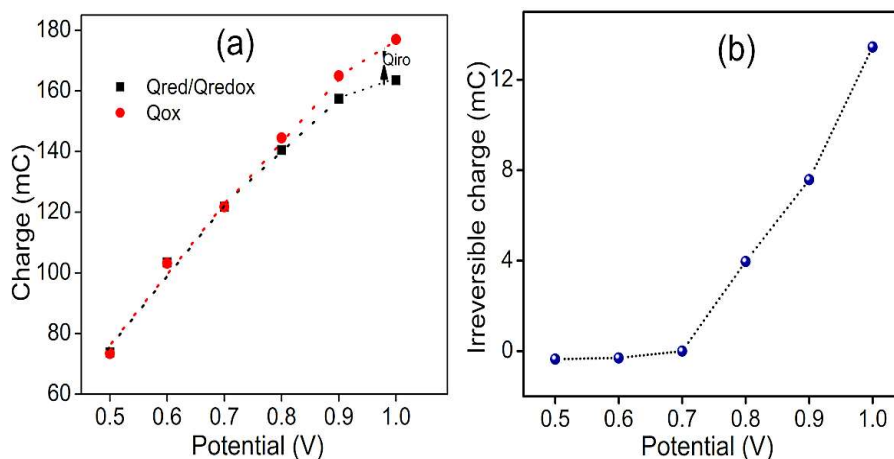


Figure 3.14 (a) Charge involved in the oxidation and reduction of PANI and (b) irreversible reduction charge for different anodic potential limits (only magnitudes of the charges are considered for plotting)

3.3. Conclusion

Though PANI has been studied extensively by researchers, a new insight into the electrochemistry of PANI is presented for the first time through assessing the electrochemical redox reaction of PANI and quantifying the charge consumed during the reaction, this has been done through analyzing QVs. Detailed analysis of QVs of PANI is also studied first time.

Chemically synthesized PANI with coral-like nanowire morphology was characterized by FTIR, TG, electrical conductivity measurements, cyclic voltammetry and coulombometry. The synthesized PANI has an electrical conductivity of $4.88 \times 10^{-2} \text{ S cm}^{-1}$. The degradation temperature of PANI is $525 \text{ }^\circ\text{C}$. The CV shows two characteristic anodic and cathodic peaks. The anodic peaks correspond to the transition from leucoemeraldine to emeraldine and emeraldine to

pernigraniline forms of PANI, respectively, and the reverse during reduction. Coulovoltammetric responses to potential cycles from PANI electrodes are presented here as a good electrochemical tool to identify and separate the different structural components of the electrode reaction: oxidation/diffusion (fast), oxidation relaxation (slow), reduction/diffusion (fast) and reduction compaction (slow). Beyond the cathodic potential of -0.3 V, the reversible process overlaps with irreversible reduction and beyond the anodic potential of 0.7 V reversible process overlaps with irreversible oxidation. That is, the PANI electrode has only a reversible process in the potential window of -0.3 V to 0.7 V. The charges consumed by each reversible and irreversible process are also quantified from the coulovoltammogram.

References

1. J. Banerjee, K. Dutta, M.A. Kader, S.K. Nayak, *Polymers for Advanced Technologies*, 30 (2019) 1902-1921.
2. S.K. Simotwo, V. Kalra, *Current Opinion in Chemical Engineering*, 13 (2016) 150-160.
3. H. Wang, J. Lin, Z.X. Shen, *Journal of science: Advanced materials and devices*, 1 (2016) 225-255.
4. Y. Chen, *IOP Conference Series: Materials Science and Engineering*, IOP Publishing, 2019, pp. 022115.
5. A. Eftekhari, L. Li, Y. Yang, *Journal of Power Sources*, 347 (2017) 86-107.
6. P. Liu, J. Yan, Z. Guang, Y. Huang, X. Li, W. Huang, *Journal of Power Sources*, 424 (2019) 108-130.
7. S. Shaheen Shah, S. Oladepo, M. Ali Ehsan, W. Iali, A. Alenaizan, M. Nahid Siddiqui, M. Oyama, A.R. Al-Betar, M.A. Aziz, *The Chemical Record*, (2023) e202300105.

8. Y. Luo, R. Guo, T. Li, F. Li, Z. Liu, M. Zheng, B. Wang, Z. Yang, H. Luo, Y. Wan, *ChemSusChem*, 12 (2019) 1591-1611.
 9. Y.A. Ismail, S.R. Shin, K.M. Shin, S.G. Yoon, K. Shon, S.I. Kim, S.J. Kim, *Sensors and Actuators B: Chemical*, 129 (2008) 834-840.
 10. K. Kaneto, M. Kaneko, Y. Min, A.G. MacDiarmid, *Synthetic Metals*, 71 (1995) 2211-2212.
 11. E. Smela, W. Lu, B.R. Mattes, *Synthetic metals*, 151 (2005) 25-42.
 12. N. Shoaie, M. Daneshpour, M. Azimzadeh, S. Mahshid, S.M. Khoshfetrat, F. Jahanpeyma, A. Gholaminejad, K. Omidfar, M. Foruzandeh, *Microchimica Acta*, 186 (2019) 1-29.
 13. J. Janata, M. Josowicz, *Nature materials*, 2 (2003) 19-24.
 14. T. Sen, S. Mishra, N.G. Shimpi, *RSC advances*, 6 (2016) 42196-42222.
 15. Q. Al-Haidary, A. Al-Mokaram, F. Hussein, A. Ismail, *Journal of Physics: Conference Series*, IOP Publishing, 2021, pp. 012062.
 16. R.J. Mortimer, *Annual review of materials research*, 41 (2011) 241-268.
 17. W. Li, T. Bai, G. Fu, Q. Zhang, J. Liu, H. Wang, Y. Sun, H. Yan, *Solar Energy Materials and Solar Cells*, 240 (2022) 111709.
 18. Q. Liu, L. Yang, W. Ling, B. Guo, L. Chen, J. Wang, J. Zhang, W. Wang, F. Mo, *Frontiers in Chemistry*, 10 (2022) 1001425.
 19. S. Liu, H. Xu, J. Ou, Z. Li, S. Yang, J. Wang, *Materials Chemistry and Physics*, 132 (2012) 500-504.
 20. E. Eskandari, M. Kosari, M.H.D.A. Farahani, N.D. Khiavi, M. Saedikhani, R. Katal, M. Zarinejad, *Separation and Purification Technology*, 231 (2020) 115901.
 21. S.L. Madaswamy, A.A. Allothman, M. mana AL-Anazy, A.A. Ifseisi, K.N. Alqahtani, S.K. Natarajan, S. Angaiah, D. Ragupathy, *Journal of Industrial and Engineering Chemistry*, 97 (2021) 79-94.
 22. K. Saranya, M. Rameez, A. Subramania, *European Polymer Journal*, 66 (2015) 207-227.
 23. S. Ghani, R. Sharif, S. Shahzadi, N. Zafar, A. Anwar, A. Ashraf, A.A. Zaidi, A.H. Kamboh, S. Bashir, *Journal of Materials Science*, 50 (2015) 1469-1477.
-

24. C.-H. Wang, C.-C. Chen, H.-C. Hsu, H.-Y. Du, C.-P. Chen, J.-Y. Hwang, L.-C. Chen, H.-C. Shih, J. Stejskal, K.-H. Chen, *Journal of Power Sources*, 190 (2009) 279-284.
25. J. Yang, P.K. Shen, J. Varcoe, Z. Wei, *Journal of power sources*, 189 (2009) 1016-1019.
26. R. Balint, N.J. Cassidy, S.H. Cartmell, *Acta biomaterialia*, 10 (2014) 2341-2353.
27. B. Kheilnezhad, A. Safaei Firoozabady, A. Aidun, *Journal of Tissues and Materials*, 3 (2020) 6-22.
28. R. Rai, J.A. Roether, A.R. Boccaccini, *Progress in Biomedical Engineering*, (2022).
29. N. Maruthi, M. Faisal, N. Raghavendra, B. Prasanna, K. Nandan, K.Y. Kumar, S.B. Prasad, *Materials Chemistry and Physics*, 259 (2021) 124059.
30. M. Zahid, R. Anum, S. Siddique, H.F. Shakir, Z. Rehan, *Journal of Thermoplastic Composite Materials*, 36 (2023) 1717-1761.
31. Y.A. Ismail, *Desalination*, 250 (2010) 523-529.
32. M. Trchova, J. Stejskal, J. Prokeš, *Synthetic Metals*, 101 (1999) 840-841.
33. W. Shao, R. Jamal, F. Xu, A. Ubul, T. Abdiryim, *Materials*, 5 (2012) 1811-1825.
34. M. Trchová, J. Stejskal, *Pure and Applied Chemistry*, 83 (2011) 1803-1817.
35. K. Wu, J. Yu, X. Jiang, *Adsorption Science & Technology*, 36 (2018) 198-214.
36. A. Kumar, A. Kumar, H. Mudila, V. Kumar, *Journal of Physics: Conference Series*, IOP Publishing, 2020, pp. 012108.
37. J.H. Shendkar, V.V. Jadhav, P.V. Shinde, R.S. Mane, C. O'Dwyer, *Heliyon*, 4 (2018) e00801.
38. L.B.J. da Silva, R.L. Oréfice, *Journal of Polymer Research*, 21 (2014) 466.
39. T.F. Otero, M. Alfaro, V. Martinez, M.A. Perez, J.G. Martinez, *Advanced Functional Materials*, 23 (2013) 3929-3940.

40. T. Otero, I. Boyano, *The Journal of Physical Chemistry B*, 107 (2003) 6730-6738.
41. J. Bisquert, *Electrochimica Acta*, 47 (2002) 2435-2449.
42. M. Levi, Y. Gofer, D. Aurbach, A. Berlin, *Electrochimica Acta*, 49 (2004) 433-444.
43. G.r. Frenning, A. Razaq, K. Gelin, L. Nyholm, A. Mihranyan, *The Journal of Physical Chemistry B*, 113 (2009) 4582-4589.
44. B. Malinowska, K. Maksymiuk, *Electroanalysis: An International Journal Devoted to Fundamental and Practical Aspects of Electroanalysis*, 15 (2003) 263-269.
45. H. Grande, T. Otero, *The Journal of Physical Chemistry B*, 102 (1998) 7535-7540.

Chapter 4

Reaction driven sensing characteristics of polyaniline: A chronopotentiometric and voltammetric investigation

The reaction driven sensing characteristics of PANI towards working conditions are studied. The electrical energy consumed during the redox reaction of PANI can respond to or senses working electrical, chemical and or thermal conditions, which is studied by chronopotentiometry. The reaction extension defined by consumed electrical charge can also sense the imposed energetic conditions such as electrical, chemical and or thermal conditions, which is studied by voltammetry. The detailed theoretical approach for the sensing of PANI through consumed electrical energy and consumed charge as sensing magnitudes are also included in this chapter.

4.1. Introduction

CPs are electroactive materials that can be oxidized/reduced by the flow of anodic/cathodic currents in suitable electrolytes. During the redox process the distribution of sigma and double bond along the polymer chain changes. It induces conformational movements of the polymeric chain. This results in the coiling/uncoiling of the polymeric chain during oxidation/reduction, which is reversible during the electrochemical reaction. Therefore, CPs are considered as a macromolecular motor [1-3]. During the reaction n electrons are extracted in n consecutive steps, each step involving one electron transfer. Therefore, CPs are considered multistep electrochemical molecular motors/machines [4, 5]. The ions and solvents are exchanged with electrolytes during the reaction for charge neutrality and osmotic pressure balance, respectively, which causes swelling and shrinking (expansion and contraction of the polymer chain) of the system. This kind of composition variation through a reaction is reminiscent of the biological processes occurring in the functional living cell [6-8]. In short, CPs are dense and reactive gels constituted by electrochemical molecular machines of the polymer chain, ions and water, therefore, they constitute a simple artificial model of the intracellular matrix of living cells.

In the sensor literature, different electroactive materials such as CPs, graphene and carbon nanotubes have been used as electrodes for classical electrochemical sensors of analytes or species in the electrolyte or species adsorbed on the electrodes [9-15]. These materials act as electrodic supports or electrodic catalysts for different sensing purposes.

A unique approach for electrochemical sensing of CPs was proposed by Otero and co-workers: the electrochemical reactions of CPs can sense by themselves (self-sensing) the reaction conditions such as mechanical, thermal, chemical, and electrical conditions [16-18]. They explored how the potential evolution, charge and electrical energy consumed during the electrodic reaction are influenced by the different physical and chemical environments.

The electrochemical reactions of CPs work outside the equilibrium condition. i.e., take place through n consecutive steps and there is a continuous composition variation during the reaction. The Nernst equation and the typical Le-Chatelier principle are not applicable in such systems. Otero and co-workers reformulated the Le-Chatelier principle that can be applied to such systems: any physical or chemical perturbation (energetic disturbances) acting on the reaction rate (during the flow of a constant current) will shift the reaction overpotential or reaction energy to adapt the new imposed energetic condition (Otero's principle) [19, 20]. That is any energetic disturbance such as chemical, thermal, electrical, or mechanical perturbations is detected, or "sensed", by the electrochemical reactions of the polymer from the potential evolution or consumed electrical energy during the reaction [17, 18]. Broadly, in any electrochemical device based on the electrochemical reaction of CPs (supercapacitors, batteries, actuators, smart windows, etc), the potential evolution or consumed electrical energy during their working will respond to or sense the changes of internal and surrounding conditions.

This multifunctionality has been studied and verified by the group of Otero using different types of polypyrrole materials by developing simultaneous sensing artificial muscle and has proposed a physicochemical self-consistent model describing, quantitatively, the dual sensing-actuating behaviours of polypyrrole [17, 18, 21, 22]. We are trying to establish the fact that; all the conducting polymers behave in a similar way and the reaction driven sensing capability is the general property of all CPs.

Since there are no studies on the reaction driven sensing of pure PANI material, this chapter addresses the self-sensing capability of chemically synthesized PANI with respect to its surrounding conditions from an aqueous HCl medium. This is a primary requirement for proposing and implementing PANI based novel sensing-motor technologies. In this chapter, the reaction driven sensing property of PANI is studied by two methods: (1) by chronopotentiometry, where consumed electrical has a sensing parameter and (2) by voltammetry, where consumed charge (reaction extension) as sensing magnitude. That is, here we studied how the reactions respond to or sense the electrical, thermal and chemical working conditions in terms of consumed electrical energy and consumed charge and put forward a theoretical explanation for this electrochemical sensing behavior of PANI. This study is useful for developing PANI based soft wet reactive sensing devices, which is noteworthy for developing bifunctional, tri-functional or multifunctional devices working based on an electrochemical reaction.

4.2. Results and Discussion

I. Reaction driven sensing characteristics of PANI: A chronopotentiometric investigation

4.2.1. Theoretical description

The rate of PANI forward reaction (reaction 3.3), r , is expressed as;

$$r = k_a[\text{PANIH}_x^*]^a [\text{Cl}^-]^b [\text{H}^+]^{-c} \quad (4.1)$$

Where, kinetic coefficient, a , b and c are the order of reaction with respect to the concentration of active polymer centers, the concentration of electrolyte and solution pH, respectively.

The reaction takes place outside the equilibrium conditions, under the flow of a constant anodic current (i_a) through the PANI electrode. According to the electrochemical kinetics for complex electrochemical reactions developed by Prof. K. J. Vetter [23], the rate can be expressed as:

$$r = k_a[\text{PANIH}_x^*]^a [\text{Cl}^-]^b [\text{H}^+]^{-c} = i_a/FV \quad (4.2)$$

$$i_a = FV k_a[\text{PANIH}_x^*]^a [\text{Cl}^-]^b [\text{H}^+]^{-c} \quad (4.3)$$

where i_a is the applied anodic current, F is the Faraday constant, and V is the volume of the electrode material. According to the Butler-Volmer fundamental equation of the electro-chemical kinetics, the rate constant (k) depends on the potential evolution during the oxidation/reduction reactions. For the anodic (oxidation) process,

$$i_a = FV k_{a0} [\text{PANIH}_x^*]^a [\text{Cl}^-]^b [\text{H}^+]^{-c} \exp\left(\frac{(1-\alpha)nF(E-E_0)}{RT}\right) \quad (4.4)$$

where E_0 is the standard potential, E is the electrode potential, α is the symmetry factor, k_{a0} is the rate constant or rate coefficient for $E = E_0$ [$k_{a0} = \exp(-\Delta G_{a0}/RT)$], R is the universal gas constant ($R = 8.314 \text{ J K}^{-1} \text{ mol}^{-1}$), and T is the reaction temperature.

From equation 4.4, it is possible to obtain an expression for the potential by taking logarithms on both sides and rearranging the equation,

$$E_a = E_0 + \frac{RT}{(1-\alpha)nF} \left(\ln\left(\frac{i_a}{FV}\right) - b \ln[\text{Cl}^-] - a \ln[\text{PANIH}_x^*] - c \text{ pH} - \ln k_{a0} \right) \quad (4.5)$$

Equation 4.5 indicates that the potential of the material is a function of the physical and chemical variables such as working temperature (T), the imposed electrical working condition (i_a), electrolyte concentration [X^-]; the concentration of active centers in the film [PANIH_x^*] and pH of the electrolyte.

The active centers [PANIH_x^*] is related to those points in the polymeric chains able to store positive charges at the end of an oxidation process. Their concentration decreases with the time of oxidation as a function of the consumed charge per unit of volume (Q/V). That is, during oxidation by the flow of an anodic current i_a , the active centers

of the polymer chains are consumed, it is related to the number of moles of electrons extracted from the chain ($n = Q/F$)[24].

$$[\text{PANIH}_x^*] = [\text{PANIH}_x]_{\text{initial}} - [\text{PANIH}_x]_{\text{consumed}} \quad (4.6)$$

$$[\text{PANIH}_x^*] = [\text{PANIH}_x]_{\text{initial}} - \frac{Q}{FV} = [\text{PANIH}_x]_{\text{initial}} - \frac{it}{FV} \quad (4.7)$$

Equation 4.5 becomes,

$$E_a = E_0 + \frac{RT}{(1-\alpha)nF} \left[\ln\left(\frac{i_a}{FV}\right) - b \ln[\text{Cl}^-] - a \ln\left([\text{PANIH}_x]_{\text{initial}} - \frac{it}{FV}\right) - c \text{pH} - \ln k_{a0} \right] \quad (4.8)$$

That is, Equations 4.8 describe the sensing properties of the PANI reaction driving the material from the same initial partial reduced state to the same final partial oxidation state every time, by the potential evolution under the flow of a constant current.

The oxidation of a polymeric chain occurs through n consecutive steps, each step involving one-electron transfer. Taking into account the above fact and considering system impedance (i.e., electrical resistances opposing to the current flow, Z , a new term of the potential can be described by Ohm's law, $Ez = i_a Z$) the most general equation is attained describing the potential of the material during the extraction of the same n^{th} electron from the different polymeric chains as a function of the different variables as:

$$E_n(t) = E_0 + i_a Z + (n-1)\Delta E + \frac{RT}{(1-\alpha)F} \left[\ln\left(\frac{i_a}{FV}\right) - b \ln[\text{Cl}^-] - a \ln\left([\text{PANIH}_x]_{\text{initial}} - \frac{i_a t}{FV}\right) - c \text{pH} - \ln k_{a0} \right] \quad (4.9)$$

where Z is the electrochemical impedance of the system; n is the number of consecutive electrons extracted from a chain; ΔE is the material potential step from the last $n-1$ electron extracted from the chains and the first n electron extracted from the polymer chains. Equation 4.9 is the quantitative expression describing the potential evolution during the reaction as a function of the experimental variables for the system working outside the equilibrium.

The electrical energy consumed during the reaction at any time of the current flow can be defined from the potential evolution and the flowing current:

$$U_a(t) = i_a \int E dt \quad (4.10)$$

where i is the constant reaction driving current and E is the potential along the time t of the current flow. By substitution of Equation 4.9 in Equation 4.10, an expression can be obtained for the evolution of the consumed energy:

$$\begin{aligned} U_a(t) = & i_a t [E_0 + Zi_a + (n - 1)\Delta E] \\ & + \frac{RTi_a t}{(1 - \alpha)F} \left[\ln \left(\frac{i_a}{FV} \right) - b \ln[\text{Cl}^-] - \text{cpH} - \ln k_{a0} \right] \\ & + \frac{RTVb}{(1 - \alpha)} \left[\ln \left([\text{PANIH}_x]_{\text{initial}} - \frac{i_a t}{FV} \right) \right. \\ & \left. - 1 \right] \left[\left([\text{PANIH}_x]_{\text{initial}} - \frac{i_a t}{FV} \right) \right] \quad (4.11) \end{aligned}$$

Equation 4.11 is the sensing equation where the consumed electrical energy (U) is the sensing magnitude: the consumed electrical energy as a function of the experimental variables such as applied current (i_a), time

of current flow (t), temperature (T), film volume (V), and electrolyte concentration ($[A^-]$, electrolyte pH, etc.

Similarly, the expression for potential evolution and consumed electrical energy for the cathodic process under the flow of constant cathodic current can also be deduced.

Equations 4.9 for potential evolution and Equations 4.11 for consumed energy state that any device based on the electrochemistry of polyaniline will be capable of sensing reaction working ambient variables such as chemical concentration, applied current, temperature, pH through the evolution of device potential and/or consumed electrical energy.

In order to prove the sensing capability of PANI synthesized here towards the applied current, electrolyte concentration and temperature, as in the sensing equation described above, the electrode was subjected to consecutive square current waves (galvanostatic experiments) after stabilizing the electrochemical response by recording up to 10 consecutive CV cycles between the potential limits -0.25 V to 0.7 V. The potential cycling was stopped at the cathodic potential limit -0.25 V (reduced state of the material) before each experiment to obtain chronopotentiometric responses.

4.2.2. Sensing electrical working conditions: current sensor

Looking into the sensing characteristics of PANI reaction, Equation 4.11 states that for the extraction of the n^{th} electron by consumption of a constant charge, ($Q = i.t = \text{constant}$) from every PANI

chain of the electrode, under constant reaction condition, the consumed electrical energy has a linear dependence with applied current.

For studying the sensing of electrical conditions (i.e., flowing current), the chronopotentiograms were recorded from the aqueous solution of 1 M HCl by applying three square current waves of different currents ranging from ± 0.5 mA to ± 5 mA (positive for anodic and negative for cathodic processes). Here, the time of the square waves was adapted to attain a constant oxidation/reduction charge of ± 60 mC ($Q=i.t$, kept constant) for obtaining the same initial and final oxidation states or the same reaction extension in each experiment.

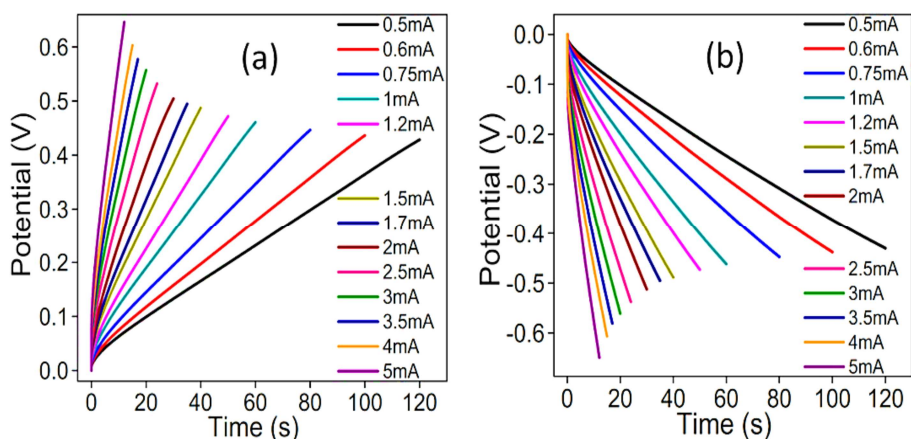


Figure 4.1 Chronopotentiograms obtained when different anodic (a) and cathodic currents (b) from 1 M HCl by passing a constant oxidation/reduction charge of ± 60 mC, in absolute values

The normalized chronopotentiometric responses for the anodic and cathodic processes are depicted in Figure 4.1a and 4.1b respectively. The figures show a sudden potential step at the initial stage before triggering the actual electrode process which is due to the various resistances offered by the electrode and electrolyte. After this initial

stage, the potential gradually increases with time during the current flow. The potential evolution occurs to higher positive potentials for higher anodic currents. Similarly, potential evolution occurs to higher negative potential during the flow of high cathodic current.

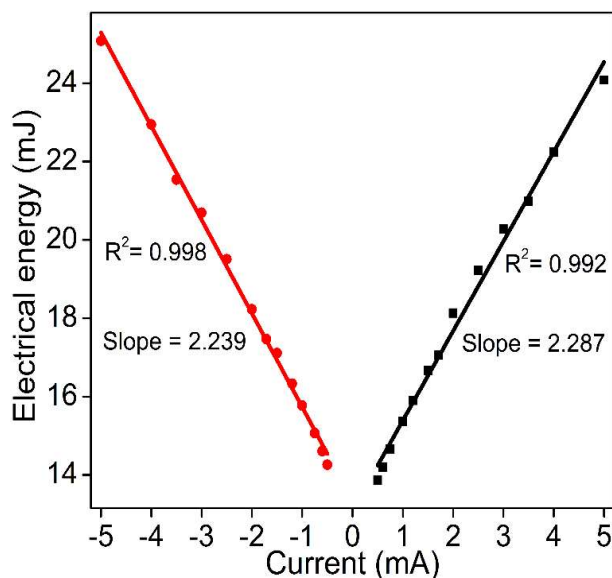


Figure 4.2 Linear dependence of consumed electrical energy with applied currents

The consumed electrical energy (U), during each oxidation or reduction process, was calculated based on Equation 4.11. Here the integral part of the equation represents the area under the chronopotentiogram obtained during the flow of constant current ' i '. Figure 4.2 indicates that the electrical energy consumed during the redox reaction of the PANI has a linear dependence on the applied electric current. That is, the reaction energy senses or responds to locally imposed electrical conditions. The slope of the concomitant calibration curve (Figure 4.2) is the sensitivity of the material as a sensor and the

sensitivity is 2.29 mJ mA^{-1} and -2.24 mJ mA^{-1} corresponding to the anodic and cathodic processes, respectively.

4.2.3. Sensing chemical working condition: concentration sensor

Equation 4.11 reveals that for the extraction of the n th electron by the flow of constant current for constant time (i and t are constant), from every PANI chain of the electrode, under constant reaction conditions, the electrical energy consumed during the reaction has a logarithmic dependence on the concentration of the electrolyte.

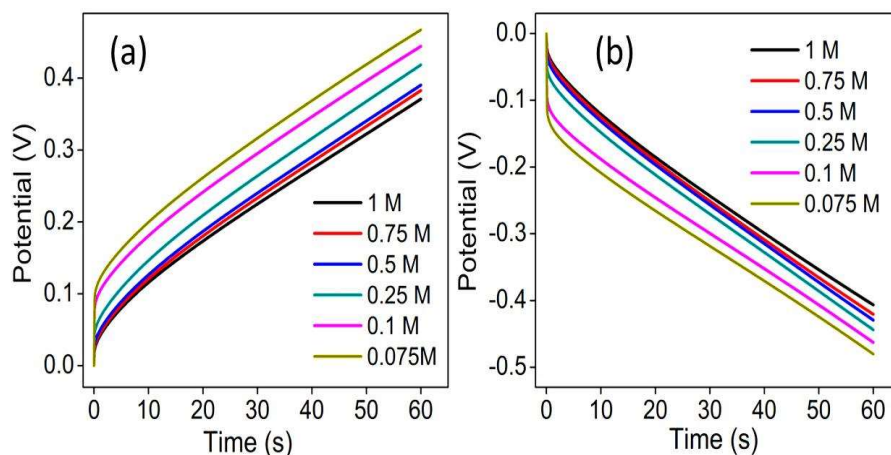


Figure 4.3 anodic (a) and cathodic (b) chronopotentiograms obtained from different concentrations of the electrolyte by the flow of $\pm 1 \text{ mA}$ current for 60 s (charge $\pm 60 \text{ mC}$) at room temperature

To investigate the concentration sensing characteristics of PANI reaction, the chronopotentiometric responses were recorded from different concentrations of HCl (from 1 M to 0.075 M) by passing consecutive square current waves of $\pm 1 \text{ mA}$ for the 60 s (at a constant charge of $\pm 60 \text{ mC}$), in each experiment at room temperature. The normalized chronopotentiometric responses for anodic and cathodic processes from

the different concentrations of electrolytes are presented in Figure 4.3a and 4.3b respectively. The full reaction process is less resistive at higher concentrations. Therefore, during the reversible oxidation/reduction reactions of polymer, the anodic and cathodic potentials evolve at lower values for increasing the concentrations of electrolyte under constant reaction extension (constant charge). In other words, the reaction requires the consumption of low electrochemical energy (chemical potential) at high available chemical energy to attain the same reaction extension.

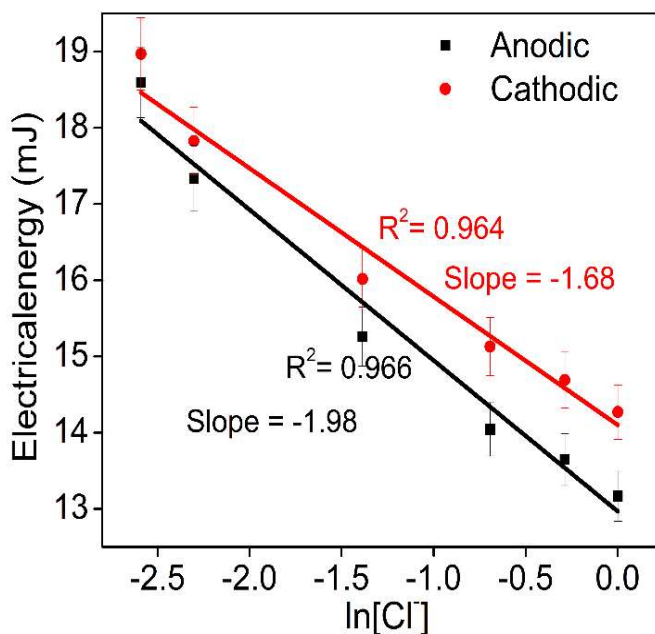


Figure 4.4 Linear dependence of consumed electrical energy with the concentration of electrolyte

The consumed electrical energy during anodic and cathodic processes in each studied concentration was obtained by the integration of the chronopotentiometric responses. Figure 4.4 shows that the

consumed electrical energies have a semi-logarithmic dependence (as in the sensing Equation 4.11 with the electrolyte concentration. That is, the PANI reaction can sense the concentration of electrolytes from the consumed electrical energy during the reaction. The slope of the calibration curve represents the sensitivity of PANI towards the concentration of electrolyte is -1.98 mJ M^{-1} and -1.68 mJ M^{-1} for anodic and cathodic processes, respectively.

4.2.4. Sensing thermal working condition: temperature sensor

Equation 4.11 also states that for the extraction of the n th electron by the flow of constant current for constant time (i and t are constant), from every PANI chain of the electrode, the electrical energy consumed during the reaction has a linear dependence on reaction temperature provided all other reaction variables are kept constant.

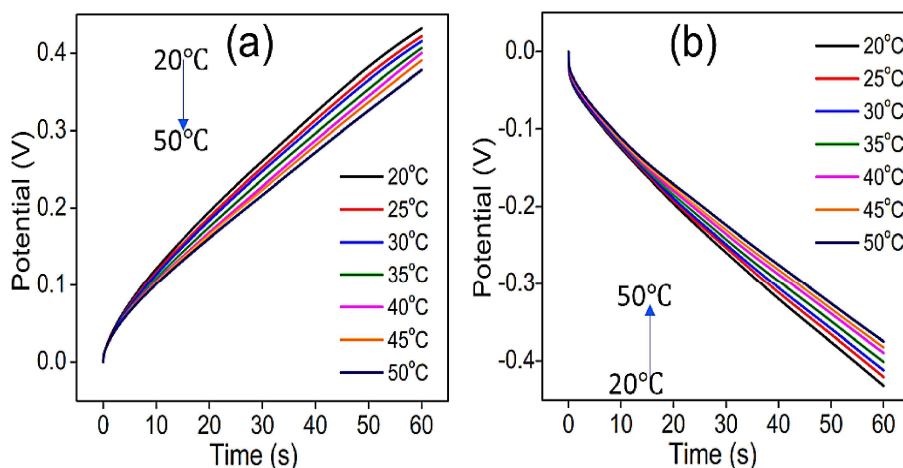


Figure 4.5 anodic (a) and cathodic (b) chronopotentiograms obtained at different temperatures by the flow of $\pm 1 \text{ mA}$ current for 60 s (charge $\pm 60 \text{ mC}$) in 1 M HCl solution

To investigate the temperature sensing characteristics of PANI reaction, the chronopotentiometric responses were recorded from the different temperatures (from 20 °C to 50 °C) by passing consecutive square current waves of ± 1 mA for the 60s (at a constant charge of ± 60 mC) in 1 M HCl by keeping all other variables constant in each experiment. The normalized chronopotentiometric responses for anodic and cathodic processes at various temperatures are presented in Figure. 4.5a and 4.5b respectively.

According to Arrhenius theory of reaction rate, as the temperature increases, available thermal energy increases, the rate of electrochemical reaction also increases and polymeric chains undergo faster and longer conformational movements, i.e., large reaction extension. This is equivalent to saying that, if a reaction is carried out at a constant rate, by passing a constant current for the same duration (constant charge), the reaction requires lower consumption of electrical energies to achieve the same reaction extension for rising temperature. Therefore, for the same reaction extension, i.e., within the same initial and final states, the material potential evolves at lower values for rising temperature. It is clear from Figures 4.5a and 4.5b that the potential (in absolute value) decreases with a gradual increase in temperature.

The consumed electrical energy during anodic and cathodic processes in each studied temperature was obtained by integrating the area under each chronopotentiometric response. Fig. 4.6 indicates that the consumed electrical energy decreases with increasing temperature. Fig. 4.6 shows that, consumed electrical energy is a linear function of reaction temperature as in the sensing Equation 4.11. That is, the PANI

reaction can sense the working temperature from the consumed electrical energy during the reaction. The sensitivity of this PANI electrode towards the working temperature (slope of calibration curve) is $-78.75 \mu\text{J K}^{-1}$ and $-64.03 \mu\text{J K}^{-1}$ for anodic and cathodic processes, respectively.

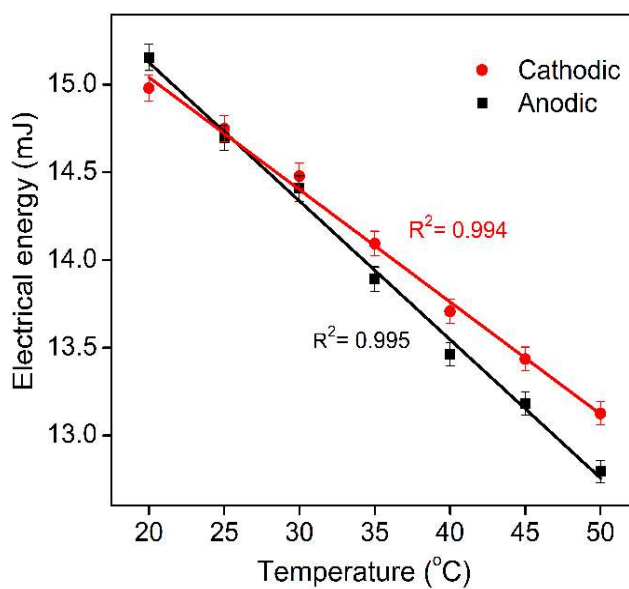


Figure 4.6 Linear dependence of consumed electrical energy with reaction temperature

II. Reaction driven sensing characteristics of PANI: A voltammetric investigation

The reaction driven sensing characteristics of PANI were further verified by voltammetry, where consumed charge during the reaction is used as the sensing parameter.

4.2.5. Sensing electrical working condition: scan rate sensor

Theoretical description

The rate of the electrochemical reaction of PANI (reaction 3.3) can be given as

$$R = k[\text{PANIH}_x^*]^a [\text{Cl}^-]^b [\text{H}^+]^{-c} \quad (4.12)$$

where R is the reaction rate ($\text{mol L}^{-1} \text{s}^{-1}$) and k is the rate constant. The volume of the polymer changes during the reaction. So, the reaction rate can be redefined in terms of the specific concentration of active centers, r ($\text{mol g}^{-1} \text{s}^{-1}$), which means per unit of mass (m) of the dry polymeric material reacting inside the electrolyte.

$$r = \frac{k}{m} [\text{PANIH}_x^*]^a [\text{Cl}^-]^b [\text{H}^+]^{-c} \quad (4.13)$$

In this study, we are investigating the influence of the electrical condition, specifically the potential scan rate, on the reaction extension of PANI. All other experimental variables are kept constant throughout the study. Following Faraday's law, the variation of the concentration of active centers $[\text{PANIH}_x^*]$ during the reaction can be obtained from the charge (Q) involved in the reaction[25] :

$$[\text{PANIH}_x^*] = \frac{Q}{mzF} = \frac{q}{zF} \quad (4.14)$$

Where Q represents the total charge involved in the reaction, $q = Q/m$ is the specific charge (charge per unit mass of the polymer) and z is the valence of the active centre (in this case 1). The specific reaction rate r (per unit of dry polymer mass) can be expressed as a rate of change of concentration of the active centre $[\text{PANIH}_x^*]$. The time can be defined using potential and scan rate (scan rate, $v = \partial E / \partial t$, $\partial t = \partial E / v$)

$$r = \frac{\partial [\text{PANIH}_x^*]}{\partial t} = \frac{\partial \left(\frac{q}{F} \right)}{\partial t} = \frac{1}{F} \frac{\partial q}{\partial t} = \frac{v}{F} \frac{\partial q}{\partial E} \quad (4.15)$$

Similarly, the average rate of reaction can be defined using the charge consumed (Q) during the reaction which is obtained from the coulovoltammogram.

$$\bar{r} = \frac{\Delta [\text{PANIH}_x^*]}{\Delta t} = \frac{q}{F \Delta t} = \frac{qv}{F \Delta E} \quad (4.16)$$

From equation 4.13 and 4.16

$$\begin{aligned} \frac{qv}{F \Delta E} &= \frac{k}{m} [\text{PANIH}_x^*]^a [\text{Cl}^-]^b [\text{H}^+]^{-c} \\ &= \frac{k}{m} [\text{Cl}^-]^b [\text{H}^+]^{-c} (q/F)^a \end{aligned} \quad (4.17)$$

Rearranging Equation 4.17, an expression showing the relationship between the specific charge consumed during oxidation/reduction of PANI and the scan rate is obtained as:

$$q^{1-a} = \frac{k\Delta EF^{1-a} [\text{Cl}^-]^b [\text{H}^+]^{-c}}{m} \frac{1}{v} \quad (4.18)$$

For the experiments carried out at different scan rate experiments, the experimental variables other than the scan rate are kept constant. The constant terms in Equation 4.18 can be combined in the new constant k_1' .

$$q^{1-a} = k_1' \frac{1}{v} \quad (4.19)$$

where,

$$k_1' = \frac{k\Delta EF^{1-a} [\text{Cl}^-]^b [\text{H}^+]^{-c}}{m} \quad (4.20)$$

Equation 4.19 is the expression that correlates the reaction extension defined by the specific reversible charge (q) consumed during the PANI oxidation/reduction and the scan rate: the extension of the reaction decreases with increasing scan rates. The rest of the experimental variables such as electrolyte concentration, working temperature, working pressure, and potential limits for the scan rate kept constant. Taking logarithms of Equation 4.19 and rearranging, a double logarithm relationship between scan rate and the reversible specific charge consumed by the PANI reversible reaction is obtained as:

$$\ln q = n_1 - m_1 \ln v \quad (4.21)$$

$$\text{where, } n_1 = \frac{\ln k_1'}{(1-a)} \quad (4.22)$$

$$\text{and } m_1 = \frac{1}{(1-a)} \quad (4.23)$$

Equation 4.21 represents the sensing equation that demonstrates the relationship between the reaction extension (i.e., the consumed charge) and the experimental scan rate. It shows that the consumed charge exhibits a double logarithmic dependence on the scan rate.

Influence of the frequency on the reaction extension

In equation 4.16, the time interval can be redefined in terms of frequency (f , s^{-1} ; $\Delta t = 1/\Delta f$, s).

$$\bar{r} = \frac{\Delta[\text{PANIH}_x^*]}{\Delta t} = \frac{q}{F\Delta t} = \frac{qf}{F} \quad (4.24)$$

From equation 4.13, 4.14 and 4.15

$$\frac{qf}{F} = [\text{Cl}^-]^b [\text{H}^+]^{-c} (q/F)^a \quad (4.25)$$

Rearranging the equation,

$$q^{1-a} = \frac{kF^{1-a} [\text{Cl}^-]^b [\text{H}^+]^{-c}}{m} \frac{1}{f} \quad (4.26)$$

The constant terms in Equation 4.26 can be combined in the new constant k_2' .

$$q^{1-a} = k_2' \frac{1}{f} \quad (4.27)$$

$$\text{where, } k_2' = \frac{kF^{1-a} [\text{Cl}^-]^b [\text{H}^+]^{-c}}{m} \quad (4.28)$$

Equation 4.27 shows that the extension of the reaction or the consumed electrical charge decreases with rising frequency. Taking

logarithms of Equation 4.27, a new relationship between frequency and the reversible specific charge consumed by the reversible reaction of PANI is attained:

$$\ln q = n_2 - m_2 \ln f \quad (4.29)$$

$$\text{where, } n_2 = \frac{\ln k'_2}{(1-a)} \quad (4.30)$$

$$\text{and } m_2 = \frac{1}{(1-a)} \quad (4.31)$$

Equation 4.29 is the sensing equation that quantifies a double logarithmic relationship between the extension of reaction and frequency.

Experimental results

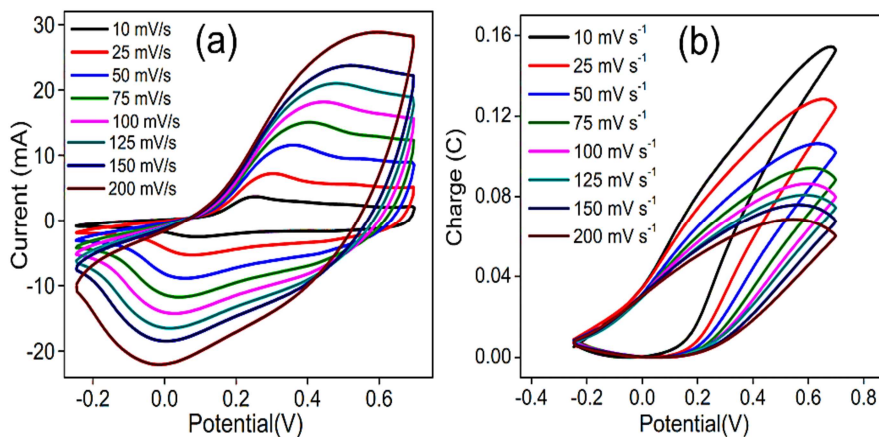


Figure 4.7 (a) CV at different scan rates and (b) QV obtained by integration of the corresponding CV

The influence of scan rate or frequency on reaction extension which is defined as the consumed charge was studied from voltammetric responses. Figure 4.7a represents the stationary CV responses of the

PANI electrode after three consecutive potential cycles for every studied scan rate. The oxidation and reduction peak currents are increased for rising scan rates. The normalized stationary coulouvoltammograms obtained by integration of the voltammetric responses attained from each of the studied scan rates are depicted in Figure 4.7b. Every coulouvoltammometric response presents a closed loop: the oxidation charge equals the reduction charge. The coulouvoltammometric maximum decreases for rising scan rates and the redox charge decreases. That is the reversible charge consumed by the PANI reversible reactions decreases with increasing scan rates.

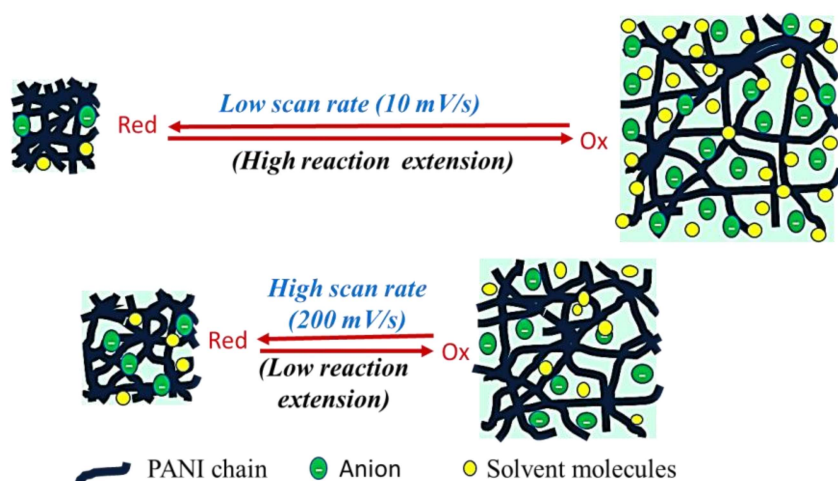


Figure 4.8 Schematic representation of extension of the electrochemically induced structural (volume) changes by reversible reaction of PANI at low and high scan rates

At lower scan rates the oxidation/reduction overpotentials are applied for a long-time range which promotes deeper conformational changes of the polymer chains, thereby generating/destroying large free volumes. A large number of ions and solvent molecules exchanged between electrode and electrolyte and attained deeper

oxidation/reduction states by consumption of high redox charges. That is a greater extension of the reaction at a lower scan rate. As the scan rate increases, relatively less time is obtained for the ion to diffuse into active sites and the polymer chains become partially oxidized/reduced: fewer electrons can be extracted per polymeric chain, hence less charge is consumed at a high scan rate. The above-described events are summarized in Figure 4.8.

The experimental result corresponding to the variation of consumed electrical charge with scan rate is presented in Figure 4.9a. The reaction extension shows a double logarithmic linear dependence with the scan rate, which aligns with the theoretical description given by Equation 4.21. The obtained linear relationships, exhibiting an excellent correlation ($R^2=0.993$), indicate that the extension of the PANI reaction is capable of sensing or responding to the working electrical condition, i.e., scan rate. The slope (-0.264) represents the sensitivity, that is how fast is the reaction extension as the consumed charge in Coulomb decreases per unit of variation of the scan rate in mV s^{-1} .

The experimental result for the variation of consumed charge with frequency is depicted in Figure 4.9b. The reaction extension demonstrates a double logarithmic linear dependence on the frequency, which aligns with the theoretical description provided by Equation 4.29. The obtained linear relationships, showing a high correlation ($R^2=0.993$), indicate that the extension of the PANI reaction is responses or sense to the working electrical condition (scan rate). Thus, Equation 4.29 is the sensing equation that quantifies how the reaction extension (consumed charge, q) responds to the frequency. The slope (-0.264)

represents the sensitivity, that is, how fast the reaction extension, as consumed charge, decreases per unit of variation of the frequency (s^{-1}).

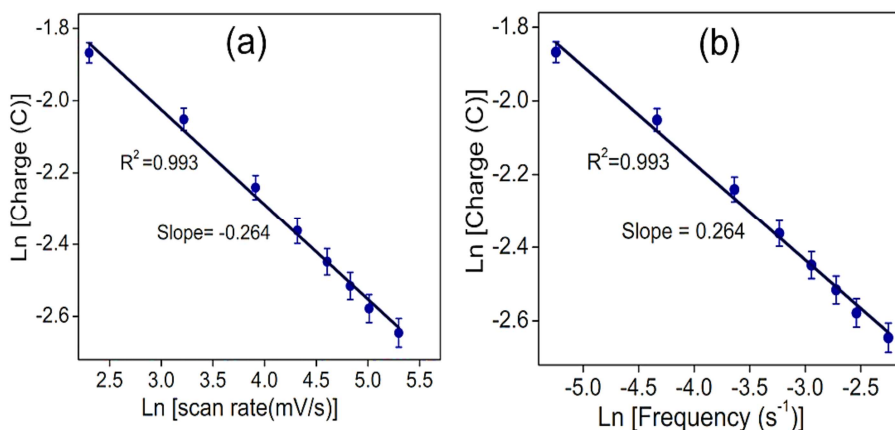


Figure 4.9 The double-logarithmic linear dependence between the charge consumed by the reaction of PANI with scan rate (a) and (b) frequency.

4.2.6. Sensing chemical working condition: concentration sensor

In this study, we present an investigation into the influence of electrolyte concentration on the reaction extension while maintaining all experimental variables other than electrolyte concentration kept constant.

Theoretical description

Rearranging Equation 4.17, an expression showing the relationship between the specific charge consumed during oxidation/reduction of PANI and electrolyte concentration can be attained:

$$q^{1-a} = \frac{k\Delta EF^{1-a}}{mv} [\text{Cl}^-]^b [\text{H}^+]^{-c} \quad (4.32)$$

The constant terms in Equation 4.32 can be combined in the new constant k_3' .

$$q^{1-a} = k_3' [\text{Cl}^-]^b [\text{H}^+]^{-c} \quad (4.33)$$

$$\text{where, } k_3' = \frac{k\Delta EF^{1-a}}{mv} \quad (4.34)$$

Equation 4.33 is the expression that correlates the reaction extension defined by the specific reversible charge (q) consumed during the PANI oxidation/reduction and electrolyte concentration. The extension of the reaction increases with increasing electrolyte concentration. Taking logarithms of Equation 4.33 and rearranging, a new relationship between the reversible specific charge consumed by the PANI reversible reaction and electrolyte concentration is attained:

$$\ln q = n_3 + m_3 \ln[\text{Cl}^-] + m_4 \ln[\text{H}^+] \quad (4.35)$$

$$\text{Or } \log q = n_3 + m_3 \log[\text{Cl}^-] - m_4 \text{ pH} \quad (4.36)$$

$$\text{where, } n_3 = \frac{\ln k_3'}{(1-a)} \quad (4.37)$$

$$m_3 = \frac{b}{(1-a)} \quad (4.38)$$

$$\text{and } m_4 = \frac{-c}{(1-a)} \quad (4.39)$$

Equations 4.33 and 4.35 are the sensing equations that show how the consumed charge varies as a function of electrolyte concentration. That is the extension of the reaction of PANI can sense the electrolyte

concentration (or the available chemical energy), provided other experimental variables are kept constant.

Experimental results

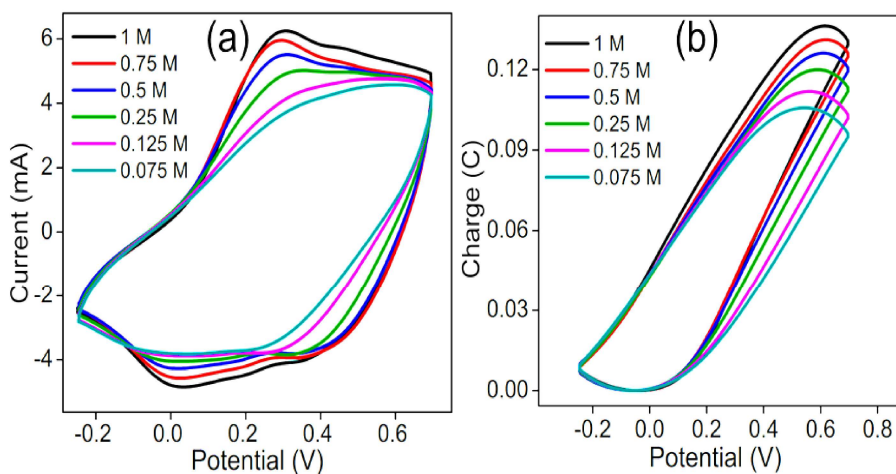


Figure 4.10 (a) CVs at different electrolyte concentrations and (b) QVs obtained by integration of the corresponding CVs

The influence of electrolyte concentration on reaction extension was studied from voltammetric responses. Figure 4.10a represents the stationary CV responses of the PANI electrode after three consecutive potential cycles in different electrolyte concentrations from 1 M to 0.075 M. The oxidation and reduction currents are found to increase with increasing electrolyte concentration. The normalized stationary coul voltammograms obtained from the voltammetric responses for different electrolyte concentrations are shown in Figure 4.10b. The coul voltammetric maximum increases for rising electrolyte concentration, i.e., the reversible charge consumed by the PANI reversible reactions increases with increasing electrolyte concentration.

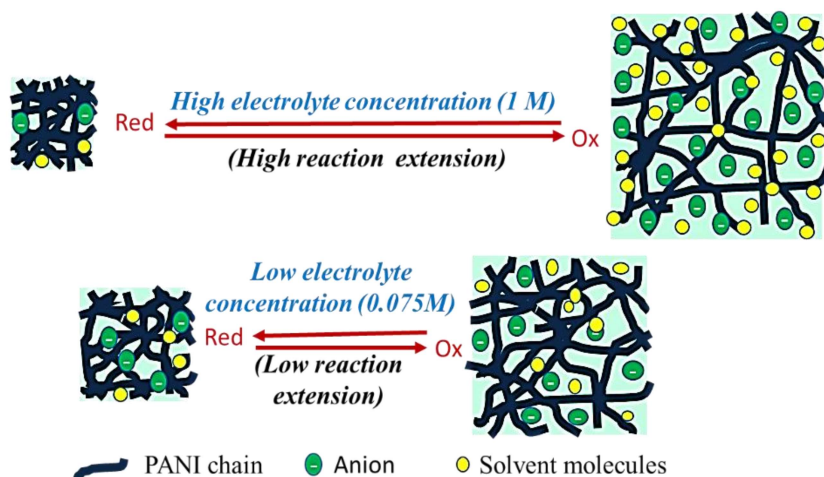


Figure 4.11 Schematic representation of extension of the electrochemically induced structural (volume) changes by reversible reaction of PANI at low and high electrolyte concentration

As the concentration of electrolyte increases, the chemical energy available for the reaction (the chemical potential) also increases. At low concentrations, the available chemical energy is low and the polymer chains become partially oxidized: fewer electrons can be extracted per polymer chain. That is only a partial convolution-deconvolution for the conformational movements of polymeric chain generate only a low amount of free volume, only a low amount of counterions and water can be lodged/expelled during the redox reaction. When the electrolyte concentration increases (the chemical energy increases), under constant experimental conditions, more electrons can be extracted per polymer chain, more free volume can be generated and followed by lodging more counterions and solvent molecules, attaining a deeper oxidation state: the reaction charge increases. The conformational movements of polymeric chains at low and high concentrations are schematically represented in Figure 4.11.

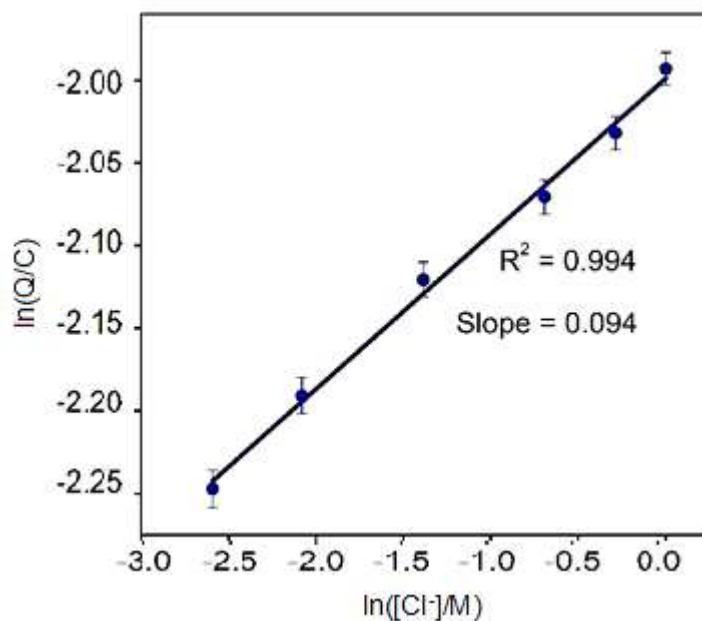


Figure 4.12 *The double-logarithmic dependence of charge consumed by the reaction of PANI with electrolyte concentration.*

The experimental result corresponding to the variation of consumed electrical charge with electrolyte concentration is presented in Figure 4.12. The reaction extension has a double logarithmic linear dependence with electrolyte concentration, as described by Equation 4.35. The attained linear relationship indicates that the extension of the reaction of PANI senses or responds to the working chemical condition (concentration of counter ion). The slope (0.094) represents the sensitivity of the PANI reaction for the electrolyte concentration.

4.2.7. Sensing thermal working condition: temperature sensor

Here, we are analyzing the influence of temperature on the reaction extension/consumed charge of PANI while maintaining all other experimental variables other than temperature kept constant.

Theoretical description

The Arrhenius equation states the dependence of the rate constant of a reaction (k) with the experimental temperature:

$$k = Ae^{-(E_a/RT)} \quad (4.40)$$

where A is the Arrhenius pre-exponential factor, R is the universal gas constant ($\text{J mol}^{-1} \text{K}^{-1}$), T is the absolute temperature (K) and E_a is the activation energy of the reaction (J mol^{-1})

Substituting Equation 4.40 in Equation 4.17

$$\frac{qv}{F\Delta E} = \frac{Ae^{-(E_a/RT)}}{m} [\text{Cl}^-]^b [\text{H}^+]^{-c} (q/F)^a \quad (4.41)$$

By rearranging the equation, a relationship between the charge consumed during the PANI oxidation/reduction reaction and working temperature is attained as:

$$q^{1-a} = \frac{A\Delta EF^{1-a} [\text{Cl}^-]^b [\text{H}^+]^{-c}}{mv} e^{-(E_a/RT)} \quad (4.42)$$

The constant terms in equation 4.42 can be combined in the new constant k_4'

$$q^{1-a} = k_4' e^{-(E_a/RT)} \quad (4.43)$$

$$\text{where, } k_4' = \frac{A\Delta EF^{1-a} [\text{Cl}^-]^b [\text{H}^+]^{-c}}{mv} \quad (4.44)$$

By taking logarithms and rearranging the equation mentioned above, a new relationship between the reversible specific charge

consumed by the PANI reversible reaction and working temperature can be derived:

$$\ln q = n_4 - m_5 \frac{1}{T} \quad (4.45)$$

$$\text{where, } n_4 = \frac{\ln k_4'}{(1-a)} \quad (4.46)$$

$$m_5 = \frac{E_a}{R(1-a)} \quad (4.47)$$

Equation 4.45 is the sensing equation. The consumed electrical charge has a semilogarithmic dependence with the inverse of the working temperature. That is the charge consumed by the reversible reaction of PANI can sense the working temperature or the available thermal energy under the same constant experimental conditions other than temperature.

Experimental results

Figure 4.13a shows the stationary CV responses obtained at different experimental temperatures after three consecutive potential cycles. The anodic and cathodic currents were increased with the increase of temperatures. The stationary coulometric responses, obtained from CV response are presented in Figure 4.13b. The redox charge consumed by the reversible reactions of the PANI increases with increasing temperatures.

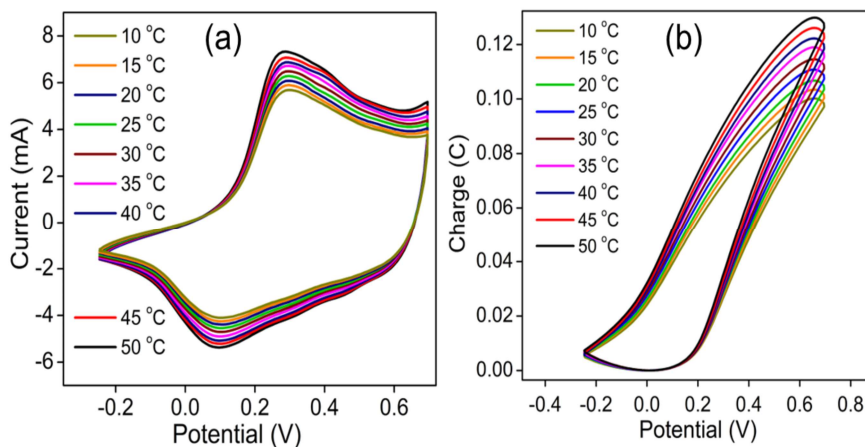


Figure 4.13 (a) CV at different temperatures and (b) Coulovoltammogram obtained by integration of the corresponding CV

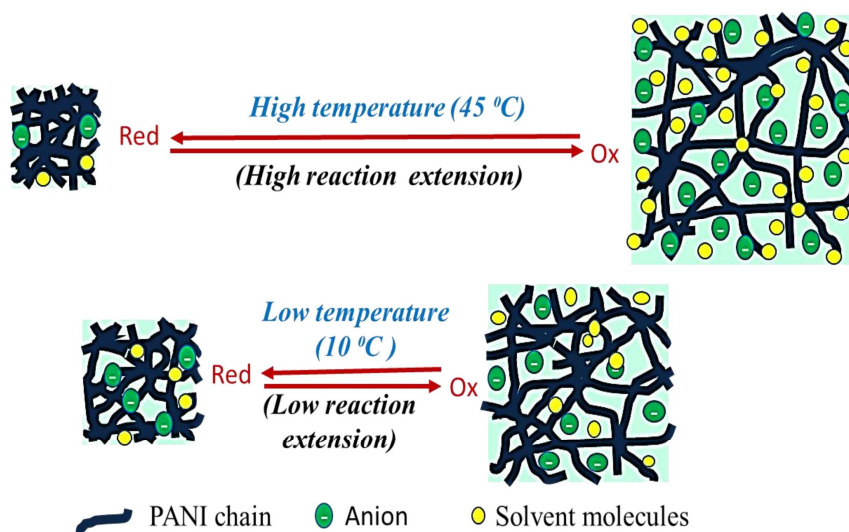


Figure 4.14 Schematic representation of extension of the electrochemically induced structural (volume) changes by reversible reaction of PANI at low and high temperatures.

As the working temperature increases, the increased thermal energy shifts the reversible reaction of PANI to deeper

oxidation/reduction states, which generate greater amounts of free volume, allowing the exchange of large amounts of counterions and solvent molecules by consumption of the concomitant greater reaction charges. The conformational movements of polymeric chains at low and high temperatures are schematically represented in Figure 4.14.

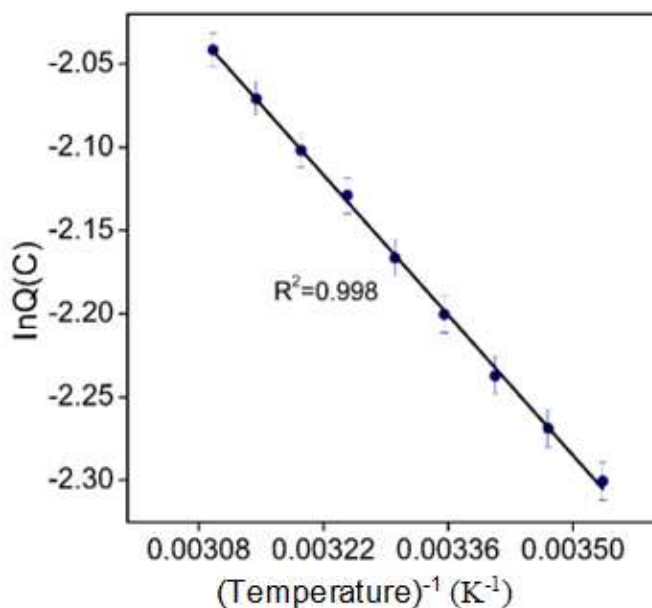


Figure 4.15 The logarithmic dependence of charge consumed by the reaction of PANI with the inverse of temperature (in Kelvin)

The experimental result for the variation of consumed charge with temperature is depicted in Figure 4.15. The reaction extension demonstrates a logarithmic linear dependence on the inverse of the temperature, as described by Equation 4.45. The observed linear relationship suggests that the extension of the PANI reaction is responsive to the working thermal condition, indicating that it can sense or respond to changes in temperature. The slope (-601.28) represents the sensitivity of the PANI reaction to the temperature.

4.3. Conclusion

The sensing characteristics of PANI reaction have been studied under galvanostatic conditions with the consumed electrical energy as sensing magnitude. The consumed electrical energy during the reaction increases as the applied current increases. Thus, shows a linear dependence with the applied current. The consumed electrical energy during the reaction decreases linearly with rising temperature. Similarly, the consumed electrical energy decreases as electrolyte concentration increases and has a logarithmic dependence on the electrolyte concentration as described through sensing equations 4.11, which is proposed theoretically.

The sensing characteristics of PANI reaction are also studied by voltammetry, where the consumed extension of reaction is defined by consumed electrical charge as sensing magnitude. The consumed charge during the reaction decreases with the increase of scan rate and shows a double logarithmic dependence with the scan rate or scan frequency. The consumed charge during the reaction increases with increasing concentration of electrolyte and has linear double logarithmic dependence. Similarly, the consumed charge during the reaction increases as rising temperature and has a logarithmic dependence with the inverse of temperature as described through sensing equations (equations 4.29, 4.35 and 4.45) which is proposed theoretically. In summary, the electrochemical reactions of polyaniline can sense their working ambient such as electrical, chemical and thermal conditions through consumed electrical energy and/or consumed charge during the reaction as sensing parameters.

Our study established the fact that the reaction of PANI can sense the working energetic conditions. Any electrochemical device, working based on the electrochemical reaction of PANI, can sense its working condition with consumed electrical energy and charge as the sensing parameters. This result will be useful for developing soft wet reactive sensing devices, which is noteworthy for multifunctional chemical devices.

References

1. T.F. Otero, *Modern Aspects of Electrochemistry*, (1999) 307-434.
2. T.F. Otero, *Physical Chemistry Chemical Physics*, 19 (2017) 1718-1730.
3. J. Heinze, B.A. Frontana-Uribe, S. Ludwigs, *Chemical Reviews*, 110 (2010) 4724-4771.
4. S. Erbas-Cakmak, D.A. Leigh, C.T. McTernan, A.L. Nussbaumer, *Chemical reviews*, 115 (2015) 10081-10206.
5. T. Otero, J. Martinez, J. Arias-Pardilla, *Electrochimica Acta*, 84 (2012) 112-128.
6. T.F. Otero, *The Chemical Record*, 18 (2018) 788-806.
7. T.F. Otero, *Polymer Reviews*, 53 (2013) 311-351.
8. T. Otero, J. Martinez, *Journal of Materials Chemistry B*, 4 (2016) 2069-2085.
9. M. Gerard, A. Chaubey, B. Malhotra, *Biosensors and bioelectronics*, 17 (2002) 345-359.
10. N. Gupta, S. Sharma, I.A. Mir, D. Kumar, (2006).
11. M.M. Barsan, M.E. Ghica, C.M. Brett, *Analytica chimica acta*, 881 (2015) 1-23.
12. G. Alici, G.M. Spinks, J.D. Madden, Y. Wu, G.G. Wallace, *IEEE/ASME Transactions on Mechatronics*, 13 (2008) 187-196.
13. Z. Song, Y. Ma, A. Morrin, C. Ding, X. Luo, *TrAC Trends in Analytical Chemistry*, 135 (2021) 116155.

14. V. Tsakova, R. Seeber, *Analytical and bioanalytical chemistry*, 408 (2016) 7231-7241.
15. M.A. Rahman, P. Kumar, D.-S. Park, Y.-B. Shim, *Sensors*, 8 (2008) 118-141.
16. T.F. Otero, *Conducting Polymers: Bioinspired Intelligent Materials and Devices*, Royal Society of Chemistry, 2016.
17. T.F. Otero, J.J. Sanchez, J.G. Martinez, *The Journal of Physical Chemistry B*, 116 (2012) 5279-5290.
18. J.G. Martinez, T.F. Otero, *The Journal of Physical Chemistry B*, 116 (2012) 9223-9230.
19. Y.A. Ismail, J.G. Martínez, T.F. Otero, *Electrochimica Acta*, 123 (2014) 501-510.
20. F.G. Córdova, Y.A. Ismail, J.G. Martinez, A.S. Al Harrasi, T.F. Otero, *Electroactive Polymer Actuators and Devices (EAPAD) 2013*, SPIE, 2013, pp. 29-43.
21. T.F. Otero, J.G. Martinez, *Progress in Polymer Science*, 44 (2015) 62-78.
22. T.F. Otero, *Journal of Materials Chemistry B*, 1 (2013) 3754-3767.
23. K.J. Vetter, S. Bruckenstein, *Electrochemical kinetics: theoretical and experimental aspects: revisions, additions, and a foreword to the English language ed. prepared by the author*, Academic Press, 1967.
24. T. Otero, E. Angulo, J. Rodriguez, C. Santamaria, *Journal of Electroanalytical Chemistry*, 341 (1992) 369-375.
25. A.J. Bard, L.R. Faulkner, H.S. White, *Electrochemical methods: fundamentals and applications*, John Wiley & Sons, 2022.

Chapter 5

Reaction driven sensing characteristics and supercapacitor application of Chitosan/polyaniline hybrid films

In this chapter, we are exploring how PANI can be used as a free-standing electrode material for sensing and supercapacitor application. Accordingly, CP/hydrogel hybrid systems are fabricated through in situ chemical polymerization of PANI using chitosan films. Then we proved that PANI/chitosan hybrid films have the reaction driven sensing capabilities. The sensing characteristics of hybrid films towards electrical, chemical and thermal working conditions have been verified by two methods: (1) by chronopotentiometry, where consumed electrical energy during the reaction as sensing parameter and (2) by voltammetry, where the consumed charge as sensing parameter. We have also proved the efficacy of Chitosan/PANI hybrid films as a free-standing electrode material for supercapacitor applications.

5.1. Introduction

In the previous chapter, it is proved that the PANI has reaction driven sensing capabilities which are noteworthy for the development of multi-sensing devices. While the poor processability due to the insolubility of PANI in common organic/aqueous solvents limits their practical application. The PANI thin films can be synthesized by electrochemical polymerization. However, the poor mechanical stability and brittleness are the major drawbacks of the electrogenerated PANI thin films hindering their direct applicability in device fabrications.

Various strategies have been proposed by researchers to overcome the drawbacks and improve the processability of PANIs: derivatization of the polymer backbone; co-polymerization with substituted monomers and introduction of lengthy substituent groups, sulphonic acid groups, or carboxyl groups into the main chain [1-5]; the preparation of composites/hybrid/blend with processable polymers [6-10]; the use of surfactants [11-13]; composite/hybrid with metallic nanoparticles, graphene, carbon nanotubes and metal-organic framework [14-18] or using polymeric/hydrogel nanofibers and microfibers as templates [19-23].

Chitosan is a naturally abundant polymer, the major derivative of chitin. Chitin is a polysaccharide present in the exoskeleton of shrimp and other crustaceans, insects and fungal cell walls. The structure of chitin consists of β -1, 4-linked glucosamine units with a high degree of acetylation. Chitosan is usually obtained by the alkaline deacetylation of chitin [24, 25]. The structure of chitin and chitosan

is shown in Figure 5.1. Owing to its negligible toxicity, biocompatibility, biodegradability, relatively good processibility, ease of derivatization and adsorption properties, chitosan has found considerable application in the commercial and biomedical fields.

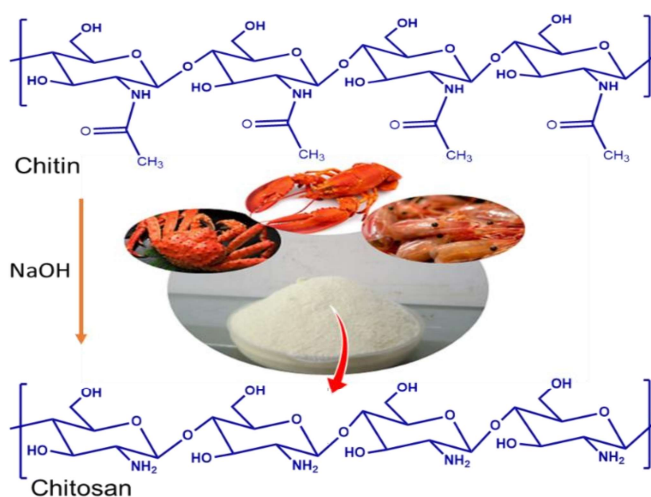


Figure 5.1 Structure of chitin and chitosan

In this work, as a strategy to fabricate an efficient freestanding electrode material based on PANI, we have selected chitosan to fabricate the hybrid films; Cs/PANI hybrid films. The films were fabricated by adopting a facile and low-cost strategy that is suitable for large-scale preparation. Here the hybrid films were fabricated by the incorporation of PANI into a biocompatible chitosan hydrogel film, for developing mechanically stable free-standing electrode materials. The reaction driven sensing characteristics of the hybrid films have been verified through consumed electrical energy and charge as sensing parameters towards electrical, chemical and thermal conditions. Besides, the charge storage properties of these hybrid films have been also studied by CV, GCD and EIS analysis.

5.2. Results and Discussion

I. Characterization of Chitosan/PANI hybrid films

The chitosan/PANI (Cs/PANI) hybrid films were prepared through an in situ chemical polymerization on a previously fabricated chitosan film. Here, four different types of films were fabricated, which are designated as CPF1, CPF2, CPF3 and CPF4 as explained in Chapter 2. It is found to be strong adhesion between chitosan and PANI due to the intramolecular hydrogen bonding between chitosan and PANI (Figure 5.2).

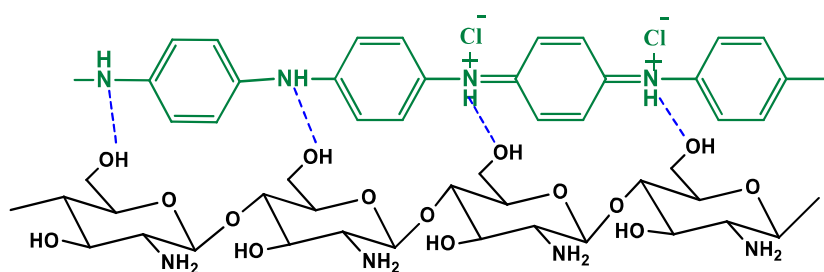


Figure 5.2 Interaction between chitosan and PANI

5.2.1. FTIR spectra

The FTIR spectra recorded for Cs, PANI, and Cs/PANI films in the range of $4000\text{--}500\text{ cm}^{-1}$ are presented in Figure 5.3. In the spectrum of Cs, the peak at 1645 cm^{-1} corresponds to C=O stretching vibration indicating the presence of N-acetyl groups. The peaks at 1025 , 1309 and 1564 cm^{-1} are assigned to C-O stretching, C-N stretching and N-H bending (amide II), respectively [26]. The peak corresponding to C-H stretching vibrations appeared at 2888 cm^{-1} as well as a broad band appeared in the region $3200\text{--}3600\text{ cm}^{-1}$ ascribed

to O-H and N-H stretching vibrations. The broadness refers to the existence of intramolecular hydrogen bonds in the chitosan film. The FTIR spectrum of PANI exhibits typical absorption peaks corresponding to C=C stretching vibrations of benzenoid and quinoid rings at 1484 cm^{-1} and 1560 cm^{-1} respectively, which corroborates that PANI is formed in the emeraldine form. The absorption peaks at 1299 cm^{-1} and 1248 cm^{-1} are ascribed to C-N stretching vibrations of the benzenoid–quinoid–benzenoid sequence. An intense peak observed around 1120 cm^{-1} is attributed to the charged defects [27].

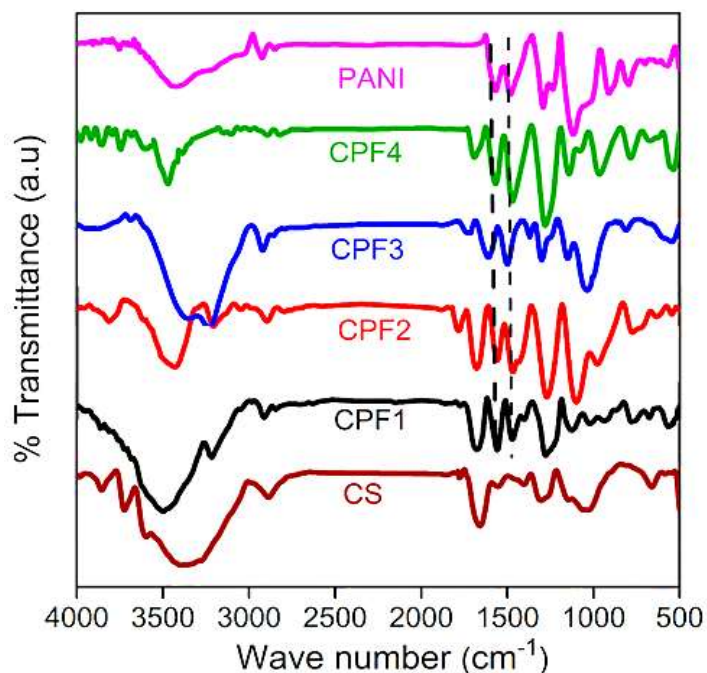


Figure 5.3 FTIR spectra of chitosan, PANI and Cs/PANI hybrid films

FTIR spectra of Cs/PANI hybrid films have characteristic peaks of both PANI and chitosan with slight variations indicating the existence of interaction between them. All the films have two characteristic peaks

corresponding to the stretching vibrations of C=C bonds of quinoid and benzenoid units of polyaniline in the region 1460-1570 cm^{-1} . The bands around 1280 cm^{-1} and 1100 cm^{-1} correspond to the C-N stretching vibration of the secondary aromatic amine and C-H in-plane bending vibration of the benzene ring respectively. Besides, the appearance of a broad peak around the region 3200 - 3600 cm^{-1} is due to the overlapping of N-H stretching of PANI with O-H and N-H stretching of Cs and indicates the hydrogen bonding interaction between chitosan and PANI [28].

5.2.2. Electrical Conductivity

Figure 5.4 represents the frequency-dependent electrical conductivities of the hybrid films obtained in the frequency range of 1 to 10^7 Hz studied using a Broadband Dielectric Spectrometer. There are effectively two specific areas in these plots. At higher frequencies, related to the alternating current (AC), the conductivity increases with increasing frequency. At lower frequencies, related to the direct current (DC), conductivity remained almost constant. The frequency-dependent electrical conductivity of Cs/PANI hybrid films follows a power-law behavior indicative of the hopping mechanism. The experimental data were fitted by Jonscher's universal power law to obtain the electrical conductivity of hybrid films [29, 30]. The electrical conductivity of CPF1, CPF2, CPF3 and CPF4 is observed to be $3.15 \times 10^{-4} \text{ S cm}^{-1}$, $2.79 \times 10^{-3} \text{ S cm}^{-1}$, $6.04 \times 10^{-2} \text{ S cm}^{-1}$ and $4.34 \times 10^{-1} \text{ S cm}^{-1}$ respectively. Cs/PANI films were found to exhibit moderately high electrical conductivity through non-conducting chitosan segments that are inherently associated with these films. This is due to the homogeneous

distribution of PANI inside as well as on the surface of chitosan films. The electrical conductivity of hybrid films is improved significantly with increasing PANI content in the film, i.e., from CPF1 to CPF4. The high electrical conductivity of the hybrid film, fabricated by in situ chemical polymerization of aniline on the chitosan hydrogel matrix, suggests that our fabrication method can be utilized in the preparation of high electroactive hydrogel-based materials.

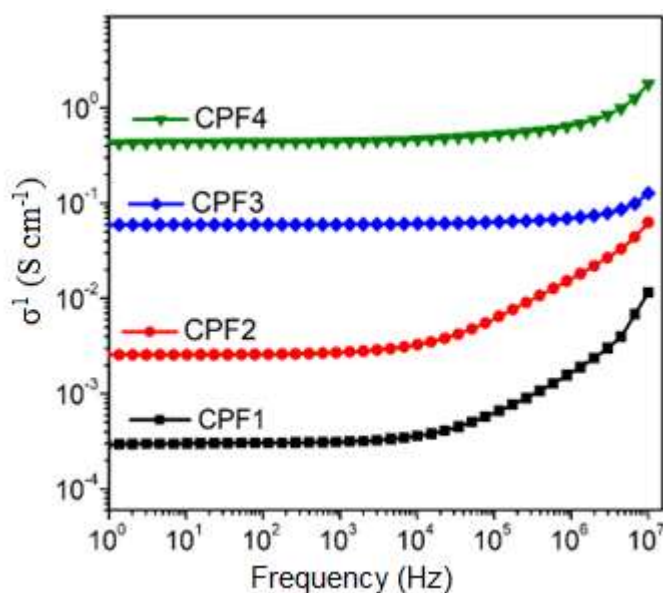


Figure 5.4 Frequency-dependent electrical conductivity of Cs/PANI hybrid films

5.2.3. Thermal characterization

Thermogravimetric analysis of Cs and Cs/PANI hybrid films was performed in the temperature range of 25-650 °C and the results are presented in Figure 5.5. The TG curve of Cs shows two stages of mass loss: the first stage corresponds to water loss which occurs up to about 120 °C with a mass loss of 14 %, while the second stage is attributed to

the decomposition of chitosan polymer chains which occurs between 270-325 °C with a mass loss of 66 %. The degradation temperature of the chitosan polymer backbone is found to be around 298 °C. The final residual mass was estimated to be 29.5 % at 650 °C [31, 32].

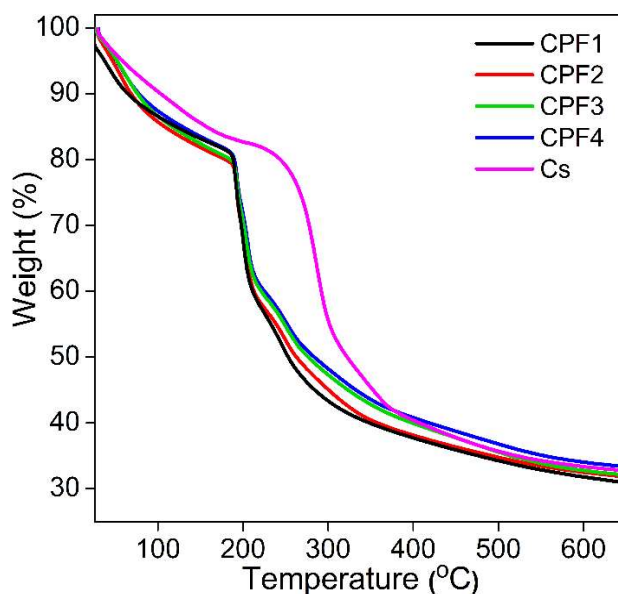


Figure 5.5 The TGA of Cs and Cs/PANI hybrid films

Cs/PANI hybrid films showed a very similar behavior as that of Cs with major two-stage mass loss. The first stage corresponds to the loss of water and volatile components including dopant ions; the second corresponds to the degradation of the polymeric backbone. The degradation of the polymer backbone of the hybrid films occurs at the temperature range of 200 °C -210 °C.

5.2.4. Mechanical characterization

Mechanical characteristics of the Cs/PANI hybrid films were analyzed using a Universal Testing Machine as described in Chapter 2.

The linear stress-strain behaviour of the films was compared. The representative stress-strain curves of all four hybrid films obtained at a crosshead rate of 50 mm/min are depicted in Figure 5.6 and the results are listed in Table 5.1.

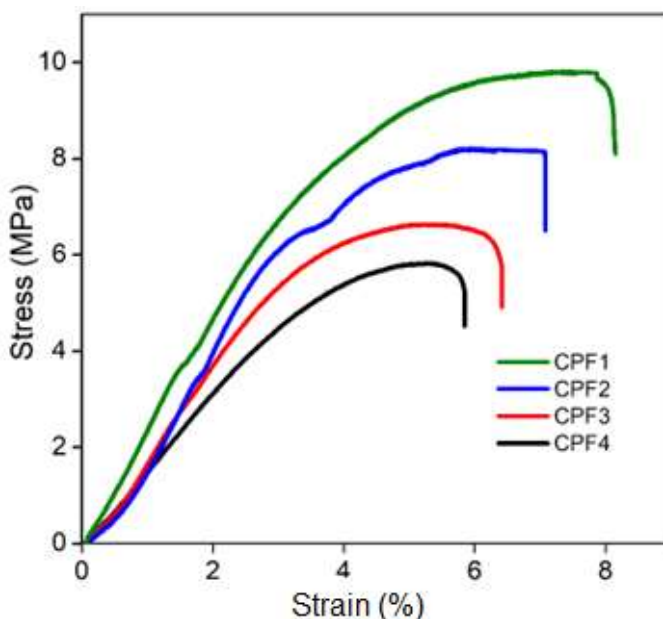


Figure 5.6 Stress-strain curve of Cs/PANI hybrid films

The stress-strain curves of Cs/PANI hybrid films show plastic behavior. The tensile strength of the film decreases from CPF1 to CPF4. This may be due to the decrease in the degree of hydrogen bonding by the interpenetration of PANI chains through a highly hydrogen bonded chitosan film matrix. Even then the table shows that the mechanical properties of the Cs/PANI hybrid films are good enough to be employed as free-standing electrode materials for electrochemical applications. The tensile strength and Young's Modulus of CPF4 film are 5.84 MPa and 1.56 MPa respectively. The maximum percentage elongation at

break decreases from CPF1 to CPF4, indicating that the stiffness of the film increases with the incorporation of more PANI content into the chitosan matrix. The result of the mechanical properties of our hybrid films suggests that the method adopted here is useful for the large-scale fabrication of conducting polymer-based stable and flexible electrodes.

Table 5.1 *Tensile strength, Young's Modulus and % elongation at break of Cs/PANI hybrid films*

Film	Tensile strength (MPa)	Young's Modulus (MPa)	% Elongation at break
CPF1	9.82	2.32	8.12
CPF2	8.22	1.99	7.08
CPF3	6.64	1.85	6.42
CPF4	5.84	1.56	5.86

5.2.5. Morphological characterization

Surface morphology of films was investigated by FESEM analysis and the images are presented in Figure 5.7.

The FESEM images indicate that the surface of the chitosan film is quite smooth without voids or cracks (Figure 5.7a). The FESEM images of Cs/PANI hybrid films reveal that the PANI has grown on the surface of the Chitosan matrix with coral-like nanowire morphology (Figure 5.7b-e). Upon repeated coating, the new polyanilines have grown on the previously formed PANI nanostructure leading to more

agglomerated morphology on the surface of those films. The nanostructures and large open channels at the nano and micro scale offer high surface area, and porosity facilitating better transport of ions and electrolytes. Besides, the swollen state of Cs/PANI hybrid films may allow facile permeation of ions and electrons in between PANI chains which provides an additional effective surface area between molecular chains and the solution phase leading to high electrochemical activities.

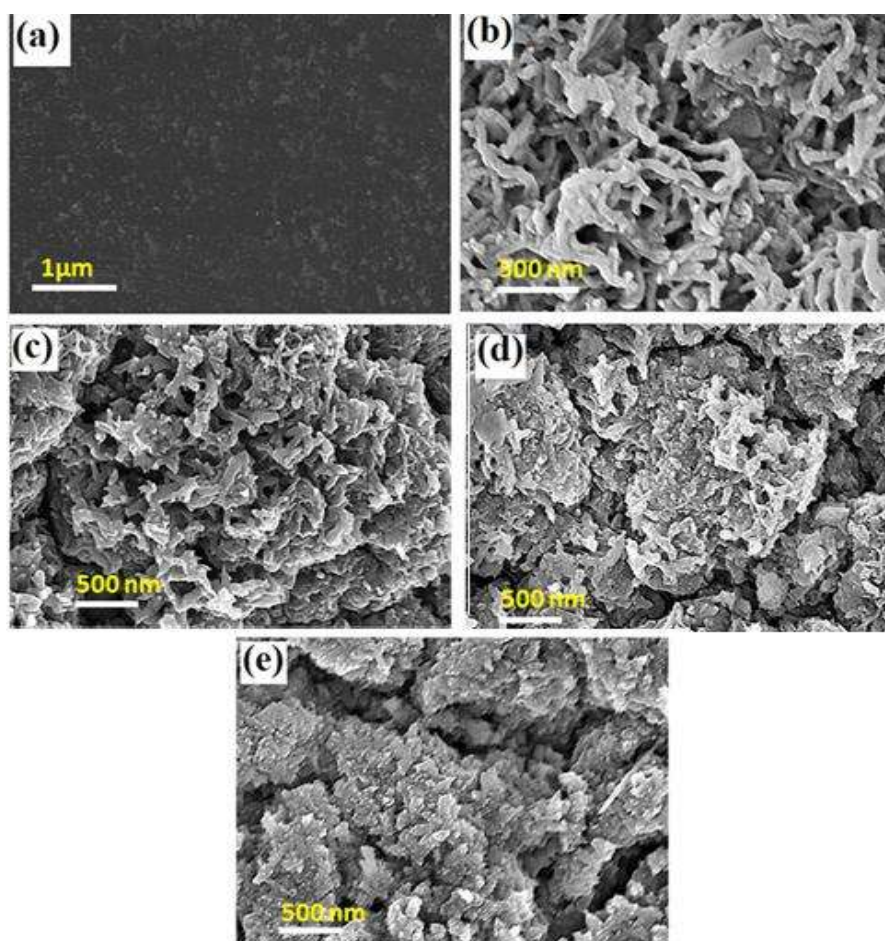


Figure 5.7 FESEM images of (a) chitosan, (b) CPF1, (c) CPF2, (d) CPF3 and (e) CPF4 films

5.2.6. Elemental analysis

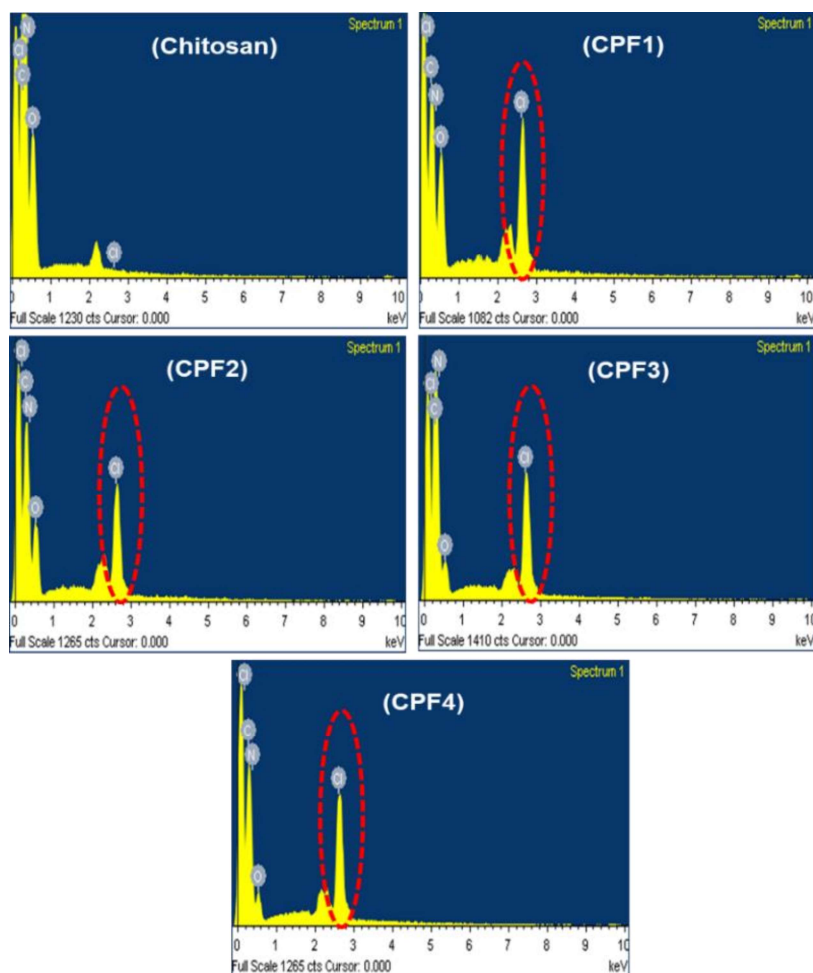


Figure 5.8 EDX spectra of chitosan and Cs/PANI hybrid films

The EDX spectra of Cs/PANI hybrid films are presented in Figure 5.8. All the hybrid films exhibit a characteristic peak of Cl^- in EDX spectra in addition to C, N and O, which is absent in chitosan film. The Cl^- is introduced as the counter ion during the acid doping of PANI. It confirms that PANI formed in the chitosan matrix is in the conductive emeraldine salt form.

5.2.7. Electrochemical characterizations

5.2.7.1. Cyclic voltammetry

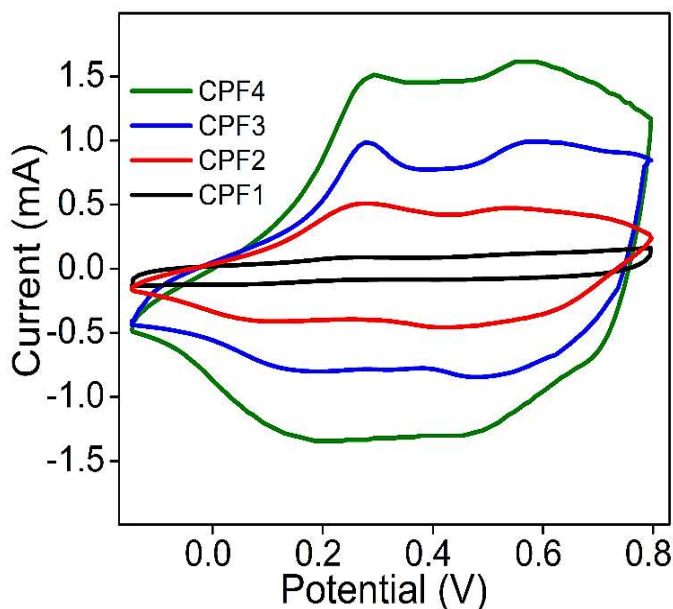


Figure 5.9 CV plot of Cs/PANI hybrid films obtained at a scan rate of 25 mV s^{-1}

The electrochemical activities of the hybrid films were analyzed by cyclic voltammetry. Figure 5.9 represents the CVs of hybrid films recorded between the potential limit of -0.15 V to -0.8 V at a scan rate of 25 mV s^{-1} in 1 M HCl solution at room temperature. The experiments were carried out in a three-electrode cell assembly after stabilizing the CV through 20 consecutive cycles. Here, hybrid films having an area of 20 mm^2 were used as working electrodes, an Ag/AgCl (3 M KCl) as the reference electrode and platinum wire as the counter electrode.

All the Cs/PANI hybrid films show two oxidation and two reduction peaks as in the case of PANI [33]. The similarity of oxidation

and reduction peaks with those of pure PANI proved that the electrochemical activity of hybrid films is imparted by the electroactive component PANI. The hybrid films showed different current responses, which are mainly ascribed to the different polyaniline content and electrical conductivity of the hybrid films (working electrodes). The current response in CV increases as the number of times of coating increases and the highest current is attained for CPF4 which is mainly ascribed to its highest electroactive PANI content, more porous structure and excellent electrical conductivity. The anodic and cathodic peak potentials of the hybrid films are listed in Table 5.2.

Table 5.2 *Anodic and cathodic peaks of Cs/PANI hybrid films at the scan rate 25 mV s⁻¹*

Film	Anodic peaks (V)		Cathodic peaks (V)	
	LE to ES	ES to PN	PN to ES	ES to LE
CPF1	0.27	0.54	0.43	0.059
CPF2	0.28	0.54	0.42	0.11
CPF3	0.28	0.59	0.48	0.19
CPF4	0.29	0.57	0.45	0.13

LE- leucoemeraldine, ES- emeraldine salt, PN- pernigraniline

The CV responses of hybrid films recorded at various scan rates from 5 mV s⁻¹ to 200 mV s⁻¹ are presented in Figure 5.10a-d. The anodic and cathodic peak currents increase linearly as a function of the square root of the scan rate as depicted in Figure 5.10e-h. It indicates that the oxidation/reduction reactions of Cs/PANI hybrid film electrodes are controlled by the ion diffusion process.

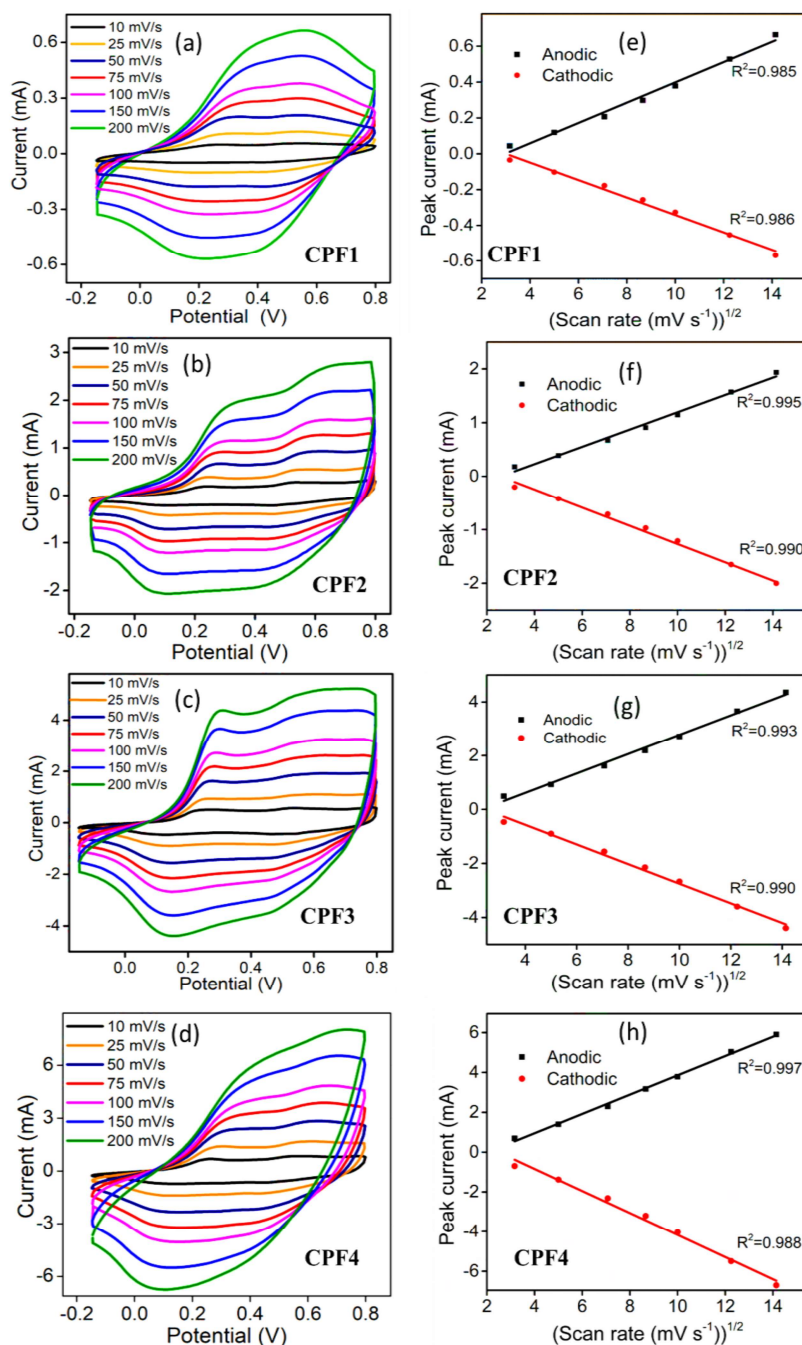


Figure 5.10 (a-d) CVs at different scan rates and (e-h) plots showing linear relation between the square root of scan rate with respect to anodic and cathodic peak currents of the Cs/PANI hybrid films

5.2.7.2. Coulvoltammetry

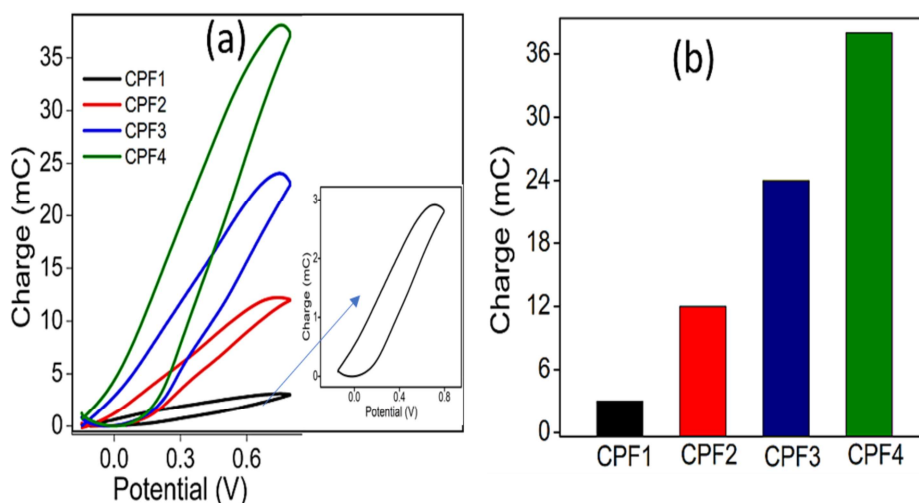


Figure 5.11 (a) *QVs of Cs/PANI hybrid films obtained by integration of CVs (Figure 5.9)* (b) *redox charges of Cs/PANI hybrid films obtained from QVs*

Figure 5.11a represents the QVs of Cs/PANI hybrid films obtained at the scan rate of 25 mV s^{-1} in 1 M HCl solution. The difference between the maxima and minima of the QV loop gives a redox charge of hybrid films at that particular experimental condition. The charge consumed by the reversible redox processes of the hybrid films is found to be 3 mC, 12 mC, 24 mC, and 38 mC respectively for CPF1, CPF2, CPF3 and CPF4 hybrid films (Figure 5.11b). The redox charge increases with increasing PANI content in the film. That is, higher PANI content leads to higher concentration of the active centers. This promotes a larger number of ions exchanged during the redox reaction and concomitant consumption of higher oxidation/reduction charges. All the hybrid films showed similar structural faradaic processes as in the case of PANI described in section 3.2.2.3.

II. Reaction driven sensing characteristics of Cs/PANI hybrid films

5.2.8. Sensing by chronopotentiometry

In this section, the reactive sensing characteristics of Cs/PANI hybrid films towards electrical, chemical and thermal working conditions are studied through consumed electrical energy as the sensing magnitude.

(a) Sensing electrical working condition: current sensor

For studying the sensing of electrical working conditions, i.e., applied current, by the hybrid films, chronopotentiograms were recorded from the aqueous solution of 1 M HCl corresponding to consecutive square currents waves of different magnitudes ranging from ± 0.1 mA to ± 1 mA. The time period of the square current waves was altered to attain constant oxidation and reduction charges ($Q = i \cdot t$, kept constant) for obtaining the same initial and final oxidation states or the same reaction extension in each experiment. Here, the chronopotentiograms of each hybrid film were recorded at a constant charge equal to their redox charge which is obtained from the coullovoltammograms at the scan rate of 25 mV s^{-1} (Figure 5.11). The normalized chronopotentiometric responses for the anodic and cathodic processes of the Cs/PANI hybrid films are shown in Figure 5.12a-d and Figure 5.12e-h, respectively. As the applied current increases, the potential evolution occurs to higher positive potential values for the anodic process and higher negative potential values for the cathodic process.

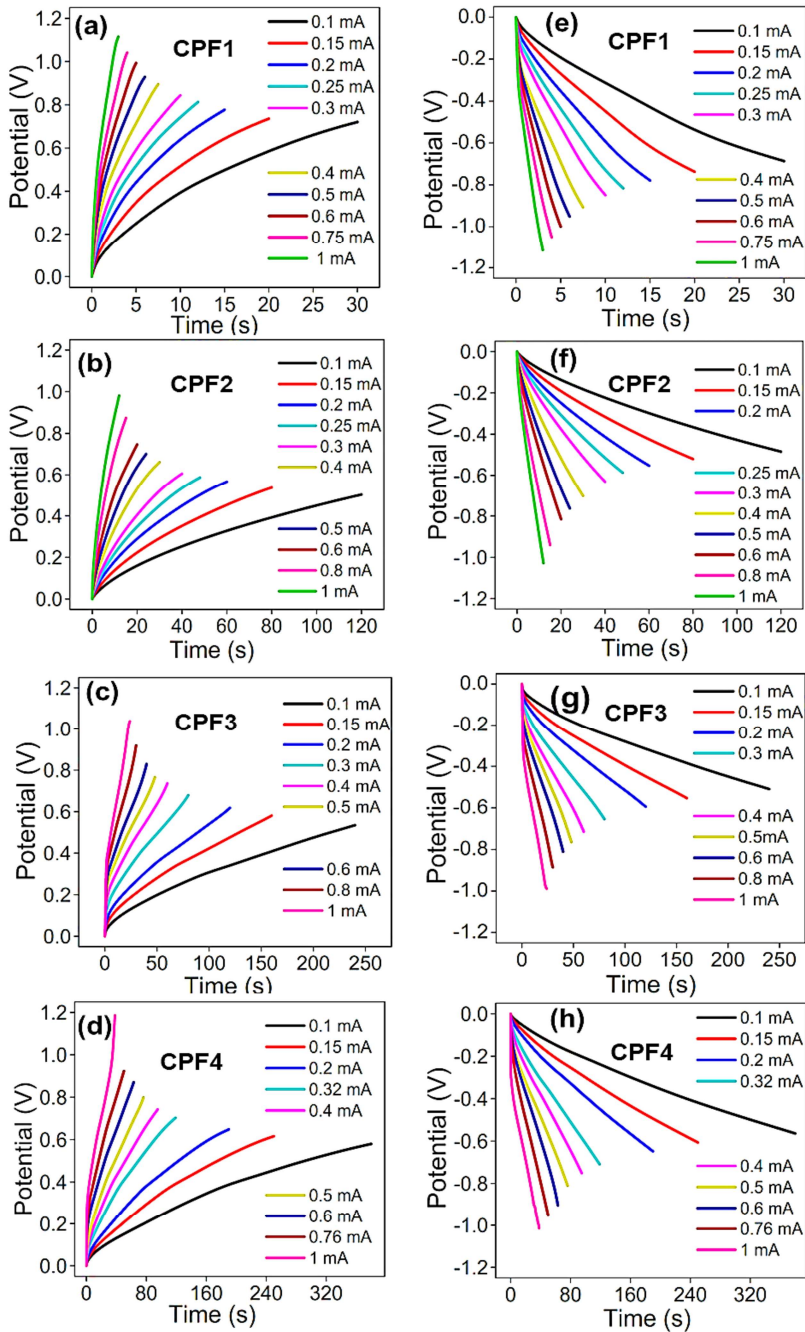


Figure 5.12 Anodic (a-d) and cathodic (e-h) chronopotentiograms were obtained when different currents were applied to Cs/PANI hybrid films by passing a constant electrical charge in 1 M HCl solution

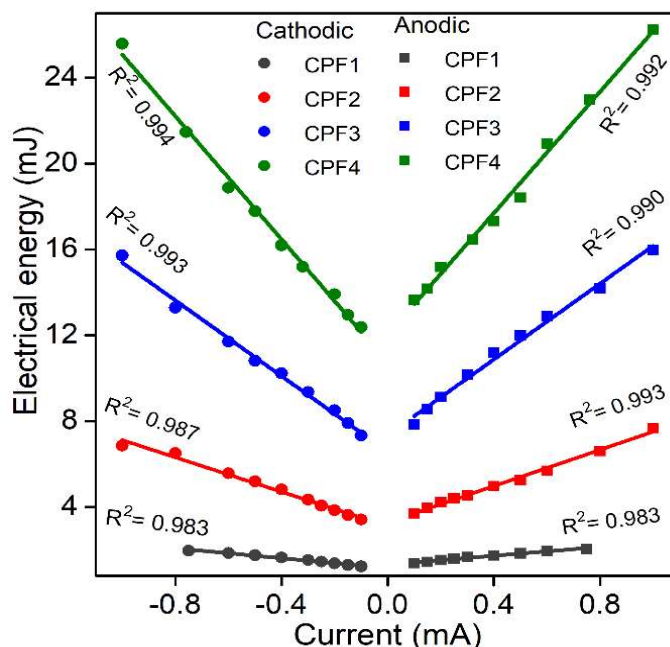


Figure 5.13 The linear variation of consumed electrical energy with the working current of Cs/PANI hybrid films

The consumed electrical energy during each oxidation/reduction process was calculated based on Equation 4.10. Figure 5.13 shows that the consumed electrical energy during the redox reaction has a linear dependence on the applied electric current for all the hybrid films. Therefore, the reaction energy senses or responds to locally imposed electrical energetic conditions. The slope of each current versus electrical energy calibration curve (Figure 5.13) denotes the sensitivity of the material as a sensor of the applied electrical current. The current sensitivities corresponding to the anodic and cathodic processes of all hybrid films are depicted in Figure 5.14. The highest sensitivity is obtained for CPF4, 14.14 mJ mA^{-1} and $-14.35 \text{ mJ mA}^{-1}$ for the anodic and cathodic processes, respectively. The sensitivity gradually increases from CPF1 to CPF4, as the number of times the coating of PANI

increases, due to increasing PANI content, which leads to a larger number of electroactive polymer active sites.

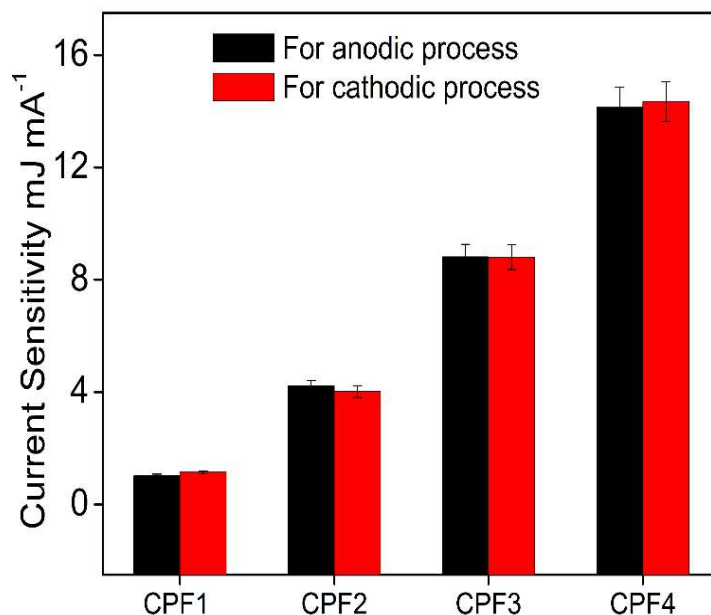


Figure 5.14 Current sensitivity of Cs/PANI hybrid films

(b) Sensing the chemical working condition: concentration sensor

To investigate the chemical working condition, i.e., the electrolyte concentration here, sensing characteristics of the Cs/PANI hybrid films, the chronopotentiograms were recorded from various concentrations of HCl ranging from 1 M to 0.05 M at a constant square wave current of ± 0.2 mA for a constant period of time to keep a constant charge ($i \cdot t = \text{constant}$) for same reaction extension in each experiment at room temperature. Figure 5.15 represents the normalized chronopotentiometric responses for the anodic (Figure 5.15a-d) and cathodic (Figure 5.15e-h) processes of the hybrid films at different concentrations of the electrolyte.

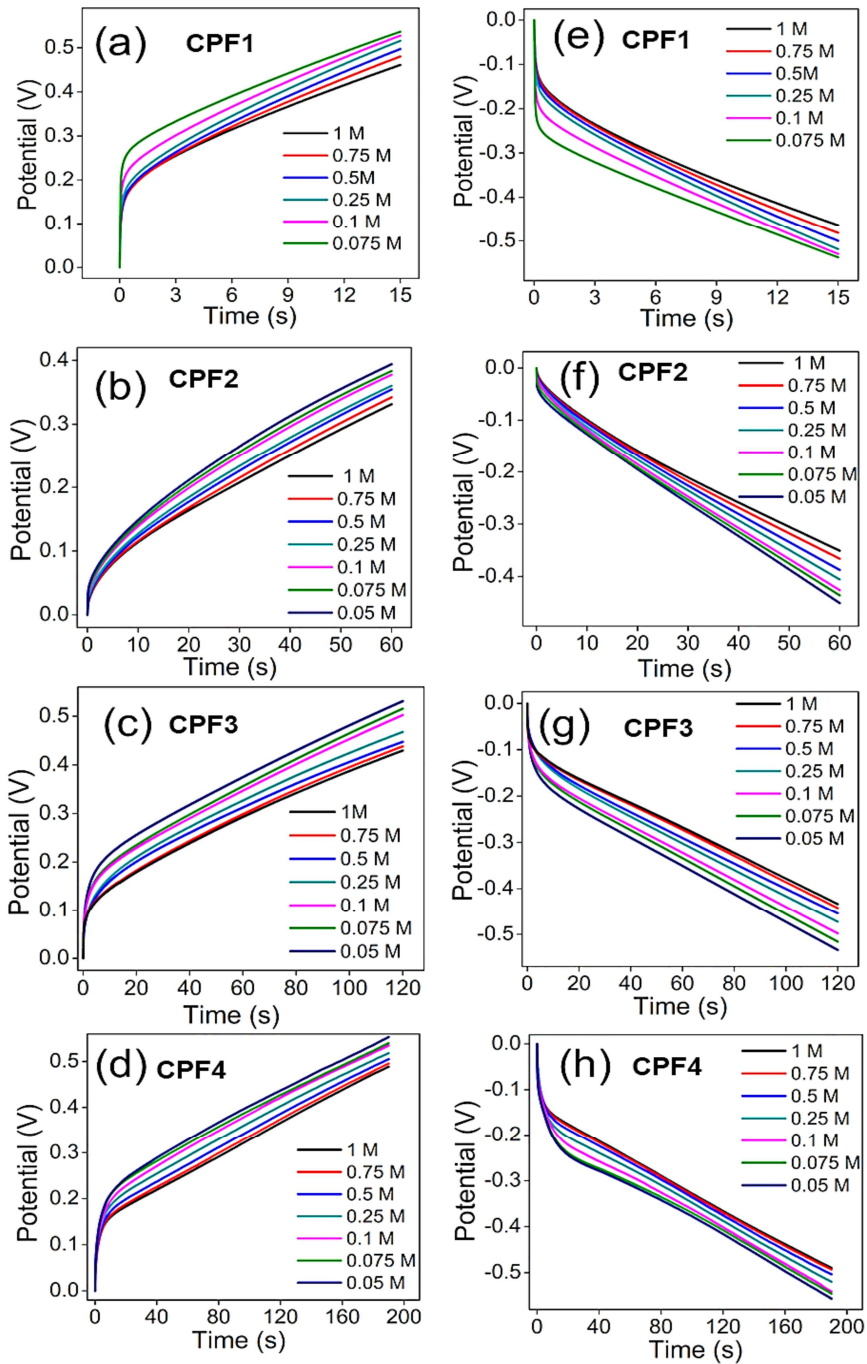


Figure 5.15 Anodic (a-d) and cathodic (e-h) chronopotentiograms obtained at different electrolyte concentrations for Cs/PANI films

During the reversible oxidation/reduction of the polymer films, the anodic and cathodic potentials evolve at lower values with increasing the electrolyte concentrations, under constant charge. That is, at higher concentrations, higher chemical energy is available and requires the consumption of lower electrochemical energy to attain the same reaction extension.

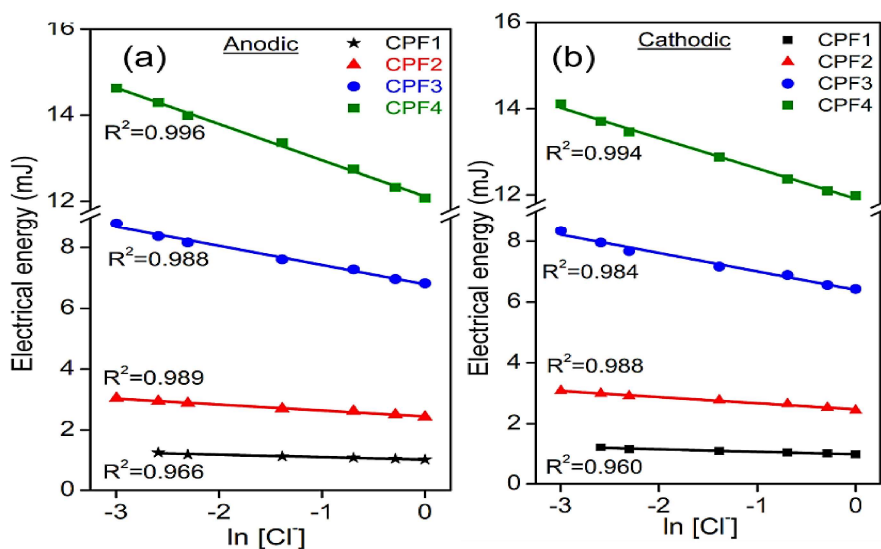


Figure 5.16 Linear variation of consumed electrical energy with the electrolyte concentration for (a) oxidation and (b) reduction process of Cs/PANI hybrid films

Upon integration of the chronopotentiometric responses at different concentrations, the electrical energy consumed during the reaction is obtained. The variation of consumed electrical energy during the oxidation and reduction of Cs/PANI hybrid films is presented in Figure 5.16. The electrical energy has a semi-logarithmic dependence on the electrolyte concentration. Hence, the reaction of Cs/PANI hybrid films can sense the chemical working condition. The slope of the calibration curve is the sensitivity of the hybrid films towards the

concentration of electrolyte, which is represented in Figure 5.17. The highest sensitivity of -0.84 mJ M^{-1} and -0.74 mJ M^{-1} for anodic and cathodic processes, respectively. As in the case of current sensing, the sensitivity gradually increases from CPF1 to CPF4 (Figure 5.17).

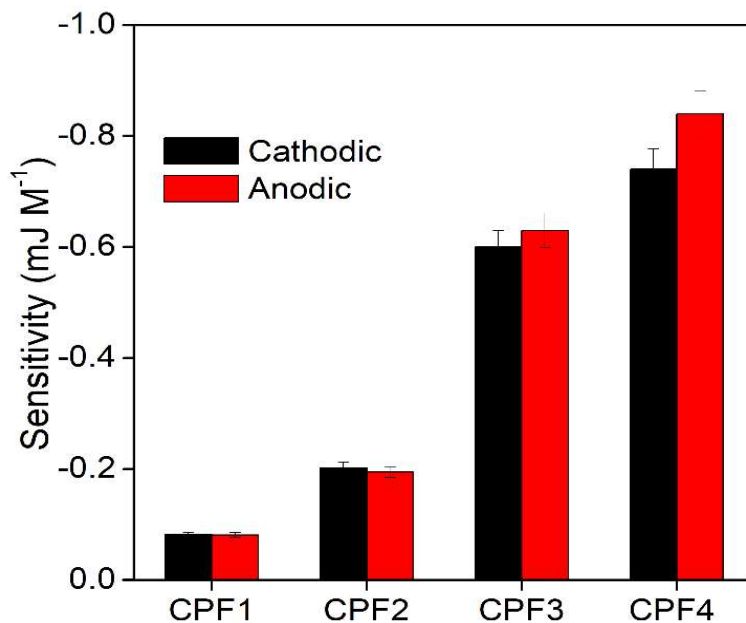


Figure 5.17 Concentration sensitivity of Cs/PANI electrodes

(c) Sensing thermal working condition: temperature sensor

To study the temperature sensing characteristics, the hybrid films were subjected to consecutive square current waves of $\pm 0.2 \text{ mA}$ at varying temperatures in 1 M HCl solution for a constant period of time, i.e., charge (i.t) is kept constant. The temperature sensing characteristics of all four synthesized hybrid films were carried out at their respective redox charges obtained from coul voltammograms. The obtained stationary and normalized chronopotentiograms corresponding to the oxidation and reduction processes of hybrid films are depicted in Figure 5.18.

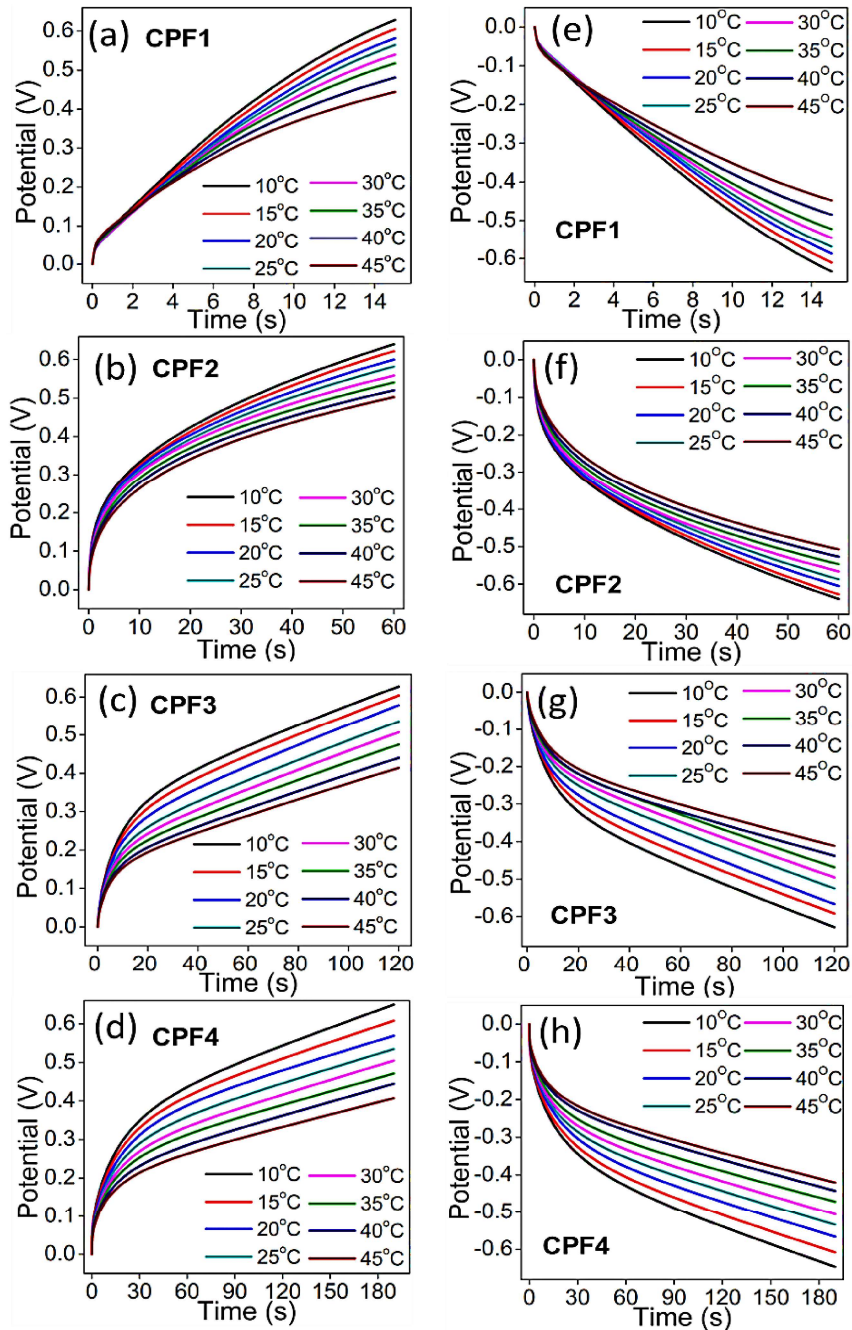


Figure 5.18 Anodic (a-d) and (e-h) cathodic chronopotentiograms obtained at different working temperatures for Cs/PANI hybrid films by passing a constant electrical charge in 1 M HCl solution

As the temperature increases, the available thermal energy increases and the electrode reaction requires lower electrical energies compared to that required at a lower temperature for attaining the same reaction extension. Therefore, the material potential evolves at lower values during the reaction taking place at higher temperatures to go from the same initial state to the same final state every time.

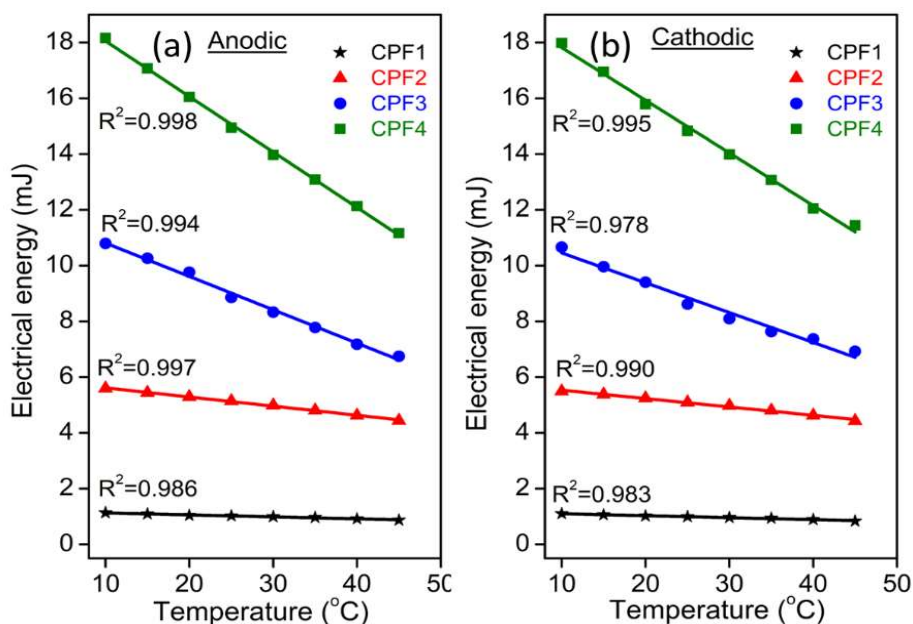


Figure 5.19 Linear variation of consumed electrical energy for (a) oxidation and (b) reduction process of Cs/PANI hybrid films with the working temperature

The electrical energy required during each oxidation-reduction reaction at different temperatures is obtained by the integration of corresponding chronopotentiograms. The consumed electrical energy during the anodic and cathodic process of Cs/PANI hybrid film has a linear dependence on the working temperature as depicted in Figure 5.19a and 19b. It reveals that Cs/PANI hybrid films can act as

sensors of the working temperature. The slope of the calibration curves represents the sensitivities of Cs/PANI hybrid films towards the working temperature which is represented in Figure 5.20. The highest sensitivity of $-198.84 \mu\text{J K}^{-1}$ and $-188.83 \mu\text{J K}^{-1}$ for anodic and cathodic processes, respectively, were obtained for CPF4 film. The temperature sensitivity gradually increases from CPF1 to CPF4 as depicted in Figure 5.20, because, the PANI content increases with the number of times of coating increases, then the resulting film has a greater number of electroactive polymer sites.

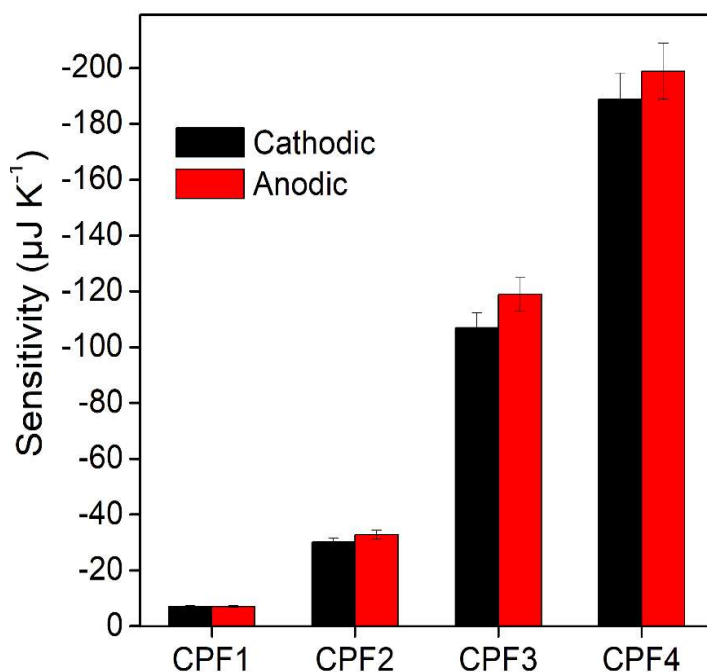


Figure 5.20 Temperature sensitivity of Cs/PANI hybrid films

5.2.9. Sensing by voltammetry

Here, the sensing characteristics of the polymer reaction of Cs/PANI hybrid films towards electrical, chemical and thermal working

conditions are studied by voltammetry and explained through the extension of reaction or consumed electrical charge as the sensing magnitude.

(a) Sensing electrical working condition

In order to study the sensing capability of Cs/PANI hybrid film towards electrical conditions, i.e., scan rate, the CVs are recorded for different scan rates from 10 mV s^{-1} to 200 mV s^{-1} in the potential window of -0.15 V to 0.8 V in 1 M HCl solution at room temperature for each of the hybrid film. The consumed electrical charge during the redox process was obtained from corresponding QVs.

Figure 5.21a-d are the stationary CV responses after two consecutive potential cycles for every studied scan rate and the corresponding QVs are presented in Figure 5.21e-f. The QV maxima decreases with increasing scan rates which indicates that the redox charge decreases at higher scan rates. At lower scan rates the oxidation/reduction potentials are applied for a long period of time which promotes deeper conformational changes of the PANI chains, thereby generating/destroying large free volumes. A large number of ions and solvent molecules are exchanged between the electrode and the electrolyte. Therefore, deeper oxidation/reduction states are attained by the consumption of high redox charges. That means the greater extension of the reaction at a lower scan rate. The slope of the QV curves (steeper portion) decreases with the increase of scan rate evidencing the decreasing of rate of electron transfer process at the interface with increasing the scan rates. Hence, decreasing the charge consumed during the reaction.

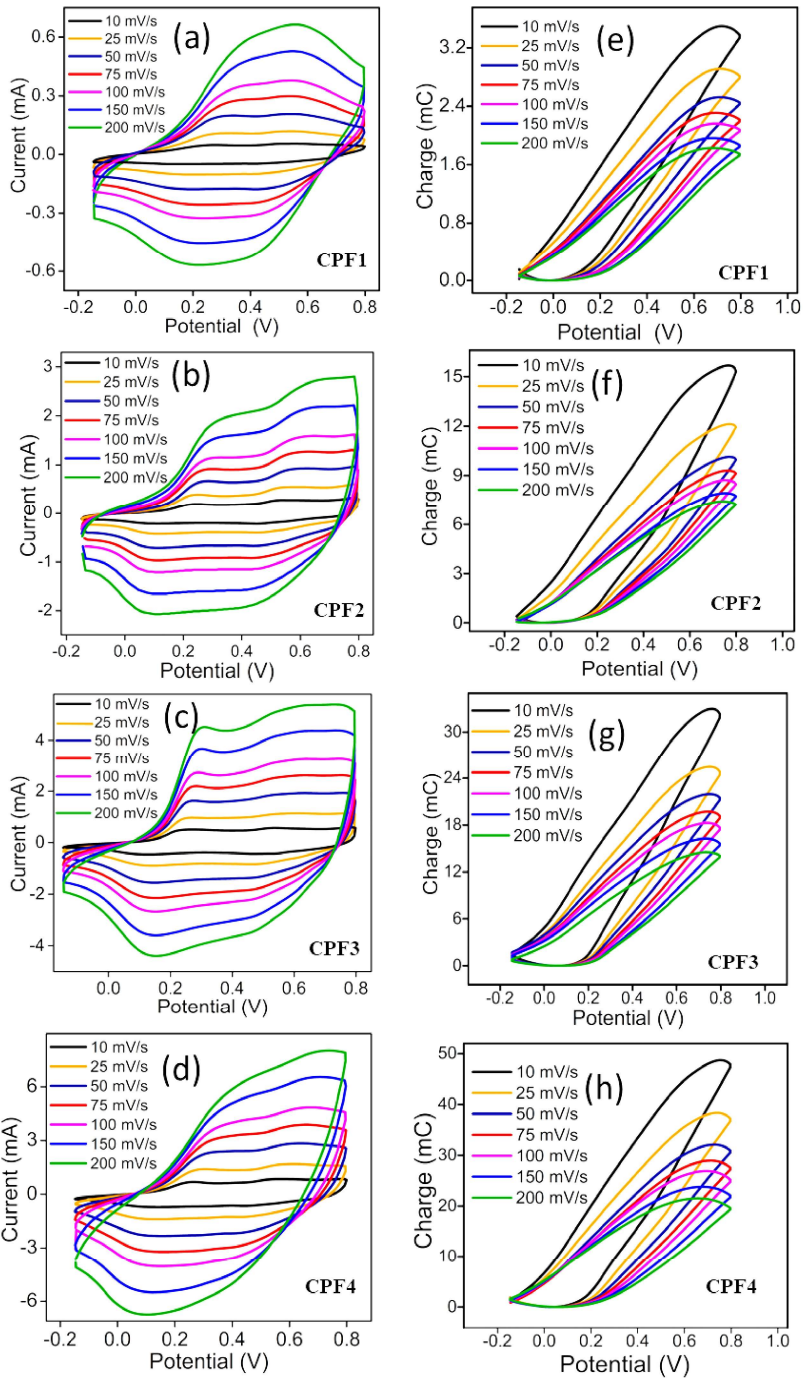


Figure 5.21 (a-d) CVs and (e-f) corresponding QVs for Cs/PANI hybrid films at different scan rates

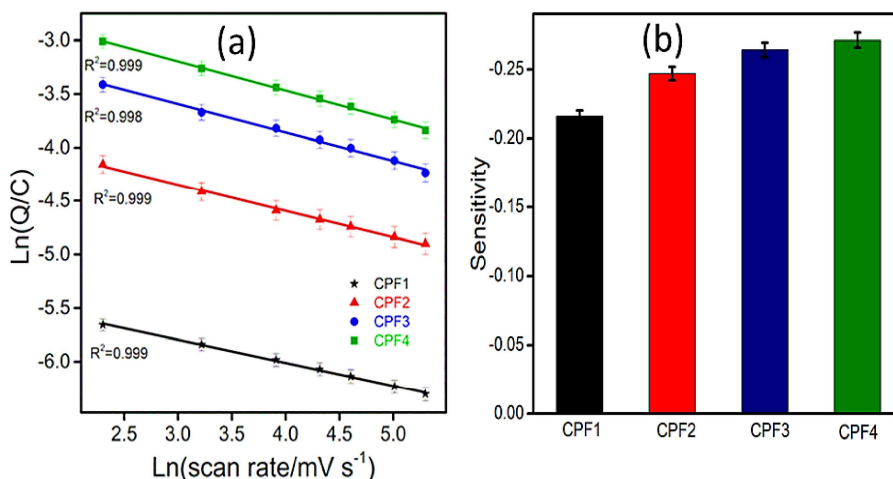


Figure 5.22 (a) The double-logarithmic linear dependence between the charge consumed by the redox reaction of Cs/PANI hybrid films with scan rate and **(b)** sensitivity of Cs/PANI hybrid films toward scan rate

Figure 5.22a shows the linear double logarithmic variation of the redox charge with the scan rate. The good linear fit for all the hybrid films indicates that the consumed redox charge during the oxidation/reduction reaction of Cs/PANI hybrid films senses the electrical working conditions. The slope of the calibration curve is the sensitivity, which increases from CPF1 to CPF4 as increasing the PANI content in the film as shown in Figure 5.22b.

(b) Sensing chemical condition: concentration sensor

For studying the sensing capability of Cs/PANI hybrid films towards chemical condition, i.e., the concentration of electrolyte, the CVs are recorded from different concentrations of HCl solution at a scan rate of 25 mV s⁻¹ in the potential window of -0.15 V to 0.8 V at room temperature for each of the hybrid film. The consumed charge during the redox process was obtained from corresponding QVs.

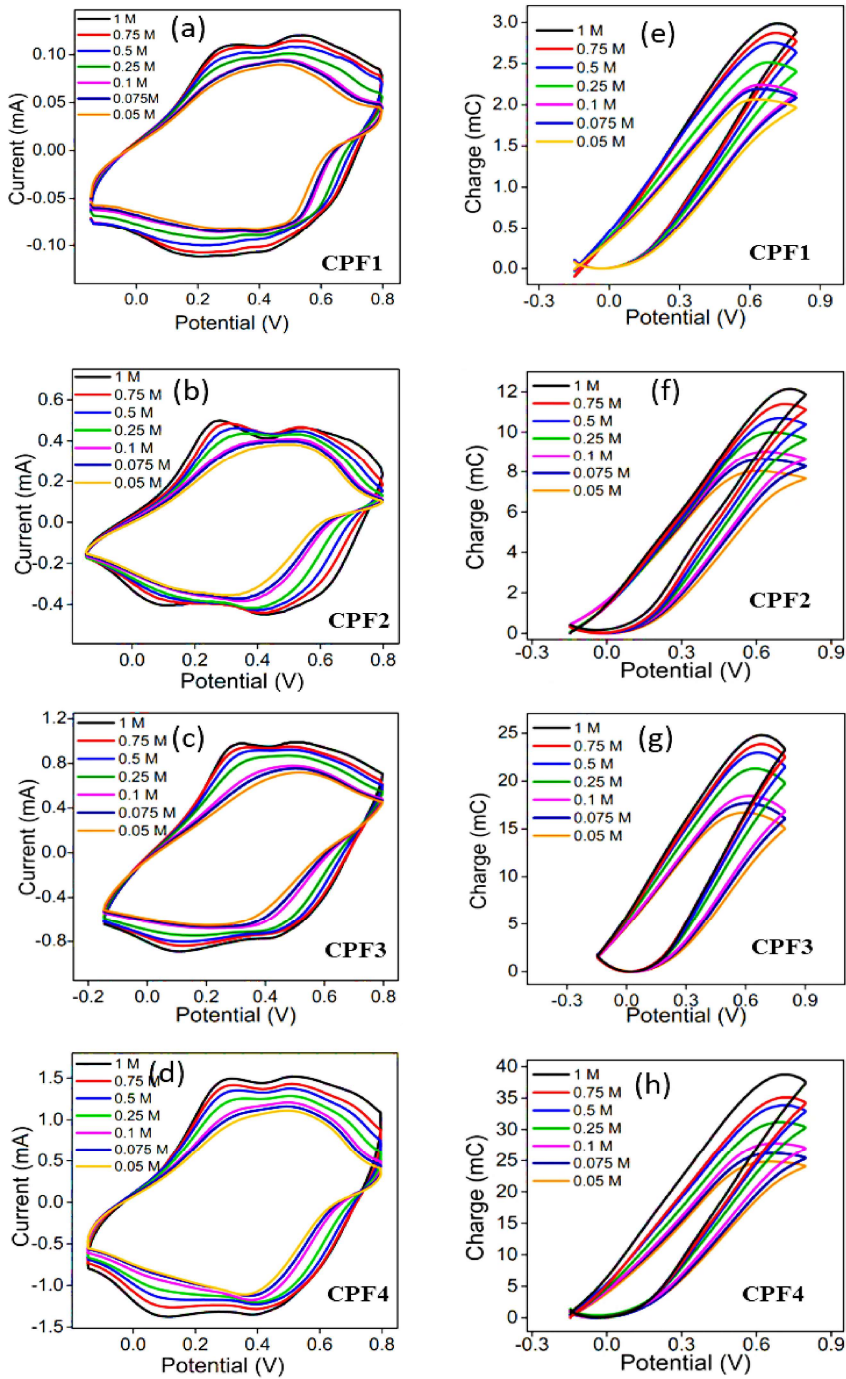


Figure 5.23 (a-d) CVs at different electrolyte concentrations and (e-f) corresponding QVs for Cs/PANI hybrid films

Figure 5.23a-d represents the stationary CV responses obtained for the hybrid films at different concentrations of electrolyte and the corresponding QV responses are presented in Figure 5.23e-h. The QV maxima increases with the increase of concentration of electrolyte. It indicates that the redox charge increases as electrolyte concentration increases. At higher concentrations, higher chemical energy is available which promotes deeper conformational movements of the polymer chains, thereby generating/destroying large free volumes. A large number of ions and solvent molecules are exchanged between the electrode and electrolyte. Therefore, deeper oxidation/reduction states are attained by the consumption of high redox charges. That means a greater extension of the reaction at a higher concentration. As the concentration decreases, available chemical energy decreases. Only partial convolutions/deconvolutions of the polymeric chain led to partial oxidation/reduction by consumption of lower redox charge compared to that obtained at higher concentration.

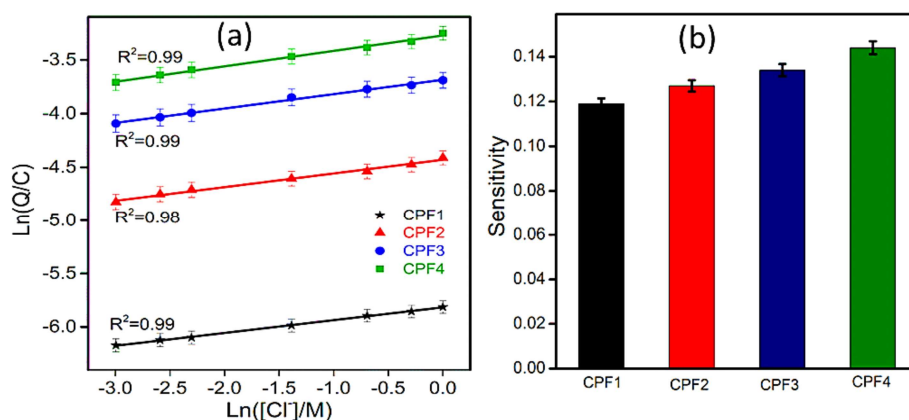


Figure 5.24 (a) *The double-logarithmic linear dependence of consumed charge with the concentration of electrolytes and* (b) *concentration sensitivity of the Cs/PANI hybrid films*

Figure 5.24a indicates that the consumed charge during the redox reaction of Cs/PANI hybrid films has a double logarithmic dependence on the concentration of the electrolyte. A good linear fit for all the hybrid films revealed that the consumed redox charge during the redox reaction of the hybrid films has the capability to respond to or sense their chemical working conditions. The slope of the calibration curve is the sensitivity, which increases from CPF1 to CPF4 with an increase in the PANI content of the films as shown in Figure 5.24b.

(a) Sensing thermal working condition: temperature sensor

To investigate the sensing capability of Cs/PANI hybrid films towards thermal conditions, i.e., working temperature, the CVs are recorded at different temperatures at a scan rate of 25 mV s^{-1} in the potential window of -0.15 V to 0.8 V from 1 M HCl solution for each hybrid film. Figure 5.25a-d represents the stationary CV responses obtained for the hybrid films at different temperatures and Figure 5.25e-h are the corresponding QVs.

The QV maxima increases as temperature increases, which indicates that the redox charge increases as temperature increases. At higher temperatures, higher thermal energy is available which promotes deeper conformational movements of the polymeric chains, thereby generating/destroying large free volumes leading to the exchange of a large number of ions and solvent molecules between electrode and electrolyte. Therefore, deeper oxidation/reduction states are attained by the consumption of high redox charges. That means a greater extension of the reaction at a higher concentration.

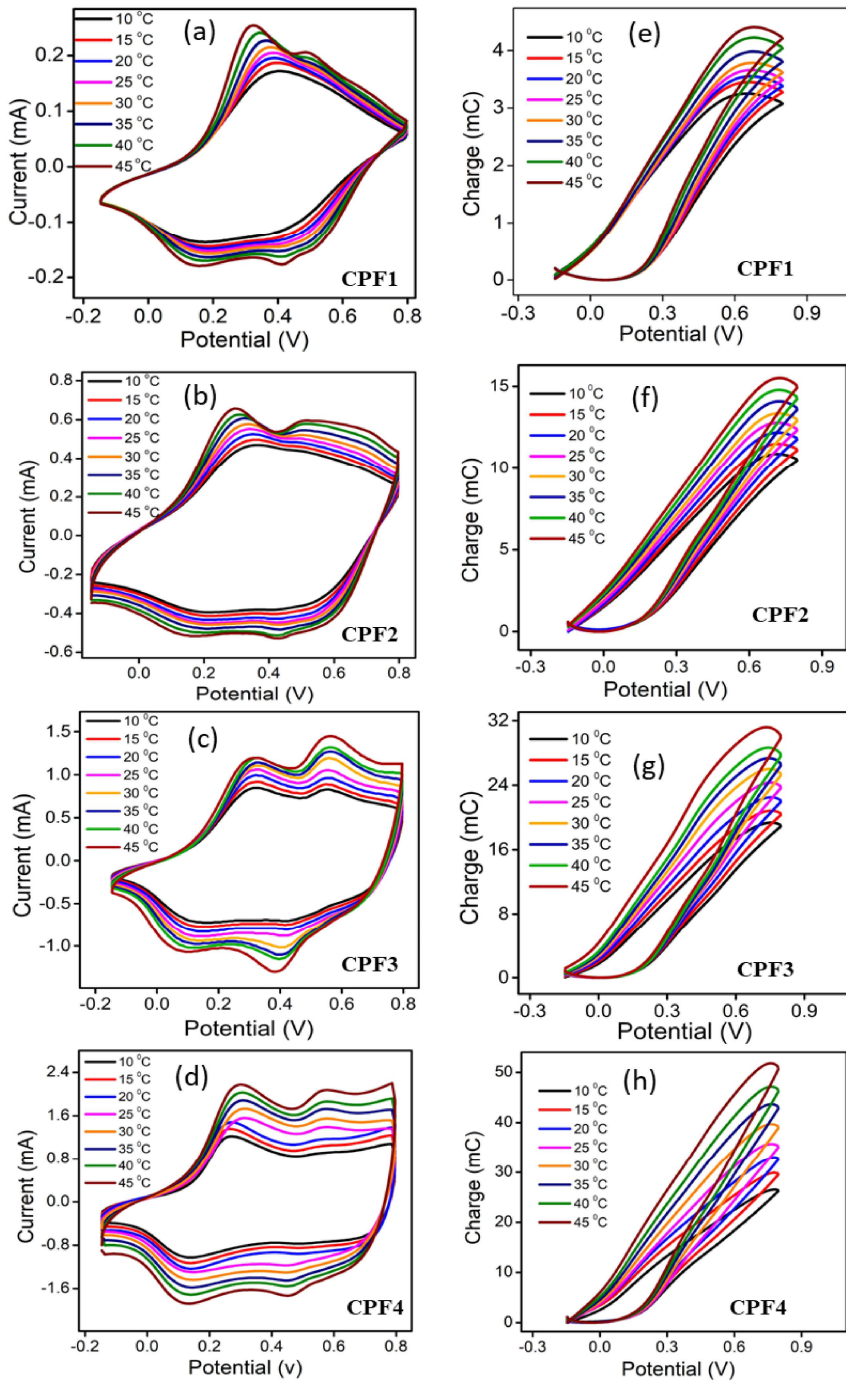


Figure 5.25 (a-d) CVs at different temperatures and (e-f) corresponding QVs for CPF1, CPF2, CPF3 and CPF4

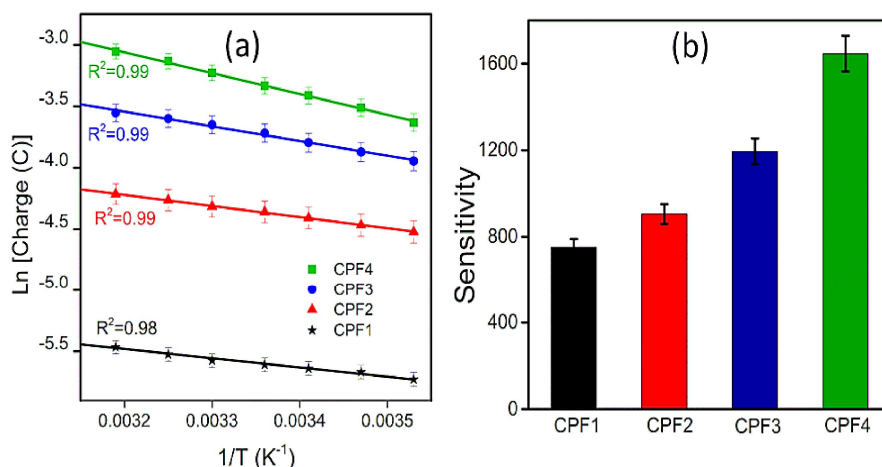


Figure 5.26 (a) The logarithmic linear dependence of consumed charge during the reaction of Cs/PANI hybrid films with the inverse of temperature and **(b)** temperature sensitivity of Cs/PANI hybrid films

Figure 5.26a indicates that the consumed charge during the redox reactions of Cs/PANI hybrid films have a logarithmic dependence on the inverse of temperature which reveals that the consumed redox charge during the redox reaction of All the hybrid films responds to or senses their thermal working conditions. The slope of the calibration curves is the sensitivities of hybrid films towards working temperature. The sensitivity increases from CPF1 to CPF4 due to increasing the PANI content. it is represented in Figure 5.26b.

In the above discussion, it is clear that PANI/hydrogel systems also have reaction driven sensing properties like PANI. The sensitivities of Cs/PANI hybrid films towards current, concentration and temperature through consumed electrical energy as well as consumed charge as sensing parameters are summarized in Table 5.3.

Table 5.3 Sensitivities of Cs/PANI hybrid films towards various working conditions, where consumed electrical energy and consumed charge during the reaction as sensing parameters

Film	<i>Consumed electrical energy as a sensing parameter</i>					
	Current sensitivity (mJ mA ⁻¹)		Concentration sensitivity (mJ mol ⁻¹)		Temperature sensitivity (μJ K ⁻¹)	
	Anodic	Cathodic	Anodic	Cathodic	Anodic	Cathodic
CPF1	1.15	-1.02	-0.081	-0.082	-7.04	-7.10
CPF2	4.02	-4.22	-0.194	-0.202	-32.76	-30.08
CPF3	8.81	-8.82	-0.635	-0.605	-119.01	-107.05
CPF4	14.35	-14.14	-0.845	-0.745	-198.84	-188.83
<i>Consumed electrical charge as a sensing parameter</i>						
film	Scan rate sensitivity (C/mV/s)		Concentration sensitivity (C/M)		Temperature sensitivity (C/K ⁻¹)	
CPF1	-0.216		0.119		751.93	
CPF2	-0.247		0.127		905.22	
CPF3	-0.264		0.134		1195.06	
CPF4	-0.271		0.144		1646.31	

III. Chitosan/PANI hybrid films as electrode materials for supercapacitors

5.2.10. The areal specific capacitance of Cs/PANI hybrid film free-standing electrodes

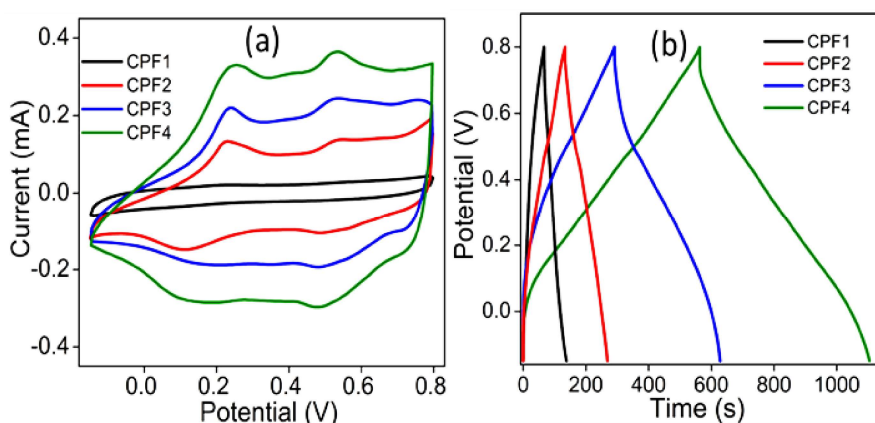


Figure 5.27 (a) CVs at a scan rate of 5 mV s^{-1} and (b) GCD curves at a current density of 0.4 mA cm^{-2} of Cs/PANI hybrid films

The charge storage performance of the hybrid films was examined through CV and GCD analysis in a three-electrode assembly. The films with an area of 0.2 mm^2 were used as working electrodes. Figure 5.27a represents the CVs obtained at a scan rate of 5 mV s^{-1} within the potential range of -0.15 to 0.8 V . The CV response of hybrid films shows non-rectangular CV curves with two pairs of redox peaks attributed to the faradaic pseudocapacitive dominance. The specific capacitance of the hybrid film electrodes was calculated from the CV curves according to Equation 2.1 and the area of the CV curve is proportional to the specific capacitance of the material. Among all hybrid films, CPF4 has the largest enclosed area ascribed to the highest specific capacitance which is consistent with the conductivity of the

films. The areal specific capacitance obtained for CPF1, CPF2, CPF3 and CPF4 is 48 mF cm^{-2} , 195 mF cm^{-2} , 309 mF cm^{-2} and 468 mF cm^{-2} , respectively, at a scan rate of 5 mV s^{-1} .

Figure 5.27b represents the GCD curves of Cs/PANI hybrid films obtained at a current density of 0.4 mA cm^{-2} within a potential range of -0.15 to 0.8 V . The discharge time is related to the energy storage property of the electrode material. Their deviation from linearity is caused by the redox process, demonstrating their pseudocapacitive behavior. CPF4 showed the highest discharge time among these hybrid films which is consistent with its high electrical conductivity and electroactive characteristics thus promoting an efficient electron transfer process. The areal specific capacitance values were calculated using Equation 2.2. The CPF1, CPF2, CPF3 and CPF4 have a specific capacitance of 31 mF cm^{-2} , 59 mF cm^{-2} , 146 mF cm^{-2} and 241 mF cm^{-2} respectively, at current density of 0.4 mA cm^{-2} .

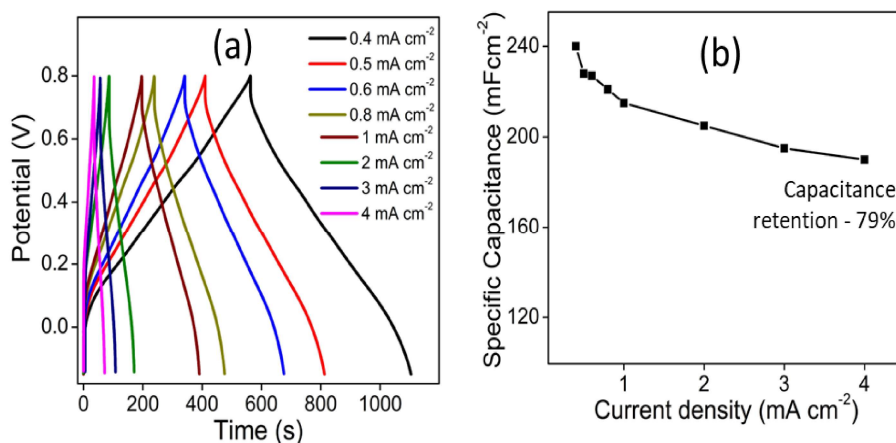


Figure 5.28 (a) GCD curves of CPF4 at different current densities and (b) variation of specific capacitance with current density

The GCD curves of CPF4 at different current densities are depicted in Figure 5.28a. The GCD curves are almost symmetrically shaped, indicating that the hybrid films have superior electrochemical reversibility and excellent coulombic efficiency. CPF4 film has only negligible IR drop in the studied potential range. Generally, the IR drop is attributed to low electron and ionic transfer rates. Here, the chitosan hydrogel matrix provides good hydrophilicity to the hybrid film. The swollen state of Cs/PANI hybrid films may allow facile permeation of ions and electrons in between PANI chains and enhance the effective surface area between molecular chains and the solution phase. It is schematically represented in Figure 5.29. The above-described events facilitate fast electron and ionic transfer leading to low IR drop as well as high electrochemical performance.

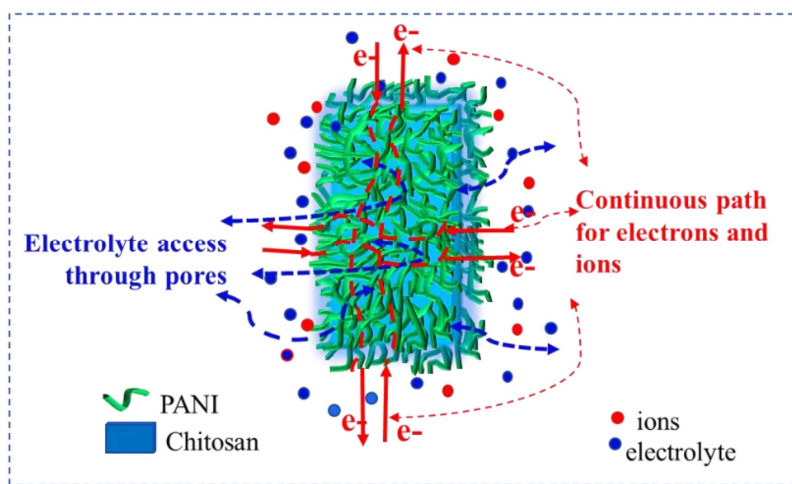


Figure 5.29 Schematic representation of structural features of Cs/PANI hybrid film enabling high electrochemical activity

The variation of specific capacitance as a function of current density from 0.4 to 4 mA cm⁻² corresponding to CPF4 is presented in

Figure 5.28b. As expected, the capacitance decreases as the current density increases due to the provision of less time for the electrolyte ions to diffuse into active sites and interact with active material at the high current densities. Interestingly, it is noted that the 79 % capacitance retained after ten times increase in current density which indicates that the electrode material has good kinetics and rate capability due to the presence of chitosan which facilitates ion transport. This value is higher than the reported values for conducting polymer based electrode materials which typically show 50–60 % capacitance retention at a 10-fold higher current density [34, 35].

Figure 5.30a shows the CVs of CPF4 films at different scan rates. The relationship between specific capacitance and scan rates for CPF4 is presented in Figure 5.30b. The specific capacitance decreases with scan rate, because, at higher scan rates the potentials are applied for a shorter time, and the electrolyte ions do not get sufficient time to interact with electrode material effectively at higher scan rates.

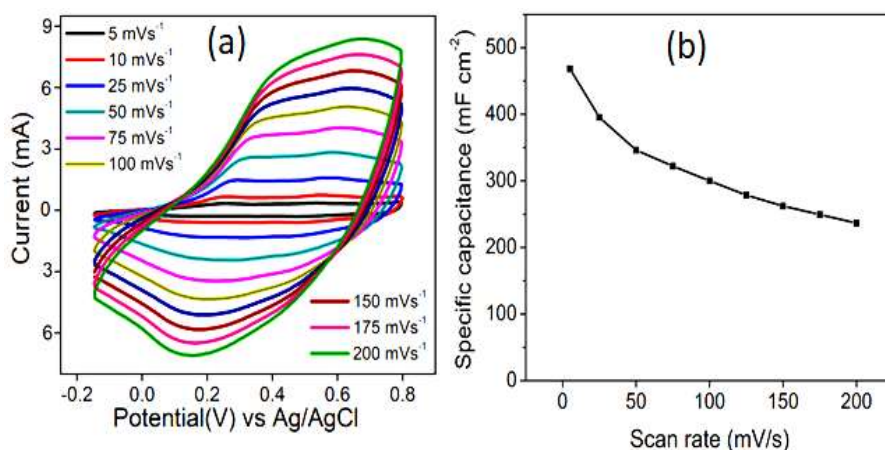


Figure 5.30 (a) CVs at different scan rates and (b) variation of specific capacitance of CPF4 electrode with scan rate

5.2.11. EIS analysis

EIS was performed to analyze the fundamental electrochemical behaviour of Cs/PANI hybrid films. Figure 5.31 represents the Nyquist plot of hybrid films (the inset shows the magnified plot of CPF3 and CPF4). The plots have a small semicircle part in the high-frequency region and a nearly straight oblique line in the low-frequency region. The semicircle mainly depicts the charge transfer process at the electrode-electrolyte interface and whose intercept to the real axis at the high-frequency region is meant for the equivalent series resistance (ESR) including solution resistance, the internal resistance of materials and the contact resistance between the electrode and electrolyte [36, 37].

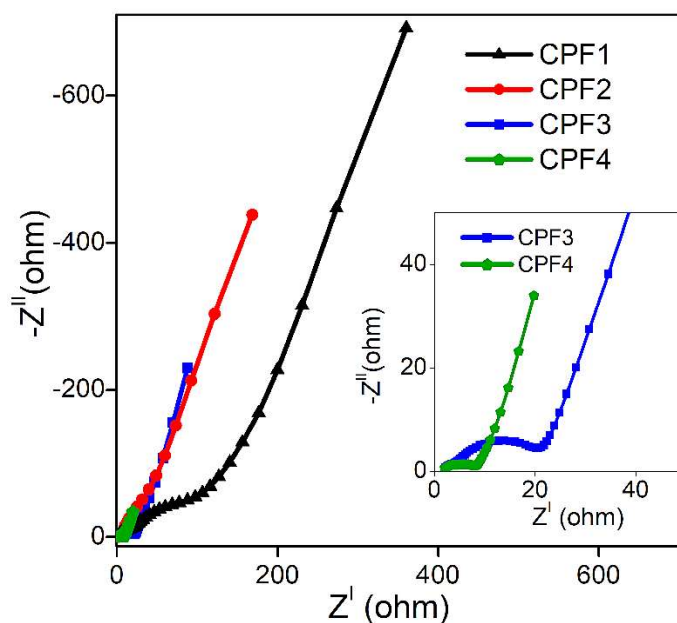


Figure 5.31 Nyquist plot of Cs/PANI hybrid film electrodes

All the Cs/PANI hybrid films have low ESR values which is attributed to the high hydrophilicity of Cs/PANI hybrid films as well as

to the better interconnection between the electrode and the electrolyte. The semicircle diameter reflects the migration impedance of charges or the charge transfer resistance (R_{ct}). The Nyquist plot showed a very small semi-circle in the high-frequency region which is ascribed to the smooth charge transfer between the electrode and the electrolyte because the polyaniline coated chitosan in the hydrogel film acts as a continuous channel for electrons and ions. The diameter of semicircles decreases from CPF1 to CPF4 suggestive of declining the charge transfer resistance, thus increasing the electron transfer in the same order due to an increase of electrical conductivity. The oblique line refers to the diffusion-limited ion transport process across the electrode surfaces, its slope gives the diffusion impedance and a larger slope of the line indicates the higher diffusion rate of ions. Here, the CPF4 films show a relatively large slope because of the highly porous nature of CPF4 films as evidenced by SEM images, which facilitate ion diffusion. The results of the EIS analysis are consistent with CV and GCD results.

5.2.12. Cycling stability

The long-term cycling stability of the CPF4 hybrid film electrode was monitored by GCD for over 1500 cycles at 2 mA cm^{-2} . The result is depicted in Figure 5.32. Conducting polymers usually suffer poor cyclic stability due to the structural degradation of the polymer chain caused by repeated intercalation/deintercalation (swelling/shrinking) of ions during the repeated charge/discharge process [38]. But, our CPF4 hybrid electrode shows good electrochemical stability, which retains 86 % of its initial capacitance after 1500 cycles, attributed to the strong synergy existing between

chitosan and polyaniline resulting in a supportive and protective effect on PANI during swelling and shrinking.

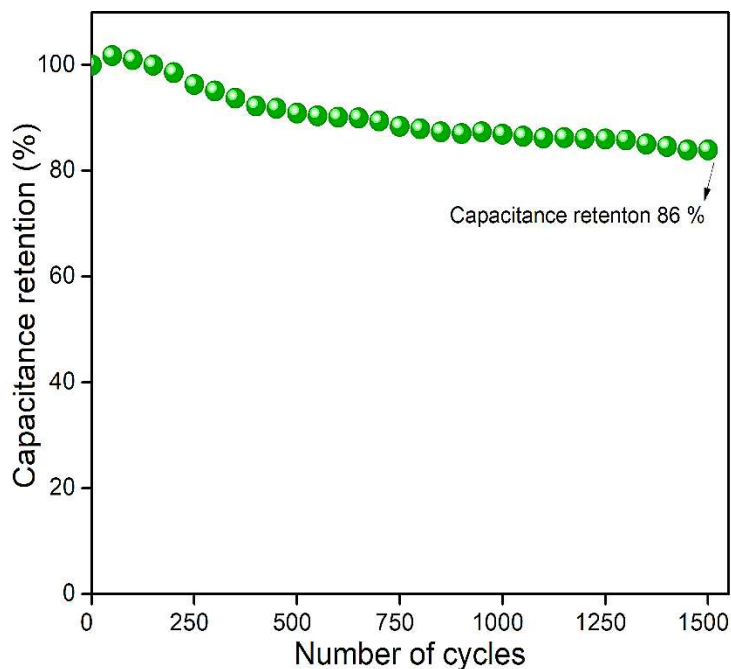


Figure 5.32 Cycling stability of CPF4 for 1500 cycles

5.2.13. Charge storage kinetics of CPF4 electrode

In addition, the charge storage behaviour of CPF4 hybrid film can be explored by applying the power law which relates the current ' i ' at a particular potential with the scan rate ' v ' by the following relationships:

$$i = av^b \quad (5.1)$$

$$\log(i) = \log(a) + b \log(v) \quad (5.2)$$

Both a and b are constants. The value of b at different potentials can be obtained by plotting $\log(i)$ against $\log(v)$ as shown in Figure 5.33a. In

general, $b = 0.5$ corresponds to the ideal diffusion controlled Faradaic process, while $b = 1$ corresponds to the outer surface non-diffusion-controlled process (double layer phenomenon) [39]. The b values at the different potentials for an anodic process are represented in Figure 5.33b. the b values lie between 0.5 and 1, which means that the charge storage comes from both diffusion-controlled and the capacitive (double layer) process. Then, the capacitive and diffusive contribution in CPF4 film is quantified by Dunn's method [39, 40]. The total current contribution at a potential is the sum of diffusive-controlled and capacitive currents which is defined as;

$$i(V) = i_{capacitive} + i_{diffusion} = k_1v + k_2v^{1/2} \quad (5.3)$$

divide equation (5.3) by $v^{1/2}$ on both sides

$$i(V)/v^{1/2} = k_1v^{1/2} + k_2 \quad (5.4)$$

Using the above equation, we determined the slope k_1 and the intercept k_2 , by plotting $i(V)/v^{1/2}$ vs $v^{1/2}$ to obtain capacitive and diffusive current at a particular potential 'V'. Figure 5.33c illustrates the graphical representation of the current contribution by the capacitive and diffusion-controlled process for a scan rate of 5 mV s^{-1} . The highlighted area with navy blue colour reveals the capacitive contribution in the CV curve. At the lower scan rate of 5 mV s^{-1} the contribution from the diffusion limited faradaic process is 51 % and from the non-faradaic process is 49 %. The bar plots of percentage contribution from the capacitive and diffusive process for different scan rates are presented in Figure 5.33d. As increasing the scan rate, the diffusive contribution is

decreased while the capacitive contribution is increased. At the highest scan rate of 100 mV s^{-1} , the CPF4 electrode has a capacitive contribution of 82 % in comparison to a diffusive contribution of 18%. This is because, at a lower scan rate, sufficient time is available to complete the redox reaction and thereby a larger diffusive contribution to the overall capacitance.

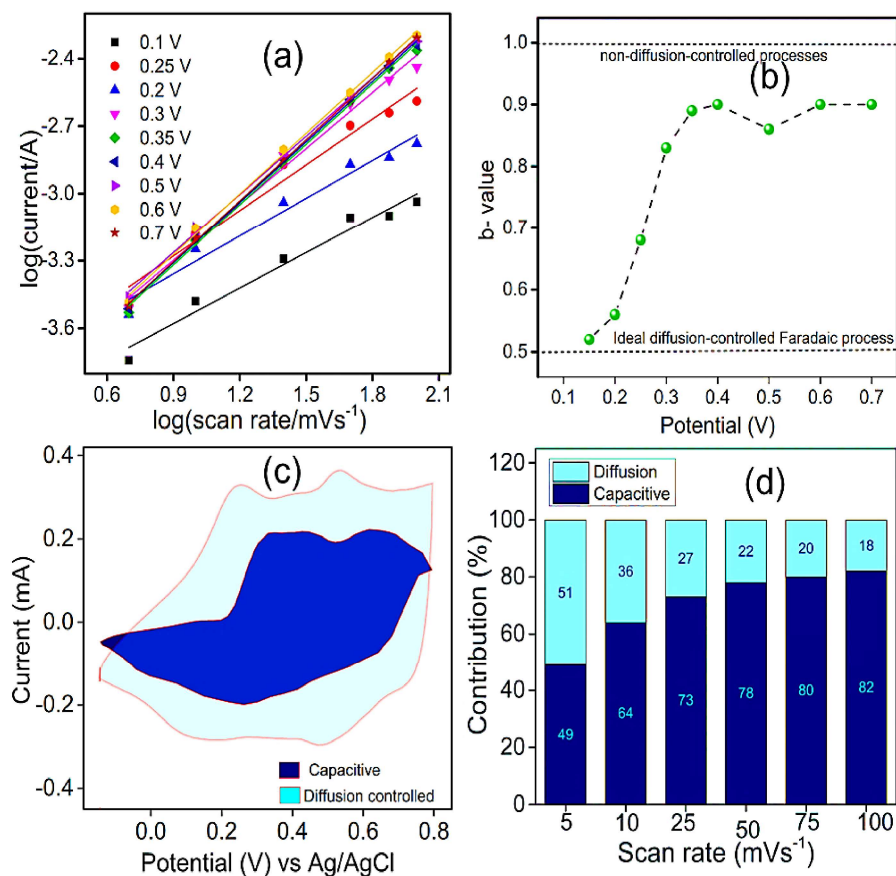


Figure 5.33 (a) The determination of 'b' values at different potential regimes, (b) the obtained 'b' values, (c) separation of the capacitive and diffusion currents at a scan rate of 5 mV s^{-1} and (d) contribution ratios from non-faradaic double layer process (capacitive) and diffusion-limited oxidation/reduction of CPF4 at various sweep rates.

5.3. Conclusions

Cs/PANI hybrid films were fabricated by a simple and inexpensive method, by in situ chemical oxidative polymerization of aniline using a previously fabricated chitosan matrix. Hybrid films were characterized by FTIR, TGA, SEM, EDAX, electrical conductivity measurement and mechanical studies. The electrical conductivity of hybrid films increases as the number of times of coating increases. The mechanical studies revealed that CPF films have moderately good mechanical stability to use them as free-standing electrodes. CV analysis revealed the electroactivity of Cs/PANI hybrid films is imparted by PANI. The redox charges of hybrid films were analyzed from QV, which increases with the number of times coating increases and thereby with an increase in the polyaniline content in the hybrid film.

The reaction driven sensing properties of Cs/PANI hybrid films towards electrical, thermal and chemical working conditions were studied through consumed electrical energy as well as consumed charge as sensing parameters. It is proved that hybrid systems have reactive sensing capabilities. The consumed electrical energy during the oxidation-reduction of Cs/PANI hybrid films has a good linear dependence with applied current and temperature as well as a logarithmic dependence with electrolyte concentration. The consumed charge during the redox reaction of Cs/PANI hybrid films has a linear double logarithmic dependence on scan rate and electrolyte concentration as well as a logarithmic dependence with the inverse of temperature. The sensitivities increase with increasing the number of

times of coating increases due to an increase in the reaction active site. Thus the Cs/PANI hybrid films were proven to act as current sensors, concentration sensors and temperature sensors.

With regard to the energy storage property of the material, the charge storage capability of the Cs/PANI hybrid films was analyzed by CV and GCD. The highest capacitance is obtained for CPF4 film due to high electrical conductivity, and low solution resistance charge transfer resistance as evidenced from EIS analysis. The highest capacitance of 468 mF cm^{-2} at the scan rate of 5 mV s^{-1} and 241 mF cm^{-2} at a current density of 0.4 mA cm^{-2} is obtained for CPF4 film. 79 % capacitance was retained after ten times increasing of current density for CPF4 film indicating that the material has good rate capability. 86 % retention initial capacitance after 1500 cycles indicating the good electrochemical stability of the hybrid film. The charge storage kinetics of CPF4 films was analyzed by Dunn's method. The CPF4 electrode has 51 % diffusive and 49 % capacitive contribution at a scan rate of 5 mV s^{-1} .

The pseudocapacitive properties and sensing properties of Cs/PANI hybrid films originated from the single oxidation/reduction reaction. Therefore, these results indicate that we can design a self-sensing supercapacitor device without additional connectivities for sensing. We argued that any electrochemical device working based on the electrochemical reaction of PANI has the inherent sensing capability to sense its working conditions.

References

1. K.S. Alva, J. Kumar, K.A. Marx, S.K. Tripathy, *Macromolecules*, 30 (1997) 4024-4029.

2. Y.A. Ismail, A. Ahmad, F. Mohammad, *Journal of Macromolecular Science®*, Part A: Pure and Applied Chemistry, 45 (2008) 650-657.
3. M. Jaymand, *Progress in Polymer Science*, 38 (2013) 1287-1306.
4. A. Yahya, A. Ahmad, F. Mohammad, (2004).
5. G. Liao, Q. Li, Z. Xu, *Progress in Organic Coatings*, 126 (2019) 35-43.
6. Y.A. Ismail, A. Shabeeba, M.P. Sidheekha, L. Rajan, *Actuators: Fundamentals, Principles, Materials and Applications*, (2020) 211-252.
7. J. Bhadra, A. Alkareem, N. Al-Thani, *Journal of Polymer Research*, 27 (2020) 1-20.
8. S.S. Athukorala, T.S. Tran, R. Balu, V.K. Truong, J. Chapman, N.K. Dutta, N. Roy Choudhury, *Polymers*, 13 (2021) 474.
9. R. Rajamany, S. Prakash, Y.A. Ismail, *Plastics, Rubber and Composites*, 51 (2022) 240-249.
10. B. Kim, G. Spinks, C. Too, G. Wallace, Y. Bae, *Reactive and Functional Polymers*, 44 (2000) 31-40.
11. S. Xing, G. Zhao, *Journal of applied polymer science*, 104 (2007) 1987-1996.
12. M. Rethi, S. Ponrathnam, C.R. Rajan, *Macromolecular rapid communications*, 19 (1998) 119-122.
13. N. Kuramoto, K. Teramae, *Polymers for Advanced Technologies*, 9 (1998) 222-226.
14. X. Li, W. Zhao, R. Yin, X. Huang, L. Qian, *Engineered Science*, 3 (2018) 89-95.
15. M. El Rhazi, S. Majid, M. Elbasri, F.E. Salih, L. Oularbi, K. Lafdi, *International Nano Letters*, 8 (2018) 79-99.
16. A. Sajedi-Moghaddam, C.C. Mayorga-Martinez, E. Saievar-Iranizad, Z. Sofer, M. Pumera, *Applied Materials Today*, 16 (2019) 280-289.
17. S. ur Rehman, R. Ahmed, K. Ma, S. Xu, T. Tao, M.A. Aslam, M. Amir, J. Wang, *Engineered Science*, 13 (2020) 71-78.
18. G. Kaur, R. Adhikari, P. Cass, M. Bown, P. Gunatillake, *RSC Advances*, 5 (2015) 37553-37567.

19. Y.A. Ismail, J.G. Martínez, A.S. Al Harrasi, S.J. Kim, T.F. Otero, *Sensors and Actuators B: chemical*, 160 (2011) 1180-1190.
20. M.P. Sidheekha, G.E. Rajendran, A. Shabeeba, Y.A. Ismail, *Journal of Materials Research*, 36 (2021) 1914-1926.
21. L. Li, J. Meng, M. Zhang, T. Liu, C. Zhang, *Chemical Communications*, 58 (2022) 185-207.
22. J. Stejskal, *Chemical Papers*, 71 (2017) 269-291.
23. B. Guo, Z. Ma, L. Pan, Y. Shi, *Journal of Polymer Science Part B: Polymer Physics*, 57 (2019) 1606-1621.
24. G.A. Roberts, G.A. Roberts, *Chitin chemistry*, (1992) 1-53.
25. S.G. Kou, L.M. Peters, M.R. Mucalo, *International Journal of Biological Macromolecules*, 169 (2021) 85-94.
26. J. Brugnerotto, J. Lizardi, F. Goycoolea, W. Argüelles-Monal, J. Desbrieres, M. Rinaudo, *Polymer*, 42 (2001) 3569-3580.
27. M. Ohira, T. Sakai, M. Takeuchi, Y. Kobayashi, M. Tsuji, *Synthetic Metals*, 18 (1987) 347-352.
28. P. Kong, H. Feng, N. Chen, Y. Lu, S. Li, P. Wang, *RSC advances*, 9 (2019) 9211-9217.
29. A.S. Roy, K.R. Anilkumar, M.A. Prasad, *Journal of applied polymer science*, 123 (2012) 1928-1934.
30. A. Fattoum, Z.B. Othman, M. Arous, *Materials chemistry and physics*, 135 (2012) 117-122.
31. A.G. Yavuz, A. Uygun, V.R. Bhethanabotla, *Carbohydrate Polymers*, 75 (2009) 448-453.
32. A. Tiwari, V. Singh, *Express Polymer Letters*, 1 (2007) 308-317.
33. Y.A. Ismail, S.R. Shin, K.M. Shin, S.G. Yoon, K. Shon, S.I. Kim, S.J. Kim, *Sensors and Actuators B: Chemical*, 129 (2008) 834-840.
34. F. Xu, G. Zheng, D. Wu, Y. Liang, Z. Li, R. Fu, *Physical Chemistry Chemical Physics*, 12 (2010) 3270-3275.
35. W. Li, F. Gao, X. Wang, N. Zhang, M. Ma, *Angewandte Chemie*, 128 (2016) 9342-9347.

36. F. Barzegar, A. Bello, O. Guellati, D.Y. Momodu, A. Harat, J.K. Dangbegnon, M. Guerioune, N. Manyala, *Electrochimica Acta*, 186 (2015) 277-284.
37. F. Ciucci, *Current Opinion in Electrochemistry*, 13 (2019) 132-139.
38. M. Zhang, A. Nautiyal, H. Du, Z. Wei, X. Zhang, R. Wang, *Electrochimica Acta*, 376 (2021) 138037.
39. T. Schoetz, L. Gordon, S. Ivanov, A. Bund, D. Mandler, R. Messinger, *Electrochimica Acta*, (2022) 140072.
40. Y. Jiang, J. Liu, *Energy & Environmental Materials*, 2 (2019) 30-37.

Chapter 6

Polyvinyl alcohol/polyaniline hybrid films as sensing macromolecular motors: electrochemical characterization and sensing supercapacitor application

Unlike Cs/PANI films, PVA/PANI hybrid films because of its high mechanical strength and much better electroactivities could be used to fabricate a sensing supercapacitor device. The sensing characteristics of PVA/PANI hybrid films with respect to the working conditions have been verified. The charge storage capabilities of the hybrid films were studied by CV, GCD and EIS. The single faradaic electrochemical reaction was responsible for both the sensing and charge storage properties. These characteristics along with high mechanical strength of the hybrid films were exploited to develop a truly integrated sensing supercapacitor device: a supercapacitor could sense the working conditions without using additional connectivities. This fundamental study provides a new direction for the development of simple and compatible self-sensing motors.

6.1. Introduction

In the previous chapter, it is proved that CP/hydrogel hybrid films have reaction-driven sensing capabilities as well as good charge storage properties. Chitosan/PANI hybrid films have reasonable mechanical strength in the dry state along with good electrochemical characteristics. They can be used for the development of various devices that work in dry conditions. In the wet state, the mechanical strength of the Cs/PANI hybrid films considerably decreased due to the high degree of swelling which limits their practical applicability in various electrochemical devices. The ultimate aim of our study is the development of sensing electrochemical motors using CPs. At first, it requires a free-standing electrode material having high mechanical stability in its wet state. Therefore, in this chapter, we focused on the development of a mechanically robust electroactive hybrid film suitable for practical applications.

Polyvinyl alcohol (PVA) is a white colour and odorless water-soluble synthetic organic polymer having an idealized formula of $[\text{CH}_2\text{CH}(\text{OH})]_n$. The structure of PVA is given in Figure 6.1. It is commercially synthesized from polyvinyl acetate through hydrolysis and it is easily degradable by biological organisms [1, 2]. Its degradability is enhanced through hydrolysis because of the presence of hydroxyl groups on the carbon atoms. PVA is a widely used thermoplastic polymer, it is nontoxic and safe for living tissues. PVA is extensively used in textile warp sizing, paper making, as a thickener and emulsion stabilizer in polyvinyl acetate adhesive formulations, in a variety of coatings, and 3D printing. PVA solution can be gelled without

an externally added crosslinking agent through repeated freezing-thawing and yield highly strong, ultrapure, biocompatible hydrogels that have been used for a variety of applications such as vascular stents, cartilages, contact lenses, etc. This polymer is widely used by blending with other polymers to enhance the mechanical properties for various industrial applications. [3].

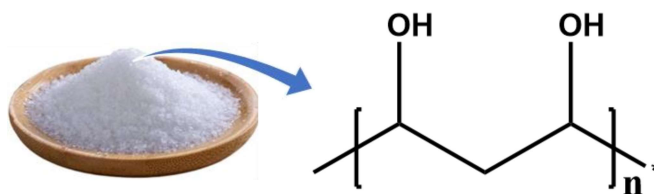


Figure 6.1: *Structure of PVA*

In this work, highly mechanically stable and electroactive PVA/PANI hybrid films were fabricated by in situ chemical polymerization of aniline on a pre-fabricated PVA film matrix. The reaction driven sensing characteristics of the hybrid film towards electrical, chemical and thermal working conditions have been verified by chronopotentiometry, where consumed electrical energy is the sensing parameter. The influence of various working conditions on the cooperative actuation of molecular motors of PANI present in the PVA/PANI hybrid film has been studied by voltammetry. Besides, the performance of PVA/PANI hybrid films as an electrode material for supercapacitors has been studied by CV, GCD and EIS analysis. The sensing and charge storage properties of hybrid film originated from its single electrochemical oxidation/reduction reaction. Therefore, it is exploited to develop a truly integrated sensing supercapacitor: a supercapacitor that can sense surroundings and working conditions.

6.2. Results and Discussion

I. Characterization of PVA/PANI hybrid films

The PVA/PANI hybrid films were prepared by in situ chemical polymerization of aniline in a prefabricated PVA film matrix. Here, four different types of films were fabricated, which are designated as PP1, PP2, PP3 and PP4 as explained in Chapter 2. The coating of PANI on PVA is very stable due to the strong intramolecular hydrogen bonding between PVA and PANI as depicted in Figure 6.2.

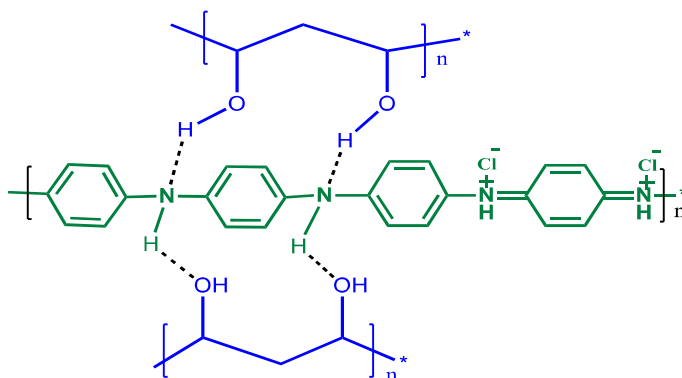


Figure 6.2 Interaction between PVA and PANI

6.2.1. FTIR spectra

The FTIR spectra recorded for PVA, PANI, and PVA/PANI hybrid films in the range of 4000-500 cm^{-1} are presented in Figure 6.3. In the spectrum of PVA, the peak at 3267 cm^{-1} corresponds to O-H stretching vibration and the broadness refers to the existence of intramolecular hydrogen bonding in the PVA film. The peak at 2940 cm^{-1} and 2916 cm^{-1} are assigned to asymmetric and symmetric vibrations of the CH_2 group. The peaks at 1416 cm^{-1} and 1325 cm^{-1} are

due to the CH₂ bending and C-H deformation vibrations, respectively. The peaks corresponding to C-O stretching and C-C stretching vibrations are observed at 1086 cm⁻¹ and 836 cm⁻¹ respectively [4-6]. The FTIR spectrum of PANI exhibits typical absorption peaks corresponding to C=C stretching vibrations of benzenoid and quinoid rings at 1484 cm⁻¹ and 1560 cm⁻¹ respectively, which indicates that PANI is in the emeraldine form. The absorption peaks at 1299 cm⁻¹ and 1248 cm⁻¹ are ascribed to C-N stretching vibrations of the benzenoid–quinoid–benzenoid sequence. An intense peak around 1120 cm⁻¹ is attributed to the charged defects [7].

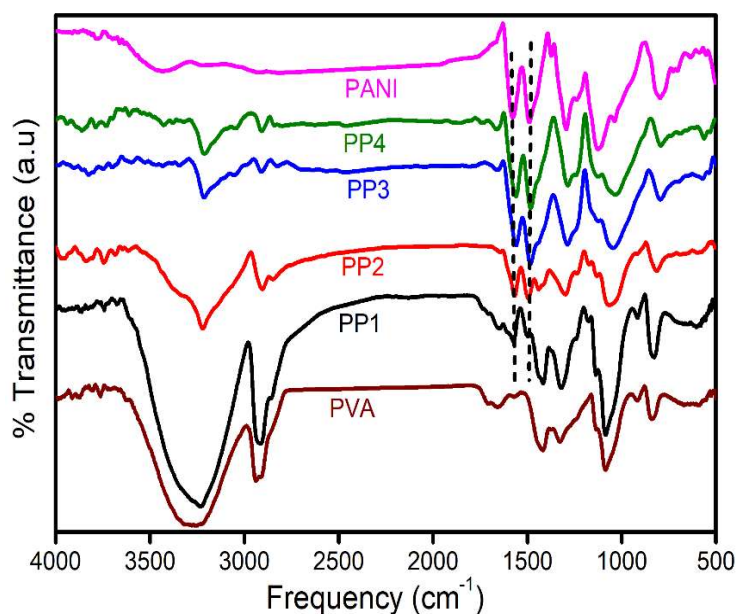


Figure 6.3 FTIR spectra of chitosan, PANI and PVA/PANI films

FTIR spectra of PVA/PANI hybrid films show characteristic peaks of both PANI and PVA with slight variations indicating the existence of interaction between them. All the films exhibit two

characteristic peaks corresponding to the stretching vibrations of C=C bonds of quinoid and benzenoid units of polyaniline in the region $1460\text{-}1575\text{ cm}^{-1}$ as observed in the FTIR spectrum of PANI. The bands present around 1280 cm^{-1} and 1100 cm^{-1} are corresponding to the C-N stretching vibration of the secondary aromatic amine and C-H in-plane bending vibration of the benzene ring respectively. Besides, the presence of a broad peak in the region $3200\text{ cm}^{-1} - 3600\text{ cm}^{-1}$ is due to the overlapping of N-H stretching of PANI and O-H and stretching of PVA [6, 8]. The broadness refers to the presence of strong hydrogen bonding interaction in the hybrid film.

6.2.2. Electrical conductivity

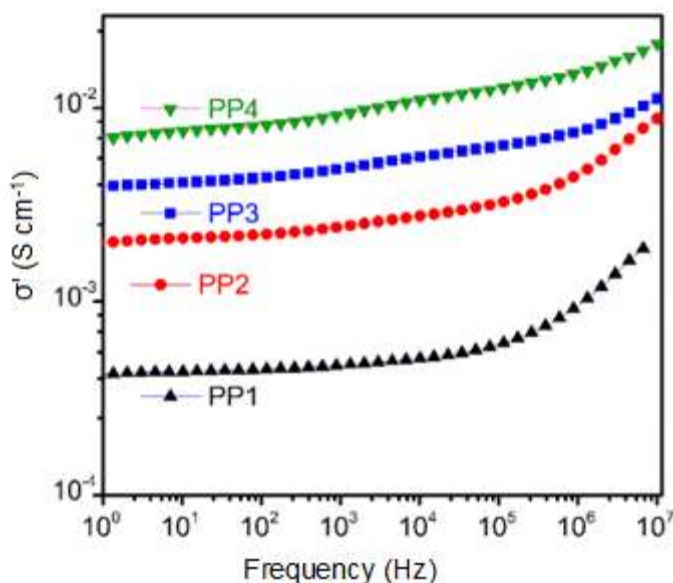


Figure 6.4 Frequency dependent conductivity of PVA/PANI films

Figure 6.4 represents the frequency-dependent electrical conductivities of the hybrid films obtained in the frequency range of

1 Hz to 10^7 Hz studied using a Broadband Dielectric Spectrometer. The frequency-dependent electrical conductivity of PVA/PANI hybrid films follows power-law behavior indicative of the hopping mechanism. The experimental data were fitted by Jonscher's universal power law to obtain the conductivity of hybrid films [9, 10]. The electrical conductivity of PP1, PP2, PP3 and PP4 is obtained as $3.75 \times 10^{-4} \text{ S cm}^{-1}$, $1.95 \times 10^{-3} \text{ S cm}^{-1}$, $3.12 \times 10^{-3} \text{ S cm}^{-1}$ and $4.48 \times 10^{-3} \text{ S cm}^{-1}$ respectively. It confirms the semiconducting nature of PVA/PANI hybrid films. The electrical conductivities of the hybrid films were significantly improved with increasing the PANI content in the hybrid film, i.e., conductivity increases from PP1 to PP4.

6.2.3. Thermal characterization

Thermogravimetric analysis of PVA and PVA/PANI hybrid films was performed in the temperature range of 25-650 °C and the resulting thermograms are presented in Figure 6.5. The TG curve of PVA shows two stages of mass loss: the first stage corresponds to water loss, while the second stage corresponds to the degradation of PVA polymer chains, in the temperature range of 245-480 °C with a mass loss of 87 % [11]. The degradation temperature of the PVA polymer backbone is found to be approximately 305 °C. The final residual mass was estimated to be around 1.24 % at 650 °C. The TGA of PVA/PANI hybrid film showed very similar behavior as that of PANI with major three-stage mass loss. The first stage corresponds to the loss of water and volatile components; the second corresponds to the loss of dopant and oligomer molecules and the third stage mass loss is due to the degradation of the polymer backbone of the hybrid films [12]. The

degradation of the polymer backbone of the hybrid films occurs at the temperature range of 425 °C - 435 °C. The final residual masses of hybrid films at 650 °C are estimated to be 3.6 %, 11.7 %, 14.5 % and 18.1 % of initial weight, respectively, for PP1, PP2, PP3 and PP4. This study shows that all four hybrid films have good thermal stability. The result indicates that the hybrid films are thermally more stable than pure PVA film and it increases with the increasing number of times of coating of PANI.

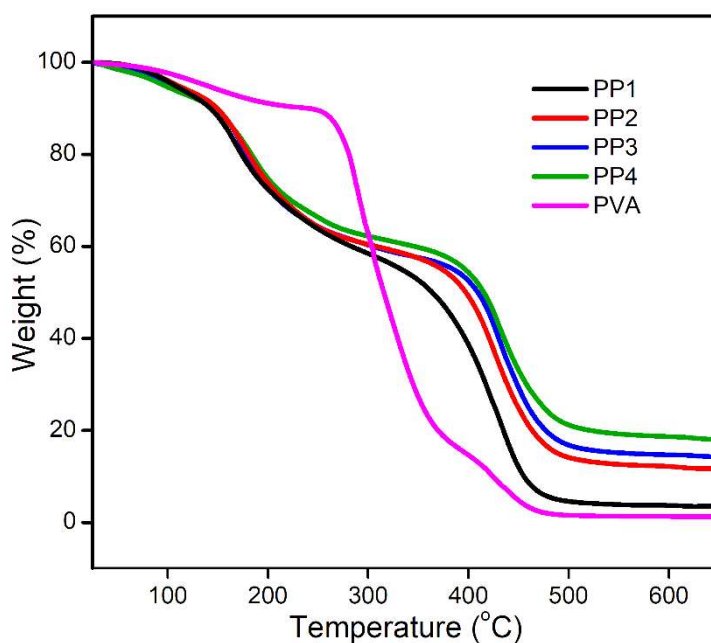


Figure 6.5 TGA of PVA and PVA/PANI films

6.2.4. Mechanical characterization

Figure 6.6 shows the photographs of the PP4 hybrid film in dry and wet conditions. It indicates that the film is mechanically stable, strong and flexible both in dry and wet states.

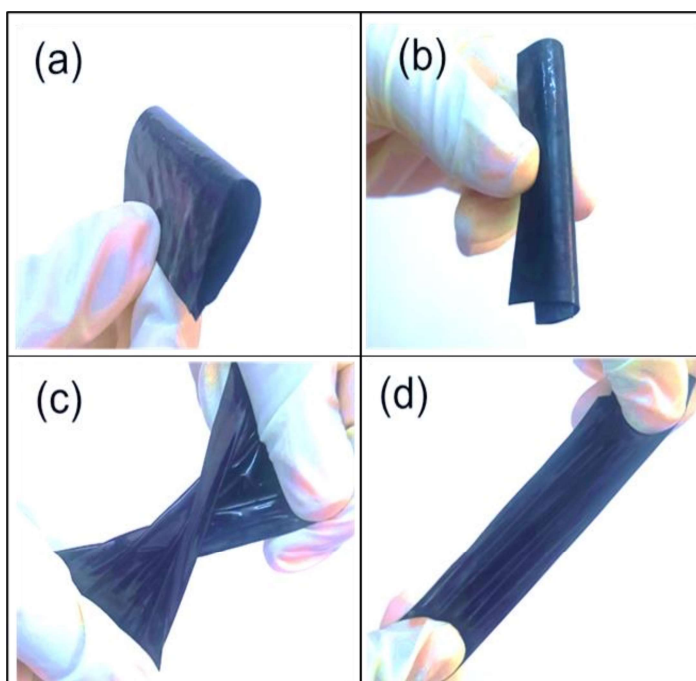


Figure 6.6 Photographs of PVA/PANI hybrid films in the dry state (a and b) and the wet state (c and d)

The mechanical characteristics of the PVA/PANI hybrid films were quantitatively analyzed using a Universal Testing Machine as described in Chapter 2. The results of the linear stress-strain behaviour of the hybrid films were then compared. The representative stress-strain curves of the PVA/PANI films obtained at a crosshead rate of 50 mm/min are depicted in Figure 6.7 and the results are listed in Table 6.1. The stress-strain curves of the hybrid films show plastic behavior. The tensile strength and Young's modulus of all the hybrid films are greater than that of pure PVA film which may be due to the PVA-PANI crosslinking. The tensile strength and Young's modulus increase with the increasing number of times of coating of PANI i.e., from PP1 to PP4. PP4 has the highest tensile strength and Young's

modulus among all the fabricated hybrid films, which are 38 MPa and 6.1214 MPa, respectively. The maximum percentage elongation of hybrid films is less than that of pure PVA and it decreases with increasing the number of times of coating of PANI in PVA. That is, the interpenetration of PANI chains through the PVA film matrix decreases the stretchability of the film. Even then PP4 has 24 % elongation at break.

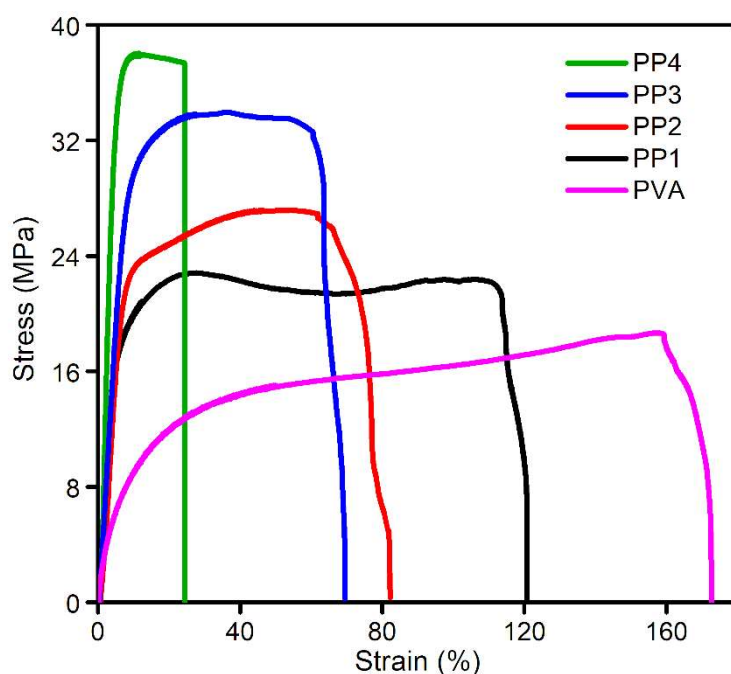


Figure 6.7 Stress-strain curve of PVA/PANI films in the dry state

The mechanical characteristics of all the hybrid films were analyzed in the wet state and corresponding representative stress-strain curves are depicted in Figure 6.8. The results are listed in Table 6.1. The tensile strength and Young's modulus of all the hybrid films are greater than that of pure PVA film even in wet conditions and it increases with

increasing the number of times of coating of PANI in the hybrid films. PP4 exhibits the highest tensile strength of 4.02 MPa and Young's modulus of 0.1624 MPa in its wet state. The percentage elongations of hybrid films are increased 2-4 times in the wet state. The result indicates that PVA/PANI hybrid films have excellent mechanical characteristics even in the wet states. Therefore, these hybrid films are suitable for the fabrication of various mechanically stable and flexible electrochemical devices.

Table 6.1 Tensile strength, Young's modulus and percentage elongation at break of PVA/PANI hybrid films in the dry and wet states

Film	Tensile strength (MPa)	Young's Modulus (MPa)	% Elongation at break
Dry state			
PVA	18.57	1.3728	173
PP1	22.8	2.8411	121
PP2	27.12	3.0676	82
PP3	33.95	3.8181	69
PP4	38	6.1214	24
Wet state			
PVA	1.44	0.0051	463
PP1	2.7	0.0168	298
PP2	3.03	0.0363	184
PP3	3.68	0.0576	107
PP4	4.02	0.1624	90

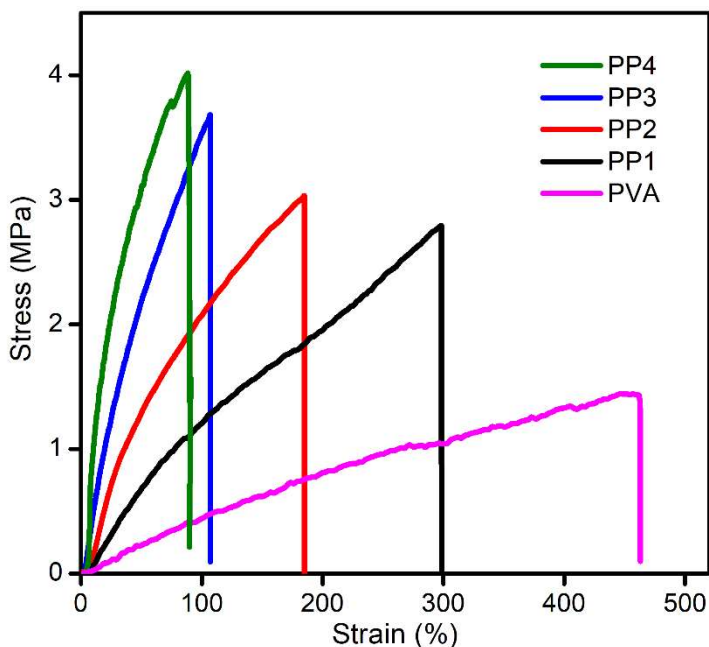


Figure 6.8 Stress-strain curve of PVA/PANI films in wet condition

6.2.5. Morphological characterization

The surface morphologies of the films were investigated by FESEM analysis and the images are presented in Figure 6.9. The FESEM images reveal that the surface of the PVA film is quite smooth without voids or cracks (Figure 6.9a). The SEM images of hybrid films (Figure 6.9 b-e) indicate that the PANI has polymerized on the surface of the PVA films with coral-like nanowire morphology. Upon repeated coating, the new polyanilines have grown on the previously formed nanostructures leading to more agglomerated morphology. The nanostructured hybrid films provide a large surface area. The presence of a large number of voids on the surface of the hybrid films facilitates better transport of ions and electrolytes for efficient electrochemical

reactions. Besides, PVA is highly hydrophilic and swells in the electrolyte. The swollen state of the hybrid films may allow facile permeation of ions and electrons in between PANI chains which provide an additional effective surface area between molecular chains and the solution phase leading to high electrochemical activities.

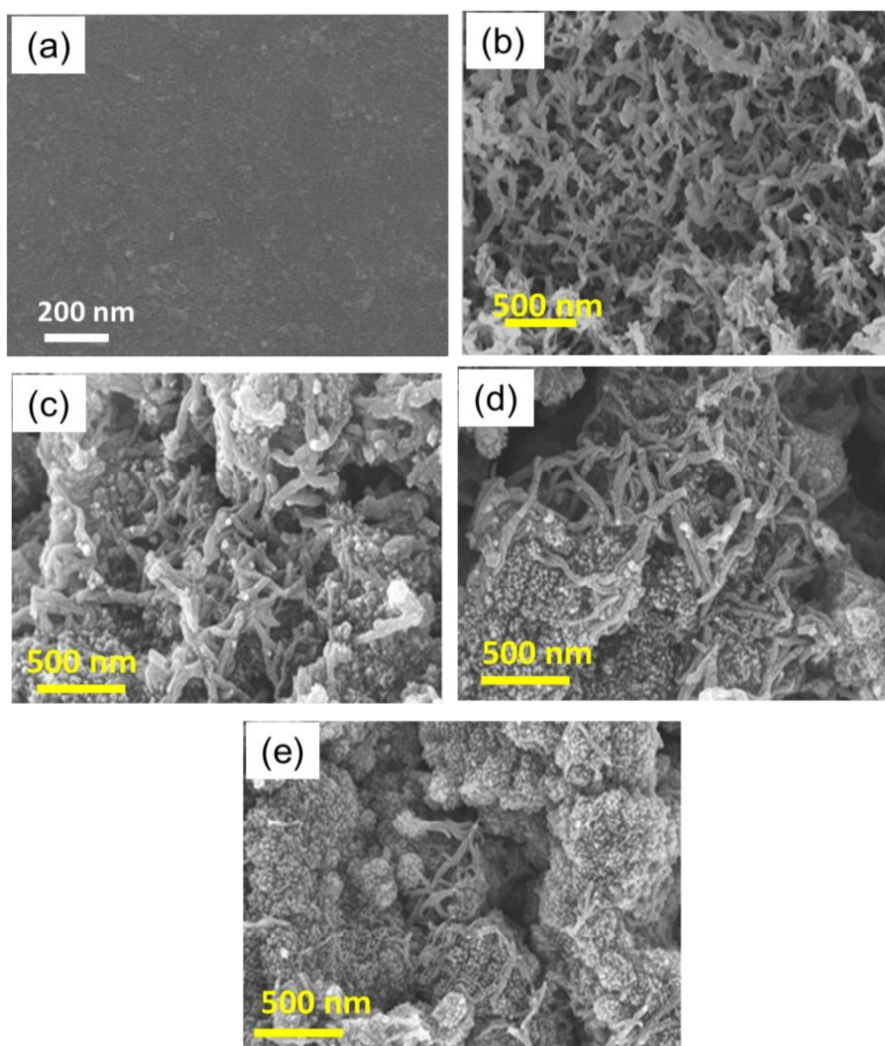


Figure 6.9 FESEM images of (a) PVA, (b) PPI, (c) PP2, (d) PP3 and (e) PP4 hybrid films

6.2.6. Elemental analysis

The EDX spectra (Figure 6.10) of all the PVA/PANI hybrid films show a characteristic peak of N and Cl^- in addition to C, and O, which are absent in PVA film. The presence of N in EDX spectra confirms the formation of PANI. The Cl^- introduced as the counter ion during the acid doping of PANI confirms that PANIs formed in the hybrid films are in the conductive emeraldine salt form.

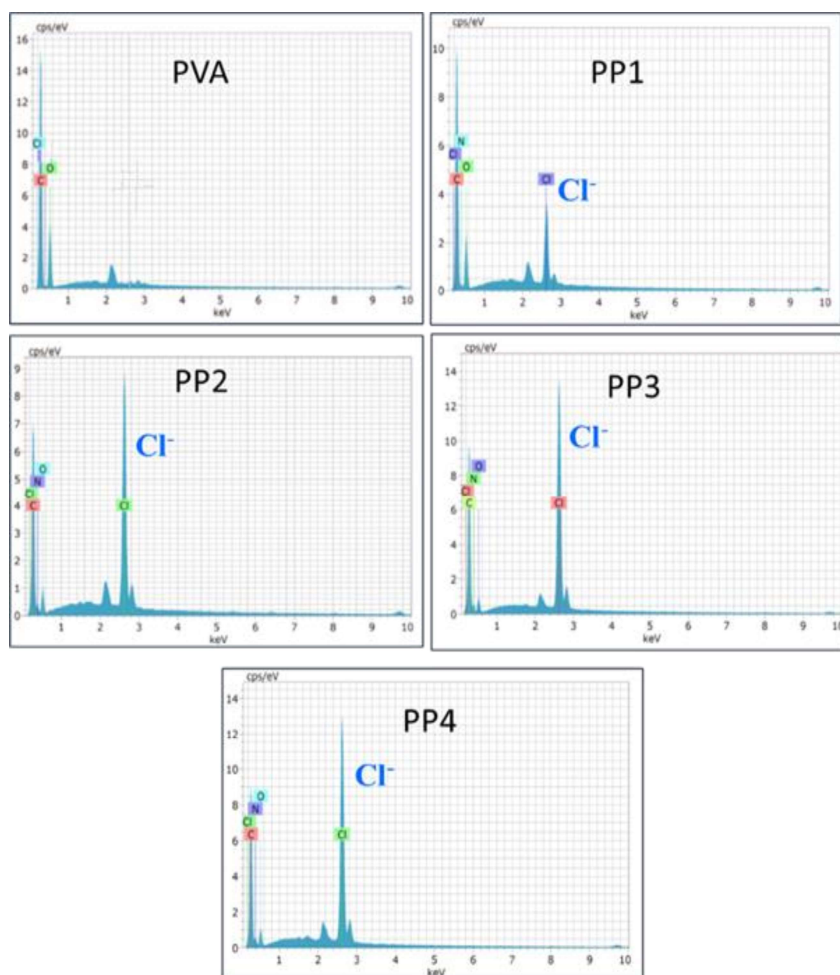


Figure 6.10 EDX spectra of PVA and PVA/PANI hybrid films

6.2.7. Electrochemical characterization

6.2.7.1. Cyclic voltammetry

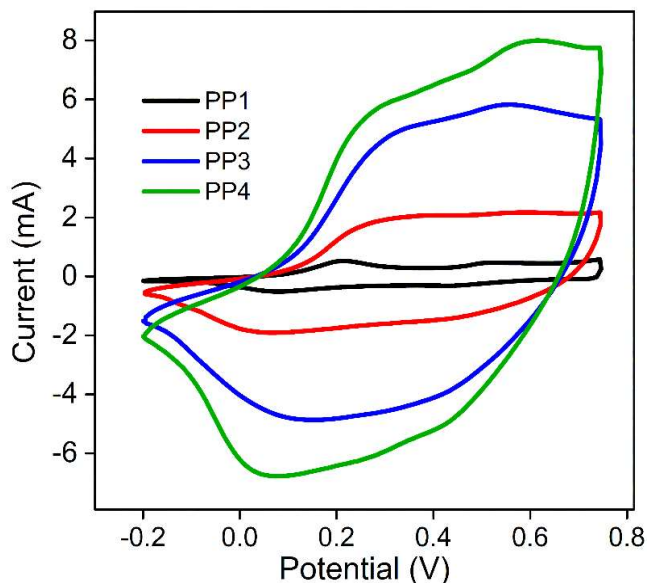


Figure 6.11 CVs of PVA/PANI hybrid films recorded at a scan rate of 25 mV s^{-1} in 1 M HCl

The electrochemical activity of the hybrid film was analyzed by cyclic voltammetry. Figure 6.11 represents the CVs of PVA/ PANI hybrid films recorded between the potential limit of -0.20 V to -0.75 V at a scan rate of 25 mV s^{-1} in 1 M HCl solution at room temperature. The experiments were carried out in a three-electrode cell assembly after stabilizing the CV through 25 consecutive cycles. All the films show two oxidation and two reduction peaks as in the case of PANI [13]. The similarity of oxidation and reduction peaks with those of pure PANI proved that the electrochemical activities of PVA/PANI films are imparted by the PANI. The hybrid films show different current

responses, which are mainly ascribed to the different PANI content and conductivity of the fabricated films. The current response in CV increases as the number of times of coating of PANI increases and the highest current is attained for PP4 which is due to relatively higher PANI content in PP4, more porous structure and good electrical conductivity compared to other films. The anodic and cathodic peak potentials are listed in Table 6.2.

Table 6.2 Anodic and cathodic peaks of PVA/PANI electrodes at the scan rate of 25 mV s^{-1}

Film	Anodic peaks (V)		Cathodic peaks (V)	
	LE to ES	ES to PN	PN to ES	ES to LE
PP1	0.21	0.52	0.43	0.082
PP2	0.27	0.57	0.44	0.062
PP3	0.29	0.55	0.40	0.14
PP4	0.23	0.61	0.42	0.072

LE- leucoemeraldine, ES- emeraldine salt, PN- pernigraniline

The CV response of PP4 hybrid film recorded at various scan rates from 5 mV s^{-1} to 150 mV s^{-1} are presented in Figure 6.12a. The anodic and cathodic peak current increases linearly as a function of the square root of the scan rate as depicted in Figure 6.12b. It reveals that

the electrochemical reaction in the PP4 hybrid film is controlled by the ion diffusion process [14].

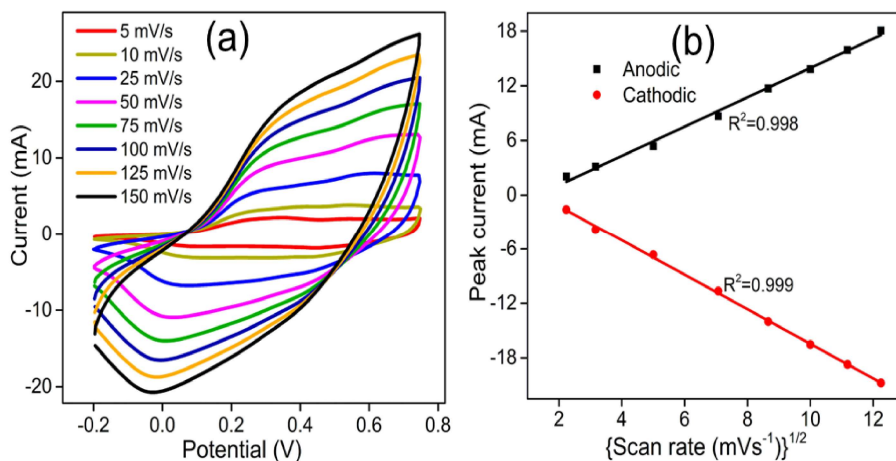


Figure 6.12 (a) CVs of PP4 at different scan rates from 1 M HCl aqueous solution at room temperature and (b) variation of peak current as a function of the square root of scan rate

6.2.7.2. Coulo Voltammetry

Figure 6.13a represents the QVs of PVA/PANI hybrid films obtained at the scan rate of 25 mV s^{-1} in 1M HCl solution at room temperature. The closed loops of QVs of PVA/PANI hybrid films indicate that only reversible oxidation/reduction is present in the studied potential window, i.e., -0.20 V to 0.75 V . The slope of the steeper portion of QV increases from PP1 to PP4. It indicates that the rate of oxidation/reduction reaction is higher in the case of PP4, i.e., increases from PP1 to PP4. The difference between the maxima and minima of the QV loops gives a redox charge of hybrid films at the same experimental conditions. The QV maxima increases from PP1 to PP4

indicating that the redox charge increases with increasing of PANI content in the film. That is, higher PANI content leads to higher concentration of the electroactive centers, thus promoting a larger number of ions exchanged during the redox reaction leading to concomitant consumption of higher oxidation/reduction charges. The charge consumed by the reversible redox processes of the hybrid films is 10 mC, 49 mC, 125 mC, and 169 mC respectively for PP1, PP2, PP3 and PP4. It is depicted in Figure 6.13b. All the PVA/PANI hybrid films show similar structural faradaic processes as in the case of PANI described in section 3.3.2.

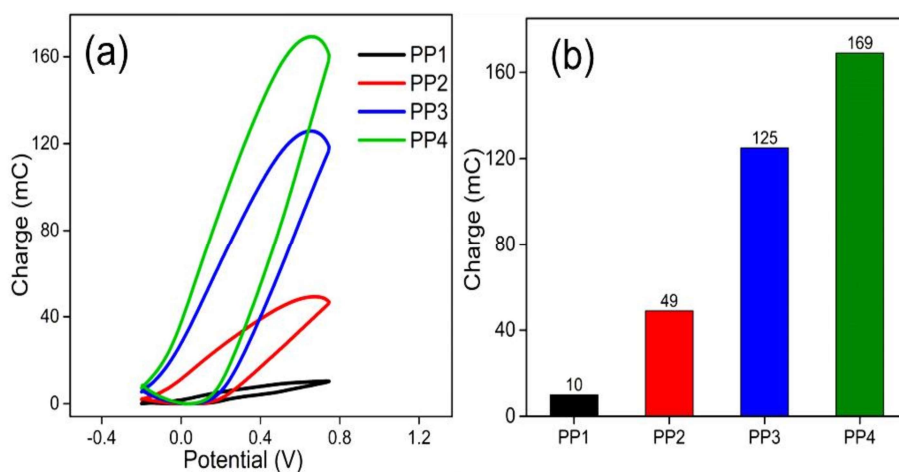


Figure 6.13 (a) *QVs of PVA/PANI hybrid films obtained by integration of CVs at the scan of 25 mV s^{-1}* (b) *redox charges of PVA/PANI hybrid films obtained from corresponding QVs*

II. Reaction driven sensing characteristics of PVA/PANI hybrid films: A chronopotentiometric study

The CV and QV analyses revealed that PP4 film is the most electroactive among the fabricated hybrid films. Therefore, in this section, the reaction driven sensing characteristics of PP4 hybrid film towards electrical, chemical and thermal working conditions are studied through consumed electrical energy as the sensing magnitude.

6.2.8. Sensing electrical working condition: current sensor

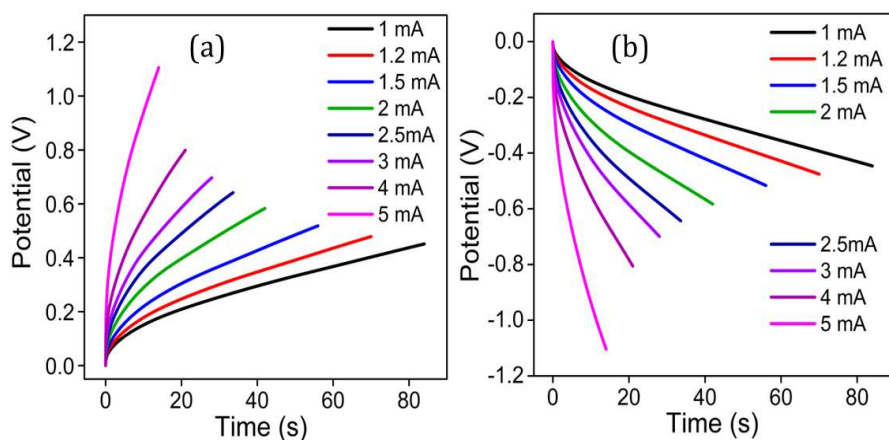


Figure 6.14 Anodic (a) and cathodic (b) chronopotentiograms were obtained when different currents were applied to PP4 hybrid film by passing a constant electrical charge of 84 mC in 1 M HCl solution

To study the sensing characteristics of PP4 hybrid film towards the electrical working conditions, i.e., applied current, the chronopotentiograms were recorded from the aqueous solution of 1M HCl corresponding to consecutive square current waves of different magnitudes ranging from ± 1 mA to ± 5 mA. The period of the square

waves was altered in each experiment to attain constant oxidation and reduction charges ($Q = i.t = 84 \text{ mC}$) to get the same initial and final oxidation states or the same reaction extension. The normalized chronopotentiometric responses for the anodic and cathodic processes of the PP4 hybrid films are depicted in Figure 6.14a and Figure 6.14b respectively. Higher anodic and cathodic currents shift the potential evolution towards higher anodic or higher cathodic potential, respectively.

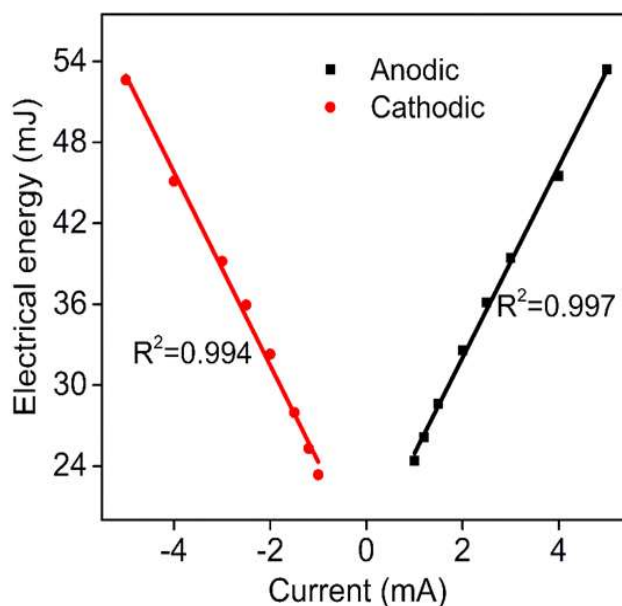


Figure 6.15 The linear variation of consumed electrical energy with the working current for the PP4 hybrid film

The consumed electrical energy during each oxidation/reduction process of PP4 was calculated by integrating chronopotentiograms. Figure 6.15 shows that the consumed electrical energy during the redox reaction has a linear dependence on the applied electric current. Therefore, the reaction energy of the PP4 hybrid film senses or responds

to locally imposed electrical conditions. The slope of the current versus electrical energy calibration curve (Figure 6.15) denotes the sensitivity of the PP4 hybrid film as a sensor of applied current. The sensitivity is 7.10 mJ mA^{-1} and -7.16 mJ mA^{-1} for the anodic and cathodic processes, respectively.

6.2.9. Sensing the chemical working condition: concentration sensor

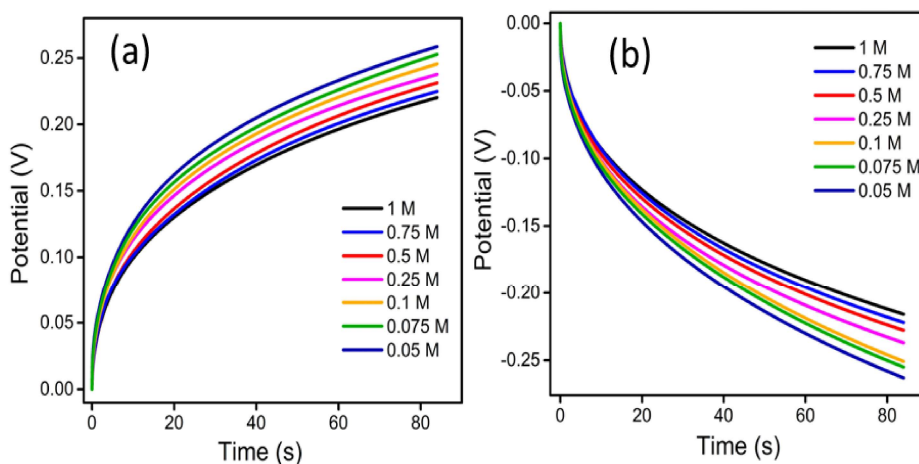


Figure 6.16 Anodic (a) and cathodic (b) chronopotentiograms obtained at different electrolyte concentrations for PP4 hybrid film

To study the sensing characteristics of the PP4 hybrid film towards the chemical working conditions, the chronopotentiograms were recorded from various concentrations of HCl ranging from 1 M to 0.075 M at room temperature by applying a constant square wave current of $\pm 1 \text{ mA}$ for 84 s, i.e., keeping the consumed charge constant at 84 mC, for attaining the same reaction extension in each experiment. Figure 6.16a and 6.16b represent the normalized chronopotentiometric responses corresponding to anodic and cathodic processes of PP4 hybrid

film at different concentrations of electrolyte respectively. During the reversible oxidation/reduction of the polymer films, the anodic and cathodic potentials evolve at lower values with increasing electrolyte concentration. That is, at higher concentrations, higher chemical energy (chemical potential) is available. Therefore, it requires only a lower consumption of electrochemical energy to attain the same reaction extension as that of the lower concentration.

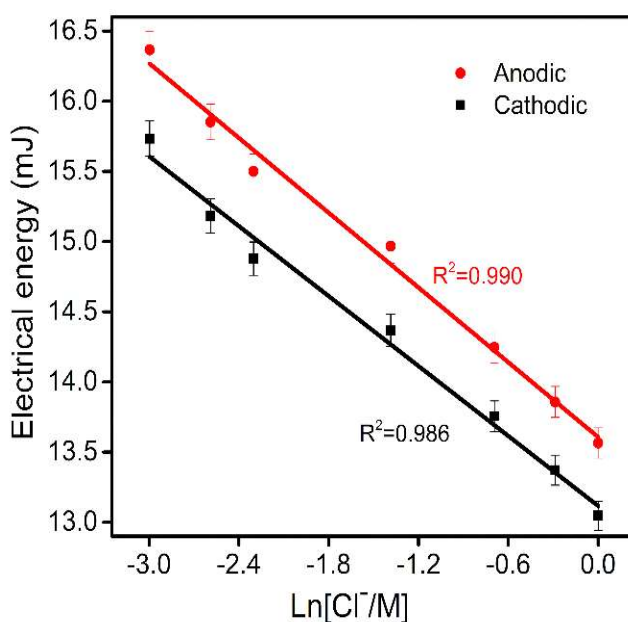


Figure 6.17 Linear variation of consumed electrical energy with the electrolyte concentration for the anodic and cathodic process of PP4 hybrid film

The variation of consumed electrical energy during the oxidation and reduction of the PP4 hybrid film is presented in Figure 6.17. The electrical energy has a semi-logarithmic linear dependence on electrolyte concentration with good correlation. Hence, the reaction of PVA/PANI hybrid films can sense the chemical working energetic

conditions. The slope of the calibration curve is the sensitivity of the PP4 towards the concentration of electrolyte, that is -0.888 mJ M^{-1} and -0.831 mJ M^{-1} for anodic and cathodic processes, respectively.

6.2.10. Sensing the thermal working condition: temperature sensor

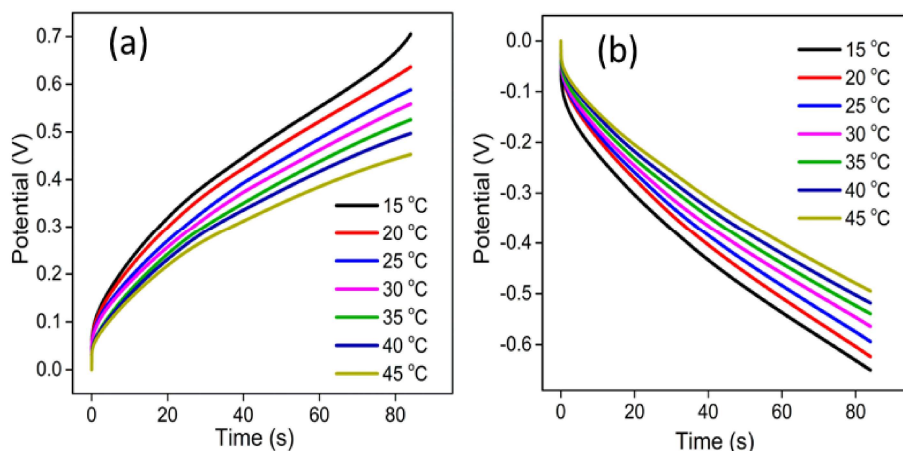


Figure 6.18 Anodic (a) and cathodic (b) chronopotentiograms obtained at different working temperatures for PP4 hybrid film by passing a constant electrical charge of $\pm 84 \text{ mC}$ in 1 M HCl solution

To study the sensing characteristics of PP4 towards thermal working conditions, here it is temperature, the chronopotentiograms were recorded at various experimental temperatures by applying consecutive square current waves of $\pm 1 \text{ mA}$ in 1 M HCl solution for a constant period of 84 s . The obtained normalized stationary chronopotentiograms corresponding to the oxidation and reduction processes of hybrid film at different temperatures are depicted in Figure 6.18a and 6.18b respectively. As the temperature increases, the available thermal energy increases and the electrode reaction requires lower consumption of electrical energies for attaining the same reaction

extension compared to that required at the lower temperature. Therefore, the material potential evolves at lower values when the reaction takes place at higher temperatures to go from the same initial state to the same final state every time.

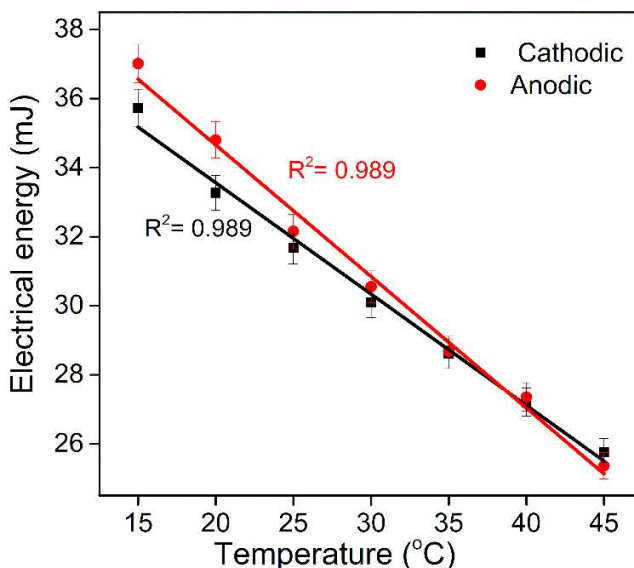


Figure 6.19 Linear variation of consumed electrical energy with the working temperature for PP4 hybrid film

The electrical energy required for the oxidation and reduction of PP4 films at various temperatures is obtained from corresponding chronopotentiograms. The consumed electrical energy during the anodic and cathodic process of PP4 hybrid film has a linear dependence on the working temperature as depicted in Figure 6.19. It reveals that PP4 hybrid films can act as a sensor of the working thermal energetic condition. The slope of calibration curves represents the sensitivity of the PP4 hybrid film towards the working temperature. The hybrid film has a high sensitivity of $-374.54 \mu\text{J K}^{-1}$ and $-317.43 \mu\text{J K}^{-1}$ for anodic and cathodic processes, respectively.

III. Influence of working conditions on the cooperative actuation of multimolecular motors of PANI: A Voltammetric study

6.2.11. Cooperative actuation in CP films

In section 1.6.2, it is discussed that conducting polymer chains are considered multistep electrochemical molecular motors. During the reversible electrochemical reactions, the polymer chains reversibly undergo uncoiling and coiling by the insertion or expulsion of counter ions. It is regarded as a molecular-level actuation of the polymeric chain [15]. At the same time, the polymer films expand or contract, i.e., the volume of the film changes, in a reversible manner during the reversible oxidation/reduction of CP films. These macroscopic changes in CP films are produced from the mutual actuation of the individual polymer chain or individual molecular motors present in the film. That is the reversible expansion or contraction of polymer film during the reversible electrochemical reaction is resulted from the cooperative actuation of multistep molecular motors present in the film [15-17]. In this section, we studied how the various reaction conditions such as chemical, thermal and electrical conditions influence the cooperative actuation of multistep molecular motors of PANI present in the PP4 film. Here, the extent of cooperative actuation is defined or quantified by the consumed charge during the reaction and verified that the extension of the reaction resulted from the cooperative actuation of molecular motors of PP4 film (here it is defined by consumed charge) can sense their working energetic conditions such as chemical, thermal and electrical conditions.

6.2.12. Influence of chemical condition on the cooperative actuation of molecular motors of PANI present in PP4 hybrid film: concentration sensor

For studying the influence of chemical conditions on the cooperative actuation of multistep molecular motors of PANI in the PP4 film, the CVs are recorded from different concentrations of HCl solution at a scan rate of 25 mV s^{-1} in the potential window of -0.2 V to 0.75 V at room temperature through the following steps:

Step 1: After stabilizing the CV response, the free-standing PP4 electrode was transferred into the control solution. In this experiment, 0.25 M HCl solution was taken as the control solution. There, the PP4 electrode was submitted to three consecutive potential cycles to get stationary CV responses.

Step 2: The electrode was then transferred into another electrochemical cell having 0.05 M HCl solution and submitted to consecutive potential cycles to get stationary CV responses.

Step 3: in the third step the electrode was transferred back to the control solution (0.25 M) and cycled again until stationary voltammetric responses were obtained.

Steps 2 and 3 were repeated for the different electrolyte concentrations such that in the first phase, the concentration of the electrolyte increases from 0.05 M to 1 M and in the second phase the concentration of the electrolyte decreases from 1 M to 0.05 M . The CVs from the control solutions are measured in between each concentration cycling during increasing and decreasing the electrolyte concentration. The procedure is schematically represented in Figure 6.20.

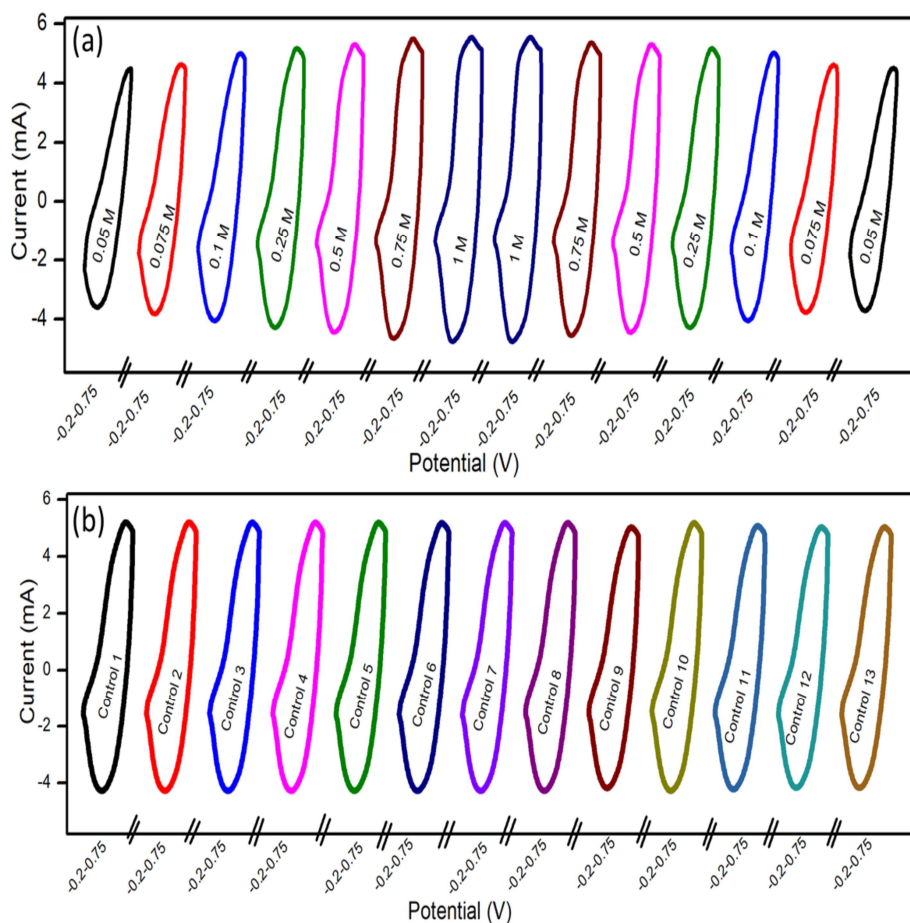


Figure 6.21 (a) Stationary CV obtained at different electrolyte concentrations of HCl solutions (indicated on each figure) in the potential window of -0.2 V to 0.75 V, (b) Control CV obtained in between every consecutive concentration under the same experimental condition from 0.25 M HCl solution.

Figure 6.21a represents the stationary CV responses obtained after two consecutive potential cycles from PP4 film in every studied electrolyte concentration. The anodic and cathodic current increases when the concentration is raised from 0.05 M to 1 M and decreases when the electrolyte concentration is decreased back to 0.05 M. Figure 6.21b presents the CV from controls, obtained in

between two consecutive concentrations. The similar control CVs corroborate that the electroactivity of the PANI remains constant during the experimental cycles.

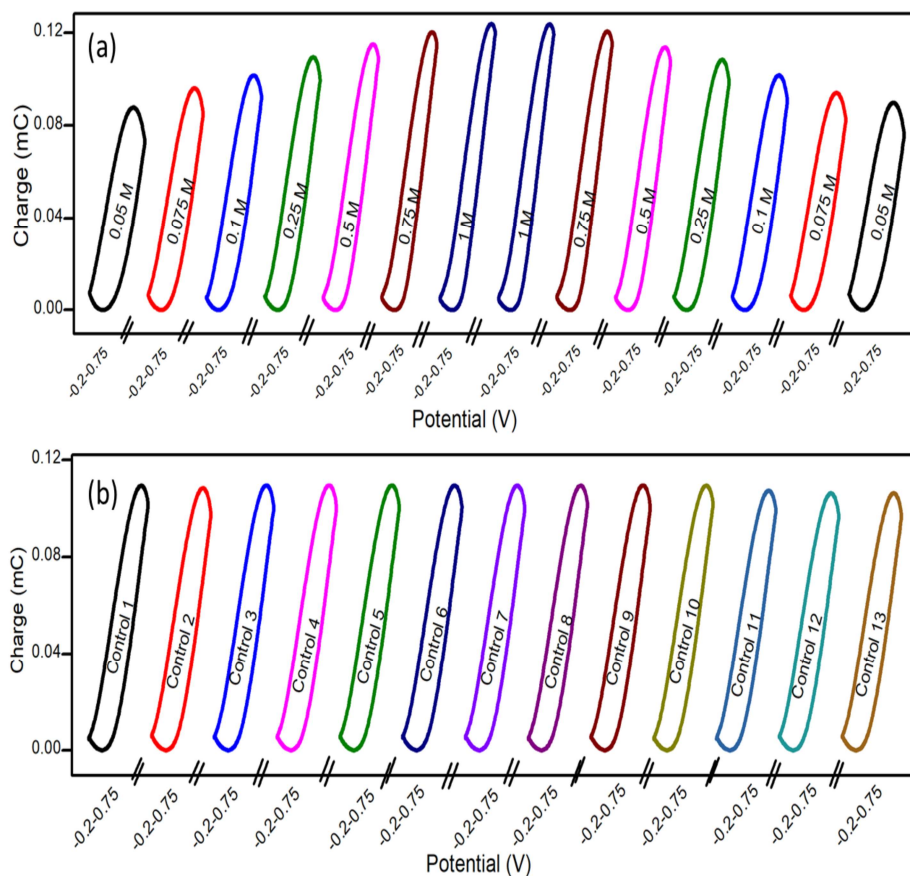


Figure 6.22: (a) *QVs at different electrolyte concentrations obtained from CVs presented in Figure 6.21a* (b) *Control QVs obtained from CVs presented in Figure 6.21b*

6.22a shows the stationary QV responses in the studied electrolyte concentrations, during the continuous increasing and decreasing cycles of concentrations obtained from corresponding CVs. All QV response presents a closed loop where the oxidation charge equals the reduction charge. The charge difference between the QV

maximum and minimum is the charge consumed during the redox process of PP4 film under the studied experimental conditions. The QV maxima increases with increasing concentration and decreases with decreasing concentration of electrolyte. That is, the reversible charge consumed by reversible reactions of PP4 film increases with increasing the electrolyte concentration and decreases with decreasing the electrolyte concentration. We obtained overlapping QVs at a particular concentration during increasing or decreasing of electrolyte concentration indicating that the extension of reaction as a result of cooperative actuation of molecular motors of PANI at a particular condition is always the same irrespective of the direction of the experiment.

Under constant reaction conditions, at higher electrolyte concentrations, higher chemical energy or chemical potential is available. Therefore, a large number of electrons can be extracted per polymer chain during oxidation. It generates a large free volume across the film to lodge a large number of anions and water molecules leading to a deeper oxidation state. Similarly, during reduction, a large number of electrons can be expelled per polymer chain which destroys large free volumes across the film and expels a large number of anions and water molecules leading to a deeper reduction state. While, at low concentrations of the electrolytes, only low chemical energy is available. So, there is only a partial convolution/deconvolution from conformational movements of the polymeric chain in the film, which generates/destroys only a low amount of free volume to lodge/expel anions and water molecules and only attain a partial oxidized/reduced

state. The above-described events are schematically presented in Figure 6.23.

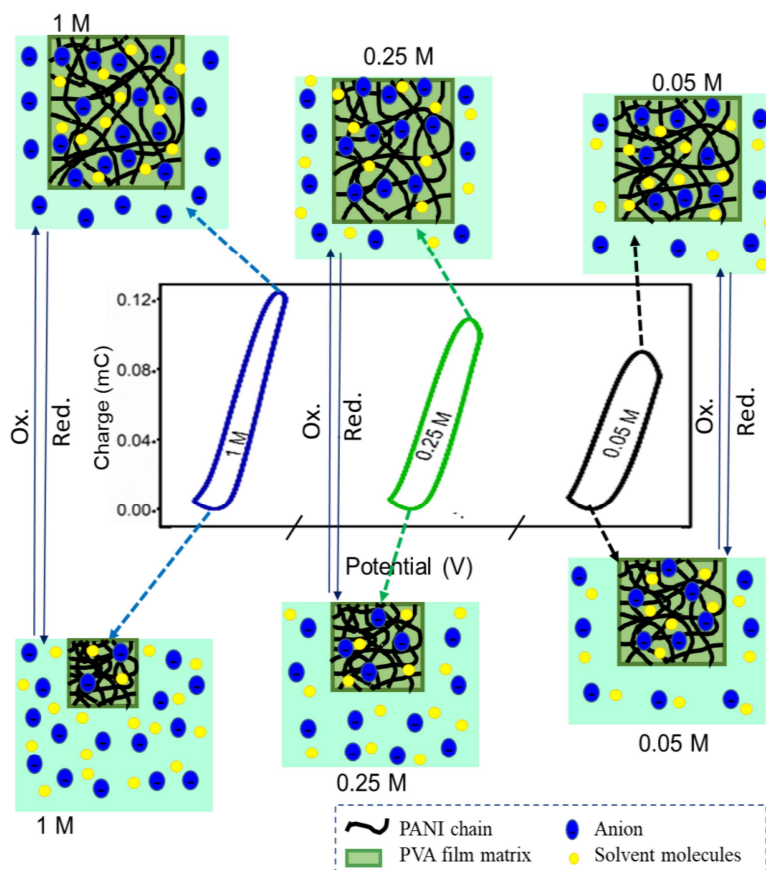


Figure 6.23 Schematic representation of extension of the electrochemically induced volume variations resulting from structural changes by reversible oxidation/reduction of the PP4 electrode at different concentrations

The QVs of the control solution obtained from corresponding CVs are depicted in Figure 6.22b. The same or overlapping QV responses are reproduced whenever the experiment comes back to the control solution in between changing concentrations. It corroborates that the electroactivity of the hybrid film or free volume variation resulting

from the cooperative actuation of molecular motors present in the hybrid film remains constant and reproducible at a particular concentration of the electrolyte when all other experimental conditions are kept constant. From the above discussions, we can conclude that the extension of reaction as a result of the cooperative actuation of the polymeric chain of PANI is always the same at a particular concentration and it is reversible.

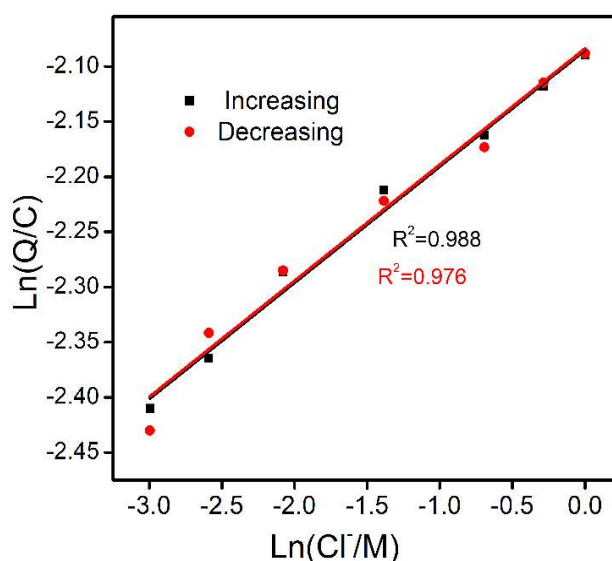


Figure 6.24 Double logarithmic variation of the charge consumed by the reversible oxidation/reduction of PP4 hybrid film with the HCl concentration.

Figure 6.24 shows that the consumed charge during the reaction of PANI has a double logarithmic linear dependence during increasing concentrations and subsequent decreasing concentrations. It can be concluded that the reversible electrochemical reactions of PANI can directly sense the available chemical energy, here it is electrolyte concentration, under the same applied electrical stimulus in such a way

that the extension of the reaction or the consumed charge is a double logarithmic function of the electrolyte concentration. The slope of the calibration curve, i.e., 0.1052 and 0.1053 respectively for increasing and decreasing electrolyte concentration, represents the sensitivity of PP4 film towards concentration.

6.2.13. Influence of thermal condition on the cooperative actuation of molecular motors of PANI present in PP4 hybrid film: temperature sensor

The influence of thermal conditions, i.e., temperature, on the cooperative actuation of multistep molecular motors of PANI in the PP4 hybrid film was studied similarly to the influence of concentration described above. Here, the CVs are recorded at different working temperatures at a scan rate of 25 mV s^{-1} in the potential window of -0.2 V to 0.75 V from 1 M HCl in the following steps:

Step 1: After stabilizing the CV response, the free-standing PP4 film was transferred into the control solution. In this experiment, 1 M HCl aqueous solution at $25 \text{ }^\circ\text{C}$ was taken as the control solution. The PP4 hybrid film was submitted to three consecutive potential cycles to get stationary CV responses.

Step 2: The electrode was then transferred into another electrochemical cell of 1 M HCl at a temperature of $10 \text{ }^\circ\text{C}$ and submitted to consecutive potential cycles until the stationary CV responses were obtained.

Step 3: Then the electrode was transferred back to the control state (temperature $25 \text{ }^\circ\text{C}$) and cycled again until stationary voltammetric responses were obtained.

Steps 2 and 3 were repeated for the different temperatures such that in the first phase the reaction temperature increases from 10 °C to 50 °C and in the second phase the temperature decreases from 50 °C to 10 °C. The CVs from the control solutions (at 25 °C) are measured in between each temperature cycle during increasing and decreasing the working temperature.

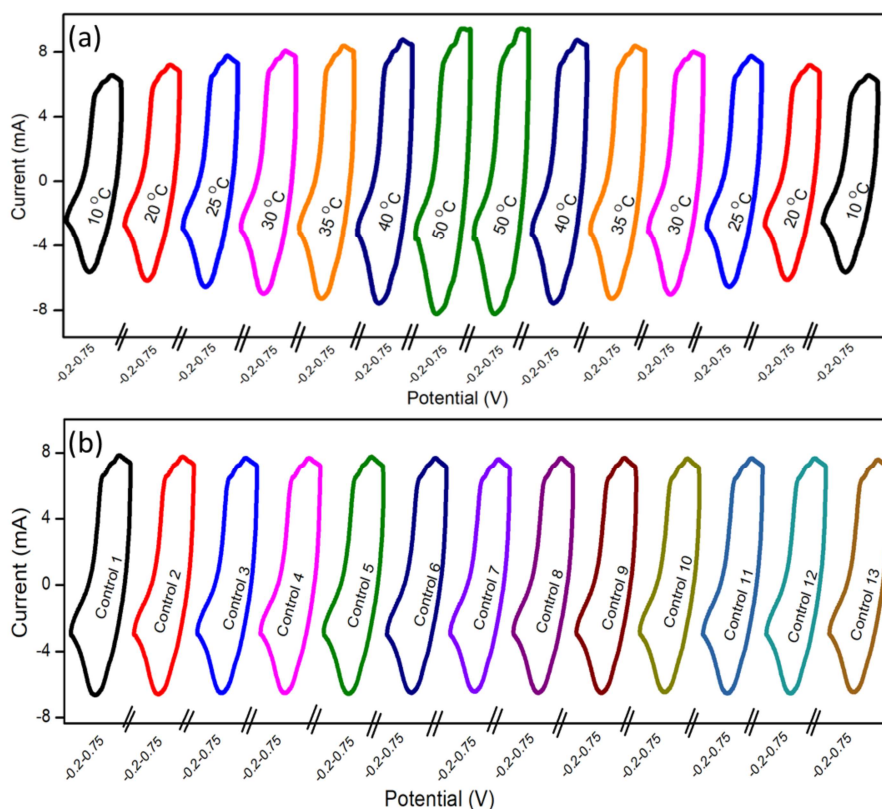


Figure 6.25 (a) Stationary CVs obtained at different working temperatures (indicated on each figure) **(b)** Control CVs obtained at 25 °C measured in between every consecutive temperature during increasing and decreasing temperature cycle under the same potential range and scan rate from 1 M HCl solution.

Figure 6.25a represents the stationary CV responses, after two consecutive potential cycles from PP4 hybrid film electrodes at every

studied temperature. The anodic and cathodic currents increase with increasing temperature and are followed by decreasing currents with decreasing working temperature. CVs from the control state, obtained between two consecutive increasing or decreasing temperatures are presented in Figure 6.25b. The similar control CVs corroborate that the electroactivity of the PP4 hybrid film remains constant during the experimental cycle.

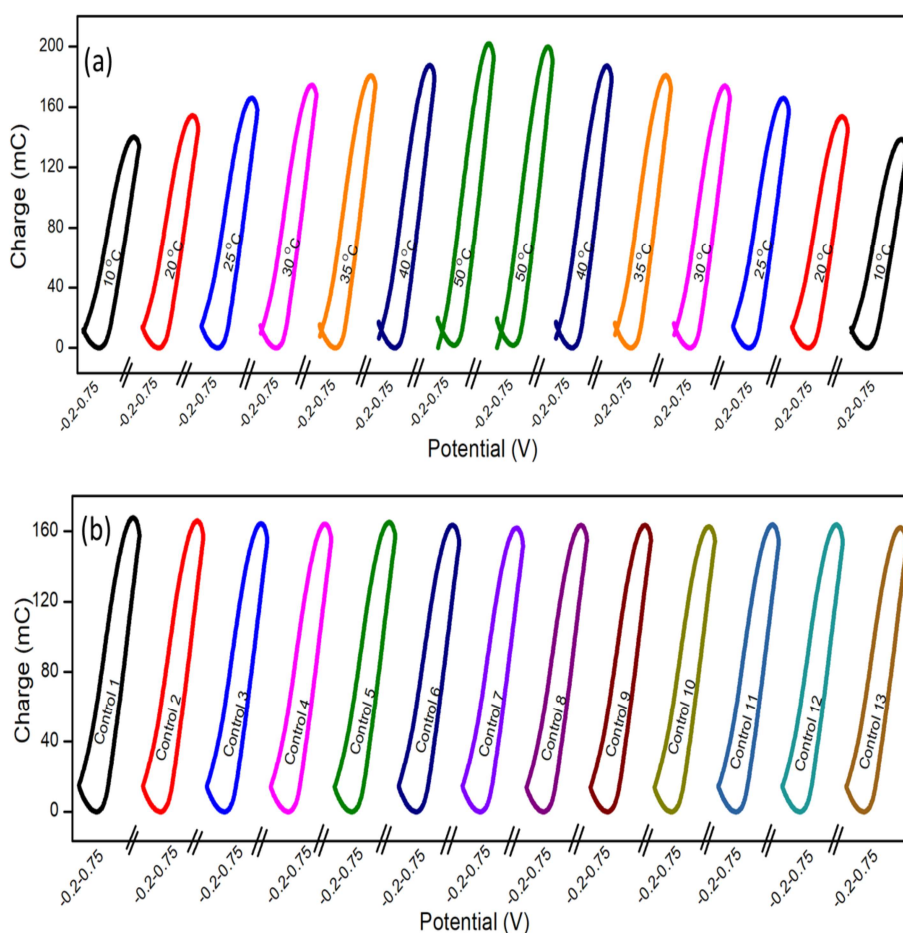


Figure 6.26 (a) *QVs at different working temperatures obtained from CVs presented in Figure 6.25a* (b) *Control QVs (at 25 °C) obtained from CVs presented in Figure 6.25b*

Figure 6.26a shows the stationary QV responses corresponding to various working temperatures, during the increasing and decreasing of experimental temperature, obtained from corresponding CVs. All QV response presents a closed loop where the oxidation charge equals the reduction charge. The QV maxima increases with increasing experimental temperature and decreases with decreasing temperature. That is, the reversible charge consumed by reversible reactions of PP4 increases with increasing working temperature and decreases with decreasing temperature. We obtained similar or overlapping QVs at a particular temperature during increasing or decreasing of temperature indicating that extension of reaction as a result of cooperative actuation of molecular motors of PANI at a particular temperature is always the same irrespective of the direction of the experiment.

Under constant reaction conditions, at higher working temperatures, higher thermal energy is available for the reaction. Therefore, a large number of electrons can be extracted per polymer chain during oxidation. It generates a large free volume across the film to lodge a large number of anions and water molecules leading to a deeper oxidation state. Similarly, during reduction, a large number of electrons can be expelled per polymer chain, destroying large free volumes across the film to expel a large number of anions and water molecules leading to a deeper reduction state. While, as the temperature decreases, only low thermal energy is available for the reaction. So, there is only a partial convolution/deconvolution of the polymeric chain resulting from conformational movements of the polymeric chain in the film, which generates/destroys only a low amount of free volume to

lodge/expel anions and water molecules leading to a partial oxidation/reduction during the electrochemical reaction. The above-described events are schematically presented in Figure 6.27.

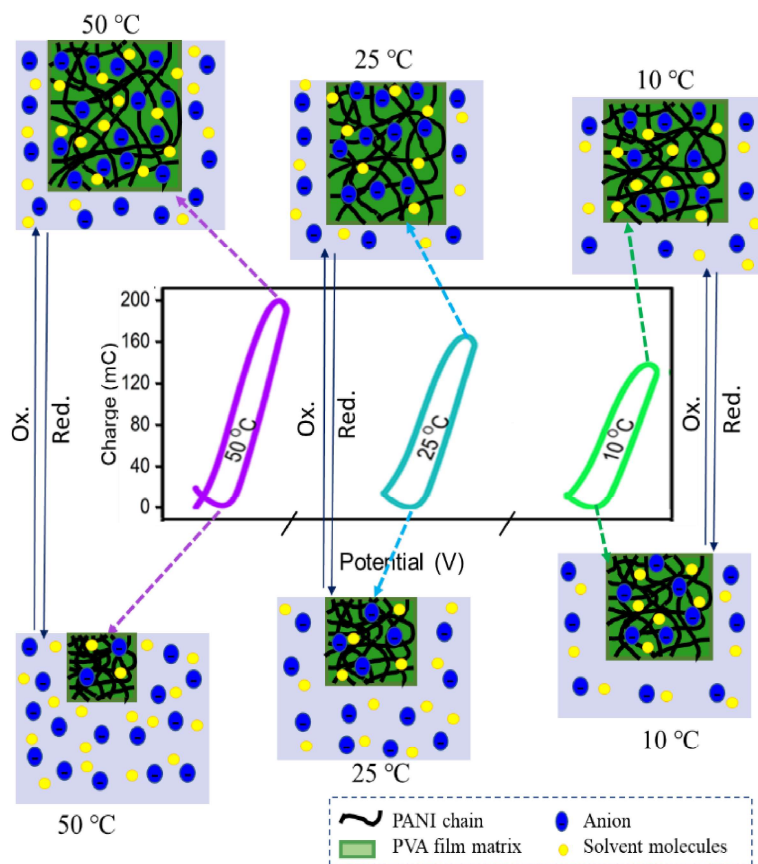


Figure 6.27 Schematic representation of extension of the electrochemically induced volume variations resulting from structural changes by reversible oxidation/reduction of the PP4 hybrid film electrode at different temperatures

The QVs of the control state, i.e., cell at 25 °C, obtained from corresponding CVs are depicted in Figure 6.26b. The same or overlapping QV responses are reproduced whenever come back to the control solution in between changing the reaction temperature. The

redox charge is constant at the control state. It corroborates that the electroactivity of the film or free volume variation resulting from the cooperative actuation of molecular motors present in the hybrid film is constant and reproducible at a particular temperature of electrolyte keeping all other experimental conditions constant. From the above discussions, we can conclude that the extension of the reaction as a result of the cooperative actuation of the polymeric chain of PANI is always constant at a particular temperature and it is reversible and reproducible.

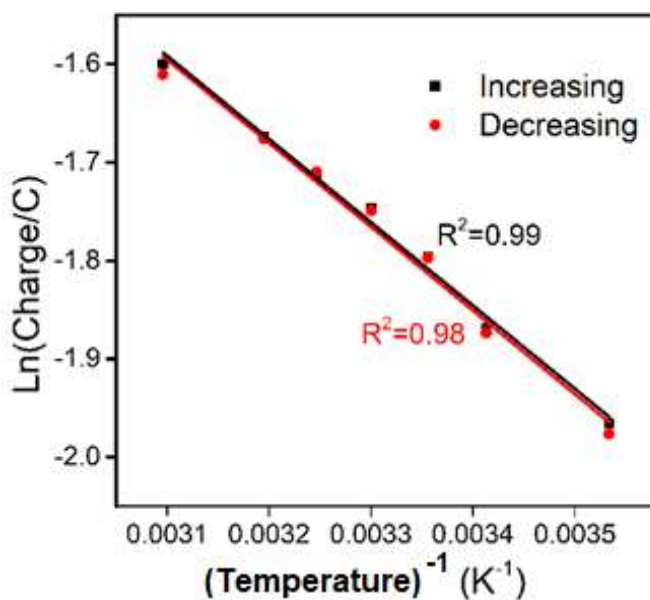


Figure 6.28 *Logarithmic variation of the charge consumed by the reversible oxidation/reduction of PP4 hybrid film with the working temperature*

Figure 6.28 shows the dependence of consumed charge during the reaction of PANI to working temperature during increasing as well as decreasing of the temperature. The extension of the reaction/consumed charge is a logarithmic function of the inverse of temperature. It fits the theoretical description by Equation 4.45. The

slope of the calibration curve, i.e., -846.9 and -850.7 respectively for increasing and decreasing working temperature, represents the sensitivity of PP4 hybrid film towards working temperature. Conclude that the cooperative actuation of molecular motors of PANI (reversible electrochemical reactions) can sense their thermal energetic conditions, here it is temperature, under the same working conditions.

6.2.14. Influence of electrical working condition on the cooperative actuation of molecular motors of PANI present in PP4 hybrid film: scan rate sensor

The influence of electrical conditions, here the scan rate, on the cooperative actuation of multistep molecular motors, that is present in the PP4 hybrid film was studied similarly as studied the influence of concentration and temperature described above. Here, the CVs are recorded at different scan rates in the potential window of -0.2 V to 0.75 V by keeping all other variables such as concentration (1 M HCl), temperature (25 °C), and pressure kept constant. The procedure is described below.

Step 1: After stabilizing the CV response the PP4 film electrode was submitted to consecutive potential cycles to get stationary CV responses at a scan rate of 50 mV s⁻¹. This is kept as a control state.

Step 2: Then the PP4 hybrid film was submitted to consecutive potential cycles to get stationary CV responses at a scan rate of 10 mV s⁻¹ under the same experimental conditions.

Step 3: Then came back to the control state, i.e., the CV recorded at a scan rate of 50 mV s⁻¹.

Steps 2 and 3 were repeated for different scan rates. In the first phase, the scan rate increases from 10 mV s^{-1} to 150 mV s^{-1} and in the second phase the scan rate decreases from 150 mV s^{-1} to 10 mV s^{-1} . The CVs from the control state (i.e., at scan rate 50 mV s^{-1}) are measured in between each scan rate cycling during increasing and decreasing the scan rate.

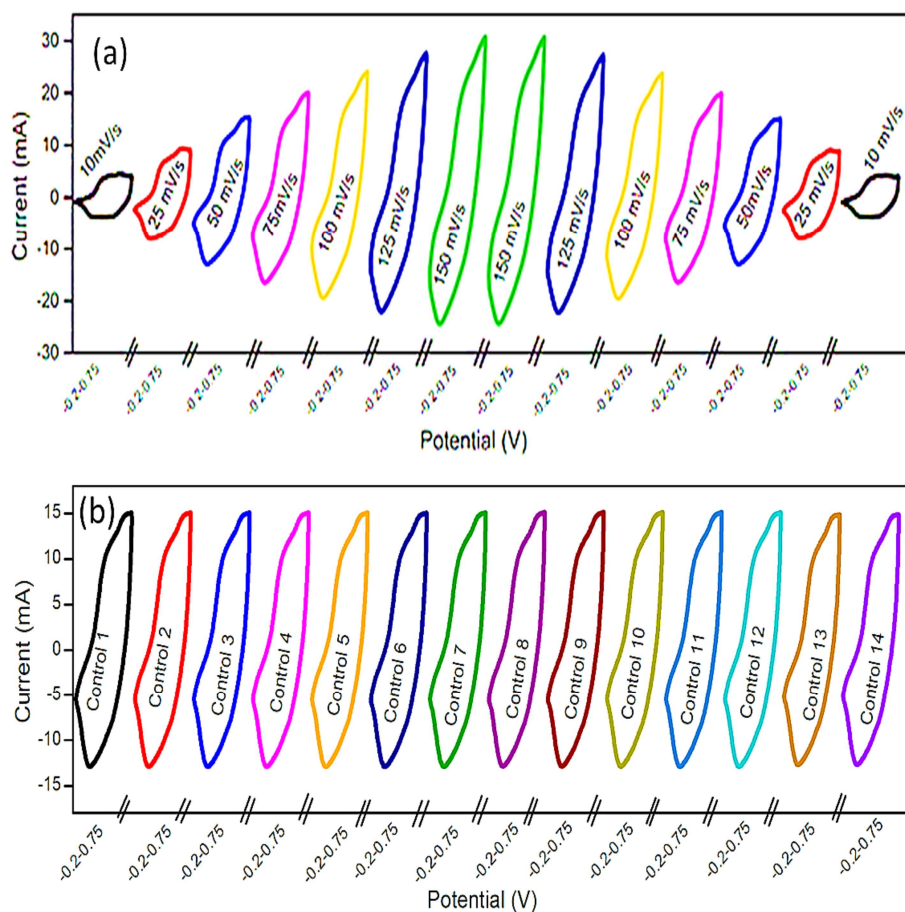


Figure 6.29 (a) Stationary CVs of PP4 hybrid film obtained at different scan rates in the potential window of -0.2 V to 0.75 V , and (b) Control CVs obtained in between every consecutive scan rate, under the same experimental conditions

Figure 6.29a represents the stationary CV responses, after two consecutive potential cycles of the PP4 film electrode at an increasing scan rate of 10 mV s^{-1} to 150 mV s^{-1} and then decreasing scan rate of 150 mV s^{-1} to 10 mV s^{-1} . The anodic and cathodic current increases with the increase of scan rate and decreases with the decrease of scan rate. Figure 6.29b is the CVs for the control state, recorded in between two consecutive increases or decreases in the scan rate. Similar or overlapping control CVs when coming back to the control state every time in between the continuous increase or decrease of scan rate cycles corroborate that the electroactivity of the PANI remains constant during the experimental cycles.

Figure 6.30a shows the stationary QV responses for increasing and decreasing scan rates, obtained from corresponding CVs. All QV responses present a closed loop where the oxidation charge equals the reduction charge. The QV maxima decreases with increasing scan rate and then increases with decreasing scan rate. That is, the reversible charge consumed by reversible reactions of the PP4 hybrid film electrode decreases with increasing scan rate. We obtained similar QVs at a particular scan rate during increasing or decreasing of scan rate indicating that the electroactivity or the free volume generation as a result of cooperative actuation of molecular motors of PANI at that particular electrical working condition remains constant irrespective of the direction of the experiment.

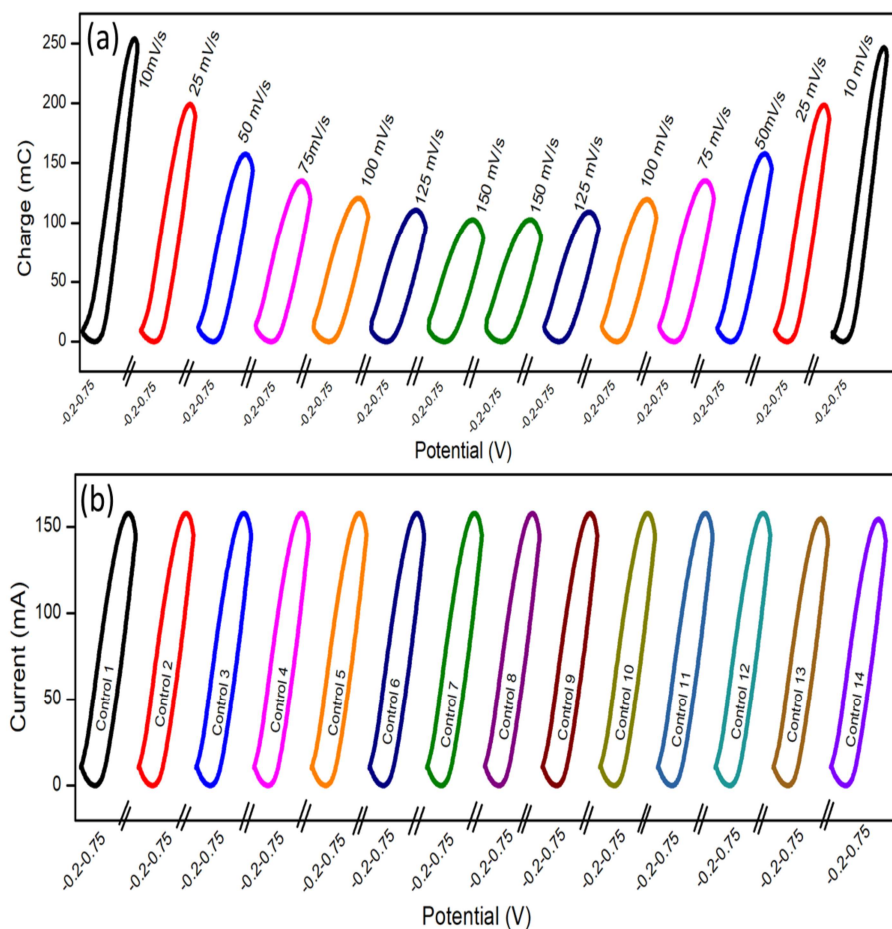


Figure 6.30 (a) QVs at different scan rates obtained from CVs presented in Figure 6.29a (b) Control QVs obtained from CVs presented in Figure 6.29b

Under constant reaction conditions, at a lower scan rate, the oxidation/reduction potentials are applied for a long period of time which promotes deeper conformational changes in the polymer chains. Therefore, a large number of electrons can be extracted per polymer chain during oxidation. It generates a large free volume across the film to lodge a large number of anions and water molecules leading to a deeper oxidation state. Similarly, during reduction, a large number of

electrons can be expelled per polymer chain, which destroys large free volume across the film to expel a large number of anions and water molecules leading to a deeper reduction state. That is a greater extension of the reaction at a lower scan rate. While, as the scan rate increases, relatively less time is available for the oxidation/reduction of the polymer chains. Therefore, only a lesser amount of free volume is generated/destroyed to lodge/expel anions and water molecules leading to a partially oxidized/reduced state. The above-described events are schematically represented in Figure 6.31.

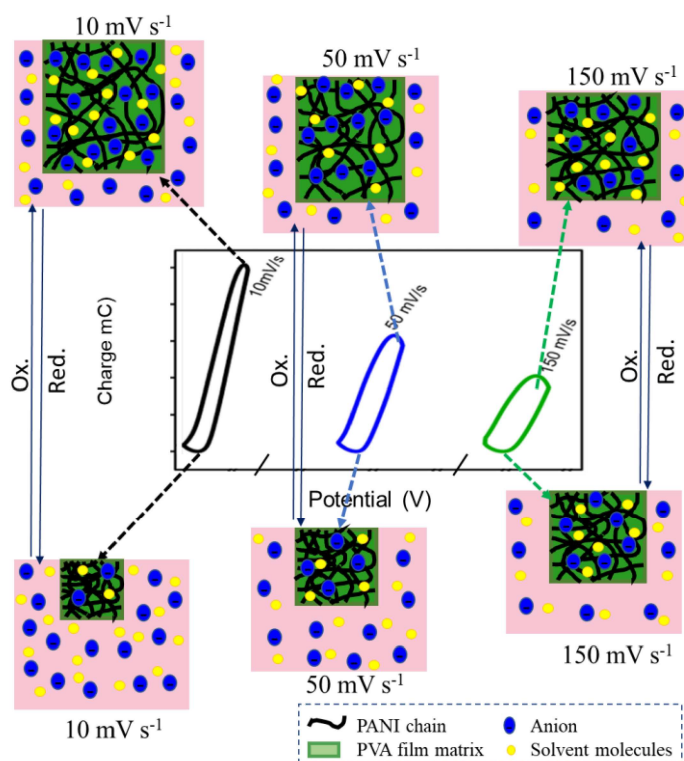


Figure 6.31 Schematic representation of extension of the electrochemically induced volume variations resulting from structural changes by reversible oxidation/reduction of the PP4 hybrid film at different scan rates

The QVs of control, i.e., at the scan rate of 50 mV s^{-1} , obtained from corresponding CVs are depicted in Figure 6.30b. The same or overlapping QV responses are reproduced whenever return to the control state from any other scan rate sweeping. That is the redox charge consumed during the reaction at a particular scan rate always almost remains constant irrespective of the direction of the experiment. Free volume variation resulting from the cooperative actuation of molecular motors present in the PP4 hybrid film is constant and reproducible at a particular scan rate keeping all other experimental conditions constant. From the above discussions, we can conclude that the extension of reaction as a result of the cooperative actuation of the polymeric chain of PANI is always the same at a particular scan rate and it is reversible in our hybrid film electrode.

Figure 6.32 shows the dependence of consumed charge during the redox reaction of PP4 hybrid film with scan rate. The extension of the reaction or consumed charge is a double logarithmic function of the scan rate. The slope of the calibration curve Figure 6.32, i.e., -0.3314 and -0.3319 respectively for increasing and decreasing scan rates, represents the sensitivity of PP4 films towards scan rate. That is, the cooperative actuation of molecular motors of PP4 hybrid films (reversible electrochemical reactions) can sense their electrical working conditions (here it is scan rate) under the same experimental conditions.

We can conclude that the electrochemical responses from PP4 hybrid film constituted by chemical molecular motors open the way for

a quantitative description of the various reaction conditions such as thermal, chemical and electrical conditions. The conformational and structural changes of PANI present in the hybrid film under faradaic control that arise due to the cooperative actuation of the constitutive chemical molecular motors (polymeric chains) are responsible for the self-sensing property of the hybrid films.

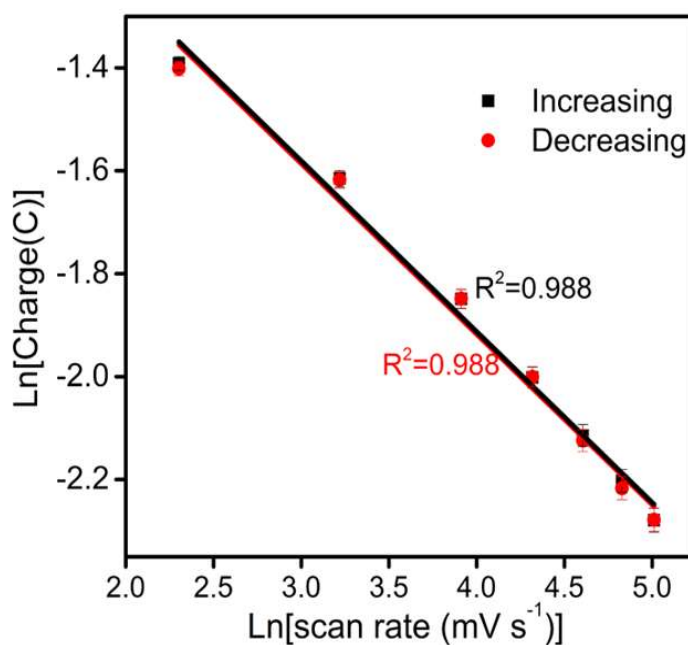


Figure 6.32 Logarithmic variation of the charge consumed by the reversible oxidation/reduction of PP4 hybrid film with the working scan rate

IV. PVA/PANI films as supercapacitor electrode

6.2.15. The specific areal capacitance of PVA/PANI hybrid film free-standing electrodes

The charge storage performances of hybrid films were examined through CV and GCD analysis in a three-electrode assembly. The films having an area of 0.2 mm^2 were used as the working electrodes. Figure 6.33a represents the CVs obtained at a scan rate of 5 mV s^{-1} within the potential range of -0.2 V to 0.75 V . The CV responses of hybrid films show non-rectangular CV curves with two pairs of redox peaks which are attributed to the faradaic pseudocapacitive dominance. The specific capacitances of the hybrid film electrodes were calculated from the CV curves using Equation 2.1. The specific areal capacitance obtained for PP1, PP2, PP3 and PP4 films is 52 mF cm^{-2} , 278 mF cm^{-2} , 584 mF cm^{-2} and 823 mF cm^{-2} respectively, at a scan rate of 5 mV s^{-1} . The highest capacitance is observed for the PP4 hybrid film.

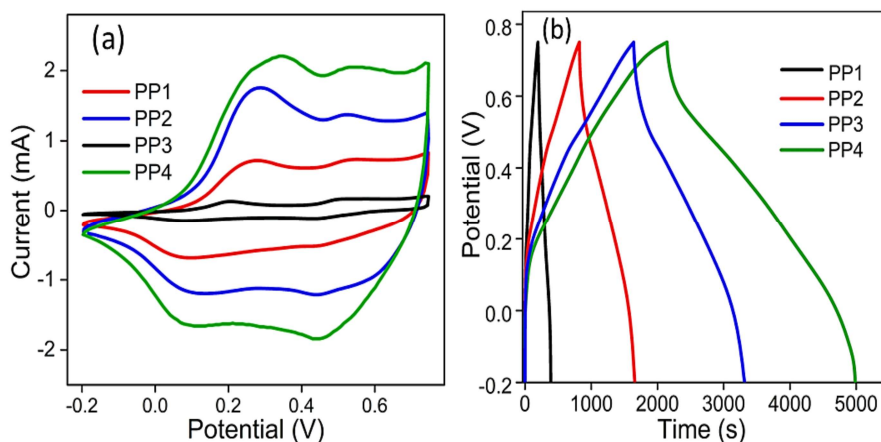


Figure 6.33 (a) CVs at a scan rate of 5 mV s^{-1} and (b) GCD curves at a current density of 0.4 mA cm^{-2} of PVA/PANI hybrid film electrodes

Figure 6.33b represents the GCD curves of PVA/PANI hybrid films obtained at a current density of 0.5 mA cm^{-2} within the potential range of -0.2 V to 0.75 V . The discharge time is related to the energy storage property of the electrode material. Their deviation from linearity is caused by the redox process of PANI, demonstrating their pseudocapacitive behavior. PP4 film electrode has the highest discharge time among these four hybrid films corresponding to its better capacitive property. It is consistent with its highest electric conductivity which is beneficial to promoting the electron transfer process. The specific capacitance values were calculated using PP1, PP2, PP3 and PP4 electrodes have a specific capacitance of 43 mF cm^{-2} , 184 mF cm^{-2} , 371 mF cm^{-2} and 630 mF cm^{-2} respectively, at current densities of 0.5 mA cm^{-2} .

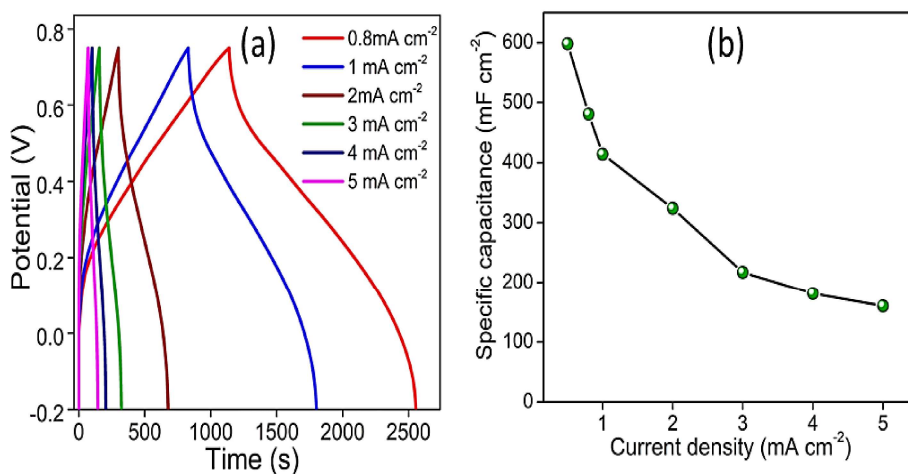


Figure 6.34 (a) GCD curves of PP4 hybrid film at different current densities and (b) variation of specific capacitance with current density

The GCD curves of the PP4 hybrid film electrode at different current densities are depicted in Figure 6.34a. The GCD curves are

almost symmetrically shaped, indicating that the PP4 film electrodes have superior electrochemical reversibility and excellent coulombic efficiency. It has only negligible IR drop in the studied potential range which is due to high electron and ionic transfer rates. Here, the PVA hydrogel matrix provides good hydrophilicity to the electrode. The swollen state of the hybrid film may allow facile permeation of ions and electrons into PANI chains leading to low IR drop as well as high electrochemical performance. The variation of specific capacitance as a function of current density from 0.5 mA cm^{-2} to 5 mA cm^{-2} for the PP4 hybrid film is presented in Figure 6.34b. The capacitance decreases as the current density increases due to the provision of less time for the electrolyte ions to diffuse into the active sites and interact with active material at the higher current densities.

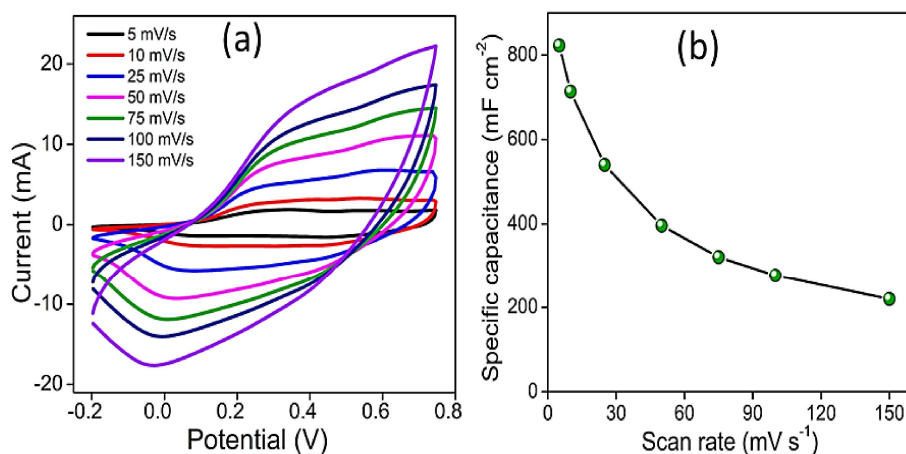


Figure 6.35 (a) CVs obtained for PP4 films at different scan rates and (b) variation of specific capacitance of PP4 hybrid film electrode with the CV scan rate

Figure 6.35a shows the CVs of PP4 hybrid film at different scan rates. The variation of specific capacitance with scan rates for PP4

hybrid film is depicted in Figure 6.35b. The specific capacitance decreases with the scan rate, because, at higher scan rates the potentials are applied for a shorter time, and electrolyte ions do not get sufficient time to interact with electrode material effectively at higher scan rates.

6.2.16. EIS analysis

EIS was performed to analyze the fundamental electrochemical behaviour of PVA/PANI hybrid films. Figure 6.36 represents the Nyquist plot of all four hybrid films. The plots have a small semicircle part in the high-frequency region and a nearly straight oblique line in the low-frequency region. The semicircle mainly depicts the charge transfer process at the electrode-electrolyte interface and whose intercept to the real axis at the high-frequency region is meant for the equivalent series resistance (ESR) including solution resistance, the internal resistance of materials and the contact resistance between the electrode and electrolyte [18, 19]

All the hybrid films have low ESR values which is attributed to the high hydrophilicity of the films as well as to the good interconnection between the electrode and the electrolyte. The semicircle diameter reflects the migration impedance of charges or charge transfer resistance (R_{ct}). The Nyquist plot showed a very small semi-circle in the high-frequency region which is ascribed to the smooth charge transfer between the electrode and electrolyte. PP4 film electrode has the smallest semicircle indicating its low charge transfer resistance and high electron transfer due to its highest conductivity. The oblique line refers to the diffusion-limited ion transport process across the

electrode surfaces. Its slope gives the diffusion impedance and a larger slope of the line indicates the higher diffusion rate of ions due to the highly porous nature of the films as evidenced by SEM images.

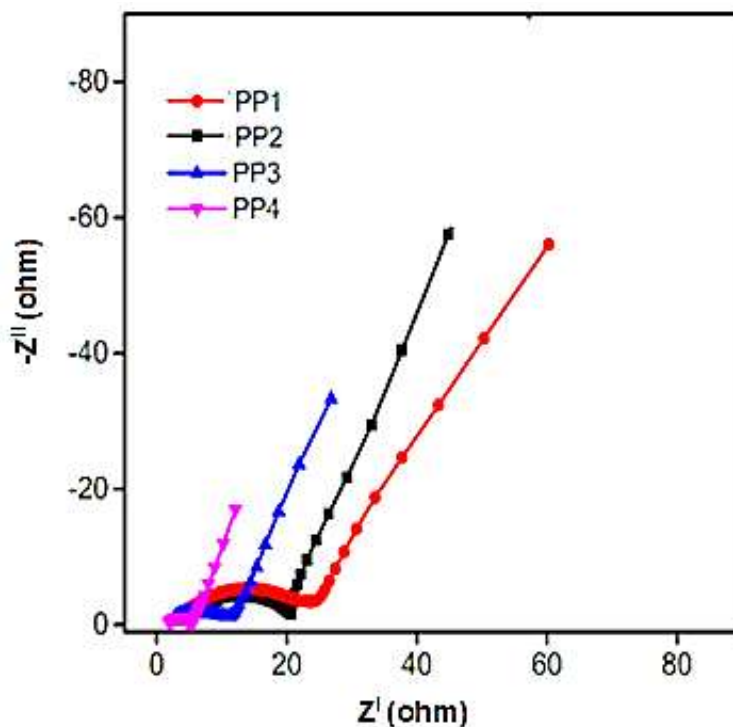


Figure 6.36 Nyquist plot of PVA/PANI hybrid films

6.2.17. Cycling stability

The long-term cycling stability of the PP4 hybrid film electrode (it has the highest specific capacitance reported) was monitored by GCD over 1500 cycles at 2 mA cm^{-2} and the result is depicted in Figure 6.37. CPs have poor cyclic stability due to the structural degradation of the polymer chain caused by repeated intercalation/deintercalation (swelling/shrinking) of ions during the repeated charge/discharge process [20]. In our study, the PP4 hybrid film electrode shows good

electrochemical stability, which retains 82 % of its initial capacitance after 1500 cycles. The relatively higher cyclic stability of PP4 film is attributed to the strong synergy existing between PVA and PANI resulting in a supportive and protective effect on PANI during swelling and shrinking process during electrochemical cycling.

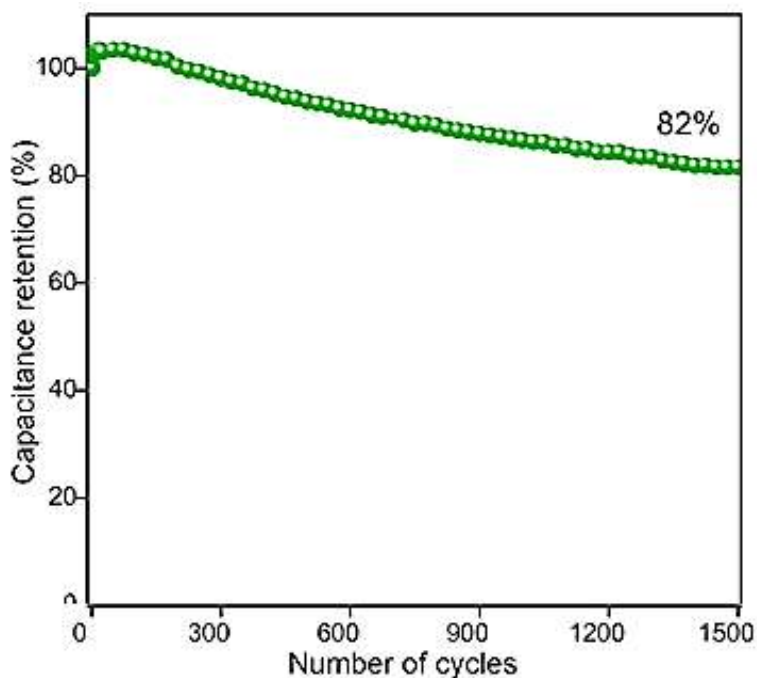


Figure 6.37 Cycling stability of PP4 hybrid film for 1500 cycles

6.2.18. Charge storage kinetics of PP4 hybrid film

The charge storage behaviour of PP4 hybrid film was analyzed from b value measurement and using Dunn's method. The b value is the indication of the charge storage mechanism. In general, $b = 0.5$ corresponds to the ideal diffusion controlled Faradaic process, while $b = 1$ corresponds to the outer surface non-diffusion-controlled process

(double layer phenomenon). It is obtained by plotting $\log(\text{current})$ against $\log(\text{scan rate})$ at different potentials as shown in Figure 6.38a (only for anodic process is depicted in the figure). The obtained b values at the various potentials are given in Figure 6.38b. It is observed from Figure 6.38b that the b values lie between 0.5 and 1. It indicates that the charge storage comes from both diffusion-controlled and capacitive (double layer) processes [21]. The capacitive and diffusive contribution in PP4 hybrid film is quantified by Dunn's method (it is detailly described in section 5.2.12). Figure 6.38c illustrates the graphical representation of the current contribution by the capacitive and diffusion-controlled process for scan rates of 5 mV s^{-1} . The highlighted area with navy blue colour in the CV curve represents the capacitive contribution. At a lower scan rate of 5 mV s^{-1} , the diffusion-limited faradaic process contributes 77 % and the non-faradaic process contributes 23 % to total capacitance suggesting the high redox nature of the PVA/PANI hybrid films. The bar plots of percentage contribution from the capacitive and diffusive process for different scan rates are presented in Figure 6.38d. At the higher scan rates, diffusion contribution is decreased while capacitive contribution is increased. Even at a higher scan rate of 100 mV s^{-1} , the PP4 film electrode has a considerable diffusive contribution of 30 %. The decreasing diffusion contribution at a higher scan rate is due to less time available for the electrode to complete the redox reaction.

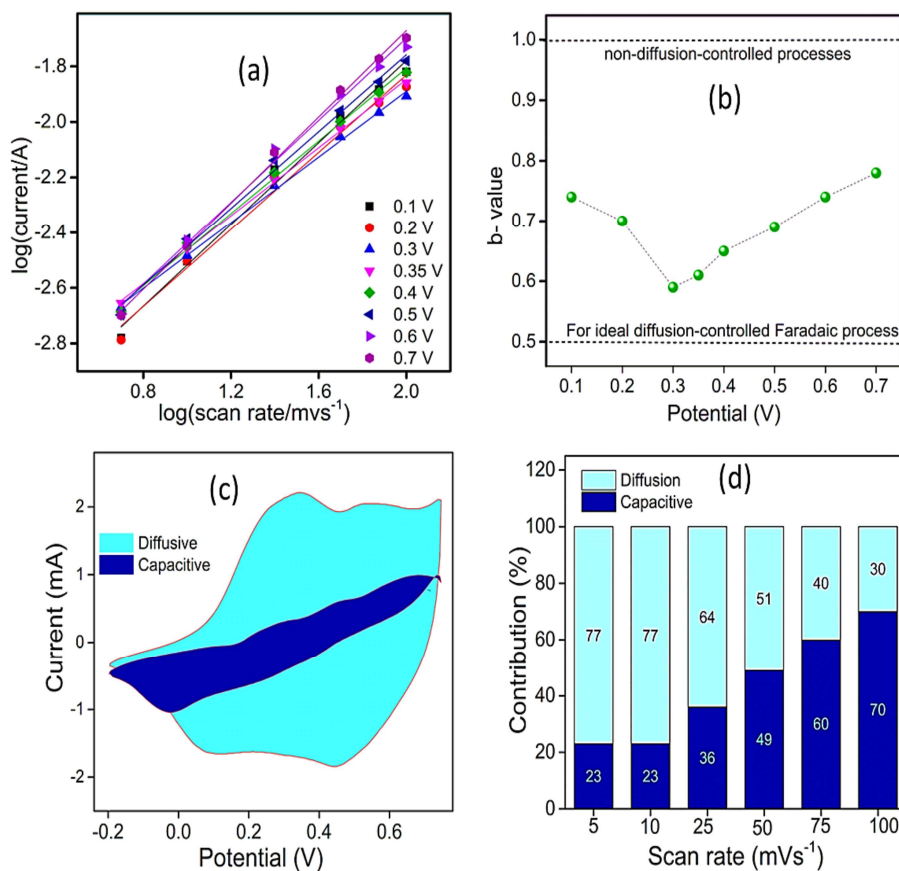


Figure 6.38 (a) Determination of b values at different potential regimes, (b) the obtained b values, (c) separation of the capacitive and diffusion currents at a scan rate of 5 mVs^{-1} and (d) contribution ratios from non-faradaic double layer process (capacitive) and diffusion-limited oxidation/reduction of PP4 hybrid films at various scan rates from 5 mVs^{-1} to 100 mVs^{-1} .

V. Sensing supercapacitor device using PVA/PANI hybrid films

One of the major objectives of this study was to fabricate a sensing motor from CPs. Towards achieving this objective, we have succeeded in fabricating highly stable electroactive hybrid films using PANI and PVA. We have fabricated a symmetric all-solid-state supercapacitor device using PVA/PANI hybrid films as described in section 2.4.

6.2.19. Charge storage performance of the device

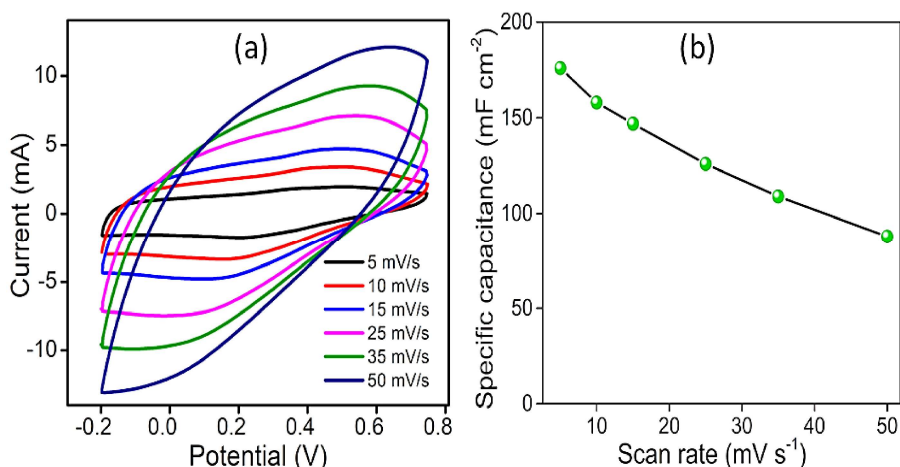


Figure 6.39 (a) CVs at different scan rates and (b) variation of specific capacitance of device with the CV scan rate

The charge storage performance of the device was tested by CV, GCD, and EIS methods. The CV diagrams obtained at different scan rates are presented in Figure 6.39a. Almost similar and symmetrical shapes of the CVs recorded at different scan rates suggest the good capacitive behavior of our supercapacitor. From CV the specific areal

capacitance of the device is calculated using Equation 2.1 and found to be 178 mF cm^{-2} at a scan rate of 5 mV s^{-1} . Figure 6.39b shows that the specific capacitance decreases with increasing the scan rate due to the provision of less time for the electrolyte ion to interact with the bulk of the electrode material.

The GCD curves obtained at different current densities in the potential window of 0.95 V are shown in Figure 6.40a. The specific capacitance of this supercapacitor device was calculated from its total area. The areal-specific capacitance of this supercapacitor device is found to be 119 mF cm^{-2} at a discharge rate of 0.5 mA cm^{-2} . It is comparable to those of various polyaniline-hydrogel-based supercapacitors reported in the literature, which are listed in Table 6.3.

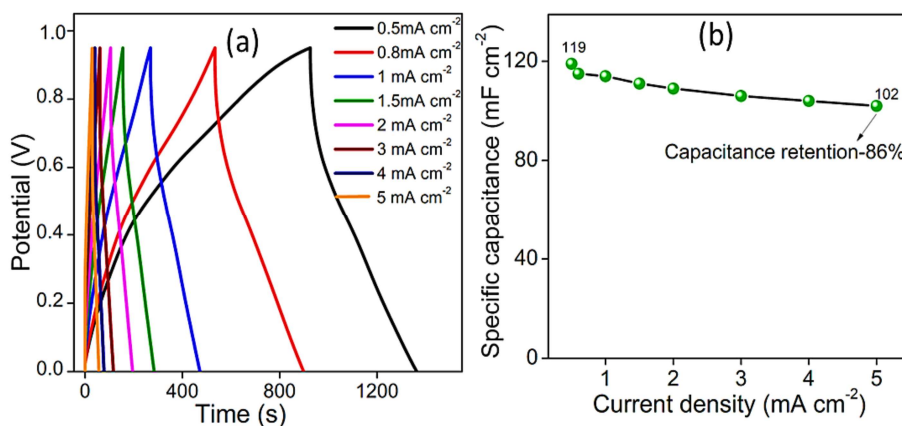


Figure 6.40 (a) GCD curves of the supercapacitor device at different current densities and **(b)** variation of specific capacitance with current density

Figure 6.40b reveals that the specific capacitance slightly decreases with increasing current density. Because at higher current densities, the electrolyte ions do not get sufficient time to interact with

the bulk of the electrodes. Interestingly, the device shows 86 % capacitance retention after a tenfold increase in current density. It indicates that the material has good kinetics as well as rate capability due to the presence of hydrophilic PVA which facilitates electrolyte and ion transport. The rate capability of the PP4 device is much better than that reported for other conducting-polymer-based supercapacitor electrodes/devices which typically give 50–60 % capacitance retention at 10-fold increases of current density [22, 23].

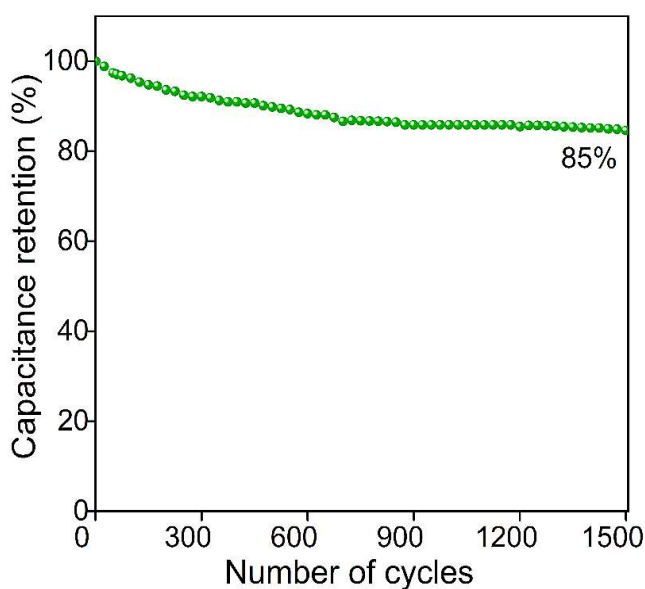


Figure 6.41 *Cycling stability of the device for 1500 cycles*

The cyclic stability of a supercapacitor is one of the significant measures for its practical application. Figure 6.41 shows the cycling stability of our supercapacitor analyzed at a scan rate of 4 mA cm^{-2} for 1500 continuous charge-discharge cycles. The device retains 85 % of its initial specific capacitance after 1500 charge-discharge cycles suggesting the good long-term electrochemical stability of the device.

Table 6.3 Comparison of PVA/PANI hybrid film supercapacitors with other PANI- hydrogel-based supercapacitors reported in the literature.

Type of electrode	Areal capacitance	Maximum energy density @ Power density	Ref.
PVA/PANI	119 mF cm ⁻² @ 0.4 mA cm ⁻² 178 mF cm ⁻² @ 5mV/s	13.8 μWh cm ⁻² @ 100 μW cm ⁻²	<i>This work</i>
Graphene / PANI	23 mF cm ⁻² @ 0.1 mA cm ⁻²	1.5 μWh cm ⁻² @ 330 μW cm ⁻²	[24]
CNFs/PANI/rGO	5.86 mF cm ⁻² @ 4.3 μA cm ⁻²		[25]
CNFs/[PANI– PEDOT: PSS	4.22 mF cm ⁻² @ 4.3 μA cm ⁻²		[25]
PVA /PANI	25.86 mF cm ⁻² @ 0.05 mA cm ⁻²		[26]
PANI/PVA/PHEA	98 mF cm ⁻² @ 0.2 mA cm ⁻²	8.48 μWh cm ⁻² @ 78.52 μW cm ⁻²	[27]
SWCNT/PANI/ PVA	15.8 mF cm ⁻² @0.044 mA cm ⁻²		[28]
rGO/PANI	6.4 mF cm ⁻² @ 0.08 mA cm ⁻²	7.07 Wh kg ⁻¹ @ 707 W kg ⁻¹	[29]
Fe ³⁺ / PANI/Cellulose	185 mF cm ⁻² @ 0.2 mA cm ⁻²	~ 6.2 μWh cm ⁻² @ ~110 μW cm ⁻²	[30]
PHE/PANI	131 mF cm ⁻² @ 0.2 mA cm ⁻²	11.6 μWh cm ⁻² @ 79.9 μW cm ⁻²	[31]
Graphite/PANI	77.8 mF cm ⁻² @ 0.1 mA cm ⁻²	0.32 mWh cm ⁻³ @ 0.054 W cm ⁻³	[32]

NiO/Graphene/ PANI	112 mF cm ⁻² @ 2 mV s ⁻¹		[33]
PVA/PANI	11.3 mF cm ⁻² @ 5 mVs ⁻¹		[34]
rGO/PANI-CH ₄	45 mF cm ⁻² @ 0.2 mA cm ⁻²		[35]
CNT/PANI	38 mF cm ⁻² @ 0.01 mA cm ⁻²		[36]
CNF/CNTs/PANI	67.31 mF cm ² @ 0.5 mA cm ⁻²		[37]
Graphene/sulfo- PANI	3.31 mF cm ⁻² @ 10 mV s ⁻¹	1.51 mWh cm ⁻³	[38]
Cellulose /PAA/PANI	1.73 mF cm ⁻² @ 5 mV s ⁻¹	0.62 μWh cm ⁻² @ 7.03 μW cm ⁻²	[39]
PANI/PLA (Symmetric)	0.20 mF cm ⁻² @ 4 μA cm ⁻²	3.60 μWh cm ⁻² @ 0.02 μW cm ⁻²	[40]
PANI/PLA (Asymmetric)	23.33 mF cm ⁻² @0.05 mA cm ⁻²	30.09 μWcm ⁻² @ 1.17μWh cm ⁻²	[40]
PANI- foamed PLA	27.73 mF cm ⁻² @ 0.05 mA cm ⁻²	1.89 μWh cm ⁻² @ 35 μW cm ⁻²	[41]
PANI–Stainless Steel wire	~19 mF cm ⁻² @ 0.1 mA cm ⁻²	0.95 μWh cm ⁻² @ ~100 μW cm ⁻²	[42]

CNFs- Cellulose nanofiber; rGO- reduced graphene oxide; PHEA- poly (N-hydroxyethyl acrylamide); SWCNT- single-walled carbon nanotube; PHE- polymer hydrogel electrolyte (polyacrylic acid crosslinked with vinyl hybrid silica nanoparticles); CNT- carbon nanotube; sulfo-PANI- sulphonated PANI; PAA- polyacrylic acid; PLA- polylactic acid.

The EIS spectra were also recorded for the device to further analyze and quantify the electrochemical kinetic parameters. The Nyquist plot is given in Figure 6.42. The inset shows an equivalent circuit used for fitting the experimental data obtained by *Zman* software and the parameters are summarized in Table 6.4. The Nyquist plot shows a semicircle at a high-frequency region resulting from the parallel combination of resistance and capacitance and an inclined line in the low-frequency region that accounts for the diffusion of ions into the porous electrode. The device has a solution resistance (R_s) value of 13.45Ω and R_{ct} of 0.5Ω , suggesting low internal resistance and fast charge transfer process even in the PVA/H₂SO₄ gel electrolyte, indicating the favorable electrochemical kinetics of fabricated supercapacitor device.

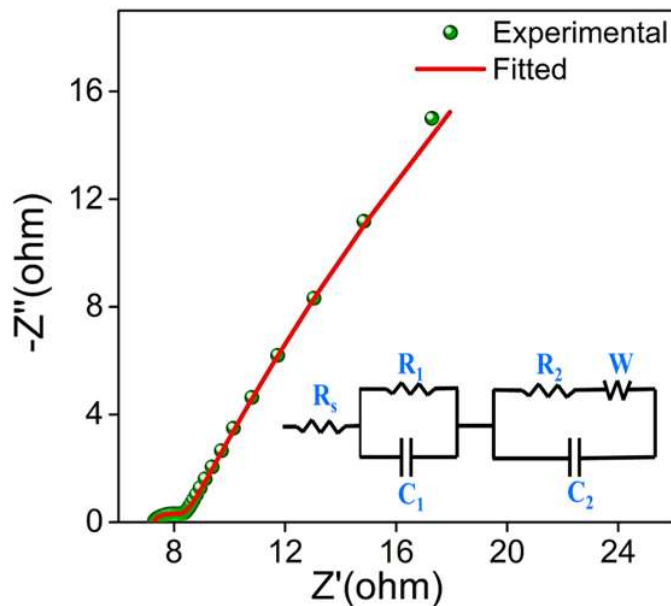


Figure 6.42 EIS Nyquist plot of the supercapacitor device

Table 6.4 EIS fitting data of the device

Parameters	R_s (Ω)	R_1 (Ω)	C_1 (mF)	R_2 (Ω)	C_2 (mF)	W ($\Omega^{0.5}$)
Values	7.43	24.69	143.08	0.598	0.252	0.141

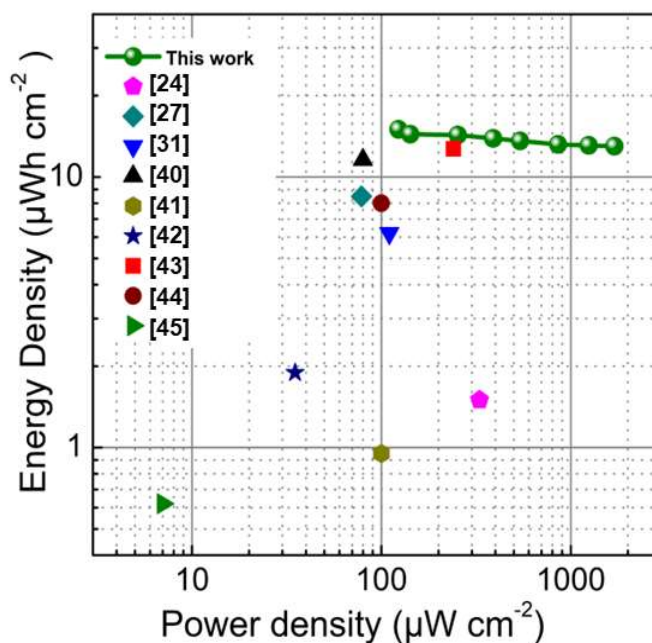
**Figure 6.43** Ragone plot of the device

Figure 6.43 is the Ragone plot which represents the areal energy density and power density of the device. The fabricated supercapacitor has an energy density of $15 \mu\text{Wh cm}^{-2}$ at a power density of $123 \mu\text{W cm}^{-2}$. It demonstrates that the device can provide remarkably high energy densities at relatively high power densities compared to those previously reported for various PANI-based supercapacitors which are depicted in the Ragone plot [24, 27, 31, 40-45] and the data

are listed in Table 6.3. When the areal power density was increased more than 10 times ($1696 \mu\text{W cm}^{-2}$), the energy density was maintained at $13 \mu\text{Wh cm}^{-2}$ for this device. That is the device has high energy density even at higher power densities.

6.2.20. Sensing characteristics of the device

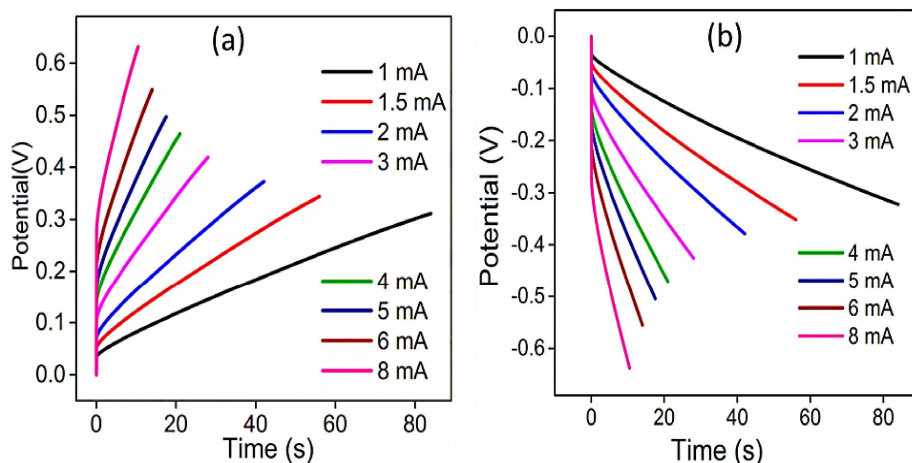


Figure 6.44 Normalized (a) anodic and (b) cathodic chronopotentiograms of the device corresponding to different working currents at the constant charge of $\pm 38 \text{ mC}$

The current sensing behaviour of the device was analyzed in a two-electrode mode at a constant charge. The normalized chronopotentiometric responses for the anodic or oxidation (charging 38 mC) and cathodic or reduction (discharging 38 mC) processes of the device are shown in Figure 6.44a and 6.44b, respectively. The electrical energy consumed during the anodic current flow, i.e., during charging and cathodic current flow, i.e., during discharging, were obtained from corresponding chronopotentiometric curves. The consumed electrical

energy has a linear dependence on the working current with excellent correlation along with well-defined sensitivity and reliability as depicted in Figure 6.45. It reveals that the fabricated supercapacitor device can sense its electrical working condition during charging/discharging without the need for additional connectivity for sensing. That is, the consumed electrical energy during the charging-discharging process can thus reveal information regarding the working ambient.

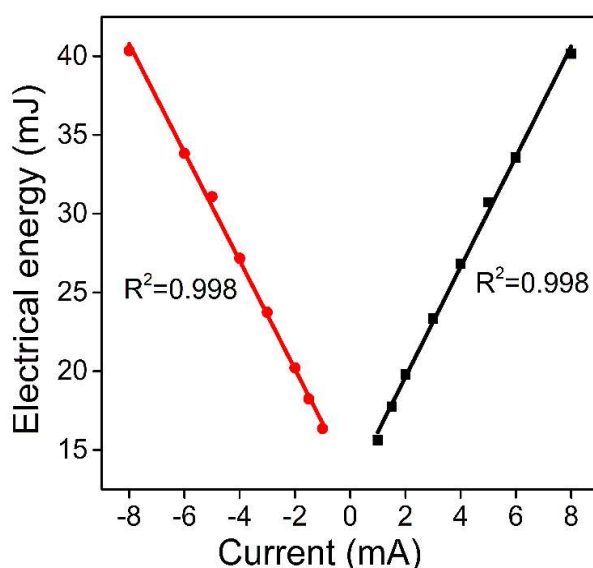


Figure 6.45 Linear variation of consumed electrical energy as a function of working current

The sensing capability of the supercapacitor device towards the thermal working condition was also analyzed by recording chronopotentiograms at different experimental temperatures. The normalized chronopotentiometric responses for the anodic (charging 38 mC) and cathodic (discharging of 38 mC) processes of the device at various temperatures are shown in Figure 6.46a and 6.46b, respectively.

The electrical energy consumed during the anodic and cathodic processes at each temperature was obtained from corresponding chronopotentiometric curves. The consumed electrical energy has a linear dependence on the working temperature with excellent correlation along with well-defined sensitivity and reliability as depicted in Figure 6.47.

It can be concluded that the PP4 supercapacitor device is capable of sensing its electrical and thermal working conditions during functioning without the need for additional connectivities for sensing. That is, the consumed electrical energy during the charging-discharging process can thus reveal information regarding the working ambient of the device. Thus, it is proved that using the PVA/ PANI hydrogel films, we can design macromolecular sensing motors.

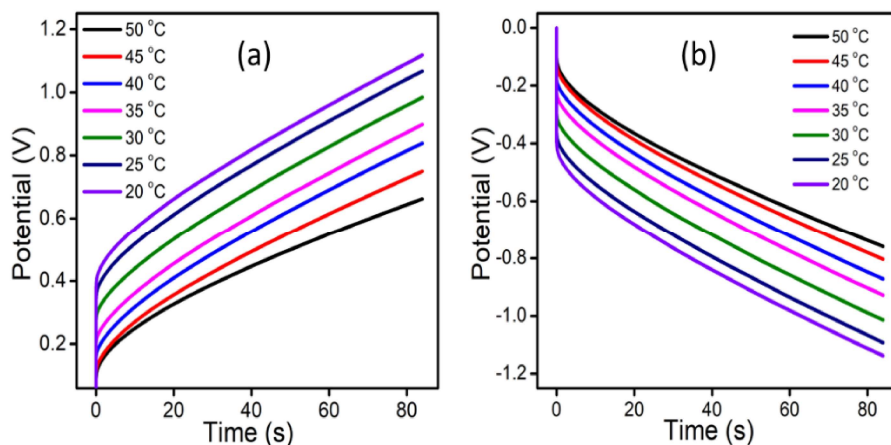


Figure 6.46 Normalized (a) anodic and (b) cathodic chronopotentiograms of the device corresponding to different working temperatures at a constant charge of ± 38 mC

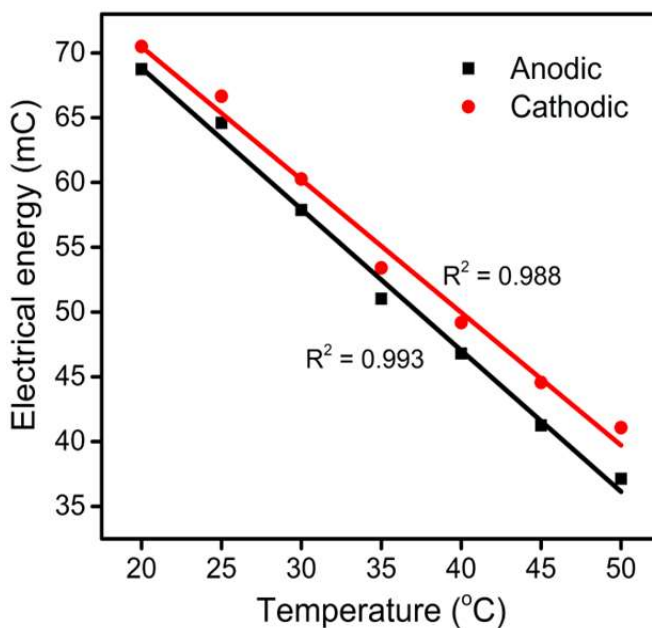


Figure 6.47 Linear variation of consumed electrical energy as a function of working temperature

6.3. Conclusion

A highly mechanically stable PVA/PANI hybrid films were fabricated through in situ chemical oxidative polymerization of PANI on a pre-fabricated PVA film matrix. The hybrid films were characterized by FTIR, TGA, SEM, electrical conductivity measurements and mechanical studies. The PANI has grown on the surface of PVA with coral-like nanowire morphology. The hybrid films are more thermally stable than PVA. The tensile strength and Young's Modulus of PVA/PANI film are higher than that of PVA and increase with increasing the number of times of coating of PANI, i.e., increases from PP1 to PP4. The hybrid films have sufficient mechanical strength even in wet states. Therefore, PVA/PANI films are suitable for the development of various devices that are working either in dry or wet

conditions. The CV studies suggest that the electroactivity of the hybrid films was imparted by the PANI component. The cyclic voltammetric and coulombometric studies revealed that PP4 film has the highest electroactivity among the fabricated hybrid films.

The results on the reaction driven sensing properties of PVA/PANI hybrid films studied through chronopotentiometry and cyclic voltammetry reveal that the consumed electrical energy and consumed charge are the sensing parameters. The QV responses detect and quantify the extension of the reaction. It is verified that the conformational and structural changes under faradaic control that arise due to the cooperative actuation of the constitutive chemical molecular machines are responsible for the self-sensing property of the hybrid film. This sensing property is verified under different reaction conditions such as concentration of electrolyte, temperature and electrical condition. That is, the extension of reaction as a result of cooperative actuation of multi-step molecular motors of polyaniline respond to or adapted to or senses the working conditions.

The above characteristics of the hybrid films were employed to design a self-sensing all-solid-state symmetric supercapacitor device using PVA/PANI hybrid hydrogel free-standing films. The device can sense their working conditions with the same connectivity. The device shows a high specific capacitance of 119 mF cm^{-2} at 0.5 mA cm^{-2} . A remarkable energy density of $15 \text{ } \mu\text{Wh cm}^{-2}$ at a power density of $123 \text{ } \mu\text{W cm}^{-2}$ and a good stability of 85 % capacitance retention after 1500 cycles was achieved for the sensing supercapacitor. Along with charge storage capability, the device has a well-defined sensitivity and

reliability towards working electrical and thermal conditions. The consumed electrical energy during the charging/discharging cycles of the supercapacitor acts as the sensing parameter. This integration strategy does not require additional connectivities for sensors and therefore, it gives a new direction for the development of a new generation of self-sensing and compact energy-related systems.

References

1. N.B. Halima, RSC advances, 6 (2016) 39823-39832.
2. M. Aslam, M.A. Kalyar, Z.A. Raza, Polymer Engineering & Science, 58 (2018) 2119-2132.
3. F. Kawai, X. Hu, Applied microbiology and biotechnology, 84 (2009) 227-237.
4. S. Adhikari, P. Banerji, Synthetic metals, 159 (2009) 2519-2524.
5. H.S. Mansur, C.M. Sadahira, A.N. Souza, A.A. Mansur, Materials Science and Engineering: C, 28 (2008) 539-548.
6. Z. Zhang, M. Wan, Synthetic metals, 128 (2002) 83-89.
7. M. Ohira, T. Sakai, M. Takeuchi, Y. Kobayashi, M. Tsuji, Synthetic Metals, 18 (1987) 347-352.
8. P. Kong, H. Feng, N. Chen, Y. Lu, S. Li, P. Wang, RSC advances, 9 (2019) 9211-9217.
9. A.S. Roy, K.R. Anilkumar, M.A. Prasad, Journal of applied polymer science, 123 (2012) 1928-1934.
10. A. Fattoum, Z.B. Othman, M. Arous, Materials chemistry and physics, 135 (2012) 117-122.
11. A.M. Omer, W.A.A. Sadik, A.G.M. El-Demerdash, T.M. Tamer, R.E. Khalifa, M.S. Mohyeldin, N.A. Abdelwahed, Polymer Bulletin, 78 (2021) 6649-6673.

12. J.M. Guerrero, A. Carrillo, M.L. Mota, R.C. Ambrosio, F.S. Aguirre, *Molecules*, 24 (2018) 63.
13. Y.A. Ismail, S.R. Shin, K.M. Shin, S.G. Yoon, K. Shon, S.I. Kim, S.J. Kim, *Sensors and Actuators B: Chemical*, 129 (2008) 834-840.
14. A.J. Bard, L.R. Faulkner, H.S. White, *Electrochemical methods: fundamentals and applications*, John Wiley & Sons, 2022.
15. T.F. Otero, *RSC advances*, 11 (2021) 21489-21506.
16. T.F. Otero, *International Journal of Smart and Nano Materials*, 8 (2017) 125-143.
17. T.F. Otero, *The Chemical Record*, 18 (2018) 788-806.
18. S. Radhakrishnan, R. Muthukannan, U. Kamatchi, C.R. Rao, M. Vijayan, (2011).
19. H.J. Nogueira Pedroza Dias Mello, M. Mulato, *The Journal of Physical Chemistry C*, 126 (2022) 12222-12229.
20. L. Lizarraga, E.M.a. Andrade, F.V. Molina, *Journal of Electroanalytical Chemistry*, 561 (2004) 127-135.
21. Y. Jiang, J. Liu, *Energy & Environmental Materials*, 2 (2019) 30-37.
22. F. Xu, G. Zheng, D. Wu, Y. Liang, Z. Li, R. Fu, *Physical Chemistry Chemical Physics*, 12 (2010) 3270-3275.
23. W. Li, F. Gao, X. Wang, N. Zhang, M. Ma, *Angewandte Chemie*, 128 (2016) 9342-9347.
24. X. Zang, X. Li, M. Zhu, X. Li, Z. Zhen, Y. He, K. Wang, J. Wei, F. Kang, H. Zhu, *Nanoscale*, 7 (2015) 7318-7322.
25. X. Wang, K. Gao, Z. Shao, X. Peng, X. Wu, F. Wang, *Journal of Power Sources*, 249 (2014) 148-155.
26. W. Li, X. Li, X. Zhang, J. Wu, X. Tian, M.-J. Zeng, J. Qu, Z.-Z. Yu, *ACS Applied Energy Materials*, 3 (2020) 9408-9416.
27. J. Yang, X. Yu, X. Sun, Q. Kang, L. Zhu, G. Qin, A. Zhou, G. Sun, Q. Chen, *ACS Applied Materials & Interfaces*, 12 (2020) 9736-9745.
28. Y. Guo, K. Zheng, P. Wan, *Small*, 14 (2018) 1704497.

29. F. Chen, P. Wan, H. Xu, X. Sun, *ACS Applied Materials & Interfaces*, 9 (2017) 17865-17871.
30. Z. Kang, C. Wu, L. Dong, W. Liu, J. Mou, J. Zhang, Z. Chang, B. Jiang, G. Wang, F. Kang, *ACS Sustainable Chemistry & Engineering*, 7 (2019) 3364-3371.
31. R. Jia, H. Du, X. Zhang, Z. Chen, D. Chen, *Journal of The Electrochemical Society*, 165 (2018) A3792.
32. B. Yao, L. Yuan, X. Xiao, J. Zhang, Y. Qi, J. Zhou, J. Zhou, B. Hu, W. Chen, *Nano Energy*, 2 (2013) 1071-1078.
33. X. Wu, Q. Wang, W. Zhang, Y. Wang, W. Chen, *Electrochimica Acta*, 211 (2016) 1066-1075.
34. R. Hu, J. Zhao, R. Jiang, J. Zheng, *Journal of Materials Science: Materials in Electronics*, 28 (2017) 14568-14574.
35. K. Wang, B. Zheng, M. Shrestha, T. Schuelke, Q.-H. Fan, *Energy Storage Materials*, 14 (2018) 230-237.
36. N. Jung, S. Kwon, D. Lee, D.M. Yoon, Y.M. Park, A. Benayad, J.Y. Choi, J.S. Park, *Advanced Materials*, 25 (2013) 6854-6858.
37. J.-h. Liu, X.-y. Xu, W. Lu, X. Xiong, X. Ouyang, C. Zhao, F. Wang, S.-y. Qin, J.-l. Hong, J.-n. Tang, *Electrochimica Acta*, 283 (2018) 366-373.
38. B. Song, L. Li, Z. Lin, Z.-K. Wu, K.-s. Moon, C.-P. Wong, *Nano Energy*, 16 (2015) 470-478.
39. S. Ke, Z. Wang, K. Zhang, F. Cheng, J. Sun, N. Wang, Y. Zhu, *Polymers*, 12 (2020) 1369.
40. L.G. Wei Huige, Wan Tong, Chen Anli, Peng Zifang, Zhang Huan, *Acta Materiae Compositae Sinica*, 39 (2022).
41. G. Li, L. Wang, X. Lei, Z. Peng, T. Wan, S. Maganti, M. Huang, V. Murugadoss, I. Seok, Q. Jiang, *Advanced Composites and Hybrid Materials*, 5 (2022) 853-863.
42. Y. Fu, H. Wu, S. Ye, X. Cai, X. Yu, S. Hou, H. Kafafy, D. Zou, *Energy & environmental science*, 6 (2013) 805-812.
43. L. Li, J. Zhang, Z. Peng, Y. Li, C. Gao, Y. Ji, R. Ye, N.D. Kim, Q. Zhong, Y. Yang, *Advanced Materials (Deerfield Beach, Fla.)*, 28 (2015) 838-845.

44. Z. Liu, J. Chen, Y. Zhan, B. Liu, C. Xiong, Q. Yang, G.-H. Hu, *ACS Sustainable Chemistry & Engineering*, 7 (2019) 17653-17660.
45. S.H. Park, J.-M. Jeong, S.J. Kim, K.H. Kim, S.H. Lee, N.H. Bae, K.G. Lee, B.G. Choi, *ACS Applied Energy Materials*, 3 (2020) 7746-7755.

Chapter 7

Summary and future outlook

In this chapter, we provide a comprehensive summary of the research conducted throughout the entire thesis. We have highlighted the major findings of our investigations with a special emphasis on the potential of PANI in the development of self-sensing electrochemical devices. The present investigation has set the stage for future research endeavors in the field of PANI-based materials for designing self-sensing macromolecular motors which is briefly described here. It also emphasizes the need for continued exploration and research in order to fully unlock the biomimetic properties of PANI and its applications in designing proprioceptive devices.

7.1. Summary

Conducting polymers, especially polyaniline, have attracted considerable research interest owing to their favourable electrical and electrochemical properties, as well as their wide-ranging applications. However, despite the attention they have received, there is still a lack of comprehensive understanding regarding the composition-dependent properties and applications of PANI within the scientific community. Although PANI is highly electroactive, its fundamental electrochemistry is not yet fully elucidated. Therefore, we initiated the thesis work by analyzing the structural faradaic process of PANI.

The thesis provides insight into the structural chemical kinetics of PANI and explains the structural faradaic process by using coul voltammograms. This study marks the first investigation of its kind in the field of PANI. QVs serve as a valuable tool for separating and quantifying reversible and irreversible reactions that occur during oxidation/reduction within the studied potential range. It is observed that the rate of reaction during the electrochemical oxidation/reduction of PANI is not constant but rather depends on structural changes with respect to the applied potential. The observed variations in the slope of the QVs are directly associated with changes in the reaction rate. By analyzing the coul voltammograms, different structural components of the electrode reaction of PANI have been identified and quantified in terms of charge. These components include fast oxidation-swelling, slow oxidation-relaxation, fast reduction-shrinking, and slow reduction compaction. This study provides valuable insights into the electrochemistry of PANI. It will help to a better understanding of

PANI's unique characteristics and pave the way for further exploration and applications in this field.

The electrochemical reaction of PANI takes place under non-equilibrium conditions due to continuous composition variation throughout the reaction. This occurs because the reaction proceeds through a series of 'n' consecutive steps, with each step involving the transfer of one electron. As a result, the system does not reach a steady-state equilibrium during the reaction. As a result, the fundamental principles of equilibrium electrochemistry, such as Le Chatelier's principle and Nernst equations, which are commonly used in traditional electrochemical sensing, are not directly applicable. In this case, Otero's principle becomes relevant and applicable. We have developed a theoretical approach for PANI sensing based on the principles outlined by Otero.

The sensing characteristics of the PANI reaction were investigated using two approaches: (1) galvanostatic conditions, i.e., chronopotentiometry, where the consumed electrical energy was found to act as the sensing parameter, and (2) potentiodynamic method, i.e., voltammetry, where the consumed electrical charge was employed as the sensing parameter. From the results, it is concluded that the PANI can sense their working energetic conditions such as electrical, chemical and thermal conditions from the consumed charge and/or consumed electrical energy during the reaction. This study gives a perspective that any electrochemical device, which works based on the electrochemical reaction of PANI, can sense its working conditions using consumed electrical energy and/or electrical charge as the sensing parameters. This

insight serves as the foundation for the development of sensing electrochemical motors. It provides new opportunities for sensing applications utilizing the distinctive electrochemical characteristics of PANI reactions.

Our primary objective was to develop electrochemical sensing motors by utilizing the sensing characteristics of PANI. However, the practical applications of PANI are hindered by its lack of processability and mechanical strength. Therefore, developing a mechanically stable PANI-based free-standing electrode material has become one of the focuses of our study. Accordingly, PANI/hydrogel hybrid films (Chitosan/PANI and PVA/PANI) were fabricated in a cost-effective and simple route to achieve this goal.

A comprehensive investigation was conducted on the Chitosan/PANI hybrid films. These films were fabricated through an in situ chemical polymerization of aniline within a chitosan film matrix. The hybrid films were subjected to detailed characterizations using various techniques. Electrochemical studies confirmed that the Chitosan/PANI hybrid films exhibit high electroactivity. Furthermore, the results demonstrated that the electrochemical reactions of the hybrid films can sense their working conditions, including electrical, thermal, and chemical conditions. Charge storage characteristics of the hybrid films studies were also conducted. The results revealed their favourable charge storage characteristics. Notably, the sensing and charge storage properties were derived from a single faradaic electrochemical reaction of hybrid film. The findings from this chapter suggest that the PANI/hydrogel films as

promising candidates for the development of sensing supercapacitor devices.

The chitosan/PANI hybrid films are moderately mechanically stable, which limits their practical applicability. Mechanical stability and flexibility are essential for device applications. Therefore, our research advances towards developing a much more mechanically stable and flexible hybrid film for device application. As a result, we succeeded in the fabrication of mechanically robust and highly flexible PVA/PANI hybrid films suitable for device design.

The studies were carried out to explore the characteristics and electrochemical properties of the PVA/PANI hybrid films. The hybrid films were subjected to detailed characterizations using various techniques. Interestingly, the results obtained revealed the remarkable electrochemical activity of the PVA/PANI hybrid films. Furthermore, the reaction-driven sensing capabilities of the hybrid films towards working energetic conditions were thoroughly examined. The consumed electrical energy was used as the sensing parameter to verify and validate the sensitivity of the hybrid films in detecting and responding to electrical, chemical, and thermal working conditions.

During the oxidation/reduction of the PANI, the conformational movements of polymeric chains generate/destroy the free volumes, anions and solvent inserted/expelled from the polymeric chain leading to swelling/shrinking of polymeric chains. This dynamic process of free volume variations has resulted from the cooperative actuation of molecular motors of PANI. It is proved that the conformational and

structural changes under faradaic control that arise due to the cooperative actuation of the constitutive chemical molecular machines are responsible for the self-sensing property of the hybrid films.

The investigation of the PVA/PANI hybrid films as electrode materials for supercapacitors yielded significant results. The hybrid films exhibited remarkable charge storage characteristics, indicating their potential as effective materials for energy storage applications. Finally, we succeeded in the fabrication of a self-sensing all-solid-state symmetric supercapacitor device using PVA/PANI hybrid hydrogel free-standing films. It has been demonstrated that the supercapacitor is capable of sensing its working conditions, such as working current and temperature. The consumed electrical energy during the charging/discharging cycles of the supercapacitor acts as the sensing parameter. This integration strategy eliminates the need for additional connectivities for sensing, unlike conventional sensing devices. Therefore, it provides a new direction for the development of compact next-generation self-sensing motors.

7.2. Future outlook

We have successfully developed mechanically stable and highly electroactive PVA/PANI hybrid films that can be easily fabricated on a large scale using a simple and cost-effective process. This achievement opens up numerous possibilities for exploring their applications across various fields. The mechanical stability and electroactivity of these PVA/PANI hybrid films make them well-suited for device fabrication, particularly in the development of self-sensing motors. In this work, we

demonstrated a self-sensing supercapacitor. Further research is necessary for their practical applications.

This work serves as a foundational milestone for the development of future biomimetic devices. Natural biological organs possess inherent sensing capabilities, they work under electrochemical reactions, allowing them to perceive and respond to their surroundings during operation (proprioception). In our research, we have successfully demonstrated that PANI (polyaniline) and PANI-based materials possess the unique ability to sense their working conditions due to their unique electrochemical reactions. That is, we established that **PANI based materials have biomimetic sensing capabilities**. Consequently, any device utilizing the electrochemical reaction of PANI, such as actuators, smart membranes, smart windows, and artificial synapses, can sense their working conditions without requiring additional sensing components. Therefore, this research has great potential for the development of various biomimetic sensing motors. By leveraging the self-sensing properties of PANI-based materials, we can replicate the functionality of biological organs, where the working signals and feedback can be transmitted through the same two connecting wires. This achievement paves the way for the creation of advanced biomimetic systems capable of self-sensing, offering significant improvements in functionality and efficiency. The possible biomimetic devices based on PVA/PANI hybrid systems are summarized in Figure 7.1.

The future scope of this study lies in the development of biomimetic sensing devices which can be termed as ‘Proprioceptive

devices' that emulate the sensing abilities of biological organs. By harnessing the high mechanical stability of PVA/PANI hybrid films and their self-sensing capabilities, we can open doors to new opportunities for enhanced performance in various biomimetic devices.

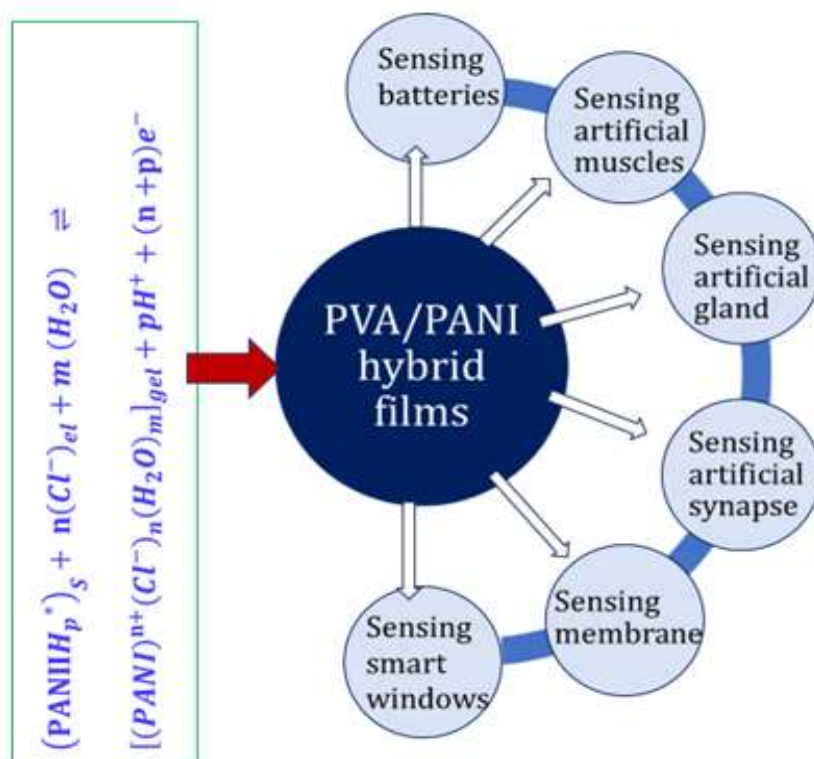


Figure 7.1 Possible biomimetic devices based on PVA/PANI hybrid films

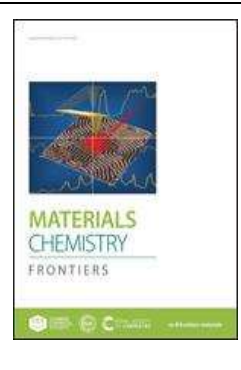
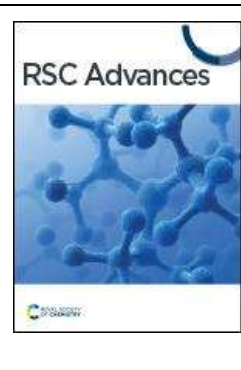
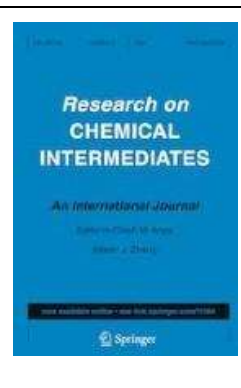


“Polyaniline, a remarkable polymer, has intrigued the world since its rediscovery in the 1980s. Its journey from the confines of laboratories to commercial markets has been within a decade. With its enticing characteristics, this polymer promises a future where smart, intelligent and functional devices dominate consumer markets with authenticity.”

“Get ready for the exciting era of polyaniline, as it enchants the world with its limitless potential.”

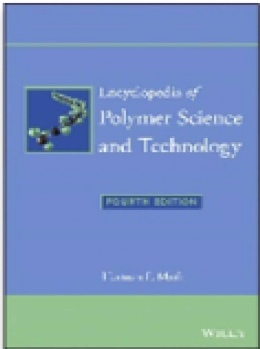
LIST OF PUBLICATIONS

	<p>M.P. Sidheekha, A. Shabeeba, L. Rajan, M. S. Thayyil, Y. A. Ismail, Conducting Polymer/Hydrogel Hybrid Free-Standing Electrodes for Flexible Supercapacitors Capable of Self-Sensing Working Conditions: Large-Scale Fabrication Through Facile and Low-Cost Route, <i>Engineered Science</i>, 2023, 23, 890. https://dx.doi.org/10.30919/es890</p>
	<p>M.P. Sidheekha, L. Rajan, Y. A. Ismail, Reaction driven biomimetic sensing characteristics of polyaniline/chitosan hybrid film: Sensing chemical and electrical reaction conditions, <i>Materials Chemistry and Physics</i>, 279, (2022) 125769. https://doi.org/10.1016/j.matchemphys.2022.125769</p>
	<p>M. P. Sidheekha, K. Nufaira, A.K. Shabeeba, L. Rajan, Y. A. Ismail, Characterization of polyanilines synthesized at different pH for electrochemical sensing and supercapacitor applications, <i>Materials Today: Proceedings</i>, 51 (2022) 2286-2292. https://doi.org/10.1016/j.matpr.2021.11.40</p>
	<p>M.P. Sidheekha, G. E. Rajendran, A. K. Shabeeba and Y. A. Ismail, Current sensing supercapacitor electrodes based on chitosan/poly-o-toluidine hydrogel composites, <i>Journal of Materials Research</i>, 36 (2021) 1914-1926 https://doi.org/10.1557/s43578-021-00241-2</p>

	<p>A. Shabeeba, L. Rajan, M. P. Sidheekha, M. S. Thayyil, Y.A. Ismail, Polypyrrole/hydrogel hybrid films as multi sensing supercapacitor electrodes, <i>Journal of Energy Storage</i>, 55 (2022) 105724 https://doi.org/10.1016/j.est.2022.105724</p>
	<p>L. Rajan, M. P. Sidheekha, A. Shabeeba and Y. A. Ismail, Conducting polymers as biomimetic multistep macromolecular sensors of working conditions: polyindole/polyvinyl alcohol hybrid film senses electrical and chemical working ambient, <i>Materials Chemistry Frontiers</i>, 6, (2022) 1706-1718 https://doi.org/10.1039/D2QM00322H</p>
	<p>A. Shabeeba, M. P. Sidheekha, L. Rajan and Y. A. Ismail, Flexible hybrid film of polypyrrole incorporated chitosan as a biomimetic multistep electrochemical sensor of working temperature: a potentiodynamic study, <i>RSC advances</i>, 12 (2022) 31911-31922 https://doi.org/10.1039/D2RA05482E</p>
	<p>L. Rajan, M. P. Sidheekha, A. Shabeeba, S. C. Unnikrishnan and Y. A. Ismail, Reactive sensing capability towards the working electrical and chemical conditions of poly (aniline-co-o-toluidine) copolymers, Research on <i>Chemical Intermediates</i>, 48 (2022) 4313-4329 https://doi.org/10.1007/s11164-022-04814-6</p>

	<p>A. K. Shabeeba, M. M. Manikandan, M. P. Sidheekha, L. Rajan, Y. A. Ismail, Poly-o-toluidine coated polyvinyl alcohol film: Reaction driven sensing capabilities, <i>Materials Today: Proceedings</i>, 51 (2022) 2293-2299. https://doi.org/10.1016/j.matpr.2021.11.403</p>
	<p>L. Rajan, A. Shabeeba, M. P. Sidheekha and Y. A. Ismail Reaction energetic condition induced conformational change in polyindole: Polyindole/PVA film as biomimetic sensor of working temperature and electrical energetic condition, <i>Chemistry-an Asian journal</i> 18 (2023) e202300742 https://doi.org/10.1002/asia.202300742</p>
	<p>L. Rajan, M. P. Sidheekha, A. Shabeeba, T. F. Otero and Y. A. Ismail Structural electrochemistry of poly(3,4-ethylenedioxythiophene) and its applicability as simultaneous sensor of environmental surroundings: self-sensing electrical, thermal, and chemical working conditions, <i>Journal of Materials Chemistry A</i>, 12(2024), 4583-4600 https://doi.org/10.1039/D3TA07081F</p>

BOOK CHAPTERS

	<p>Y. A. Ismail, A. K. Shabeeba, M. P. Sidheekha, L. Rajan, Conducting polymer/hydrogel systems as soft actuators, <i>Actuators: In: Fundamentals, Principles, Materials and Applications</i>, Wiley-Scrivener publishers, (2020) 211-252</p>
	<p>Y. A. Ismail, A. Shabeeba, M. P. Sidheekha, L. Rajan, Electroactive Polymer Actuators, <i>In: Encyclopedia of Polymer Science and Technology</i> (Ed.), Wiley publishers (2024).</p>

PRESENTATIONS

1. Oral presentation at the international conference ‘Frontiers in Chemical Sciences -FCS-2020’ organized by the Department of Chemistry, University of Calicut, Kerala, January 2020 (***Title: Synthesis and electrochemical characterization of conducting polymer/chitosan hybrid film as concentration sensor***)
2. Oral presentation at the International Conference on ‘Advances in material science –ICAMS-2021’ jointly organized by Arunai International Research Foundation, Tamilnadu, in association with the Department of Chemistry, University of Calicut, Kerala during 11-12 September 2021 (***Title: Characterization of polyanilines synthesized at different pH for electrochemical sensing and supercapacitor applications***)